Universidade de Aveiro
Departamento de Electrónica, Telecomunicações e Informática,
2012

Daniel Filipe
Marques Castanheira

Cancelamento de Interferência em Sistemas Celulares Distribuidos

Interference Cancellation for Distributed Wireless Systems

Universidade de Aveiro
Departamento de Electrónica, Telecomunicações e Informática,
2012

Daniel Filipe Marques Castanheira

Cancelamento de Interferência em Sistemas Celulares Distribuidos

Interference Cancellation for Distributed Wireless Systems

"We should be taught not to wait for inspiration to start a thing. Action always generates inspiration. Inspiration seldom generates action."

— Frank Tibolt

Universidade de Aveiro
Departamento de Electrónica, Telecomunicações e Informática,
2012

Daniel Filipe
Marques Castanheira

Cancelamento de Interferência em Sistemas Celulares Distribuidos

Interference Cancellation for Distributed Wireless Systems

Tese apresentada à Universidade de Aveiro para cumprimento dos requesitos necessários à obtenção do grau de Doutor em Engenharia Electrotécnica, realizada sob a orientação científica do Doutor Atílio Manuel da Silva Gameiro, Professor Associado do Departamento de Electrónica, Telecomunicações e Informática da Universidade de Aveiro

Apoio financeiro da FCT e do FSE no âmbito do III Quadro Comunitário de Apoio.

o júri / the jury

presidente / president

Prof. Doutor António Carlos Matias Correia
Professor Catedrático da Universidade de Aveiro

vogais / examiners committee

Prof. Doutor Francisco António Bucho Cercas
Professor Associado com Agregação do ISCTE - Instituto Universitário de Lisboa

Prof. Doutor Rui Miguel Henriques Dias Morgado Dinis
Professor Auxiliar com Agregação da Faculdade de Ciências e Tecnologias da Universidade Nova de Lisboa

Prof. Doutor Sílvio Almeida Abrantes Moreira
Professor Auxiliar da Faculdade de Engenharia da Universidade do Porto

Prof. Doutor Adão Paulo Soares Silva
Professor Auxiliar da Universidade de Aveiro

Prof. Doutor Atílio Manuel da Silva Gameiro
Professor Associado da Universidade de Aveiro (Orientador)

agradecimentos / acknowledgements

Queria usar este pequeno espaço para deixar os meus mais sinceros agradecimentos aqueles que foram essenciais neste percurso.

Desde já agradeço ao meu orientador professor Dr. Atílio Gameiro pela orientação, ajuda e confiança demonstradas ao longo destes anos.

À Fundação para a Ciência e Tecnologia pelo apoio financeiro.

Ao Instituto de Telecomunicações pelos excelentes meios e recursos disponibilizados.

Aos colegas do grupo MOTION/MOBNET pela entre ajuda e partilha de ideias.

Aos meus amigos pelos momentos de descontração passados juntos.

Aos meus pais pela inspiração que sempre foram para mim.

palavras-chave

Sistema de Antennas Distribuidas, Sistemas Multi-Utilizador, Precodificação Linear e Não-Linear, Minimização da Probabilidade de Erro, Capacidade de Canal, Cancelamento de Interferência, Codificação com Perdas, Codificação de Canal, Dirty Paper Coding

resumo

O tema principal desta tese é o problema de cancelamento de interferência para sistemas multi-utilizador, com antenas distribuídas. Como tal, ao iniciar, uma visão geral das principais propriedades de um sistema de antenas distribuídas é apresentada. Esta descrição inclui o estudo analítico do impacto da ligação, dos utilizadores do sistema, a mais antenas distribuídas. Durante essa análise é demonstrado que a propriedade mais importante do sistema para obtenção do ganho máximo, através da ligação de mais antenas de transmissão, é a simetria espacial e que os utilizadores nas fronteiras das células são os mais beneficiados. Tais resultados são comprovados através de simulação. O problema de cancelamento de interferência multi-utilizador é considerado tanto para o caso unidimensional (i.e. sem codificação) como para o multidimensional (i.e. com codificação). Para o caso unidimensional um algoritmo de pré-codificação não-linear é proposto e avaliado, tendo como objectivo a minimização da taxa de erro de bit. Tanto o caso de portadora única como o de multipla-portadora são abordados, bem como o cenário de antenas colocadas e distribuidas. É demonstrado que o esquema proposto pode ser visto como uma extensão do bem conhecido esquema de zeros forçados, cuja desempenho é provado ser um limite inferior para o esquema generalizado. O algoritmo é avaliado, para diferentes cenários, através de simulação, a qual indica desempenho perto do óptimo, com baixa complexidade. Para o caso multi-dimensional um esquema para efectuar "dirty paper coding" binário, tendo como base códigos de dupla camada é proposto. No desenvolvimento deste esquema, a compressão com perdas de informação, é considerada como um subproblema. Resultados de simulação indicam transmissão fidedigna proxima do limite de Shannon.

keywords

Distributed Antenna System, Multiuser Systems, Linear/Non-linear Precoding, Minimum Bit-Error-Rate, Shannon Capacity, Interference Cancellation, Lossy Coding, Channel Coding, Dirty Paper Coding

abstract

This thesis focus on the interference cancellation problem for multiuser distributed antenna systems. As such it starts by giving an overview of the main properties of a distributed antenna system. This overview includes, an analytical investigation of the impact of the connection of additional distributed antennas, to the system users. That analysis shows that the most important system property to reach the maximum gain, with the connection of additional transmit antennas, is spatial symmetry and that the users at the cell borders are the most benefited. The multiuser interference problem has been considered for both the one dimensional (i.e. without coding) and multidimensional (i.e. with coding) cases. In the unidimensional case, we propose and evaluate a nonlinear precoding algorithm for the minimization of the bit-error-rate, of a multiuser MIMO system. Both the single-carrier and multi-carrier cases are tackled as well as the co-located and distributed scenarios. It is demonstrated that the proposed scheme can be viewed as an extension of the well-known zero-forcing, whose performance is proven to be a lower bound for the generalized scheme. The algorithm was validated extensively through numerical simulations, which indicate a performance close to the optimal, with reduced complexity. For the multi-dimensional case, a binary dirty paper coding scheme, base on bilayer codes, is proposed. In the development of this scheme, we consider the lossy compression of a binary source as a sub-problem. Simulation results indicate reliable transmission close to the Shannon limit.

Contents

List of Figures

List of Tables

List of Acronyms

3GPP	3rd Generation Partnership Project.
AMPS	Advanced Mobile Telephone System.
AWGN	Additive White Gaussian Noise.
BC	Broadcast Channel.
BD	Block Diagonalization.
BEC	Binary Erasure Channel.
BEQ	Binary Erasure Quantization.
BER	Bit Error Rate.
BFGS	Broyden-Fletcher-Goldfarb-Shanno.
BiP	Bias Propagation Algorithm.
BLAST	Bell Laboratories Layered Space-Time.
BMS	Binary Memoryless Symmetric Channel.
BP	Belief Propagation.
BPSK	Binary Phase Shift Keying.
BS	Base Station.
BSC	Binary Symmetric Channel.
C-Netz	Radio Telephone Network C.
CAS	Co-located Antenna System.
CDMA	Code Division Multiple Access.
CoMP	Coordinated MultiPoint.
CSI	Channel State Information.
CU	Central Unit.

DAS	Distributed Antenna System.
DCAP	Differential CAPacity.
DE	Density Evolution.
DPC	Dirty Paper Coding.
EDGE	Enhanced Data Rates for GSM Evolution.
eNB	evolved NodeB.
ETSI	European Telecommunications Standards Institute.
FCC	United State's Federal Commission.
FDD	Frequency Division Duplex.
FDMA	Frequency Division Multiple Access.
FFT	Fast Fourier Transform.
FUTON	Fibre-Optic Networks for Distributed Extendible Heterogeneous Radio Architectures and Service Provisioning.
GPRS	General Packet Radio Service.
GSM	Global System for Mobile Communications.
HSDPA	High-Speed Downlink Packed Access.
IC	Interference Cancellation.
IMTS	Improved Mobile Telephone Service.
ITU	International Telecommunications Union.
KKT	Karush-Kuhn-Tucker.
LDGM	Low Density Generator Matrix.
LDPC	Low Density Parity Check.
LTE	Long Term Evolution.
M2M	Machine to Machine.
MAC	Multiple Access Channel.
MAP	Maximum a Posteriori.
MBMUT	Minimum Bit-Error-Rate multiuser transmission.
MGF	Moment Generating Function.
MIMO	Multiple Input Multiple Output.

MISO	Multiple Input Single Output.
ML	Maximum Likelihood.
MMSE	Minimum Mean Square Error.
MRT	Maximum Ratio Transmission.
MTA	Mobile Telephone System A.
MTS	Mobile Telephone Service.
MUT	MUltiuser Transmission.
NMT	Nordic Mobile Telephone.
OFDM	Orthogonal Frequency Division Multiplexing.
OSTBC	Orthogonal Space Time Block Codes.
PDC	Personal Digital Cellular.
PDF	Probability Density Function.
PGS	Projected Gauss Seidel.
PHOTON	Distributed and Extendible Heterogeneous Radio Architectures using Fibre Optic Networks.
QAM	Quadrature Amplitude Modulation.
QP	Quadratic Program.
QPSK	Quadrature Phase Shift Keying.
RAT	Radio Access Technology.
RAU	Remote Antenna Units.
RBP	Reinforced BP.
RRU	Remote Radio Units.
RTMI	Radio Telefono Mobile Integrato.
RV	Random Variable.
SIR	Signal to Interference Ratio.
SISO	Single Input Single Output.
SNR	Signal to Noise Ratio.
SON	Self Optimizing Networks.
SP	Survey Propagation.

SQP	Sequential Quadratic Programming.
SVD	Singular Value Decomposition.
TACS	Total Access Communication System.
TDD	Time Division Duplex.
TDMA	Time Division Multiple Access.
TPC	Total Power Constraint.
UE	User-Equipment.
UMTS	Universal Mobile Telecommunications System.
WiMAX	Worldwide Interoperability for Microwave Access.
ZF	Zero-Forcing.

List of Abbreviations

$(.)^H$	Hermitian transpose operator
$(.)^T$	Transpose operator
$(\bar{.})$	Real vector representation of a complex vector
$\setminus$	Set subtraction operator
$\circ$	Hadamard product
$\lambda(.)$	Variable node degree distribution
$\mathcal{I}(\mathbf{A})$	Imaginary part of matrix $\mathbf{A}$
$\mathcal{R}(\mathbf{A})$	Real part of matrix $\mathbf{A}$
$\mathbb{1}(.)$	Indicator function
$\mathbb{E}[.]$	Expectation operator
$\rho(.)$	Check node degree distribution
σ^2	Noise variance
$\sim x_i$	Set of all entries of vector $\mathbf{x}$ except x_i
$\tilde{\mathcal{N}}_p(\mu, \mathbf{\Sigma})$	p-variate complex Gaussian distribution, with mean μ and covariance $\mathbf{\Sigma} \in \mathbb{C}^{p \times p}$
$\tilde{\mathcal{N}}_p(\boldsymbol{\mu}, \mathbf{\Sigma})$	p-variate complex Gaussian distributed vector with mean μ and covariance $\mathbf{\Sigma}$
$\tilde{\mathcal{W}}_p(n, \mathbf{\Gamma})$	complex Wishart distributed $(p \times p)$ matrix with n degrees of freedom and mean $\mathbf{\Gamma}$
$\mathbf{0}_N$	$1 \times N$ all zeros column vector
$\mathbf{1}_N$	$1 \times N$ all ones column vector
$\mathbf{G}$	Generator matrix
$\mathbf{G}_i$	Column i of matrix $\mathbf{G}$
$\mathbf{H}$	Parity check matrix/Channel Matrix

$\mathbf{n}$	Noise introduced by the channel
$\mathbf{x}$	Channel input
$\mathbf{x}_i$	Entry i of vector $\mathbf{x}$
$\mathbf{y}$	Channel output
C	Maximum possible rate of transmission over a channel
$H(.)$	Entropy of a random variable
$I(.,.)$	Mutual information
I_N	$(N \times N)$ Identity Matrix
M	Constellation order
N	Codeword length
N_c	Number of available sub-carriers
P	Available power for transmission
p	Binary symmetric channel flipping probability
$tr(.)$	Trace operator
$\mathrm{Ber}(p)$	Bernoulli distribution with probability p

Chapter 1

Introduction

In this chapter we give a brief overview of the historic evolution of the wireless cellular systems, leading to the adoption of cooperation techniques in the latest standards. We then present the main motivation for the work developed within this thesis. The main contribution resulting from this thesis is outlined, followed by a description of the structure of this document.

1.1 Evolution of Cellular Systems

Public mobile telephone history begins in the 1940s, after World War II. On July 28, 1945, the principles of today wireless cellular systems were first described, in print, by J. K. Jett [19]. Nevertheless, the United States' Federal Communications Commission (FCC) never allocated the spectrum needed for this service. In 1946, AT&T and South Western Bell introduced the Mobile Telephone Service (MTS) [2], at Saint Louis, Missouri [19]. In MTS the traffic was manually routed by an operator, at the central office. Eighteen years later, in 1964, Bell System launched an enhanced version of MTS the Improved Mobile Telephone Service (IMTS) [3, 19]. The IMTS was a full duplex system, unlike MTS, with direct-dial and caller identification.

The first nationwide public radiotelephone system was inaugurated in 1949 by the Dutch National radiotelephone network and the first fully automatic phone system, the Mobile Telephone System A (MTA), was designed by Swedish Telecommunications Administration's Sture Lauhrén and Ragnar Berglund, in 1951, and did not become entirely operational until 1956 [19].

In 1947, at Bell Labs, D. H. Rings, with the help from W. R. Young, clearly proposed the cellular concept for mobile wireless systems in an internal company memorandum [4]. The cellular concept is based on the divide and conquer principle, namely the main idea behind it is to replace a high-power base station, covering a large geographical area and using all available frequency channels, by a set of low powered base stations, covering a small area, called cell, and using only a subset off all frequency channels. With the help of frequency reuse, BSs in non-adjacent cells could reuse the same set of channels with little interference. However, only thirteen years later, in 1960, the final portrait of the entire wireless cellular system was drawn when two papers, discussing the handoff process, were published in the *Institute of Radio Engineers Transactions on Vehicle Communications* [19]. Nevertheless, the first commercial cellular radio system, the Metroliner [5], just became operational in 1969.

In Europe, the Analog cellular was also widely accepted. Namely, in 1981, Sweden, Finland,

Denmark and Norway began operating the first multinational cellular system, the NMT 450, which offered roaming [19]. In the same decade, Great Britain introduced the Total Access Communications System (TACS), the West German C-Netz, the French Radiocom 2000 and the Italian RTMI/RTMS. In the United States, the first commercial cellular services began in 1983, using Advanced Mobile Phone Service (AMPS) [6], [7] .

The main characteristics of the 1G systems are: analog frequency modulation for voice transmission, digital signaling, handover and the use of frequency division multiple access (FDMA) for channel allocation. The increasing diversity of incompatible cellular systems working in Europe led the Europeans to draw a plan to create a single European wide digital mobile service with advanced features and easy roaming [19]. The Global System for Mobile Communications (GSM) [8] was born. GSM has no backward compatibility with previous existing systems and is fully digital. The move from analog to digital clearly defines another major technological step, a turning point to the 2G. The advances made within the area of micro-electronics, in the seventies, with the introduction of the microprocessor, by Intel, and also the development of low-rate digital speech coding techniques, were among the most important contributions to the full development of 2G [6] [8]. With the advent of the 2G systems, the infrastructure and handsets' cost has become lower, the spectral efficiency increased, new services have been offered (such as data, messaging, fax and roaming) and the privacy increased [9]. Unlike Europe, in the US, the newly adopted digital standard, IS-54, had backward compatibility with existing AMPS systems [19]. However, like most 2G systems, it used time division multiple access (TDMA) to separate the channels of different users [19]. Among the most important 2G systems, we have: GSM which started in Europe and is now all over the world, spread around 130 countries, IS-54 in the United States and the Personal Digital Cellular (PDC) in Japan [10].

In the nineties, we started to assist a paradigm shift. Namely, the mobile phone, a device primarily built to make voice calls started to be more and more used to access the Internet, check the email, receiving faxes, etc. Nonetheless, its effectiveness for doing that stuff was limited, since it and the associated network were not built for data traffic [19]. Consequently, a fundamental change was needed from circuit switching to packet switching, since unlike voice, data is not efficiently handled by circuit switching [19]. To tackle this problem two technologies were developed: General Packet Radio Service (GPRS) and its improvement, Enhanced Data Rates for GSM Evolution (EDGE), well known as 2.5G systems [19]. The 3G systems were designed to add mobility not only to voice but also to the new data applications that were emerging. This new generation of systems has been designated by the International Telecommunications Union (ITU) as International Mobile Telecommunications 2000 (IMT-2000). In 1991, ETSI standardized Universal Mobile Telecommunications System (UMTS), the European 3G system [19]. UMTS key features include the support to basic modes (FDD and TDD), variable transmission rates, intercell asynchronous operation, adaptive power control, increased coverage and capacity, etc. Other examples of 3G systems are the American CDMA2000 and the Chinese Time-Division Synchronous CDMA (TD-SCDMA), just to name a few. All these systems were specified by the 3rd Generation Partnership Project (3GPP) [11], all use the Code Division Multiple Access (CDMA) technology and offered from 144 kbps (high mobility) to 2 Mbps (low mobility). Nevertheless, with the High-Speed Downlink Packet Access (HSDPA) technology it is possible to achieve up to 8-10Mbps over a 5 MHz bandwidth.

The full deployment of 3G systems has been slow and expensive, since the upgrade from 2G to 3G requires a change of access technology, from time to code division, and a costly infrastructure [19]. In between, 4G has begun to see the light of the day, driven by the

steady increase of user requirements unable to be met by the limitations of the current mobile communication systems. Worldwide Interoperability for Microwave Access (WiMAX) and Long Term Evolution (LTE) are considered as the two pre-4G technologies, sometimes called 3.9G technologies. Although these two technologies have made a great leap into the 4G world, they have failed to achieve the full vision of the ITU IMT-advanced project [12]. The key features of IMT-Advanced are [12], [13]:

- improved spectral efficiency and peak rates (100 Mbit/s for high and 1 Gbit/s for low mobility were established as targets for research);
- low latencies;
- ubiquitous Access;
- transparent mobility and worldwide roaming capability;
- low cost and low-complexity terminals;
- high quality mobile services;
- user equipment suitable for worldwide use;
- user-friendly applications, services and equipment;

To comply fully with the IMT-Advanced project specifications LTE-Advanced, the next milestone along the evolution path of LTE, has been developed. LTE and LTE-Advanced use orthogonal frequency division multiplexing (OFDM) as its radio access technology (RAT). The main improvements of LTE-advanced over LTE Release 8 are [14]:

- Wider bandwidth, enabled by carrier aggregation;
- Advanced MIMO techniques;
- Support for heterougenous network;
- Relaying;
- Coordinated multipoint transmission and reception (CoMP);
- LTE Self Optimizing Networks SON enhancements;
- Home Node B (HNB) and Home enhanced Node B (HeNB) mobility enhancements;

Indeed, LTE-Advanced has been accepted, by ITU, as a 4G technology, in 2010, by complying with or exceeding the ITU established criteria in all aspects. One of the main technologies introduced in LTE Advanced, which promises to bring increased data rates and system coverage, is CoMP [14], [15]. In CoMP, a user-equipment (UE), at the cell-edge, may receive signals from multiple cell sites and can also transmit its signal, to be jointly processed, by several cell sites. The way the different intervening cell sites cooperate, and the cell coordination process influences the final performance of the system. The cooperation/coordination can go from simple interference avoidance techniques to full cooperation. If the coordination is within a cell, we have the intra-site CoMP. On the other hand, if CoMP involves multiple cells, we

call it inter-site CoMP [16], [17]. Intra-site CoMP does not involve the exchange of information through the backhaul, since the communication is within a site. However, inter-site CoMP, does need a backhaul infrastructure to pass information between the different cell sites, for cooperation. An interesting CoMP architecture is the one where a set of geographically distributed Remote Radio Units (RRU) are connected by optical fiber to an evolved NodeB (eNB), where all the coordination/processing is done. This architecture can be considered to be in between the intra-site and the inter-site architecture, since the coordination process is done in the corresponding site eNB, but the transmission behaves like the inter-site CoMP. More recently, a similar architecture has been pursued in the FUTON European project [18].

1.2 Motivation

Current cellular networks and architecture support over 6 billion mobile devices worldwide, and the total number is expected to increase substantially in the forthcoming years, with the advent of machine to machine (M2M) systems. The demand for wireless data traffic is expected to increase by 33-fold (relatively to 2010), achieving an expected mark of more than 127 Exabytes (10^18 bytes) in 2020 [1]. Evolution of the network architecture is required to achieve these goals, along with the use of cooperation/coordination techniques.

To cope with the current trend of higher rates, the operators are shrinking cell sizes (e.g. using femtocells, M2M clusters, relaying, etc) [1]. If not carefully managed, this process could lead to unsustainable levels of interference, since the percentage of cell-edge users are also increasing. To alleviate this problem inter-cell interference cancellation techniques can be used, but this requires cooperation between base stations. By sharing information, the base stations are able to jointly apply MIMO techniques.

It is well known that for a MIMO system the capacity scales linearly with the minimum number of transmit and receive antennas, as long as the different channels are uncorrelated. Unfortunately due to the physical limitations in the size of the transceivers, the number of antenna elements cannot be large and the spacing between them is limited, which implies that the degree of channel independence achieved is insufficient in most scenarios to reach the high capacities envisioned. To alleviate this problem the antenna elements should be distributed geographically, leading to the distributed antenna system concept. In order to enable the application of MIMO techniques the antennas must be connected, through a transparent medium, to a central unit, where all the processing is done. This allows the antennas to be treated as physically distributed antennas of one composite base station.

1.3 Thesis Contribution

The work described in this thesis has been done in parallel with the European FUTON project (Fibre-Optic Networks for Distributed Extendible Heterogeneous Radio Architectures and Service Provisioning) and also with the Portuguese PHOTON project (Distributed and Extendible Heterogeneous Radio Architectures using Fibre Optic Networks). This work is mainly focused on the multiuser interference cancellation topic. Succinctly, the main aspects addressed during the course of this journey were:

- Analytical investigation of the gains obtained by the joint processing of more antennas at a central base station, for a scenario with single antenna users and a base station with distributed antennas.

- Proposal of a nonlinear multiuser MIMO precoding algorithm for the minimization of the bit-error-rate (BER) of the downlink of a conventional co-located multiuser MIMO based system. The algorithm was derived assuming the high signal to noise ratio. By taking into account the properties of the BER function in that regime it is possible to simplify the minimization problem from a quadratic nonlinear optimization one to a simple quadratic program. The final quadratic formulation is shown to have close connections to the well-known zero-forcing. The previous formulations are also extended to a multiuser distributed antenna system (DAS) and in addition to the multicarrier case.

- An algorithm for binary quantization over the low density generator matrix (LDGM) codes is proposed. The typical algorithm to solve such a problem is the belief propagation (BP) with hard decimation. However, its complexity grows quadratically with the codeword length of the code. To solve this problem is proposed to replace the hard constraints, imposed by hard decimation, by soft constraints, to guide the BP algorithm, like already done in the interior point method, for convex optimization problems.

- A bilayer LDGM code is proposed for practical binary dirty paper coding (DPC). With the careful concatenation of a high-rate Low Density Parity Check code (LDPC) to the lower layer of the bilayer LDGM code, the bilayer LDGM code will be able to work not only at two different rates, but also to be a good channel code globally and to be a good lossy source code locally, in the upper LDGM code. These two important features of the code make it well suited for DPC. Using the density evolution (DE), erasure channel approximation, and linear programming a method is introduced to optimize the bilayer LDGM code parameters, for DPC.

Over the years, the research done over the previous topics had given rise to the following scientific publications:

Book Chapters

[1] A. Gameiro, D. Castanheira, "System Concept for Central Processing of Signals" - Chapter in *Next Generation Wireless Communications using Radio over Fiber*, Nathan Gomes, Atilio Gameiro, and Paulo Monteiro, Wiley, United Kingdom, 2012.

[2] D. Castanheira, A. Gameiro, "Single/Multi-User MIMO Differential Capacity" - Chapter in *Radio Communications*, Alessandro Bazzi, In-Tech, Austria, 2010.

Scientific Journals/Magazines

[3] D. Castanheira, R. Holakouei, A. Silva, A. Gameiro, "Linear and Nonlinear Precoding Schemes for Centralized Multicell MIMO-OFDM Systems", submitted to *Journal Springer Wireless personal communications*, -, 2012

[4] D. Castanheira, A. Gameiro, A. Silva, "Minimum bit error rate nonlinear precoding for multiuser MIMO and high SNR", *Physical Communication*, Volume 4, Issue 4, December 2011, Pages 296-304, ISSN 1874-4907, 10.1016/j.phycom.2011.07.003.

[5] D. Castanheira, A. Gameiro, "Distributed antenna system capacity scaling [Coordinated and Distributed MIMO]," *Wireless Communications*, IEEE , vol.17, no.3, pp.68-75, June 2010

Scientific Conferences

[6] D. Castanheira, A. Gameiro, A. Silva, "Minimum Bit-Error-Rate Nonlinear Precoding For Multi-User Distributed Antenna Systems," in proc. *IEEE GLOBECOM First Workshop on Distributed Antenna Systems for Broadband Mobile Communications*, Houston, Texas, USA, December 2011

[7] D. Castanheira, A. Gameiro, "Lossy source coding using belief propagation and soft-decimation over LDGM codes," in proc. *IEEE International Symposium on Personal Indoor and Mobile Radio Communications* (PIMRC), Istambul, Turkey, Sept. 2010

[8] D. Castanheira, A. Gameiro, "Binary dirty paper coding," in Proc. *IEEE Future Network and Mobile Summit*, Florence, Italy, June 2010

[9] D. Castanheira, A. Gameiro, "High SNR Broadcast Channel Differential Capacity", in proc. *Future Network and MobileSummit*, Santander, Spain, June 2009

[10] D. Castanheira, A. Gameiro, "Distributed MISO system capacity over Rayleigh flat fading channels," in proc. *IEEE International Symposium on Personal, Indoor and Mobile Radio Communications*, Cannes, France, Sept. 2008

1.4 Thesis Organization

This thesis is organized into six chapters, and the main theme of focus is interference cancellation (IC). For ease of reading we have divided the central theme into three main topics: capacity analysis and interference cancellation without coding and with coding (DPC). The first topic is discussed in chapter 3 the second in chapter 4 and the last in the subsequent chapter.

In the first chapter, chapter 2, a brief revision of the basic concepts needed for a clear understanding of the contents of this thesis is presented. First, we describe the main definitions and concepts of information theory. Then we present some capacity results, for the most important channel models, some of which will be used in the following chapters. Finally, an overview of linear block codes is given, with special emphasis on LDPC and LDGM codes. In particular, their factor graph representation is presented, the sum-product decoding algorithm revisited, and a brief overview of density evolution made.

In chapter 3, a model for DAS and CAS is described. Using this model a connection between DAS and CAS is presented which displays why the additional degrees of freedom provided by DAS are essential to get its benefits over CAS. The benefits of the DAS over a co-located antenna system (CAS) are delineated, in terms of efficiency, diversity and capacity. To accomplish that, the exact capacity expression for the single-user case is derived and a new concept proposed, the differential capacity. Taking into account the introduced definition, it is shown that are the users at the cell borders the ones that obtain most of the gains, by the connection of additional transmit antennas.

The standard linear precoding techniques, zero-forcing and minimum mean square error, are revisited in chapter 4. A minimum bit-error-rate optimization problem for the downlink of a co-located multiuser MIMO based system is formulated. By taking into account the

properties of the BER function in the high SNR regime this minimization is simplified from a quadratic constrained nonlinear optimization problem to a simple quadratic program. This results in significant complexity reduction. The final quadratic problem is shown to have close connections to the well-known zero-forcing (ZF) precoding scheme. Enabling the proposal of a Minimum Mean Square Error (MMSE) like scheme with improved performance at low SNR. The algorithm is further extended to the multicarrier and to the distributed antenna case. Results show significant gains relatively to ZF and MMSE, demonstrating that the algorithm is well suited for practical implementation as it combines close to optimum performance, with reduced complexity.

An overview of the lossy source coding problem is drawn in Chapter 5, followed by a brief description of the BP and BP with hard decimation algorithms. Supported by the BP, with decimation, algorithm, an equivalent representation of it is drawn with the help of an indicator function. This allows to transform the hard constraint into a soft one by replacing the indicator function by a linear function, to guide the BP algorithm. Results indicate linear complexity in the block length and close to the state-of-the-art performance.

Furthermore, in Chapter 5, the DPC problem and framework are briefly reviewed. The DPC problem is decoupled into a channel and a lossy coding problem, to obtain a low complexity scheme. The main idea behind this separation is that one can group the bits to be transmitted into two parts. One for real data transmission and another to use as an approximation to the interference. The use of bilayer codes, duals of the ones proposed for the relay channel, are proposed to implement the DPC scheme. Additionally, a simple linear programming approach is suggested to optimize the corresponding bilayer DPC code. Simulation results indicate reliable transmission close to the Shannon limit, with reduced complexity.

1.5 References

[1] BelAir Networks, “Small Cell Networks for Mobile Network Offload.” *White paper*, Nov. 2011.

[2] Peterson, A. C., Jr. “Vehicle Radiotelephony Becomes a Bell System Practice.” *Bell Laboratories Record*, 137, April, 1947.

[3] Douglas, V. A. “The MJ Mobile Radio Telephone System.” *Bell Laboratories Record*, 383, December, 1964.

[4] Roessner, D et al. “The role of NSF’s Support of Engineering in Enabling Technological Innovation: Phase II, chapter 4: The Cell Phone. Final Report to the National Science Foundation.’ Arlington, Virginia: SRI International, 89, 1998. citing Ring, D H, “ Mobile Telephony - Wide Area Coverage,"’ *Bell Laboratories Record Technical Memorandum*, December 11, 1947.

[5] Paul, C.E. Telephones Aboard the ’Metroliner’. *Bell Laboratories Record*, 77, March, 1969

[6] Padgett, J.E.; Gunther, C.G.; Hattori, T.; , "Overview of wireless personal communications," *Communications Magazine*, IEEE , vol.33, no.1, pp.28-41, Jan 1995 doi: 10.1109/35.339877

[7] G. L. Stï¿½ber, Principles of Mobile Communications, Springer, 2011.

[8] M. Mouly and M.-B. Pautet, Mobile Communications Advanced Systems and Components, vol. 783, Springer Berlin / Heidelberg, 1994, pp. 13 20.

[9] R. Bekkers and J. Smits, Mobile telecommunications: standards, regulation, and applications. Artech House, 1999.

[10] T. Rappaport, Wireless Communications: Principles and Practice, Upper Saddle River, New Jersey, USA, Prentice Hall, 1996.

[11] Third Generation Partnership Project, http://www.3gpp.org.

[12] ITU, Visions, Framework and Overall Objectives of the Future Development of IMT-2000 and Systems Beyond IMT-2000, ITU-R, Rec. ITU-R M.1645, June 2003.

[13] IMT-ADV, Background on IMT-Advanced, May 2008

[14] Agilent, Introducing LTE-Advanced, pg. 6 , March 8, 2011

[15] S. Parkvall, E. Dahlman, A. Furuskar, Y. Jading, M. Olsson, S. Wanstedt, K. Zangi, LTE-Advanced - Evolving LTE towards IMT-Advanced, in Proc. *IEEE 68th Vehicular Technology Conference*, pp. 1-5, Calgary, Canada, September 2008.

[16] Sawahashi, M.; Kishiyama, Y.; Morimoto, A.; Nishikawa, D.; Tanno, M.; , "Coordinated multipoint transmission/reception techniques for LTE-advanced [Coordinated and Distributed MIMO]," *Wireless Communications*, IEEE , vol.17, no.3, pp.26-34, June 2010 doi: 10.1109/MWC.2010.5490976

[17] Irmer, R.; Droste, H.; Marsch, P.; Grieger, M.; Fettweis, G.; Brueck, S.; Mayer, H.-P.; Thiele, L.; Jungnickel, V.; , "Coordinated multipoint: Concepts, performance, and field trial results," *Communications Magazine*, IEEE , vol.49, no.2, pp.102-111, February 2011 doi: 10.1109/MCOM.2011.5706317

[18] Fibre optic networks for distributed, extendible heterogeneous radio architectures and service provisioning. FUTON project. [Online]. Available: http://www.ict-futon.eu/

[19] Farley, T. (2005). Mobile telephone history. *Teletronikk*

Chapter 2

Brief Revision of Concepts

In this chapter we review the most fundamental concepts used in this document. First, we give a brief overview of the main concepts used in information theory and derive the capacity expression of some representative channels. Then we go through the basic properties of linear block codes with special emphasis on LDPC and LDGM codes. In this overview we introduce the code factor graph representation, the well known sum-product decoding algorithm and the main technique used in code optimization, density evolution.

2.1 Introduction

In 1948, Claude Shannon introduced the field of information theory to the research community and to the world with his remarkable paper entitled "A Mathematical Theory of Communication" [1]. In this paper Shannon formulates and solves one of the most important and challenging problems in communications, of his time. He shows that it is possible to transmit information through a noisy channel, reliably and with a positive rate, with the help of coding. The maximum information rate that can be achieved through a channel with an arbitrarily small probability of error, is the channel capacity. Over the years, the capacity of various channels, such as the Additive White Gaussian Noise (AWGN) channel [1], the MIMO channel [2], the Multiple Access channel [3, 4] and the Broadcast channel [5, 6], has been derived using the tools provided by Shannon. However, such tools have not been provided for the construction of codes able to achieve the capacity, which led to an intense research in the area. Recently, the proposal of turbo coding [7–10] and the reappearance of LDPC codes [11–16] have made practical the achievement of rates close to capacity. These codes can be represented by sparse graphical models, and the corresponding encoding/decoding algorithms operate locally in the associated graph. The algorithm operates locally, but the complex code structure guarantees reliable transmission, since as the algorithm iterates the local information propagates along the graph. Another important feature of these codes, like in the original work of Shannon, is their inherent randomness, with which the notion of a graph ensemble enabled the analysis of such codes by methods like density evolution. These methods, allow, for example, to calculate the theoretical capacity, and to optimize the structure of LDPC codes.

This chapter is organized as follows. We begin in the following section with a brief description of the main definitions and concepts of information theory. Then we present capacity

results for some channel models. Finally, an overview of linear block codes is given, with special emphasis on LDPC and LDGM codes. In particular, their factor graph representation is presented, the sum-product decoding algorithm revisited, and a brief overview of density evolution made.

2.2 Information Theory Overview

2.2.1 Introduction

"The fundamental problem of communications is that of reproducing at one point either exactly or approximately a message selected at another point" [1]. Shannon work, in the field of information theory [1], leaned over the answer of a fundamental problem: the reliable transmission of information over an unreliable medium, at a positive rate.

Let us consider, as shown in Figure 2.1, a transmission system decomposed into its main components, by applying the source-channel separation principle. The main blocks of a transmission system are the information source, the source encoder/decoder, the channel encoder/decoder, the channel and the destination. As the name indicates the information source produces messages to be sent through the channel. The source encoder removes all the redundancy present in the message, sent by the source. On the other hand, the channel encoder adds additional redundancy to the message to protect it from the noise added by the channel. The destination is just the final recipient (user or machine) of the message.

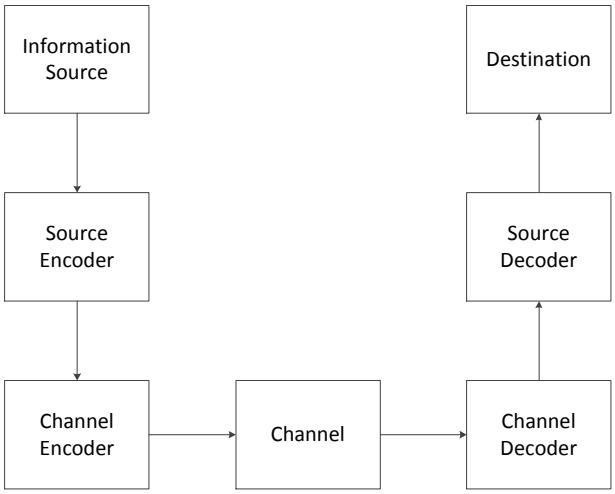

Figure 2.1: Block diagram of a communication link by applying the source-channel separation theorem.

For simplicity and as a way to facilitate the introduction of concepts, let us consider a simple model for the channel. Namely, let us consider that the channel is a binary symmetric channel (BSC) with probability of error p. The BSC is a simple channel model used to model efficiently a large number of communication systems, where a bit (a 0 or a 1) is transmitted correctly with probability $1 - p$ and in error with probability p. Let us also consider that the information source is a binary Bernoulli random variable with probability 1/2. Such an

assumption implies that no source encoder/decoder is needed, as will be seen next, since this source has no redundancy. Assume that the source is transmitting N bits of data to the destination, per second, and the channel is introducing pN errors, on average, in such bits. In such a case, the number of correct bits received at destination is $(1-p)N$, per second. However, this is not the true rate of transmission of information over the channel. The real rate is lower, since a user at the destination cannot extract any actual "information" from this message, since he does not know where the errors occurred. For instance, consider a particular long sample of the error sequence, with length N. It will contain, with probability approaching one, pN ones and $(1-p)N$ zeros. Therefore, a particular instance, of this sequence, has a probability of occurrence of approximately

$$P_i = p^{pN}(1-p)^{(1-p)N} = 2^{N(p\ log_2(p)+(1-p)\ log_2(1-p))} = 2^{-NH(p)} \tag{2.1}$$

where $H(p) = -p\ log_2(p) - (1-p)\ log_2(1-p)$ is the noise entropy, as will be defined next. In the previous analysis, we have not taken into account the small-scale fluctuations of the probability around the average. Namely, by the law of large numbers, the error sequences can be divided into two sets, the typical set, which has a probability of occurrence around the average ($2^{-N(H(p)+\epsilon)} \leq P_i \leq 2^{-N(H(p)-\epsilon)}, \epsilon \to 0$) and the atypical set. By the law of large numbers, a large enough random sequence belongs, with high probability, to the typical set. Since this set has a uniform distribution, the number of error sequences will be with high probability $2^{NH(p)}$ and not 2^N, as one might expect. Consequently, the transmitted sequence is transformed into one of a set of $2^{NH(p)}$ possible sequences, at an average hamming distance of Np, as shown graphically in Figure 2.2. Hence, to achieve a low as desired probability of error, the possible causes of each transmitted sequence must be disjoint from the likely causes of the others, like in Figure 2.2. Since, if an overlap between this sets occurs the decoder is unable to decide between the sequences labeling these sets. As a result, one can see that the limiting rate of transmission of information, for the BSC, is given by

$$R = \frac{1}{N} log_2\left(\frac{2^N}{2^{NH(p)}}\right) = 1 - H(p) \tag{2.2}$$

If the channel has no noise ($p = 0$) $R = 1$ as expected. However, with noise, the rate is reduced by the constant value $H(p)$. Therefore $H(p)$ represents the reduction in the information rate that the noisy channel imposes. One might also see $H(p)$ as the uncertainty introduced in the transmitted message, by the noise, from the viewpoint of the destination [1].

2.2.2 Entropy and Information

As seen in the previous section the noise in the channel adds uncertainty to the transmitted message decreasing the communication information rate. In this section, we will define in more detail the concept of information. To begin we will start with a single discrete source and next progress to multiple sources of information, characterizing the mutual information between them and their interaction. All concepts will be given for discrete random variables.

Consider a discrete source drawn from a random variable, X, with an alphabet of length K, where p_k is the probability of production of character k. A particular long instance, of length N, of this source will have with high probability $p_1 N$ occurrences of the first character, $p_2 N$ occurrences of the second character and so on. Therefore, the probability of occurrence

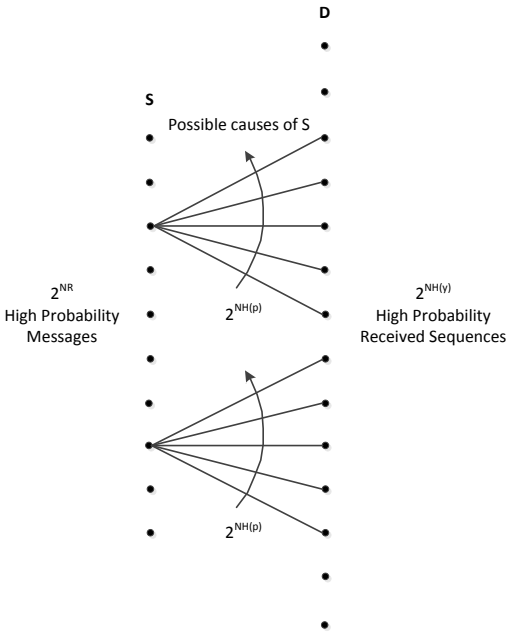

Figure 2.2: Transmitted/received messages correspondence.

---

of a specific instance, of length N, of this source is

$$P_i = \prod_{k=1}^{K} p_k^{p_k N} = 2^{N\left(\sum_{k=1}^{K} p_k \ log_2(p_k)\right)} = 2^{-NH(X)} \tag{2.3}$$

where $H(x)$ is defined as the entropy of the random variable x. Namely, the entropy gives us a measure of the uncertainty of the information content of a given variable.

$$H(X) = -\sum_{k=1}^{K} p_k \ log_2(p_k) \tag{2.4}$$

As an example consider a totally unfair coin, that can be modeled by a binary Bernoulli random variable, with probability 1. The entropy of this source is zero, since the uncertainty of the process is zero. We know the result before the coin is thrown into the air. On the other hand, for a fair coin, the entropy is one, since one bit is enough to describe the process and remove the user uncertainty. Looking at these examples and to equation (2.3) one can look at the entropy as the number of bits[1], needed to represent an event from the source.

The entropy can also be defined using another useful concept, the self-information, $I(x_k)$

$$H(X) = -\sum_{k=1}^{K} p_k \ log_2(p_k) = \mathbb{E}_X[I(x_k)] \tag{2.5}$$

[1]If another unit of measure is chosen, like nats, the entropy must be scaled accordingly by the appropriate constant.

where $I(x_k)$ is defined as the self-information associated with the outcome x_k, with probability p_k, which is given by $-log_2(p_k)$ and $\mathbb{E}_X[.]$ is the expectation operator over the space of X. The self-information gives a measure of the information content for a particular outcome of a random variable. Hence the entropy is the expected value of the associated self-information events. As a result of the self-information definition, the less probable events are the ones that provide the higher information content when they occur, as expected. Furthermore, if an event is the intersection of two independent events, the information content of the first is the sum of the other two, a consequence of the usage of the $log(.)$ operator.

Equipped with the concepts and definitions presented in the case of a single random variable then we move to the case of the interaction of more than one random variable, more specifically to the case of two random variables.

From the definition presented in equation (2.5) the concept of entropy can be easily extended to the multivariate case

$$H(X,Y) = -\sum_{k=1,m=1}^{K,M} p(x_k, y_m)\, log_2(p(x_k, y_m)) \tag{2.6}$$

If two variables are taken separately the number of typical sequences, for a long instance of length N, for the source X is $2^{NH(X)}$ and for the source Y, $2^{NH(Y)}$. On the other hand, if they are considered jointly the total number of typical sequences will be $2^{NH(X,Y)}$. Nevertheless, if X is drawn independently of Y, the number of such sequences is just $2^{NI(X,Y)}$. There are $2^{NH(X)}2^{NH(Y)}$ independent typical pairs and $2^{NH(X,Y)}$ jointly typical pairs, consequently, the probability of hitting one of these pairs is $2^{NH(X,Y)}/2^{NH(X)+NH(Y)} = 2^{-NI(X,Y)}$, where $I(X,Y)$ represents the mutual information between X and Y

$$\begin{aligned} I(X,Y) &= H(X) + H(Y) - H(X,Y) \\ &= H(X) - H(X|Y) \\ &= H(Y) - H(Y|X) \end{aligned} \tag{2.7}$$

and $H(X|Y) = -\sum_{m=1}^{M} p(y_m) \sum_{k=1}^{K} p(x_k|y_m)\, log_2(p(x_k|y_m))$ is the conditional entropy of X, given random variable Y. The mutual information is an important concept, in the analysis of the capacity of a communication channel, since its value defines the probability that a sequence different than the one transmitted, and the one received are jointly typical. Namely, it defines the average probability of error of the typical set decoder [17], allowing to prove that if the rate of information transmission is lower than $I(X,Y)$ the obtained probability of error can be made as low as required. The relations, present in equation (2.7), between entropy, joint entropy, conditional entropy and mutual information are shown graphically in Figure 2.3.

With all the previous definitions, the capacity of a communication link, C, can be defined as the maximum possible rate of information over all potential information source distributions

$$C = \max_{p(X)} I(X,Y) \tag{2.8}$$

Using the previous formula, for the BSC channel with flipping probability p, we get $C = I(X,Y) = H(Y) - H(Y|X) = H(Y) - H(p)$. The input distribution that maximizes the mutual information is the binary Bernoulli distribution with probability $1/2$, since it implies that the distribution of Y is also Bernoulli, with probability $1/2$. Hence, $H(Y) = 1$, and the corresponding BSC channel capacity is $C = 1 - H(p)$ as already argued previously.

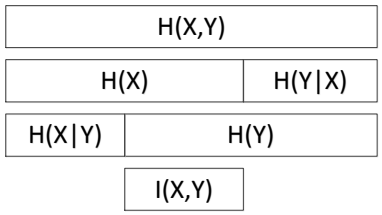

Figure 2.3: Entropy, joint entropy, conditional entropy and mutual information relations.

2.3 Channel Capacity

In this section, we will present and review the capacity expressions of some of the most well known channel models. First, the capacity of the erasure channel will be reviewed, due to its simplicity and to introduce the corresponding channel model that will be used in the following chapters. Next the AWGN channel, SISO and MIMO channel's capacity expressions and channels are presented.

2.3.1 Erasure Channel

The binary erasure channel (BEC) is a simple channel model commonly used in coding and information theory. Its output, Y, can assume three different values, a zero, a one or an erasure $Y \in \{0, 1, ?\}$, see Figure 2.4. The erasure represents that a complete loss of the transmitted information bit has occurred. Each transmitted bit, X, is erased with probability ϵ. As an example of a simple input and its corresponding output, we have: $X = \{0, 1, 1, 1, 0, 1, 0, 0\}$; $Y = \{0, 1, ?, ?, 0, 1, ?, 0\}$. It is easy to get an upper bound on the capacity of this channel.

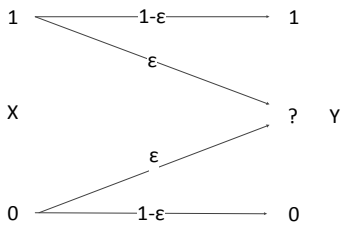

Figure 2.4: Erasure channel model, with erasure probability ϵ.

Consider that the transmitter knows in advance which positions are going to be erased at the receiver. If he knows that, he can just send his data in the remaining $(1-\epsilon)N$ positions of the message. By doing that the receiver gets all the information without any erasure, but obviously at a rate of $1-\epsilon$. Since, in the real world the transmitter does not know, with prior advance, the erasure positions the capacity of the erasure channel is upper bounded by $1-\epsilon$. Indeed it can be shown that the upper bound, $1-\epsilon$, can be attained. Indeed, it is not difficult to see that. Let us consider a random linear code [2] with a generator matrix $\mathbf{G} \in \{0,1\}^{N \times N(1-\epsilon)}$, for large N. The associated input/output relationship can be described by $\mathbf{y} = \mathbf{G}\mathbf{x}$, see Figure 2.5. At the output, $\mathbf{y}$, the erasures imply a reduction in the dimensionality of the previous system of equations. Namely, erasing the element n from vector $\mathbf{y}$ is the same as removing the row n

[2] For more details on linear codes see section 2.4

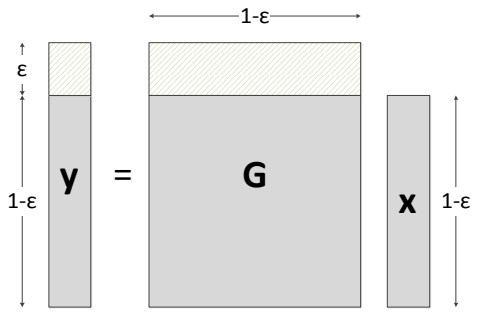

Figure 2.5: Input/Output relationship of the erasure channel using a linear code. The erasures are represented in light gray.

from matrix **G**. Consequently, the $N\epsilon$ erasures, at the output, imply that the decoder must solve a system of equations where the reduced matrix is with high probability full rank, if X has dimensionality $N(1-\epsilon)$. Thus reliable transmission is possible over the binary erasure channel, for rates lower than $1-\epsilon$.

2.3.2 AWGN Channel

The AWGN channel is one of the simplest time-discrete continuous input, output channels and can be used to model from radio to satellite links. This channel can be described mathematically by

$$y_i = x_i + n_i \tag{2.9}$$

where x_i, y_i and n_i are the channel input, output and noise, at time i. The noise n_i is independent and identically Gaussian distributed (i.i.d.) with variance σ^2. Let us consider that the transmit signal has an average power constraint P ($\mathbb{E}[x] \leq P$). Such a constraint is necessary, since if not imposed the capacity of the channel would be infinite. Although there is noise in the channel (i.e. n_i with variance greater than zero), with unlimited power, it would be always possible to generate a codebook, with far enough codewords, that can be decoded, at the destination, with as small as desired probability of error.

By incorporating the power constraint in the capacity definition given in (2.8) one can obtain the capacity expression for the AWGN channel

$$\begin{aligned}
C &= \max_{p(x):\mathbb{E}[X^2]\leq P} I(X,Y) \\
&= \max_{p(x):\mathbb{E}[X^2]\leq P} (H(Y) - H(Y|X)) \\
&= \max_{p(x):\mathbb{E}[X^2]\leq P} (H(Y) - H(N)) \\
&= \max_{p(x):\mathbb{E}[X^2]\leq P} \left(H(Y) - \frac{1}{2} log_2(2\pi e\sigma^2) \right) \\
&= \frac{1}{2} log_2(2\pi e(P+\sigma^2)) - \frac{1}{2} log_2(2\pi e\sigma^2) \\
&= \frac{1}{2} log_2 \left(1 + \frac{P}{\sigma^2} \right)
\end{aligned} \tag{2.10}$$

For a given variance, the normal distribution maximizes the entropy. Since $y = x+n$, and x and n are independent, the power of y is $P + \sigma^2$. Therefore the input distribution that maximizes the channel mutual information is the normal distribution, which implies that Y is also normal distributed, with variance $P + \sigma^2$, and has an entropy equal to $1/2\ log_2(2\pi e(P + \sigma^2))$.

2.3.3 SISO Channel

Like the AWGN channel, the SISO channel is a point to point channel. It is also a time-discrete continuous input, output channel. Its model is quite similar to the AWGN channel. The main difference is the introduction of a gain (h_i) in between the transmitter and receiver

$$y_i = h_i x_i + n_i \tag{2.11}$$

For a fixed channel gain, the corresponding channel capacity can be easily obtained from the Gaussian one, as

$$C_i = \frac{1}{2} log_2 \left(1 + \frac{h_i^2 P}{\sigma^2}\right) \tag{2.12}$$

Assuming ergodic channels, so that their randomness can be averaged out over time, the channel capacity becomes a random variable, for which taking the expectation over time, with respect to h, generates the ergodic capacity. For that case, the capacity can be defined by

$$C = \mathbb{E}_h\{C_i\} = \mathbb{E}_h \left\{ \max_{p(x):\mathbb{E}[X^2]\leq P} I(X,Y) \right\} \tag{2.13}$$

For H Rayleigh distributed the ergodic capacity of the channel is given by [18]

$$C = e^{-\frac{\sigma^2}{P}} E_i \left(-\frac{\sigma^2}{P}\right) \tag{2.14}$$

where $E_i(x)$ is the exponential integral function, given by $\int_{-\infty}^{x} e^t/t\ dt$.

2.3.4 MIMO Channel

A MIMO channel with n_T transmit and n_R receive antennas can be modeled as a set of $n_T \times n_R$ SISO links, where each group of n_R received signals are summed up at the destination, see Figure 2.6

$$\mathbf{y} = \mathbf{H}\mathbf{x} + \mathbf{n} \tag{2.15}$$

where $\mathbf{x}$ is the $(n_T \times 1)$ transmit vector, $\mathbf{y}$ is the $(n_R \times 1)$ receive vector, $\mathbf{H}$ is the $(n_R \times n_T)$ channel matrix and $\mathbf{n}$ is a vector with n_R elements each Gaussian distributed, with zero mean and variance σ^2. If full channel state information (CSI) is available at the transmitter and receiver, the MIMO channel can be converted into a series of parallel channels. This can be accomplished by decomposing the $\mathbf{H}$ matrix, using singular value decomposition (SVD), into $\mathbf{H} = \mathbf{U}\mathbf{D}\mathbf{V}^H$. To diagonalize the channel the transmitter should apply the transmit precoding matrix $\mathbf{U}^H$ to the data to be transmitted and at the receiver, the received signals must be equalized with the linear transformation $\mathbf{U}\mathbf{y}$. The resulting equivalent channel is $\mathbf{D}$, a diagonal channel, with $rank(\mathbf{H}) \leq min(n_T, n_R)$ entries different from zero. If the matrix $\mathbf{H}$ is full rank, the number of parallel channels obtained by the SVD method is equal to min(n_T,n_R).

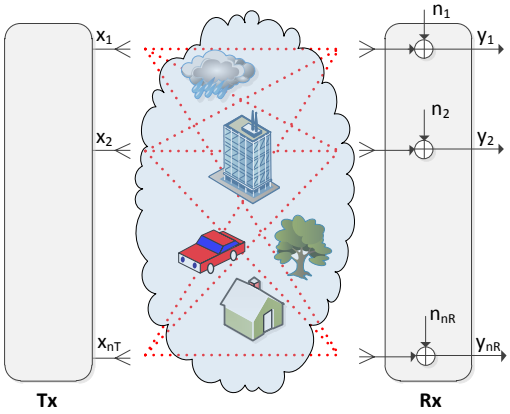

Figure 2.6: MIMO channel model.

Considering perfect CSIR, the capacity expression for a MIMO channel is given by [2, 19]

$$\begin{aligned} C &= \max_{p(x):Tr(\mathbf{R_x})\leq P} I(X,Y) \\ &= \max_{p(x):Tr(\mathbf{R_x})\leq P} (H(Y) - H(Y|X)) \\ &= \max_{p(x):Tr(\mathbf{R_x})\leq P} (H(Y) - H(N)) \\ &= \max_{p(x):Tr(\mathbf{R_x})\leq P} \left(H(Y) - log_2|\pi e\sigma^2\mathbf{I}|\right) \\ &= \max_{\mathbf{R_x}:Tr(\mathbf{R_x})\leq P} log_2\left(\pi e|\sigma^2\mathbf{I} + \mathbf{H}\mathbf{R_x}\mathbf{H}^H|\right) - log_2|\pi e\sigma^2\mathbf{I}| \\ &= \max_{\mathbf{R_x}:Tr(\mathbf{R_x})\leq P} log_2\left|\mathbf{I} + \frac{\mathbf{H}\mathbf{R_x}\mathbf{H}^H}{\sigma^2}\right| \end{aligned} \tag{2.16}$$

where $R_X = \mathbb{E}[\mathbf{x}\mathbf{x}^H]$ is the covariance matrix of the MIMO channel input. The covariance of the output is given by $\mathbf{R_y} = \sigma^2\mathbf{I} + \mathbf{H}\mathbf{R_x}\mathbf{H}^H$. For a given covariance, the entropy is maximized when the associated distribution is zero mean circularly symmetric complex Gaussian (ZMCSCG) [2]. Therefore, $\mathbf{x}$ must be also ZMCSCG.

If the channel is perfectly known at transmitter, it is optimal to use the so-called water-filling principle. On the other hand, if the channel is unknown to the transmitter, the optimum power allocation matrix is uniform, $\mathbf{R_x} = P/n_T\mathbf{I}_{n_T}$ and the respective capacity can be expressed as

$$C = log_2\left|\mathbf{I} + \frac{P}{n_T\sigma^2}\mathbf{H}\mathbf{H}^H\right| \tag{2.17}$$

which grows linearly with $min(n_T, n_R)$ [2]. Even if the channel realization is not available at the transmitter the capacity still grows linearly with the number of transmit and receive antennas. However, more processing is needed at the receiver side to separate the received symbols [19]. Maximum likelihood decoding or, for example, the simpler and more efficient Bell Laboratories Layered Space-Time (BLAST) technique [20, 21] can be used to achieve this.

2.3.5 Wireless Multipath Channel

The propagation of a signal, in a wireless channel, can be completely described by the Maxwell equations [19], by taking into account the properties of the medium, i.e. dielectric constants, location and size of objects, etc. However, such a model is too complex to be implemented and to be taken into account, for simulations, and system design. Hence, the modelling of the wireless channel, is commonly divided into three distinct phenomena: the path loss, shadowing and multipath, which can be treated independently. The first two phenomena can be included into the slow fading category and the last into the fast fading category. This subdivision reflects the different scales of signal variation. Indeed, the slow fading category includes the phenomena that vary slowly with distance. The path loss is slower than shadowing. In Figure 2.7 we present a simple example illustrating this three phenomena.

The first effect, the path loss, models the fact that an electromagnetic wave propagating through the space has its energy density decreased. Path loss takes into account, for example, the propagation loss caused by the expansion of the radio wave front, in free space, which takes the form of a sphere, with increasing radius. For this case the power falls off quadratically with the distance. One of the simplest path loss models [19] and the most commonly used considers an exponential decay of the power with the distance, i.e. can be mathematically described as $P_t = P_r K (d_0/d)^{\gamma}$, where K is a unitless constant that depends on the average channel attenuation and antenna characteristics, d_0 is a reference distance, γ the path loss exponent, P_t the transmit power and P_r the received power. Contrary to the free space case, for non line of sight scenarios the decaying factor (γ) is higher, typically between 3 and 5.

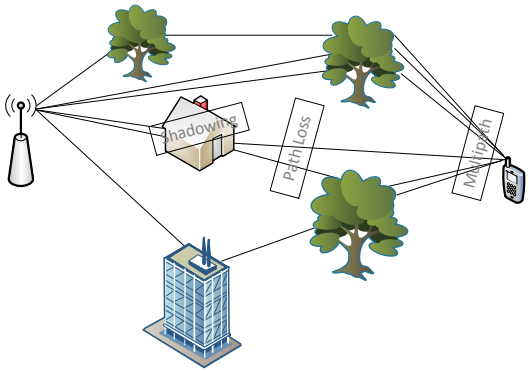

Figure 2.7: Example propagation Scenario.

Shadowing is caused by the obstruction of the electromagnetic wave path by buildings, hills and other big objects, resulting in fluctuations of the average signal power. This type of fading is normally modelled by a log-normal distribution [19].

The multipath, as the name refers to, corresponds to the existence of multiple reflective paths, between the transmitter and receiver. This is a consequence of the existence of multiple objects along the wave propagation path, that reflect the incident wave. At the receiver these multiple paths, scaled copies of the transmitted signal, are received at different time instants and with unequal phases. The different times of arrival lead to a time-spreading of the transmitted signal. A small variation in the position of these objects or even of the

transmitter or receiver results in a phase change of the received multipath signals, which can add destructively. If the transmitter/receiver pair and all scatterers are stationary, the channel appears to be time invariant. On the other hand, if the receiver/transmitter or the scatterers are moving then the channel change. This leads to a time varying channel and to the appearance of the Doppler spectrum. Indeed, for a receiver moving at a velocity v the corresponding Doppler frequency is given by [22]

$$f_D = \frac{v}{\lambda_c} cos(\theta) \tag{2.18}$$

where λ_c is the carrier wavelength and θ the angle between received path and the receiver moving direction. From equation (2.18) we see that the maximum Doppler shift is $f_{D_{max}} = v/\lambda_c$.

To model these phenomena a time variant system is usually considered, where the channel impulse response is modelled by the superposition of L_p paths with different amplitudes and delays [22, 23]

$$h(\tau, t) = \sum_{p=1}^{L_p} \alpha_p(t)\delta(\tau - \tau_p) \tag{2.19}$$

In the previous equation, τ_p represents the delay of path p, $\alpha_p(t)$ the path p complex amplitude gain, t the time, τ the delay and L_p the number of paths considered.

Equation 2.19 already considers that the L_p paths are resolvable. In practice each of the L_p paths corresponds to the merging of L_{sp} sub-paths, each with a delay τ_p^l, similar to τ_p. These sub-paths are normally formed at a cluster of objects. By similar delay we mean, a delay difference $\tau_p^l - \tau_p^m, \forall\, l, p \in \{1, \ldots, L_{sp}\}$ much lower than the system sampling time. Such paths are non-resolvable [19], i.e. they cannot be separated, at the receiver, since the system is unable to distinguish between them. Therefore, at the receiver, they are considered as one, i.e. $\alpha_p(t) = \sum_{l=1}^{L_{sp}} \alpha_p^l(t)$ and $\tau_p^l \approx \tau_p \; \forall\, l \in \{1, \ldots, L_{sp}\}$, where $\alpha_p^l(t)$ is the complex amplitude gain of sub-path l. For a practical cellular system, especially in urban environments, the number of non-resolvable paths (L_{sp}), with delay close to τ_p, is high [19]. Hence, if each sub-path gain is considered to be a random variable, then, by the central limit theorem, the resulting total gain ($\alpha_p(t)$) is complex Gaussian distributed. This leads to a Rayleigh distributed path amplitude, with uniform phase [19]. It is also commonly assumed that there is no correlation between the gain $\alpha_p(t)$ of different replicas, since they arrive from different paths, i.e. they are formed at different scatterer objects. We say that such a channel has uncorrelated scattering (US).

As a linear system the channel can be represented also by the following equivalent functions

$$\begin{aligned} H(f, t) &= \mathcal{F}_\tau(h(\tau, t)) \\ H(\tau, f_D) &= \mathcal{F}_t(h(\tau, t)) \\ H(f, f_D) &= \mathcal{F}_\tau(H(\tau, f_D)) \end{aligned} \tag{2.20}$$

where $\mathcal{F}_t(.)$ denotes the Fourier transform, relative to parameter t, f_D represents the Doppler frequency shift, f the frequency domain equivalent of the delay, $H(f, t)$ is the system transfer function and $H(\tau, f_D)$ the deterministic scattering function [19], that captures the Doppler characteristics of the channel, via f_D.

Autocorrelation of the channel fading process

To characterize the channel the autocorrelation function, of the channel impulse response, can be used [19, 24]

$$R_h(\tau_1, \tau_2; t, \Delta t) = \mathbb{E}[h^*(\tau_1, t)h(\tau_2, t + \Delta t)] \tag{2.21}$$

In practice, most channels are wide sense stationary (WSS), i.e. the statistics of a channel at time t and $t + \Delta t$ depend only on the time difference Δt.

$$R_h(\tau_1, \tau_2; \Delta t) = \mathbb{E}[h^*(\tau_1, t)h(\tau_2, t + \Delta t)] \tag{2.22}$$

As stated earlier, we can also consider that there is no correlation between two replicas, with delay τ_1 and τ_2, hence

$$R_h(\tau_1, \tau_2; t_1, \Delta t) = R_h(\tau, \Delta t) = \mathbb{E}[h^*(\tau, t)h(\tau, t + \Delta t)] \tag{2.23}$$

where the function, $R_h(\tau, \Delta t)$, gives the average output power of the channel for a delay τ and a difference Δt in the observation time. The Fourier transform of $R_h(\tau, \Delta t)$, with respect to Δt is denominated by scattering function

$$S_h(\tau, f_D) = \int_{-\infty}^{+\infty} R_h(\tau, \Delta t)e^{-j2\pi f_D \Delta t} d\Delta t \tag{2.24}$$

which gives the average channel output power for a Doppler f_D and a delay τ. With the previous two functions the most important channel characteristics can be obtained, namely the power delay profile, the coherence bandwidth, the Doppler power spectrum and the coherence time. The power delay profile is identical to $R_h(\tau, 0)$. It represents the average channel output power for a delay τ. From the power delay profile two important characteristics of the channel can be derived, the average delay ($\bar{\tau}$) and root mean square (rms) delay spread (σ_τ) [19, 25]

$$\begin{aligned} \bar{\tau} &= \frac{\int_0^{+\infty} \tau R_h(\tau) d\tau}{\int_0^{+\infty} R_h(\tau) d\tau} \\ \sigma_\tau &= \sqrt{\frac{\int_0^{+\infty} (\tau - \bar{\tau})^2 R_h(\tau) d\tau}{\int_0^{+\infty} R_h(\tau) d\tau}} \end{aligned} \tag{2.25}$$

which can be also obtained as the first and second moment of a random variable T_h with pdf $p_{T_h}(\tau) = R_h(\tau) / \int_0^{+\infty} R_h(\tau) d\tau$, i.e. the normalized power delay profile. Indeed, we can think of $p_{T_h}(\tau)$, in the calculation of the average delay and rms delay spread, as a weighting factor that assigns more weight to high power delays. The delay spread gives a measure of the spread a signal incurs when it passes through the considered multipath channel. It is an important measure to assess the performance loss introduced due to inter-symbol interference (ISI). Due to the WSS and US characteristics of process $h(t, \tau)$, the autocorrelation of the random process $H(f, t)$, is given by [19]

$$R_H(f_1, f_2; \Delta t) = \mathbb{E}[H^*(f_1, t)H(f_2, t + \Delta t)] = R_H(\Delta f, \Delta t) \tag{2.26}$$

Defining $R_H(\Delta f) = R_H(\Delta f, 0)$ we get [19]

$$R_H(\Delta f) = \int_0^{+\infty} R_h(\tau)e^{-j2\pi \Delta f \tau} d\tau \tag{2.27}$$

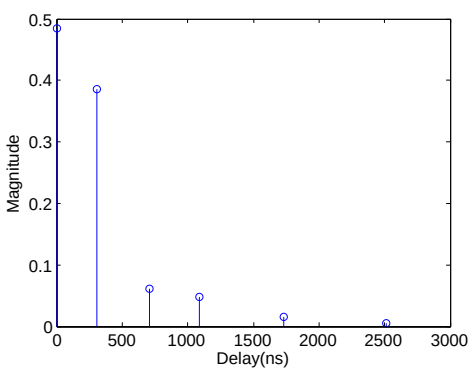

(a) Power delay profile, $R_h(\tau)$.

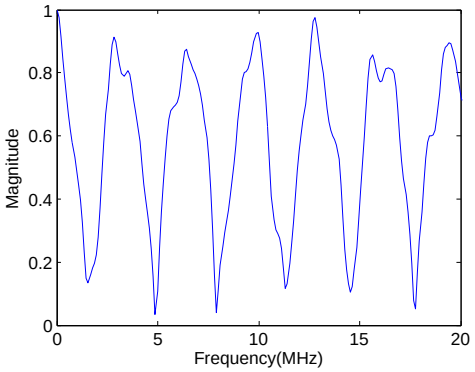

(b) Frequency correlation function, $R_H(\Delta f)$.

Figure 2.8: ITU Veh. A channel profile and its corresponding frequency correlation function.

Namely, $R_H(\Delta f)$ is the Fourier transform of the power delay profile. Figure 2.8 presents, as an example, the power delay profile and frequency correlation function of the ITU vehicular A channel. If $R_H(B_c) \approx 0$ then the channel response at frequencies f and $f + \Delta$, where $\Delta \geq B_c$, are approximately independent. B_c is the channel coherence bandwidth. One can think of it as a measure of the bandwidth where the multipath channel has approximately equal gain and linear phase. Due to the connection between the power delay profile function and $R_H(\Delta f)$ one can obtain an approximation for B_c. Namely, B_c is proportional to the inverse of the rms delay spread, where the constant of proportionality varies for different channel correlation values. If the channel has a coherence bandwidth higher than the one of the signal to be transmitted, through it, then all parts of the signal will be similarly affected. This type of channels are non frequency selective. On the contrary, if the coherence bandwidth is lower than the signal bandwidth, the channel is frequency selective, since multiple coherence zones exist. Each of these zones can be considered as frequency non selective and roughly independent between them.

The variation of the channel with time can be described by taking the Fourier transform of $R_H(\Delta f, \Delta t)$ relative to Δt [19]

$$S_H(\Delta f; f_D) = \int_{-\infty}^{+\infty} R_H(\Delta f, \Delta t) e^{-j2\pi f_D \Delta t} d\Delta t \tag{2.28}$$

The Doppler power spectrum of the channel is defined by $S_H(f_D) = S_H(0; f_D)$. Using the same type of analysis, as for the average delay and rms delay spread, one can obtain the average Doppler shift and rms Doppler spread. $R_H(0; \Delta t)$ measures the correlation between a complex exponential sent at time t_1 and a similar complex exponential sent at time t_2, where $\Delta t = t_2 - t_1$. As for the coherence bandwidth, for this case, we can define coherence time as the time span where the channel characteristics are approximately the same. If the coherence time is lower than the transmit symbol duration, then the channel is denominated time selective.

2.4 Linear Block Codes

As stated earlier in this chapter, coding allows to transmit information reliably over a noisy channel. The space of codes available for study is big, but here we will focus on the family of linear block codes. More specifically, in this section, the LDPC and LDGM codes will be described in more detail.

An error correction code can be fully described by a mapping from one high dimensional vector space to another high dimensional vector space. In the following, we consider as scalars of the aforementioned vector spaces the elements of the binary field, $\{0,1\}$. As such a code C can be mathematically defined as

$$C = \{\mathbf{y} \in \{0,1\}^N | \mathbf{y} = \boldsymbol{\mathcal{E}}(\mathbf{x}), \forall\, \mathbf{x} \in \{0,1\}^K\} \tag{2.29}$$

where K and N are the length of the input and output codewords, respectively, $\boldsymbol{\mathcal{E}}(.)$ is the mapping function and $\mathbf{x}$, $\mathbf{y}$ are the input and output sequences, correspondingly. One can see from the code definition that the encoding process implies a space expansion factor of $R = K/N$ and this is defined as the rate of the code. If the mapping function is linear, $\boldsymbol{\mathcal{E}}(\mathbf{x}) = \mathbf{G}\mathbf{x}$, as will be in the following, we have a linear code

$$C_{Linear} = \{\mathbf{y} \in \{0,1\}^N | \mathbf{y} = \mathbf{G}\mathbf{x}, \forall\, \mathbf{x} \in \{0,1\}^K\} \tag{2.30}$$

where $\mathbf{G} \in \{0,1\}^{N \times K}$ is what we call the code generator matrix. A linear code has many special features:

- the zero codeword belongs always to the code. ($\mathbf{0} = \mathbf{G0}$)
- the sum of two codewords is still a codeword. ($\mathbf{c}_1 + \mathbf{c}_2 = \mathbf{G}\mathbf{x}_1 + \mathbf{G}\mathbf{x}_2 = \mathbf{G}(\mathbf{x}_1 + \mathbf{x}_2)$)
- the set of codewords is in the subspace spanned by the columns of $\mathbf{G}$, i.e. it is in the set of linear combinations of the columns of the matrix $\mathbf{G}$, ($\mathbf{G}_i$). $\left(\mathbf{c} = \mathbf{G}\mathbf{x} = \sum_{i=1}^{K} \mathbf{G}_i \mathbf{x}_i\right)$

An important metric used to measure the performance of an error correcting code, introduced by Hamming [26], is the Hamming distance. The Hamming distance between two sequences of the same length is equal to the number of positions in which they differ. For error correction codes an important measure derived from this is the minimum Hamming distance that is defined as the minimal distance between any two codewords. For a general code, the computation of the minimum distance is a difficult problem. However, for linear codes, the computation task is simplified, since $\mathbf{c}_1 - \mathbf{c}_2$ is also a codeword, and thus we only need to compute the Hamming distance between $\mathbf{c}_1$ and the $\mathbf{0}$ codeword.

Linear codes can be both specified by the corresponding generator matrix, $\mathbf{G} \in \{0,1\}^{N \times K}$, and by the associated parity check matrix $\mathbf{H} \in \{0,1\}^{(N-K) \times N}$. The parity check matrix as the name suggests may be used to check if the $M = N - K$ parity bits, generated by encoding, were decoded correctly, for example. Namely, the columns of $\mathbf{H}$ generate the orthogonal complement of C

$$\mathbf{H}\mathbf{c} = \mathbf{0} \tag{2.31}$$

The parity check matrix can also be used for encoding, like the generator matrix, and sometimes with complexity advantages over its counterpart [27, 28]. To encode a block $\mathbf{x}$ of K bits of data with $\mathbf{H} = [\mathbf{H}_s\ \mathbf{H}_p]$ ($\mathbf{H}_s \in \{0,1\}^{M \times K}$, $\mathbf{H}_p \in \{0,1\}^{M \times M}$) we first compute $\mathbf{v} = \mathbf{H}_s\mathbf{s}$ and then compute the parity bits by solving $\mathbf{H_p p} = \mathbf{v}$, which can be done by inverting $\mathbf{H_p}$.

Consequently, the sub-matrix $\mathbf{H_p}$ must be properly selected so that the resulting matrix is full rank. The previous, scheme is equivalent to obtaining the solution of the following system of linear equations

$$[\mathbf{H}_{s_{(M\times K)}}\ \mathbf{H}_{p_{(M\times M)}}]\begin{bmatrix}\mathbf{s}_{(K\times 1)}\\ \mathbf{p}_{(M\times 1)}\end{bmatrix}=\mathbf{0} \tag{2.32}$$

where $M=N-K$, $\mathbf{H}=[\mathbf{H}_s\ \mathbf{H}_p]$ and $\mathbf{s}$ is the data to be encoded.

2.5 Low Density Parity Check Codes

Low density parity check codes were firstly proposed by Gallager [14], in the sixties, but were almost forgotten, during thirty years, since they were still too complex for the processing power available at that time. Some exceptions to this rule where the works of Zyablov and Pinsker [29], Margulis [30] and Tanner [31]. Nevertheless, Gallager introduced in his thesis the underlying principles of the most successful codes today. Namely, the iterative decoding algorithms, the graphical representation of a code, the basis for stochastic analysis of iterative algorithms, just to name a few. In the nineties, the introduction of turbo codes [7] renewed the interest of LDPC codes [13]. Namely, new analytical tools have been developed to analyze the behavior of the message passing decoders over the BEC and the BSC [32] [33], which were later extended for more general channels [15]. These techniques combined with the continuation of the LDPC code definition to irregular codes have enabled to achieve rates close to capacity for many channels [34].

An LDPC code is a linear error correcting code. Namely it belongs to the subclass of linear codes with low density parity check matrices.

$$C_{LDPC}=\{\mathbf{y}\in\{0,1\}^N:\mathbf{Hy}=\mathbf{0}\mid\mathbf{H}\ sparse\} \tag{2.33}$$

A low-density matrix is one with a high percentage of zeros, in other words, it is a sparse matrix.

The first LDPC codes, proposed by Gallager [14], were regular. One important concept introduced by Gallager, in the analysis and design of codes, was the notion of an ensemble of codes. The parity check matrix of a regular code is designed to have a small fixed number n of ones in each row and a small fixed number k of ones in each column. As an example, we present in Figure 2.9 a sample of a low-density parity check matrix of a regular (3,6) LDPC code[3], with length 10000. Regular codes due to their simpler structure make them better suited for practical hardware implementation than their irregular counterparts [35], even if they have worse BER performance. Irregular LDPC codes were introduced by Luby et al. [32] as an extension to regular LDPC codes, as a way to achieve better performance.

An irregular LDPC code is described by two probability distributions $\mathbf{L}=\{L_1,\ldots,L_i,\ldots,L_{n_{max}}\}$, $\mathbf{R}=\{R_1,\ldots,R_i,\ldots,R_{k_{max}}\}$, where L_i and R_i correspond to the probability of a column or row of the parity check matrix having i 1's, respectively. Using this notation, a regular (3, 6) code can be described by $\mathbf{L}=\{0,0,0,0,0,1\}$, $\mathbf{R}=\{0,0,1\}$. A more compact notation can be used, by the introduction of the polynomials

$$L(x)=\sum_{i=1}^{n_{max}}L_ix^i \qquad\qquad R(x)=\sum_{i=1}^{k_{max}}R_ix^i \tag{2.34}$$

[3] A regular (3, 6) LDPC code has 3 ones per column ($k=3$) and 6 ones per row ($n=6$).

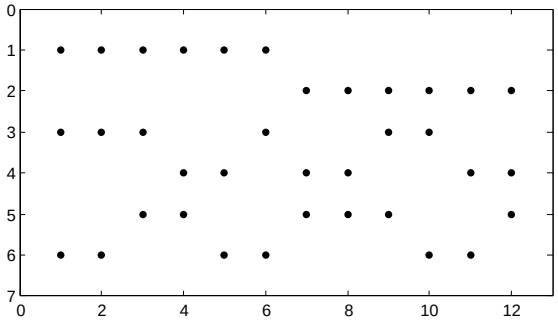

Figure 2.9: Regular LDPC (3, 6) parity check matrix sample of size 6×12.

---

through which one can get the code rate

$$R = 1 - \frac{K}{N} = 1 - \frac{K}{N}\frac{\sum_i i\Lambda_i}{\sum iP_i} = 1 - \frac{\sum_i i\Lambda_i/N}{\sum iP_i/K} = 1 - \frac{\sum_i iL_i}{\sum iR_i} \tag{2.35}$$

where Λ_i denotes the number of columns with i 1's ($\sum_i \Lambda_i = N$) and P_i is the number of rows with i 1's ($\sum_i P_i = K$). Consequently, $\sum_i i\Lambda_i = \sum iP_i$ corresponds to the total number of 1's in the parity check matrix. With the previously introduced notation the (3, 6) code can be represented by $L(x) = x^6$, $R(x) = x^3$. On the other hand, a LDGM has a low-density generator matrix and can be considered a dual of LDPC [36].

$$C_{LDGM} = \{\mathbf{y} \in \{0,1\}^N | \mathbf{y} = \mathbf{G}\mathbf{x}, \forall\, \mathbf{x} \in \{0,1\}^K \textit{ and } \mathbf{G} \textit{ sparse}\} \tag{2.36}$$

However, LDGM codes are asymptotically bad, i.e. they exhibit an error floor that is independent of the considered block size. The poor distance properties of a LDGM code can be easily controlled with proper concatenation of two codes, while maintaining the low complexity advantages [37].

2.5.1 Sum-Product/Belief Propagation Algorithm

Let us assume a channel, with transitional probability $p(Y|X)$ and a transmitter whose objective is to transmit one message from a set of M messages to a destination. For that he uses a codebook, C, to encode the corresponding message. There is a one to one correspondence between the messages and the codewords. After encoding, the generated codeword $\mathbf{x}$, is transmitted through the channel. The associated probability of each codeword/message is denoted by $p(X)$. At the destination, the channel observation Y, corrupted by the channel, is decoded to recover the transmitted codeword. Assuming that the output codeword is $\mathbf{x}$ the corresponding probability of error is given by $1 - p(\mathbf{x}|\mathbf{y})$. Therefore, to minimize the probability of error the decoder should choose $\mathbf{x}$ in such a way to maximize $p(\mathbf{x}|\mathbf{y})$. This is the so-called Maximum A Posteriori (MAP) decoding rule

$$\begin{aligned} \mathbf{x}_{MAP} &= \underset{\mathbf{x}\in C}{\operatorname{argmax}}\, p(\mathbf{x}|\mathbf{y}) \\ &= \underset{\mathbf{x}\in C}{\operatorname{argmax}}\, p(\mathbf{y}|\mathbf{x})\frac{p(\mathbf{x})}{p(\mathbf{y})} \\ &= \underset{\mathbf{x}\in C}{\operatorname{argmax}}\, p(\mathbf{y}|\mathbf{x})p(\mathbf{x}) \end{aligned} \tag{2.37}$$

where the second equality follows from the Bayes's theorem [38] and the last because $p(\mathbf{y})$ is constant (after knowing the channel output $\mathbf{y}$). If the prior information $p(\mathbf{x})$ is uniform, i.e. all codewords are equally likely, the MAP rule is transformed into the Maximum Likelihood (ML) decoding rule

$$\mathbf{x}_{MAP} = \underset{\mathbf{x}\in C}{\operatorname{argmax}}\, p(\mathbf{y}|\mathbf{x})p(\mathbf{x}) = \underset{\mathbf{x}\in C}{\operatorname{argmax}}\, p(\mathbf{y}|\mathbf{x}) = \mathbf{x}_{ML} \tag{2.38}$$

To solve the MAP problem, 2.37, let us assume that the channel is memoryless. That is to say $p(\mathbf{y}|\mathbf{x}) = \prod_n p(y_n|x_n)$. For a LDPC code the prior distribution over codewords can be described [17] by $\mathbb{1}[\mathbf{Hx} = \mathbf{0}]$, where $\mathbb{1}[.]$ is an indicator function that is equal to one when the condition inside brackets is respected and zero when it is not. Thus, the MAP rule is equivalent to

$$\begin{aligned}
\mathbf{x}_{MAP} &= \operatorname{argmax} p(\mathbf{y}|\mathbf{x})\mathbb{1}[\mathbf{Hx} = \mathbf{0}] \\
&= \operatorname{argmax} \prod_n p(y_n|x_n) \prod_k \mathbb{1}[\mathbf{H}_k\mathbf{x} = 0] \\
&= \operatorname{argmax} \prod_n p(y_n|x_n) \prod_k \mathbb{1}\left[\sum_{v\in\mathcal{N}(k)} x_v = 0\right]
\end{aligned} \tag{2.39}$$

where $\mathcal{N}(k)$ denotes the set of variables involved into the parity check k.

Each of the k indicator functions can be represented graphically, using a bipartite graph. A bipartite graph is a graph composed of two disjoint vertex sets, V and C, with edges connecting them. Let us consider a function $f(x_1, \ldots, x_N)$. This function is dependent on $\{x_1, \ldots, x_N\}$, the set of independent variables. To represent $f(x_1, \ldots, x_N)$ graphically, we represent each variable from the set of independent variables with a circle and the operator $f(.)$ by a square. The dependence of $f(.)$ on the set of independent variables is represented by an edge connecting each of the circles (variables) and the square (operator). With that idea in mind we can represent graphically the indicator function, associated with a parity check, with $\mathcal{N}(k) = \{1, 3, 5, 6\}$, as shown in Figure 2.10(a).

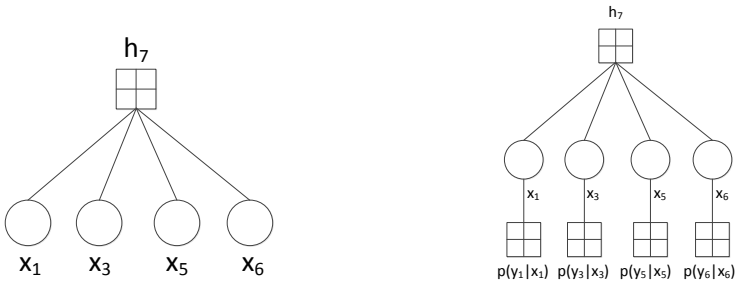

(a) Parity check.

(b) Parity check with channel priors.

Figure 2.10: Graphical representation of a parity check, example.

Following the above graphical representation, for the overall code, a LDPC code of length N and rate R can be represented by a bipartite graph with N variable nodes, circles, and $(1-R)N$ parity check nodes, squares, see Figure 2.11. The overall probability distribution can also be represented graphically by a factor graph, using the same idea. A factor graph is a bipartite

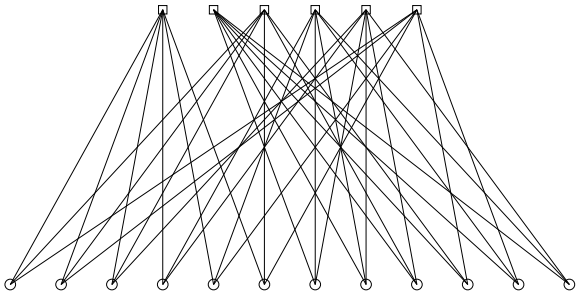

Figure 2.11: Graphical representation of the global parity check matrix of a regular (3, 6) random generated code with length 12.

---

graph representing the factorization of a function. For the MAP problem to be described by a factor graph the channel priors, $p(y_n|x_n)$, should be also included in the representation previously presented. That can be accomplished by drawing more squares in the graph, one for each prior. Each additional square represents the function $p(y_n|x_n)$ and connects to variable node x_n, since function $p(.)$ is dependent on variable x_n. As an example we present in figure 2.10(b) the graphical representation of a parity check with $\mathcal{N}(k) = \{1, 3, 5, 6\}$, as previously, but now with the associated channel priors incorporated into the graphical representation.

If instead of minimizing the block error rate, we want to minimize the bit error rate, the rule to be used for decoding is the bit-wise MAP

$$\begin{aligned} x_i^{MAP} &= \underset{\substack{x_i \in \{0,1\} \\ \mathbf{x} \in C}}{\operatorname{argmax}} p(x_i|\mathbf{y}) \\ x_i^{MAP} &= \underset{\substack{x_i \in \{0,1\} \\ \mathbf{x} \in C}}{\operatorname{argmax}} \sum_{\sim x_i} p(\mathbf{x}|\mathbf{y}) \\ x_i^{MAP} &= \underset{\substack{x_i \in \{0,1\} \\ \mathbf{x} \in C}}{\operatorname{argmax}} \sum_{\sim x_i} p(\mathbf{y}|\mathbf{x}) p(\mathbf{x}) \end{aligned} \tag{2.40}$$

In the second equality, the law of total probability has been used [39]. By $\sum_{\sim x_i}$ we denote a summation over all variables except x_i, i.e. a marginalization over x_i. The main difference between 2.37 and 2.40 is that in the bit-wise MAP decoding rule the maximization is replaced by an addition.

Example

As an example let us consider that $i = 1$ and that $p(\mathbf{x}|\mathbf{y}) = F(x_1, x_2, x_3, x_4, x_5) = f_A(x_1) f_B(x_2) f_C(x_1, x_2, x_3) f_D(x_3, x_4) f_E(x_3, x_5)$. The corresponding bipartite graph representation of function $F(.)$ is shown in Figure 2.12. Hence, according to equation (2.40), to obtain the MAP estimate of the bit variable x_1 we need to marginalize the function $p(\mathbf{x}|\mathbf{y}) = F(.)$

$$\begin{aligned} x_1^{MAP} &= \underset{x_1 \in \{0,1\}}{\operatorname{argmax}} \sum_{\sim x_1} F(x_1, x_2, x_3, x_4, x_5) \\ x_1^{MAP} &= \underset{x_1 \in \{0,1\}}{\operatorname{argmax}} \sum_{x_2, \ldots, x_5} f_A(x_1) f_B(x_2) f_C(x_1, x_2, x_3) f_D(x_3, x_4) f_E(x_3, x_5) \end{aligned} \tag{2.41}$$

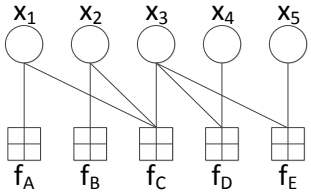

(a) 1st representation: standard form.

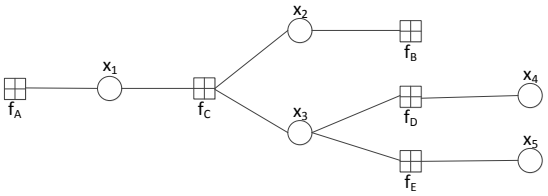

(b) 2nd representation: expanded into a tree

Figure 2.12: Bipartite graph representation of function $F(.)$

If one uses exhaustive search one would need to sum $2 \times 2^4 = 32$ terms, one for each different assignment of variables $x_2, \ldots, x_5$, both for $x_1 = 0$ and $x_1 = 1$. Nevertheless, due to the special characteristics of the function $F(.)$ this number can be decreased. Namely, we can use the distributive law, in equation (2.41), to obtain

$$\begin{aligned}
x_1^{MAP} &= \underset{x_1 \in \{0,1\}}{\text{argmax}} \sum_{x_2,\ldots,x_5} f_A(x_1) f_B(x_2) f_C(x_1, x_2, x_3) f_D(x_3, x_4) f_E(x_3, x_5) \\
x_1^{MAP} &= \underset{x_1 \in \{0,1\}}{\text{argmax}}\, f_A(x_1) \left[\sum_{x_2,x_3} f_C(x_1, x_2, x_3) f_B(x_2) \left(\sum_{x_4} f_D(x_3, x_4) \right) \left(\sum_{x_5} f_E(x_3, x_5) \right) \right] \\
x_1^{MAP} &= \underset{x_1 \in \{0,1\}}{\text{argmax}}\, f_A(x_1) \left[\sum_{x_2,x_3} f_C(x_1, x_2, x_3) f_B(x_2) f_{II}(x_3) f_I(x_3) \right] \\
x_1^{MAP} &= \underset{x_1 \in \{0,1\}}{\text{argmax}}\, f_A(x_1) \left[\sum_{x_2,x_3} f_C(x_1, x_2, x_3) f_B(x_2) f_{III}(x_3) \right] \\
x_1^{MAP} &= \underset{x_1 \in \{0,1\}}{\text{argmax}}\, f_A(x_1) f_{IV}(x_1) = \underset{x_1 \in \{0,1\}}{\text{argmax}}\, f_V(x_1)
\end{aligned} \tag{2.42}$$

By using the distributive law we reduced the complexity from 2×2^4 sums to $2^3 + 2^2 + 2^2 = 16$ sums (2^2 sums to obtain $f_I(x_3) = \sum_{x_5} f_E(x_3, x_5)$, 2^2 sums for $f_{II}(x_3) = \sum_{x_4} f_D(x_3, x_4)$ and 2^3 sums for $f_{IV}(x_1) = \sum_{x_2,x_3} f_C(x_1, x_2, x_3) f_B(x_2) f_{III}(x_3)$). This has been made possible due to the fact that the factor graph representation of the function $F(.)$ can be expanded into a tree, as shown in Figure 2.12. If instead of the bit-wise MAP we use the MAP decoding rule, equation (2.37), we have

$$\begin{aligned}
x_1^{MAP} &= \underset{x_1 \in \{0,1\}}{\text{argmax}} \max_{\sim x_1} F(x_1, x_2, x_3, x_4, x_5) \\
x_1^{MAP} &= \underset{x_1 \in \{0,1\}}{\text{argmax}} \max_{x_2,\ldots,x_5} f_A(x_1) f_B(x_2) f_C(x_1, x_2, x_3) f_D(x_3, x_4) f_E(x_3, x_5)
\end{aligned} \tag{2.43}$$

As the distributive law can be applied to both the *sum* and *max* operators the same techniques can be used for both problems.

General Case

Now, that an example has been provided, let us consider the more general case of the bit-wise MAP problem. Before starting to explain how to solve the aforementioned problem

let us define some notation. Namely, in the following, elementary functions, i.e. functions that cannot be further decomposed into products of other functions, are denoted by lower case letters, like $f_c(x_i, \mathbf{x}_{v(c)})$ (c is just an index). Global functions, i.e. functions that are products of elementary functions, are represented by uppercase letters, like $G_j(x_j, \mathbf{x}_{V(j)})$ and $F_c(x_i, \mathbf{x}_{V(c)})$. $G_j(x_j, \mathbf{x}_{V(j)})$ denotes a global function that can be decomposed as the product of global functions. On the other hand, $F_c(x_i, \mathbf{x}_{V(c)})$ denotes a global function that can be decomposed into the product of elementary and global functions. Two types of inputs have been considered, both for elementary and global functions, one scalar (x_j) and another vectorial ($\mathbf{x}_{v(c)}$ and $\mathbf{x}_{V(j)}$), where the last is indexed by a set $V(j)$. To differentiate the indexing sets of elementary and global functions lower and uppercase letters have been used, respectively. It should be emphasized that this sets do not take into account the index j, since x_j is already included explicitly as an input. Hence, $\{x_j, \mathbf{x}_V(j)\}$ ($\{x_i, \mathbf{x}_V(c)\}$) is the set of independent variables of function $G_j(.)$ ($F_c(.)$).

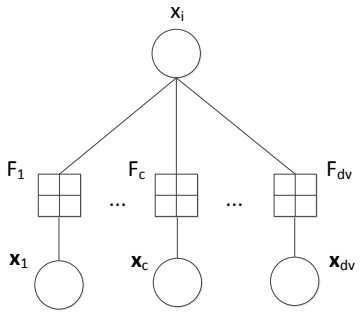

Figure 2.13: First expansion of function $F(\mathbf{x}) = p(\mathbf{y}|\mathbf{x})p(\mathbf{x})$.

Therefore, to solve the MAP decoding problem let us assume, [40] that $F(\mathbf{x}) = p(\mathbf{y}|\mathbf{x})p(\mathbf{x})$ has a specific distribution, or more precisely that it factorizes accordingly to a specific pattern. Namely, let us consider, that $F(\mathbf{x}) = \prod_{c \in C(i)} F_c(x_i, \mathbf{x}_{V(c)}) = G_i(x_i, \mathbf{x}_{V(i)})$, see Figure 2.13, where $C(i)$ denotes the indexing set of the functions that factorize $F(x)$, $V(b) \cap V(c) = \emptyset$, for $b \neq c$ and $\cup_{c=1}^{K} V(c) = \{1, \ldots, N\} \backslash i$, i.e. i, $V(c_1)$, ..., $V(c_k)$, ..., $V(c_K)$, is a partition of the set $\{1, \ldots, N\}$ [40]. The symbol $\backslash$ denote the set subtraction operator, N the length of vector $\mathbf{x}$, $c_k \in C(i)$ and K is the dimension of set $C(i)$. Therefore the bit-wise MAP problem simplifies to

$$\begin{aligned} x_i^{MAP} &= \underset{\substack{x_i \in \{0,1\} \\ \mathbf{x} \in C}}{\operatorname{argmax}} g_i(x_i) = \underset{\substack{x_i \in \{0,1\} \\ \mathbf{x} \in C}}{\operatorname{argmax}} \sum_{\sim x_i} F(\mathbf{x}) \\ &= \underset{\substack{x_i \in \{0,1\} \\ \mathbf{x} \in C}}{\operatorname{argmax}} \sum_{\sim x_i} G_i(x_i, \mathbf{x}_{V(i)}) \\ &= \underset{\substack{x_i \in \{0,1\} \\ \mathbf{x} \in C}}{\operatorname{argmax}} \sum_{\sim x_i} \prod_{c \in C(i)} F_c(x_i, \mathbf{x}_{V(c)}) \\ &= \underset{\substack{x_i \in \{0,1\} \\ \mathbf{x} \in C}}{\operatorname{argmax}} \prod_{c \in C(i)} \sum_{\mathbf{x}_{V(c)}} F_c(x_i, \mathbf{x}_{V(c)}) \end{aligned} \tag{2.44}$$

From the third to the fourth line we have used the distributive law and the fact that i, $V(c)$, ..., $V(K)$ defines a partition of the set of integers, between 1 and N. A careful look to this

line, shows that the use of the distributive law allowed a reduction of complexity from 2^{Kd_c} to 2^{d_c}, where d_c is the size of each set $V(c)$, which is considered to be equal for all c, for simplicity of calculations.

Now let us assume that $F_c(x_i, \mathbf{x}_{V(c)}) = f_c(x_i, \mathbf{x}_{v(c)}) \prod_{j \in v(c) \backslash i} G_j(x_j, \mathbf{x}_{V(j)})$, see Figure 2.14, where again $V(i) \cap V(j) = \emptyset$, for any $i \neq j$, $v(c) \cap V(j) = \emptyset$, for $j \in v(c) \backslash i$ and $V(c) = (\cup_{j \in v(c)} V(j)) \cup v(c)$, (a partition of the set $V(c)$). This in turn allow to simplify again the bit-wise MAP problem

$$
\begin{aligned}
x_i^{MAP} &= \underset{\substack{x_i \in \{0,1\} \\ \mathbf{x} \in C}}{\operatorname{argmax}} g_i(x_i) = \underset{\substack{x_i \in \{0,1\} \\ \mathbf{x} \in C}}{\operatorname{argmax}} \prod_{c \in C(i)} \sum_{\mathbf{x}_{V(c)}} F_c(x_i, \mathbf{x}_{V(c)}) \\
&= \underset{\substack{x_i \in \{0,1\} \\ \mathbf{x} \in C}}{\operatorname{argmax}} \prod_{c \in C(i)} \left(\sum_{\mathbf{x}_{V(c)}} f_c(x_i, \mathbf{x}_{v(c)}) \prod_{j \in v(c) \backslash i} G_j(x_j, \mathbf{x}_{V(j)}) \right) \\
&= \underset{\substack{x_i \in \{0,1\} \\ \mathbf{x} \in C}}{\operatorname{argmax}} \prod_{c \in C(i)} \left(\sum_{\mathbf{x}_{v(c)}} f_c(x_i, \mathbf{x}_{v(c)}) \prod_{j \in v(c) \backslash i} \left[\sum_{\mathbf{x}_{V(j)}} G_j(x_j, \mathbf{x}_{V(j)}) \right] \right) \\
&= \underset{\substack{x_i \in \{0,1\} \\ \mathbf{x} \in C}}{\operatorname{argmax}} \prod_{c \in C(i)} \left(\sum_{\mathbf{x}_{v(c)}} f_c(x_i, \mathbf{x}_{v(c)}) \prod_{j \in v(c) \backslash i} \left[\sum_{\sim x_j} G_j(x_j, \mathbf{x}_{V(j)}) \right] \right) \\
&= \underset{\substack{x_i \in \{0,1\} \\ \mathbf{x} \in C}}{\operatorname{argmax}} \prod_{c \in C(i)} \left(\sum_{\sim x_i} f_c(x_i, \mathbf{x}_{v(c)}) \prod_{j \in v(c) \backslash i} g_j(x_j) \right)
\end{aligned}
\tag{2.45}
$$

In the third line we have used the fact that $(\cup_{j \in v(c)} V(j)) \cup v(c) = V(c)$ and the distributive law. For a clearer view of the factorization process and of the assumptions made the graphical representation of the first and second successive considered expansions of $F(\mathbf{x})$ are shown in Figures 2.13 and 2.14. In these figures $dv = K$, and dc is the dimension of sets $V(j)$, which were considered equal for simplicity. In Figure 2.15 we progress further with the function $F(\mathbf{x})$ factorization and represent the corresponding graph expansion by considering the calculation of each $g_j(x_j)$. For that the same methodology as for $g_i(x_i)$ has been used. Obviously, this could continue until a point where we end up with elementary $g_j(x_j)$ functions. Indeed this is the case for finite codes respecting the considered assumptions. For such a code, the associated factor graph is a tree as can be attested by Figure 2.15.

From equation (2.45) one finds that

$$
g_i(x_i) = \prod_{c \in C(i)} \left(\sum_{\mathbf{x}_{v(c)}} f_c(x_i, \mathbf{x}_{v(c)}) \prod_{j \in v(c) \backslash i} g_j(x_j) \right) \tag{2.46}
$$

However, it should be stressed out that to calculate $g_j(x_j)$ the factor $f_c(x_i, \mathbf{x}_{v(c)})$ should not be taken into account, even if the variable x_j belongs to the independent set of function $f_c(.)$, unlike for $g_i(x_i)$, where all factors should be considered. This happens since this factor is included explicitly in the previous function expansion ($g_i(x_i)$), see equation (2.46). As a consequence for all $g_j(x_j), j \in \{1, \ldots, N\}$, except $g_i(x_i)$, the following transformation should

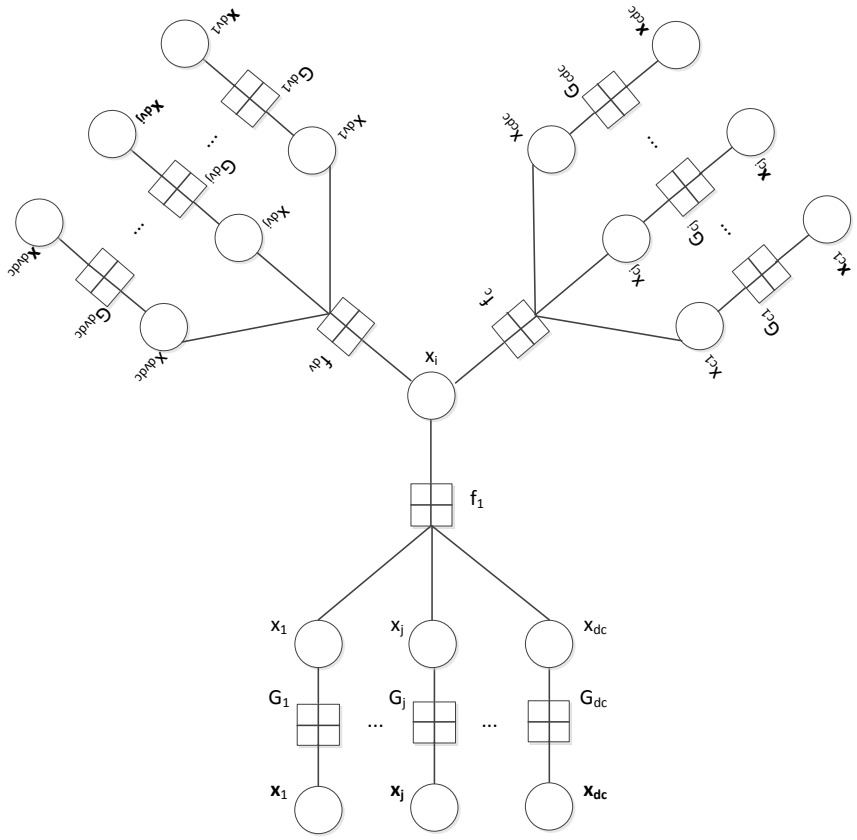

Figure 2.14: Second iteration of the expansion of function $F(\mathbf{x}) = p(\mathbf{y}|\mathbf{x})p(\mathbf{x})$.

---

be used, instead of equation (2.46)

$$g_j(x_j) = \prod_{b \in C(j) \setminus c} \left(\sum_{\mathbf{x}_{v(b)}} f_b(x_j, \mathbf{x}_{v(b)}) \prod_{k \in v(b) \setminus j} g_k(x_k) \right) \tag{2.47}$$

Equations (2.46) and (2.47) completely define the factorization process of $F(\mathbf{x})$, if the same factorization is used for all the remaining global functions. The first equation is used in the first factorization and the second in all the following factorizations. Namely, we can identify the $g_i(x_i)$ function as the probability of variable x_i being equal to $\{0, 1\}$ and the function $g_j(x_j)$ as the probability of variable x_j equals $\{0, 1\}$, given the information from factors other than $f_c(.)$ [17]. Hence, to compute $g_i(x_i)$, equations (2.46) and (2.47) can be used, since they define completely the factorization process of $F(\mathbf{x})$. Before showing up how to evaluate the recursive function $g_j(x_j)$ let us broke it into two parts

$$\begin{aligned} m_{j \to c}(x_j) &= \prod_{b \in C(j) \setminus c} m_{b \to j}(x_j) \\ m_{b \to j}(x_j) &= \sum_{\sim x_j} f_b(x_j, \mathbf{x}_{v(b)}) \prod_{k \in v(b) \setminus j} m_{k \to b}(x_k) \end{aligned} \tag{2.48}$$

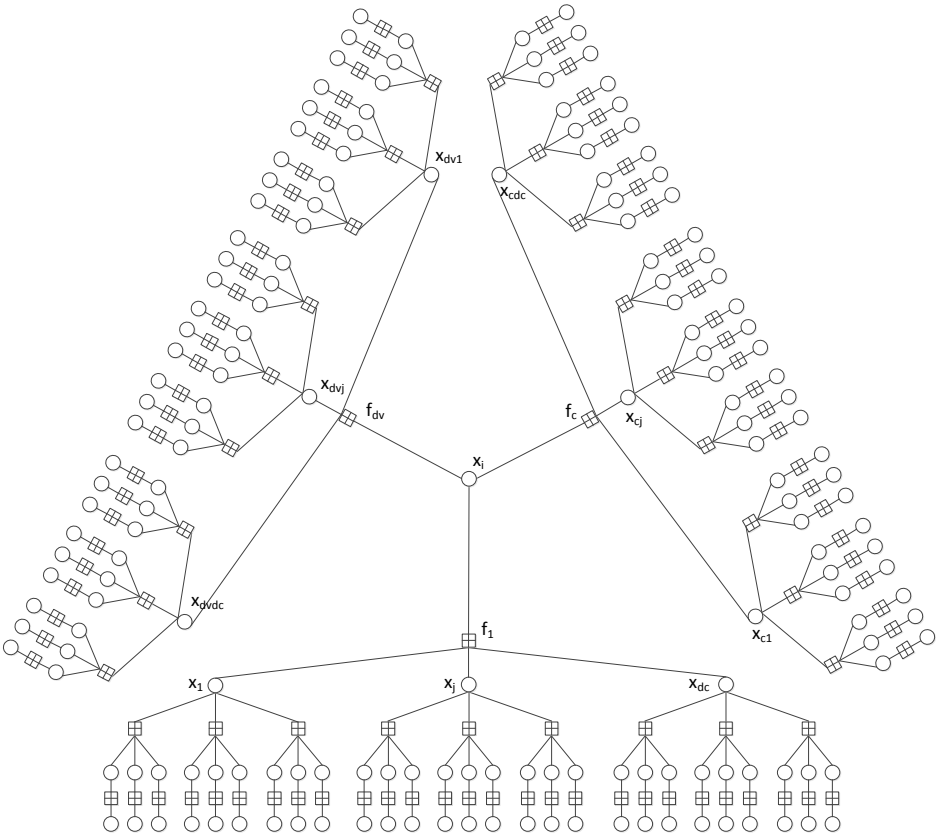

Figure 2.15: Third iteration of the expansion of function $F(\mathbf{x}) = p(\mathbf{y}|\mathbf{x})p(\mathbf{x})$.

---

where $g_j(x_j) = m_{j\to c}(x_j)$, $g_k(x_k) = m_{k\to b}(x_k)$ and the intermediate function $m_{j\to c}(x_j)$ has been defined implicitly. The previous functions denomination start with a letter m, since they will be associated with messages in the corresponding factor graph, to facilitate the visualization of the processing done, and to provide a way to simplify its implementation. Namely, function $m_{j\to c}(x_j)$ will be associated to the edge connecting variable node j and check node c and function $m_{b\to j}(x_j)$ to the edge connecting check node b and variable node j. The arrow just indicates the direction of the information transmission, in the graph. For example, $j \to c$, in $m_{j\to c}(x_j)$, indicates that the information is processed at variable node j and sent to check node c. We use the indices a, b, c to denote check nodes and i, j, k to denote variable nodes. The index c, in function $m_{j\to c}(x_j)$, indicate that the factor $f_c(.)$ has not been taken into account in the calculation of $g_j(x_j)$ and the index j denote that the processing is done for variable x_j. The same for indices b and k in $m_{k\to b}(x_k)$. If we consider that the value of X_j is fixed to x_j and that the probability of the event $X_k = x_k$, $k \in v(b)\backslash j$, is $m_{k\to b}(x_k)$, then the function $m_{b\to j}(x_j)$ represents the probability of factor $f_b(.)$ being respected. It should be stressed that the factor $f_b(.)$, in the MAP decoding problem, is an indicator function representing the check b. Equations (2.48) are the so-called Sum-Product/Belief-Propagation update equations. To obtain the true marginal of a given variable $m_j(x_j)$ we should consider all factors involved, as in equation (2.46)

$$m_j(x_j) = \prod_{b\in C(j)} m_{b\to j}(x_j) \tag{2.49}$$

Therefore, to compute the marginal of variable x_i one just need to apply equations (2.48) recursively. Using the edge assignment previously discussed, this recursive process can be mapped to the factor graph defined by the factorization of function $F(\mathbf{x})$, which has a tree topology (see Figure 2.15). Therefore, the evaluation of the marginal of variable x_i results in the propagation of messages, computed accordingly to equations (2.48, from the tree leafs (full recursion depth) to the root x_i. For a tree instead of propagating messages from the leafs to the root, to obtain the marginal, one can apply equation (2.48) in parallel, to all nodes, until convergence. The results obtained by these two methods are equal, since the messages sent from the leafs will overwrite the ones previously sent, in the parallel working version.

The sum-product algorithm expressed by equations (2.48) implies that a pair of messages $(m_{j\to c}(0), m_{j\to c}(1))$ or $(m_{b\to j}(0), m_{b\to j}(1))$ is transferred between nodes, at each iteration. However, it can be simplified so that only one value, per iteration per edge, is needed. For decoding, one only needs to know if $p(x_j = 0|\mathbf{y}) \geq p(x_j = 1|\mathbf{y})$. Consequently, the fraction $\frac{m_{j\to c}(0)}{m_{j\to c}(1)}$ or its logarithm is all that we need for decoding

$$\begin{aligned}
L_{j\to c} = log\left(\frac{m_{j\to c}(1)}{m_{j\to c}(0)}\right) &= \sum_{b\in C(j)\backslash c} log\left(\frac{m_{b\to j}(1)}{m_{b\to j}(0)}\right) = \sum_{b\in C(j)\backslash c} R_{b\to j} \\
&= \sum_{b\in C(j)\backslash c} log\left[\frac{\sum_{\sim x_j}\left(f_b(1,\ldots)\prod_{k\in v(b)\backslash j} m_{k\to b}(x_k)\right)}{\sum_{\sim x_j}\left(f_b(0,\ldots)\prod_{k\in v(b)\backslash j} m_{k\to b}(x_k)\right)}\right] \\
&= \sum_{b\in C(j)\backslash c} log\left[\frac{\sum_{\sim x_j}\left(f_b(1,\ldots)\prod_{k\in v(b)\backslash j} \frac{m_{k\to b}(x_k)}{m_{k\to b}(0)}\right)}{\sum_{\sim x_j}\left(f_b(0,\ldots)\prod_{k\in v(b)\backslash j} \frac{m_{k\to b}(x_k)}{m_{k\to b}(0)}\right)}\right] \\
&= \sum_{b\in C(j)\backslash c} log\left[\frac{\sum_{\mathbf{x}}\left(f_b(1,\mathbf{x})\prod_{k\in v(b)\backslash j} e^{L^{x_k}_{k\to b}}\right)}{\sum_{\mathbf{x}}\left(f_b(0,\mathbf{x})\prod_{k\in v(b)\backslash j} e^{L^{x_k}_{k\to b}}\right)}\right]
\end{aligned} \tag{2.50}$$

The function $f_b(\mathbf{x})$ can only take values on the set $\{0,1\}$, since for a LDPC code this is the indicator function represented in function (2.39). Namely, it is equal to zero for $\mathbf{x}\in\mathcal{O}$ and equal to one for $\mathbf{x}\in\mathcal{E}$, where $\mathcal{O}$ and $\mathcal{E}$ denote the set of binary vectors of length $|v(b)|+1$ with a odd and even number of entries equal to one, respectively. Consequently, the likelihood values sent by the variable nodes to the check nodes are given by

$$\begin{aligned}
L_{j\to c} &= \sum_{b\in C(j)\backslash c} log\left[\frac{\sum_{\mathbf{x}\in\mathcal{E}}\prod_{k\in v(b)\backslash j} e^{L^{x_k}_{k\to b}}}{\sum_{\mathbf{x}\in\mathcal{O}}\prod_{k\in v(b)\backslash j} e^{L^{x_k}_{k\to b}}}\right] \\
&= \sum_{b\in C(j)\backslash c} log\left[\frac{\prod_{k\in v(b)\backslash j}(e^{L_{k\to b}}+1)+\prod_{k\in v(b)\backslash j}(e^{L_{k\to b}}-1)}{\prod_{k\in v(b)\backslash j}(e^{L_{k\to b}}+1)-\prod_{k\in v(b)\backslash j}(e^{L_{k\to b}}-1)}\right] \\
&= \sum_{b\in C(j)\backslash c} log\left[\frac{1+\prod_{k\in v(b)\backslash j}\frac{e^{L_{k\to b}}-1}{e^{L_{k\to b}}+1}}{1-\prod_{k\in v(b)\backslash j}\frac{e^{L_{k\to b}}-1}{e^{L_{k\to b}}+1}}\right] \\
&= \sum_{b\in C(j)\backslash c} 2atanh\left[\prod_{k\in v(b)\backslash j} tanh\left(\frac{L_{k\to b}}{2}\right)\right]
\end{aligned} \tag{2.51}$$

Thereafter the log-domain version of the sum-product algorithm can be mathematically represented by the pair of messages

$$\begin{aligned} L_{j\to c} &= \sum_{b\in C(j)\setminus c} R_{b\to j} \\ R_{b\to j} &= 2atanh\left[\prod_{k\in v(b)\setminus j} tanh\left(\frac{L_{k\to b}}{2}\right)\right] \end{aligned} \tag{2.52}$$

For a tree the sum-product, or belief propagation, algorithm is exact. However, for factor graphs with loops that is not the case, the algorithm is suboptimal, but its performance has been shown to be very good in practice [12, 13].

2.5.2 Density Evolution

In the previous sections it was seen that with the help of a random code and of the optimal decoding algorithm it is possible to achieve the channel capacity. Here, in this section, we present the tools to obtain the capacity of a channel when specific codes and decoding algorithms are used [15]. Namely, we will analyze the case of graphical codes and of the message passing algorithms with special focus on LDPC codes and the sum-product algorithm.

The performance of a code is independent of the transmitted codeword, due to the symmetry properties of the decoding algorithm and also of the own code [39]. Consequently we are free to choose any codeword for analysis purposes. Since the all zero codeword is present in all linear codes, as stated in the Linear Codes section 2.4, it is obviously the best choice for analysis. The analysis of individual codes would be difficult and specific, since the model for such a process would be highly detailed. Nevertheless, there is a result stating that with high probability the performance of an individual code is identical to the ensemble average of the codes describing that individual code [15]. Equipped with this result, it is possible to make a statistical analysis of the code performance. Given a distribution pair ($\mathbf{\Lambda}$, $\mathbf{P}$) we define a *LDPC($\Lambda(x), P(x)$) code ensemble* in the following way [15]: Each graph has $\Lambda(1)$ variable nodes and $P(1)$ check nodes. Λ_i variable nodes and P_i check nodes have degree i. A degree i node has i sockets, to which the edges connect. The total number of sockets, in each side, is $\sum_i i\Lambda_i = \sum_i iP_i = \Lambda'(1) = P'(1)$. $\Lambda'(1)$ denotes the derivative of function $\Lambda'(x)$ evaluated at point 1. Label the sockets on one side with $\mathbf{s} = \{1, \ldots, \Lambda'(1)\}$ and label the sockets on the other side with a uniform random permutation, P, of $\{1, \ldots, \Lambda'(1)\}$, $\mathbf{s}(P)$. Connect the sockets with the same labellings with an edge.

In the following, two important simplifications are made: that the all zero codeword was sent and that the average performance concentrates around the average ensemble performance. The performance of the codes are thus analyzed in the infinite blocklength limit for which the corresponding factor graph has a tree like structure with probability one [39].

Previously, we have presented a way to describe an irregular LDPC code from the node perspective, but here, to analyze the code performance, the edge perspective is better suited (the messages are sent over the edges)

$$\lambda(x) = \sum_i \lambda_i x^{i-1} = \frac{L'(x)}{L'(1)} \qquad\qquad \rho(x) = \sum_i \rho_i x^{i-1} = \frac{R'(x)}{R'(1)} \tag{2.53}$$

where $\lambda_i(\rho_i)$ is equal to the fraction of edges that connect to variable (check) nodes with degree i.

Erasure Channel

In the following, we will start by revising how the performance of a LDPC code can be analyzed over the BEC. First, regular LDPC codes are reviewed and next the results are extended to the irregular case. Finally, we revisit optimization techniques for irregular LDPC codes.

To start the analysis the BP update equations are simplified, since for the BEC channel they are much simpler.

At each iteration, the check nodes modeling the channel send to the neighborhood variable, the corresponding channel messages, i.e. $\{0, 1, ?\}$, with equivalent likelihoods $\{+\infty, -\infty, 0\}$. Since the channel never introduces errors, the values of the incoming messages to a variable node belong to the set $\{0, +\infty\}$ (or $\{0, -\infty\}$). This in conjunction with the fact that the BP processing rule, at the variable nodes (2.52), amounts to just a summation of the set of incoming messages implies that the output message value is within the same set of the inputs.

For the check nodes the set of input message values is $\{-\infty, +\infty, 0\}$. After the processing of the input message with the function $tanh(.)$ the input set is transformed into $\{-1, +1, 0\}$. The product operation, in the check node update equation, (2.52), is equivalent to a mod-2 sum over the binary field ($\{0, 1\}$), where $+1$ is the bipolar representation of 0 and -1 of 1, when no input message is equal to zero. When any of the inputs are equal to zero the product and the corresponding check to variable node message is equal to zero. Looking to the check node update equation, (2.52), one see that the $2atanh(.)$ restores again the set of values to the original set ($\{-\infty, +\infty, 0\}$).

Thus, as previously explained, the BP algorithm update equations can be simplified to [39]

Variable node: the output message is an erasure if and only if all the inputs are erased, otherwise the output message is equal to the incoming message from the other edges.

Check node: the output message is equal to an erasure if one or more of the incoming messages are erased, otherwise its value is the mod-2 sum of the incoming messages.

Since we are considering the infinite blocklength case the computation neighborhood graph of a node will be tree like with high probability and consequently the messages exchanged by the BP algorithm are independent and all marginals are correct. Therefore the sum-product update equations, with independent inputs, are sufficient to describe the decoding process.

Let us assume an ensemble of regular (n, k) LDPC codes and a BEC with erasure probability ϵ. To describe the decoding process it is sufficient to analyze the erasure probability of the messages sent, over the edges, at each iteration. The erasure probability of the variable to check messages is given by

$$x = \epsilon y^{n-1} \tag{2.54}$$

where y is the erasure probability of the check to variable messages. Since the variable to check messages are only erased if all incoming messages from the other checks are erased, including the one coming from the factor representing the channel, which is erased with probability ϵ.

The check to variable messages are only not erased if all incoming messages from the neighborhood variable nodes are not erased. Consequently the erasure probability of the

check to variable node messages is

$$y = 1 - (1 - x)^{k-1} \tag{2.55}$$

Thereafter, for a regular (n, k) LDPC code its performance over the BEC can be characterized by the following equation

$$x = \epsilon(1 - (1 - x)^{k-1})^{n-1} \tag{2.56}$$

As an example we plot in Figures 2.16 and 2.17 the performance of the BP algorithm over an infinite blocklength regular (3,6) LDPC code, by iterating equation (2.56), for a BEC channel with erasure probability $\epsilon = 0.4$ and $\epsilon = 0.5$, respectively. One can see from these two figures that from one of the channels it is possible to transmit reliably, with an erasure probability of zero (after running the BP algorithm for around 25 iteration), but for the other channel it is not. The algorithm gets stuck at an erasure probability of around 0.45.

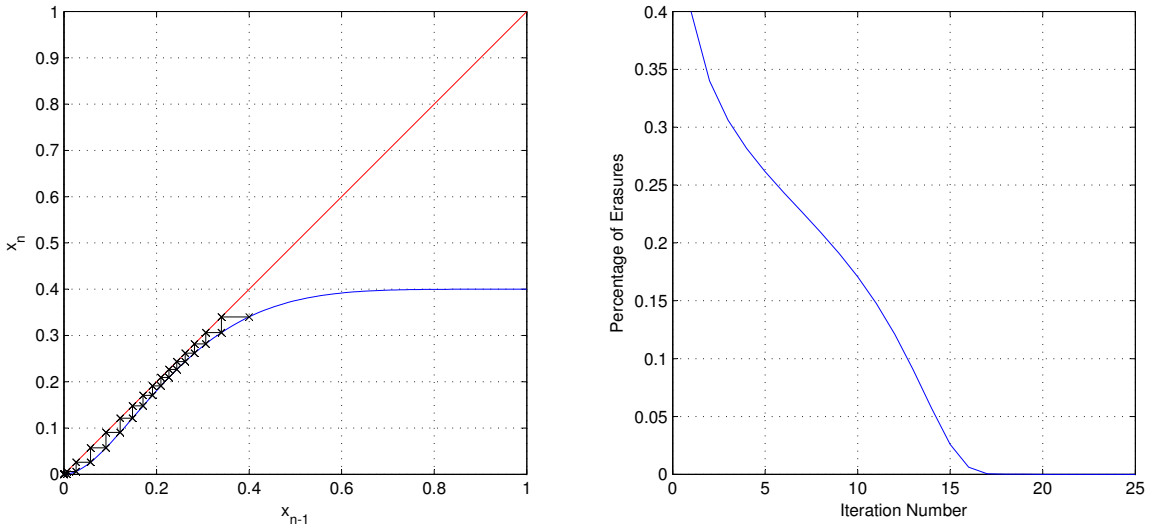

Figure 2.16: Regular $(3, 6)$ LDPC code variable to check erasure probability over the iterations for a BEC with $\epsilon = 0.4$.

To extend the previous result to the case of irregular codes one needs to average these results over the code uniform edge degree distributions. Assume an ensemble of LDPC(λ, ρ) codes. For such an ensemble, since the percentage of edges connected to variable nodes with degree i is given by λ_i, the variable to check node erasure probability is

$$x = \sum_i \lambda_i \epsilon y^{i-1} = \epsilon\lambda(y) \tag{2.57}$$

For the check to variable nodes the same way of thinking applies

$$y = \sum_i \rho_i (1 - (1 - x)^{k-1}) = 1 - \rho(1 - x) \tag{2.58}$$

Therefore, an irregular LDPC(λ, ρ) code performance is characterized by the following density evolution equation

$$x = \epsilon\lambda(1 - \rho(1 - x)) \tag{2.59}$$

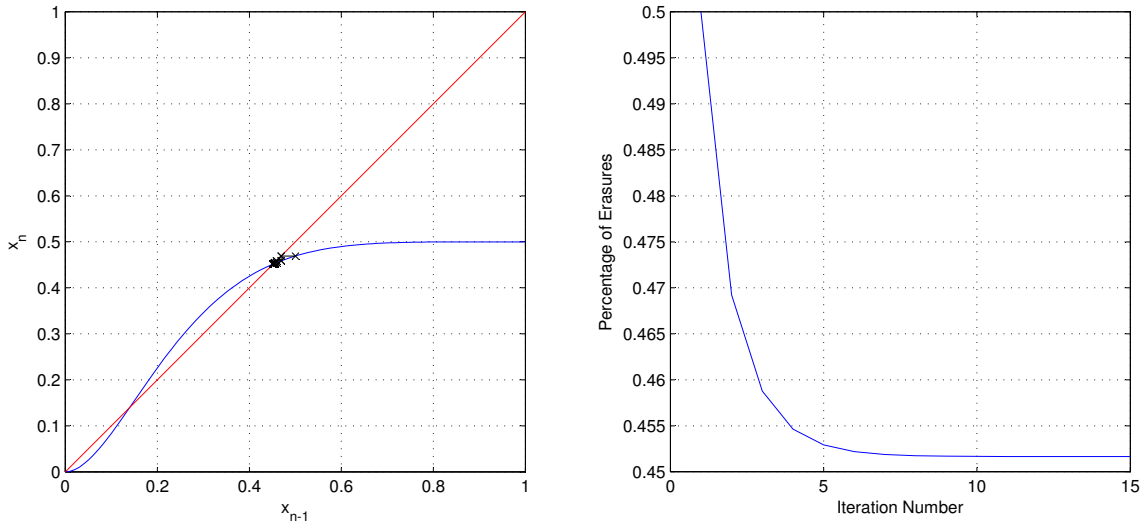

Figure 2.17: Regular $(3, 6)$ LDPC code variable to check erasure probability over the iterations for a BEC with $\epsilon = 0.5$.

This function is monotonically increasing in both of its arguments x, and ϵ [39]. If applied iteratively, using the fixed point iteration, it gives a monotone sequence converging to the nearest solution of the function [39]. If the erasure probability converges to zero for a BEC(ϵ) then it also converges to zero for a BEC(ϵ') for all $0 \leq \epsilon' \leq \epsilon$ [39]. This two monotonicity conditions with the fact that one of the fixed points of the previous iteration is $x = 0$ implies the existence of a well defined upper limit for which reliable transmission over the BEC(ϵ) is possible [39]. This upper limit is called threshold. For the regular $(3, 6)$ LDPC code the value of this threshold can be obtained numerically and is equal to $\epsilon = 0.4294$. Consequently, with a regular (3, 6) LDPC code and the BP decoder one can only transmit data reliably over a BEC with erasure probability lower than 0.4294.

Getting the Taylor series expansion of the right hand side of equation (2.59), around zero, one gets [39]

$$x = \epsilon\lambda'(0)\rho'(1)x + \mathcal{O}(x^2) \tag{2.60}$$

For sufficiently small x the convergence properties of (2.59) are determined by $\epsilon\lambda'(0)\rho'(1)$. More precisely if this factor is lower than one the sequence converges, otherwise no. This is the so called stability condition [39]. The more important consequence of such condition is the implied upper bound on the threshold of a code (ϵ)

$$\epsilon\lambda'(0)\rho'(1) \leq 1 \Leftrightarrow \epsilon \leq \frac{1}{\lambda'(0)\rho'(1)} \tag{2.61}$$

Now equipped with a code description and with a code performance evaluation tool it is possible to optimize the code structure so that better codes are obtained. The usual approach to optimize LDPC codes is to maximize the rate of the code for a given channel erasure probability, while ensuring that reliable transmission is obtained [39]. If the obtained rate for the code is higher than the one we expect, we can increase slightly the channel erasure probability and run the optimization problem again, to lower it. For a LDPC(λ, ρ) the rate

can be expressed by, see equation 2.35

$$R = 1 - \frac{\sum_i \rho_i / i}{\sum_i \lambda_i / i} \tag{2.62}$$

Fixing the check node distribution ($\rho(x)$) the objective of the optimization ($\max R$) become linear ($\max \sum_i \lambda_i / i$). The reliability constraint is enforced by imposing that the erasure probability decreases at each iteration: $\epsilon\lambda(1-\rho(1-x)) < x, \forall x \in [0,1]$. For a finite set of linear constraints the set $x \in [0,1]$ must be discretized. Therefore to avoid numerical problems around $x = 0$, caused by the discretization, the stability condition is used. With all the previous statements the LDPC(λ, ρ) code optimization task can be mathematically expressed by

$$\begin{aligned} \lambda = & \max_{\lambda} \sum_i \lambda_i / i \\ s.t. \;\; & \epsilon\lambda(1-\rho(1-x_i)) \leq x_i, \; x_i \in [0,1]; \; i \in \{0, \ldots, N_s\} \\ & \epsilon\lambda'(0)\rho'(1) \leq 1 \\ & \sum_i \lambda_i = 1, \; \lambda_i \geq 0; \end{aligned} \tag{2.63}$$

where N_s is the number of samples taken in the interval $[0,1]$ to discretize the constraints. As can be seen from equation (2.63) the LDPC code optimization task is a linear program. If we want also to optimize the check node distribution we can do it in the same way as done for the variable nodes, but using the $1 - y - \rho(1 - \epsilon\lambda(y)) \leq 0, \forall y \in [0,1]$ constraint and the merit function $-\sum_i \rho_i / i$. Iterating both problems the two degree distributions can be optimized.

Binary Memoryless Symmetric Channel

The analysis of the performance of LDPC codes over a binary memoryless channel (BMS) [39] follow the same structuring lines as the previous section. Thus, to start the analysis the BP update equations are transformed so that the analysis becomes simpler. Just to remember the BP update equations are

$$\begin{aligned} L_{v \to k} &= R_{0 \to v} + \sum_{n \in \mathcal{N}(v) \setminus k} R_{n \to v} \\ R_{k \to v} &= 2atanh \left[\prod_{n \in \mathcal{N}(k) \setminus v} tanh \left(\frac{L_{n \to k}}{2} \right) \right] \end{aligned} \tag{2.64}$$

where $R_{0 \to v}$ denotes the message sent by the factor representing the channel to variable node v, which corresponds to the associated channel log-likelihood ratio.

Let us define $d(y) : \mathbb{R} \to [-1, 1]$, $f(x, y) : \mathbb{R}^2 \to \mathbb{R}$ and $\mathbf{g}(y) : \mathbb{R} \to \{-1, +1\} \times [0, +\infty[$

$$\begin{aligned} d(y) &= tanh(y/2) \\ f(x, y) &= 2atanh(x \; Exp(-y)) \\ \mathbf{g}(y) &= (sign(y), -log(|d(y)|)) \end{aligned} \tag{2.65}$$

Thereafter, after some manipulations, the check node update equation can be rewritten as

$$\begin{aligned} R_{k\to v} &= 2atanh\left(\left[\prod_{n\in\mathcal{N}(k)\setminus v} sign(d(L_{n\to k}))\right]\left[Exp\left(-\sum_{n\in\mathcal{N}(k)\setminus v} log(|d(L_{n\to k})|)\right)\right]\right) \\ &= f\left(\prod_{n\in\mathcal{N}(k)\setminus v} sign(d(L_{n\to k})), \sum_{n\in\mathcal{N}(k)\setminus v} log(|d(L_{n\to k})|)\right) \\ &= f(\oplus_{n\in\mathcal{N}(k)\setminus v}\mathbf{g}(d(L_{n\to k})) \end{aligned} \tag{2.66}$$

where the sum operator ($\oplus$) is defined as

$$\oplus_i \mathbf{g}(y_i) = \left(\prod_i sign(y_i), -\sum_i log(|d(y_i)|)\right) \tag{2.67}$$

Hence the BP update equations, (2.64), can be reformulated as

$$\begin{aligned} L_{v\to k} &= R_{0\to v} + \sum_{n\in\mathcal{N}(v)\setminus k} R_{n\to v} \\ R_{k\to v} &= f(\oplus_{n\in\mathcal{N}(k)\setminus v}\mathbf{g}(d(L_{n\to k})) \end{aligned} \tag{2.68}$$

From 2.68 we see that apart from the $f(.)$ transformation the BP update equations amount to just a summation of the input messages. Since we are considering the infinite blocklength case the computation neighborhood of a given node is a tree with probability equal to one.

Let us assume a BMS, described by the probability distribution $p(Y|x)$ The associated log-likelihood ratio is defined as

$$l(y) = \frac{p(y|1)}{p(y|0)} \tag{2.69}$$

For a given random variable Y the associated log-likelihood ratio is L = l(Y), a random variable, with probability distribution $\mathtt{l}$. This corresponds to the messages exchanged by the factor nodes representing the channel to the variable nodes. At the first iteration this is the only information available to the algorithm, localized at the tree leafs. As the iterations proceed the information converges from the leafs to the root. Since all messages are drawn independently and from the same distributions[4], at a given iteration, the analysis of the overall tree simplifies to the analysis of a part of the tree, as already done before. Therefore it is sufficient to analyze the processing done at a variable and check node. Let us consider a variable node with degree n and with input message distribution $\mathtt{y}$. At the variable nodes the messages are processed, by the associated BP updating rule (2.48), which amounts to just a summation of the $n-1$ incoming messages plus the one coming from the factor node representing the channel. This implies that the resulting distribution of the variable to check messages, $\mathtt{x}$, is the convolution of the $n-1$ incoming check to variable distributions, $\mathtt{y}$, convolved with the channel log-likelihood ratio distribution [39]

$$\mathtt{x} = \mathtt{l} \circledast \mathtt{y}^{\circledast(n-1)} \tag{2.70}$$

[4]The messages are considered statistically independent since an infinite code is assumed and at each iteration the output distributions of the BP update equations are the same since their input distributions are also the same.

Apart from the map $f(.)$ the check node processing is a summation in the $\{-1,+1\} \times [0,+\infty[$ domain. Therefore the output distribution of a check node edge, $\mathtt{y}$, amounts to the convolution of the input distributions $\mathtt{x}$, in the $\{-1,+1\} \times [0,+\infty[$ domain. Namely, assuming a check node with degree k, the output distribution is given by [39]

$$\mathtt{y} = \mathtt{x}^{\boxtimes(k-1)} \tag{2.71}$$

where $\mathtt{y}$ represents the check node edge output distribution after the $f(.)$ transformation and $\boxtimes$ represents the convolution operator defined for the sum operator $\oplus$ and $g(.)$ function.

For a LDPC(λ, ρ) the corresponding variable to check message distribution is a weighted sum over the edge degree distribution of the code [39]

$$\mathtt{x} = \sum_i \lambda_i \mathtt{l} \circledast \mathtt{y}^{\circledast(i-1)} = \mathtt{l} \circledast \lambda(\mathtt{y}) \tag{2.72}$$

the same applies to the check to the variable message distribution

$$\mathtt{y} = \sum_i \rho_i \mathtt{x}^{\boxtimes(i-1)} = \rho(\mathtt{x}) \tag{2.73}$$

where $\rho(x) = \sum_i \rho_i \mathtt{x}^{\boxtimes(i-1)}$ and $\lambda(x) = \sum_i \lambda_i \mathtt{x}^{\circledast(i-1)}$. Thereafter, an irregular LDPC(λ, ρ) code performance is characterized by the following density evolution equation [39]

$$\mathtt{x} = \mathtt{l} \circledast \lambda(\rho(\mathtt{x})) \tag{2.74}$$

The corresponding log-likelihood ratio density of the corresponding variable, v, is given by the convolution of all n incoming messages including the channel likelihood

$$\mathtt{x}_v = \mathtt{l} \circledast \sum_i \lambda_i \mathtt{y}^{\circledast i} \tag{2.75}$$

From the probability distribution $\mathtt{x}_v$ one can get the bit error probability

$$P_e = \int_{-\infty}^{0} \mathtt{x}_v(x) dx \tag{2.76}$$

Since the all-zero codeword assumption has been made an error occurs if the corresponding log-likelihood ratio is lower than zero. On the other hand the probability that the information content sent on a message from a variable node to a check node is in error is given by

$$P_{e_\rightarrow} = \int_{-\infty}^{0} \mathtt{x}(x) dx \tag{2.77}$$

For a code to transmit reliably over a BMS channel either the P_e or $P_{e_\rightarrow}$ must go to zero as the iteration number increases [39].

2.6 References

[1] C. E. Shannon, "A mathematical theory of communication," *Bell System Technical Journal*, vol. 27, pp. 379–423 and 623–656, July and October 1948.

[2] I. E. Telatar, "Capacity of Multi-antenna Gaussian Channels," *AT&T Bell Laboratories, Murray Hill, NJ*, 1999.

[3] R. Ahlswede, "Multi-way communication channels," in *Proc. 2nd. Int. Symp. Information Theory (Tsahkadsor, Armenian S.S.R.)*. Publishing House of the Hungarian Academy of Sciences, 1971.

[4] H. Liao, "A coding theorem for multiple access communications," in *Proceedings of IEEE International Symposium on Information Theory*, 1972.

[5] G. Caire and S. Shamai, "On the achievable throughput of a multiantenna Gaussian broadcast channel," *Information Theory, IEEE Transactions on*, vol. 49, no. 7, pp. 1691–1706, 2003.

[6] H. Weingarten, Y. Steinberg, and S. Shamai, "The Capacity Region of the Gaussian Multiple-Input Multiple-Output Broadcast Channel," *Information Theory, IEEE Transactions on*, vol. 52, no. 9, pp. 3936–3964, Sept. 2006.

[7] C. Berrou, A. Glavieux, and P. Thitimajshima, "Near Shannon limit error-correcting coding and decoding: Turbo-codes. 1," vol. 2, 1993, pp. 1064–1070 vol.2.

[8] R. McEliece, D. MacKay, and J.-F. Cheng, "Turbo decoding as an instance of Pearl's ldquo;belief propagation rdquo; algorithm," *Selected Areas in Communications, IEEE Journal on*, vol. 16, no. 2, pp. 140 –152, feb 1998.

[9] M. Tuchler, R. Koetter, and A. Singer, "Turbo equalization: principles and new results," *Communications, IEEE Transactions on*, vol. 50, no. 5, pp. 754 –767, may 2002.

[10] M. C. Valenti and J. Sun, "The UMTS turbo code and an efficient decoder implementation suitable for software defined radios," *International Journal of Wireless Information Networks*, vol. 8, pp. 203–216, 2001.

[11] D. MacKay, "Good error-correcting codes based on very sparse matrices," in *Information Theory. 1997. Proceedings., 1997 IEEE International Symposium on*, Jun-4 Jul 1997, pp. 113–.

[12] M. Davey and D. MacKay, "Low density parity check codes over GF(q)," in *Information Theory Workshop, 1998*, Jun 1998, pp. 70–71.

[13] D. MacKay and R. Neal, "Near Shannon limit performance of low density parity check codes," *Electronics Letters*, vol. 33, no. 6, pp. 457–458, Mar 1997.

[14] R. G. Gallager, *Low-Density Parity-Check Codes*. The MIT Press, Sep. 1963.

[15] T. Richardson and R. Urbanke, "The capacity of low-density parity-check codes under message-passing decoding," *Information Theory, IEEE Transactions on*, vol. 47, no. 2, pp. 599–618, Feb 2001.

[16] S.-Y. Chung, J. Forney, G.D., T. Richardson, and R. Urbanke, "On the design of low-density parity-check codes within 0.0045 dB of the Shannon limit," *Communications Letters, IEEE*, vol. 5, no. 2, pp. 58–60, Feb 2001.

[17] D. MacKay, *Information theory, inference, and learning algorithms.* Cambridge Univ Pr, 2003.

[18] W. Lee, "Estimate of channel capacity in Rayleigh fading environment," *Vehicular Technology, IEEE Transactions on*, vol. 39, no. 3, pp. 187 –189, aug 1990.

[19] A. Goldsmith, *Wireless Communications.* Stanford University, 2005.

[20] G. J. Foschini, "Layered space-time architecture for wireless communication in a fading environment when using multi-element antennas," *Bell Labs Technical Journal*, vol. 1, no. 2, pp. 41–59, 1996. [Online]. Available: http://dx.doi.org/10.1002/bltj.2015

[21] *V-BLAST: an architecture for realizing very high data rates over the rich-scattering wireless channel*, 1998. [Online]. Available: http://ieeexplore.ieee.org/xpls/abs_all.jsp?arnumber=738086

[22] I. IST-Winner, "WINNER II Channel Models-Deliverable D1. 1.2 V1. 2," 2007.

[23] E. Biglieri, J. Proakis, and S. Shamai, "Fading channels: Information-theoretic and communications aspects," *Information Theory, IEEE Transactions on*, vol. 44, no. 6, pp. 2619–2692, 1998.

[24] P. Bello, "Characterization of randomly time-variant linear channels," *Communications Systems, IEEE transactions on*, vol. 11, no. 4, pp. 360–393, 1963.

[25] M. Patzold, *Mobile Fading Channels: Modelling, Analysis, & Simulation*, 1st ed. Wiley, Feb. 2002.

[26] R. Hamming, "Error detecting and error correcting codes," *Bell System Technical Journal*, vol. 29, no. 2, pp. 147–160, 1950.

[27] T. Richardson and R. Urbanke, "Efficient encoding of low-density parity-check codes," *Information Theory, IEEE Transactions on*, vol. 47, no. 2, pp. 638 –656, feb 2001.

[28] J. Lu and J. M. F. Moura, "Linear Time Encoding of LDPC Codes," *CoRR*, vol. abs/0810.2781, 2008.

[29] V. Zyablov and M. Pinsker, "Estimation of the error-correction complexity for Gallager low-density codes," *Problemy Peredachi Informatsii*, vol. 11, no. 1, pp. 23–36, 1975.

[30] G. Margulis, "Explicit constructions of graphs without short cycles and low density codes," *Combinatorica*, vol. 2, no. 1, pp. 71–78, 1982.

[31] R. Tanner, "A recursive approach to low complexity codes," *Information Theory, IEEE Transactions on*, vol. 27, no. 5, pp. 533–547, 1981.

[32] M. Luby, M. Mitzenmacher, M. Shokrollahi, D. Spielman, and V. Stemann, "Practical loss-resilient codes," in *Proceedings of the twenty-ninth annual ACM symposium on Theory of computing.* ACM, 1997, pp. 150–159.

[33] M. Luby, M. Mitzenmacher, A. Shokrollah, and D. Spielman, "Analysis of low density codes and improved designs using irregular graphs," in *Proceedings of the thirtieth annual ACM symposium on Theory of computing.* ACM, 1998, pp. 249–258.

[34] T. Richardson, M. Shokrollahi, and R. Urbanke, "Design of capacity-approaching irregular low-density parity-check codes," *Information Theory, IEEE Transactions on*, vol. 47, no. 2, pp. 619–637, 2001.

[35] C. Cole, S. Wilson, E. Hall, and T. Giallorenzi, "Regular $\{4, 8\}$ LDPC Codes and Their Lowerror Floors," in *Proceedings of the 2006 IEEE conference on Military communications*. IEEE Press, 2006, pp. 1490–1496.

[36] E. Martinian and J. Yedidia, "Iterative quantization using codes on graphs," *Arxiv preprint cs/0408008*, 2004.

[37] J. Garcia-Frias and W. Zhong, "Approaching Shannon performance by iterative decoding of linear codes with low-density generator matrix," *Communications Letters, IEEE*, vol. 7, no. 6, pp. 266–268, June 2003.

[38] J. Milton and J. Arnold, *Introduction to probability and statistics: principles and applications for engineering and the computing sciences*. McGraw-Hill New York, 1990.

[39] T. Richardson and R. Urbanke, *Modern coding theory*. Cambridge Univ Pr, 2008.

[40] F. Kschischang, B. Frey, and H. Loeliger, "Factor graphs and the sum-product algorithm," *Information Theory, IEEE Transactions on*, vol. 47, no. 2, pp. 498–519, 2001.

Chapter 3

Distributed Antenna System Overview

The DAS concept promises to enhance the capacity and diversity of the next generation wireless communication networks, due to the inherently added micro and macro diversity. In this chapter, we first give an overview of the main benefits of a DAS in relation to a CAS. Next we study the sum-capacity scaling of a multi-user DAS with the number of jointly processed transmit antennas, in the downlink. In a practical system, this scaling will have implications on the number of antennas that are worth being jointly processed, since the costs of processing an additional antenna can be higher than the extra benefits obtained. Results show that the most important system property to attain the highest capacity gains is symmetry and that the users who attain the maximum gain are those at the cell border. They also confirm that the main DAS feature that makes possible his gains over the CAS architecture is the additional degrees of freedom/diversity provided by such an architecture, which increase the probability of finding a system state with high symmetry and of each user being near to one of the transmit antennas.

3.1 Introduction

In response to the increasing demand of higher spectral efficiencies the MIMO antenna concept has gained a lot of attention during the last years. From theory [1], it is expected that the system capacity will increase far beyond that of the single antenna systems, in rich scattering propagation environments. On the other hand, for limited scattering propagation environments, the capacity and the diversity order achieved will be limited, due to the existence of strong correlation between channel paths. This is indeed what happens for a CAS, where typically, the antennas are only few wavelengths apart. This can be explained by the fact that if the antennas are close together and one of the links has poor quality, then the others will have a poor quality with high probability. Such a fact implies that the overall received signal strength will be low. On the opposite, for a system with independent links, if one of the links has a poor quality, then at least one of the other links will have a good quality with a fairly high probability, which increases with the number of considered links. Therefore, to achieve high spectral efficiencies and to attain big diversity gains, the channels should be independent. Nevertheless, due to physical limitations at the transceivers the number of antennas deployed and the degree of channel independence achieved, in a CAS, cannot be high. One possible solution to cope with this problem is to have the mobiles simultaneously communicating with a group of geographically distributed antennas, which are jointly processed at a central

point [2]. The key element to achieve this is to have the signals transparently connected to a central unit (CU), by fiber, for example, where they are jointly processed. This leads us to the DAS concept, and thus not only capacity and diversity gains will be obtained but also the access distance and transmit power will be reduced, due to the inherent added macro-diversity. In [3] the authors quantify the capacity gains provided by a single-user DAS in the presence of inter-cell interference, showing that DAS reduces other-cell interference, in a multi-cell environment, and hence significantly improves performance and capacity, especially for users near cell boundaries. When more users are to be served simultaneously, the additional degrees of freedom provided by the DAS architecture can be used to spatially separate users, expanding in that way the system capacity. Nonetheless, at the mobile terminals, the number of antennas is generally low, only one or two. Therefore, from the law of diminishing returns it is expected that when the number of jointly processed antenna's increase, the complexity will increase, but the improvement in throughput may not increase in the same way. As a result, a tradeoff between the added complexity/costs and obtained benefits, from the joint processing of more transmit antennas, has to be made. One possible way to ease this problem is the use of low complexity/sub-optimal precoding schemes, like ZF and Block-Diagonalization (BD), at the CU. Following this line of thought, in [4, 5] the authors study the incurred losses, in terms of rate/power offsets, between ZF/BD and the optimal scheme, which is well known to be DPC [6]. The authors conclude that the incurred losses are more pronounced when the number of transmit antennas is close to the number of aggregate receive antennas. On the other hand, in [7] the authors analyze the complexity/costs' tradeoff by considering as a measure for the network performance the normalized system capacity or more precisely the maximum achievable rate per channel use normalized by the number of cooperating remote antenna units (RAU). Another key performance measure considered, in the previous article, is the signal-to-interference ratio (SIR). Considering full frequency reuse among RAUs different cooperation schemes were theoretically analyzed. The authors observe that cooperation is not always beneficial, i.e. when the users are close to the RAUs. Based on those results the authors propose to adaptively optimize the network operation mode, i.e. the number of cooperative RAUs, to combine the advantages of cooperative and non-cooperative schemes to maximize the system throughput. Results show that adaptive cooperation becomes more significant when shadowing effect's increase, with more than 20% cell-average gain for up to 3 RAUs cooperation. In this chapter, we give an overview of the gains provided by RAUs cooperation in terms of the ergodic channel sum-capacity, in the downlink. In that context, we define Differential CAPacity (DCAP) as the increase in ergodic sum-capacity when one additional RAU is connected to the system users, to quantify the gains provided by the processing of one extra RAU, at the CU. Work on the achievement of a closed-form expression for particular cases of the ergodic distributed MISO channel capacity was already carried on [8] and [3]. In [8] the authors study the ergodic capacity of a orthogonalized (by orthogonal space time block codes (OSTBC)) distributed MISO channel. In [3] the authors study the more general case of a distributed MISO channel, but they consider that all channels gains are different. While numerically the results can be obtained through the formulas of [8] and [3], no theoretical expression was given in the referred papers, for DCAP. Here we derive an expression for this differential capacity and provide upper bounds that are simple to compute and give us information on the maximum capacity increase one can expect by connecting the terminal to additional RAUs. Such a result is of interest when managing the radio resources, since assuming that one wants to connect to the RAUs providing the best SNRs it gives us indication when for a given network state, we should add or drop an RAU and can also provide

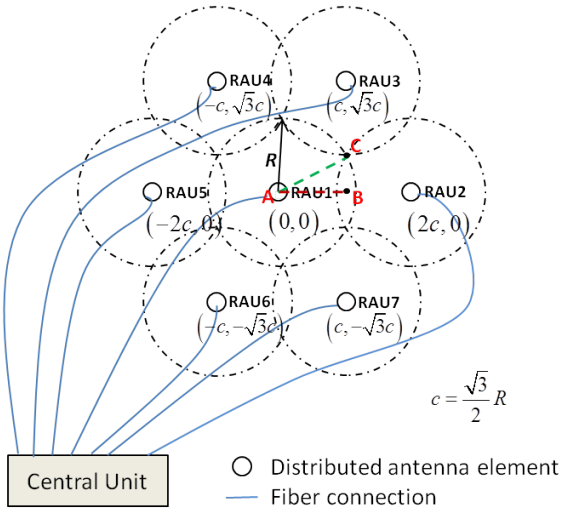

Figure 3.1: Distributed antenna system cell.

---

guidelines for the deployment of the distributed RAUs. We begin in the following section with a description of the system model. Next we give a small overview of the main benefits of DAS over CAS. Then we describe the behavior of the DCAP for the single-user case, to introduce the topic. Finally, we access the benefits of the connection of more transmit RAUs to the CU, for the multi-user case.

3.2 System Model

In the following we model the downlink of a multiuser DAS/CAS system. Both the DAS and CAS have unique properties to be modeled. As a result of the existing different access distances, in a DAS, there is a significant path loss variation among received signal paths. On the other hand, for a CAS, all received paths experience the same path loss [9], [10], since all transmit antennas are co-located. Nevertheless, the small separation between the transmit antennas has also its drawbacks. The small antenna separation implies the appearance of correlation between channel paths. In contrast, for a DAS the different scattering properties around each of the RAUs enrich the corresponding channel statistics, offering channel independence.

To model all the previous stated channel characteristics, a broadcast channel (BC) [6] with N transmit antennas and K users, each with only one receive antenna is considered for the downlink of a DAS/CAS. For such a system, if there is no correlation between the channel paths of different users, the user k received signal can be modeled by

$$y_k = \mathbf{h}_k \mathbf{x} + n_k,\ k = 1, \ldots, K;\ \ \mathbf{h}_k = \mathbf{h}_k^w \mathbf{R}^{1/2} \boldsymbol{\rho}_k^{1/2} \tag{3.1}$$

where $\mathbf{x}$ is the transmitted signal vector, $\boldsymbol{\rho}_k$ is a diagonal matrix where each element i denotes the path loss factor between transmit antenna i and user k, $\mathbf{h}_k^w$ models the microscopic independent Rayleigh fading component, $\mathbf{R}$ represents the correlation between transmit antennas [11] and n_k is additive white Gaussian noise. $\mathbf{R}$ and $\boldsymbol{\rho}_k$ are deterministic.

In the following sections, ideal DAS and CAS systems are considered, i.e. for DAS we consider no correlation between transmit antennas ($\mathbf{R} = \mathbf{I}$), and for CAS all path losses are regarded as equal ($\boldsymbol{\rho}_k = \mathbf{I}$). It is also assumed that the receiver has perfect knowledge of its own channel and that the transmitter has perfect instantaneous knowledge of all channels. In practice this can be achieved using training data and feedback channels between the CU and the system users. All analysis presented in this chapter consider, for simplicity, a single cell, with all RAUs connected to a unique CU, where all signals are jointly processed. Therefore, the system is considered to be noise limited. Additionally, the cable connection is regarded as transparent to the signals transported. In all results presented, the SNR at a distance of 1000 meters, relative to each transmit antenna, is assumed to be equal to 0dB. It is also considered that the RAU connection order is from the closest RAU to the farther one and that the propagation path loss only depends on the distance between user i and RAU j, d_{ij}, and on the path loss exponent α ($d_{ij}^{-\alpha}$), which is considered to be equal to 3. In next sections, for the single-user case, by circular ring we mean a group of antennas with the same mean SNR to the user.

3.3 Power Efficiency

Power efficiency gives a measure of the required power for supporting a given coverage area. One of the main benefits of DAS over CAS is in terms of power efficiency. This is mainly due to the fact that for a DAS the access distance is reduced, mitigating in that way the path loss effects of the channel onto the transmitted signals.

To demonstrate the power benefits of DAS over CAS let us consider a deployment scenario as in [3]. This is illustrated in Figure 3.1, where we consider one central antenna and a tier of 6 distributed antennas, each with a coverage radius equal to R. This corresponds to a coverage area of $7\pi R^2 - 24(\pi/6R^2 - \sqrt{3}/4R^2) = (3\pi + 6\sqrt{3})R^2$, for each distributed antenna. The radius of a circle with the same area is $R\sqrt{3 + 6\sqrt{3}/\pi}$. For a fair comparison, with a DAS, consider this circle as the coverage area of a CAS cell [9]. Let us also consider that for a RAU to support a coverage area with radius R the required power is P. Thus to support the overall coverage area a total power of $7P$ is needed. On the other hand, for the CAS, the needed power is equal to $(3+6\sqrt{3}/\pi)^{\alpha/2}P$, if the propagation path loss is assumed to be given by $d^{-\alpha}$, where α is the path loss exponent. In other words, the power efficiency of the DAS is $(3 + 6\sqrt{3}/\pi)^{\alpha/2}/7$. For a path loss exponent equal to 3 the DAS power efficiency gain is 3.6 dB and is even higher for bigger path loss exponents. In conclusion, this simple example, illustrates the power efficiency benefits of a DAS with respect to a CAS, meaning that a DAS needs a much lower power budget to support the same coverage area.

3.4 Diversity/Power Loss

To analyze the impact of the channel correlation in a CAS and of the path loss asymmetries in a DAS, let us consider as a measure the average BER and let us also consider the downlink of a single user transmit diversity system with N transmit antennas and one receive antenna. Let us also consider, for simplicity, BPSK modulation and the high SNR regime. To maximize the received SNR, the signal sent on transmit antenna i is pre-multiplied by a gain a_i. Under those circumstances, the optimal gain value is obtained using the maximum ratio transmission

(MRT) algorithm. If MRT is used, at the transmitter, the instantaneous received SNR is equal to $\frac{P}{\sigma^2}\mathbf{h}^w\mathbf{\Sigma}\mathbf{h}^{w^H}$, where P is the transmit power, $\mathbf{\Sigma} = \mathbf{R}^{1/2}\boldsymbol{\rho}^{1/2}(\mathbf{R}^{1/2}\boldsymbol{\rho}^{1/2})^H$ and $\mathbf{h}^w$ represents the channel matrix, with complex Gaussian distributed entries, zero mean and variance one. Therefore, the system BER can be mathematically expressed by

$$P_e = \mathbb{E}_{\mathbf{h^w}}\left[Q\left(\sqrt{\frac{P}{\sigma^2}\mathbf{h}^w\mathbf{\Sigma}\mathbf{h}^{w^H}}\right)\right] \tag{3.2}$$

The deterministic matrix $\mathbf{\Sigma}$ can be decomposed using the singular value decomposition, $\mathbf{\Sigma} = \mathbf{U}\mathbf{\Lambda}\mathbf{U}^H$, and the corresponding left and right singular vectors integrated into the channel matrix without affecting their distribution, since they are unitary and $\mathbf{h}^w$ is isotropic. Thus, $\mathbf{h}^w\mathbf{\Sigma}\mathbf{h}^{w^H}$ and $\mathbf{h}^w\mathbf{\Lambda}\mathbf{h}^{w^H}$ follow the same distribution, the weighted chi-square distribution. Therefore, by evaluating the expectancy operator, of equation (3.2), one gets

$$\begin{aligned}
P_e &= \mathbb{E}_{\mathbf{h}^w}\left[Q\left(\sqrt{\frac{P}{\sigma^2}\mathbf{h^w}\mathbf{\Lambda}\mathbf{h}^{w^H}}\right)\right] \\
&= \mathbb{E}_{\mathbf{h^w}}\left[Q\left(\sqrt{\frac{P}{\sigma^2}\sum_{i=1}^{N}\mathbf{\Lambda}_{ii}|(\mathbf{h}_i^w)|^2}\right)\right] = \mathbb{E}_{\mathbf{x}}\left[Q\left(\sqrt{\frac{P}{\sigma^2}\sum_{i=1}^{N}\mathbf{x}_i}\right)\right], \quad \mathbf{x}_i = \mathbf{\Lambda}_{ii}|(\mathbf{h}_i^w)|^2 \\
&= \int_0^{+\infty}\cdots\int_0^{+\infty} Q\left(\sqrt{\frac{P}{\sigma^2}\sum_{i=1}^{N}\mathbf{x}_i}\right)\prod_{i=1}^{N} f_{\mathbf{X}_i}(\mathbf{x}_i)d\mathbf{x}_1\ldots d\mathbf{x}_N
\end{aligned} \tag{3.3}$$

Using the alternate $Q(.)$ function representation [12, 13] $Q(z) = 1/\pi\int_0^{\pi/2} exp[-z^2/(2sin^2\theta)]d\theta$ and the fact that $f_{\mathbf{X}_i}(\mathbf{x}_i) = \mathbf{\Lambda}_{ii}^{-1}e^{-\mathbf{\Lambda}_{ii}^{-1}\mathbf{x}_i}$, $\mathbf{x}_i = \mathbf{\Lambda}_{ii}|(\mathbf{h}_i^w)|^2$ this simplifies to

$$\begin{aligned}
P_e &= \int_0^{+\infty}\cdots\int_0^{+\infty}\frac{1}{\pi}\int_0^{\frac{\pi}{2}} Exp\left(-\frac{P}{\sigma^2}\frac{\sum_{i=1}^{N}\mathbf{x}_i}{2sin^2\theta}\right)d\theta\prod_{i=1}^{N}\mathbf{\Lambda}_{ii}^{-1}e^{-\mathbf{\Lambda}_{ii}^{-1}\mathbf{x}_i}d\mathbf{x}_1\ldots d\mathbf{x}_N \\
&= \frac{1}{\pi}\int_0^{\frac{\pi}{2}}\prod_{i=1}^{N}\int_0^{+\infty}\mathbf{\Lambda}_{ii}^{-1}Exp\left[-\mathbf{x}_i\left(\frac{P}{\sigma^2}\frac{1}{2sin^2\theta}+\mathbf{\Lambda}_{ii}^{-1}\right)\right]d\mathbf{x}_i d\theta \\
&= \frac{1}{\pi}\int_0^{\frac{\pi}{2}}\prod_{i=1}^{N}\mathbf{\Lambda}_{ii}^{-1}\left(\frac{P}{\sigma^2}\frac{1}{2sin^2\theta}+\mathbf{\Lambda}_{ii}^{-1}\right)^{-1}d\theta = \frac{1}{\pi}\int_0^{\frac{\pi}{2}}\prod_{i=1}^{N}\mathbf{\Lambda}_{ii}^{-1}\left(\frac{\mathbf{\Lambda}_{ii}2sin^2\theta}{\frac{P}{\sigma^2}\mathbf{\Lambda}_{ii}+2sin^2\theta}\right)d\theta \\
&\approx \frac{1}{\pi}\int_0^{\frac{\pi}{2}}\prod_{i=1}^{N}\mathbf{\Lambda}_{ii}^{-1}\left(\frac{2sin^2\theta}{\frac{P}{\sigma^2}}\right)d\theta = \frac{2^N}{\pi}\left(\frac{P}{\sigma^2}\right)^{-N}\prod_{i=1}^{N}\mathbf{\Lambda}_{ii}^{-1}\int_0^{\frac{\pi}{2}} sin^{2N}\theta d\theta \\
&= \frac{(2N)!}{(N!)^2 2^{2N+1}}\left(\frac{P}{\sigma^2}\right)^{-N}\prod_{i=1}^{N}\mathbf{\Lambda}_{ii}^{-1} = \frac{(2N)!}{(N!)^2 2^{2N+1}}\left(\frac{P}{\sigma^2}|\mathbf{\Sigma}|^{\frac{1}{N}}\right)^{-N}
\end{aligned} \tag{3.4}$$

where in the the fourth line we have considered the high SNR regime, i.e. that $P/\sigma^2\mathbf{\Sigma}_{ii} \gg 2sin^2\theta$. As a consequence, if $\mathbf{\Sigma}$ is full rank, it is not difficult to verify, from equation (3.4), that the correlation at the transmitter side, for a CAS, or the path loss asymmetries inherent to a DAS, imply a BER power penalty of $|\mathbf{\Sigma}|^{1/N}$, in the high SNR regime. If instead, the rank of $\mathbf{\Sigma}$ is equal to $n < N$, the system looses $N - n$ degree of freedom, since $N - n$ channels become linearly dependent.

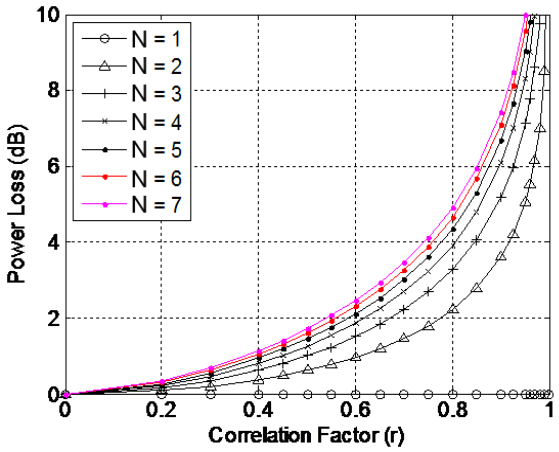

Figure 3.2: CAS Power loss versus correlation factor (r).

Hence, for a DAS, if one of the channel path losses increases by a factor of 2, the power loss will increase by 3 dB, since the determinant of a diagonal matrix is equal to the product of their diagonal entries. On the other hand, the correlation effects are not so easy to visualize since the correlation matrix is not diagonal, like the path loss matrix. To have a better insight of the correlation effects into the BER performance, let us consider a CAS with a simplified correlation structure, namely let us consider a correlation r between the channel paths of different transmit RAUs. For such correlation structure, the resulting power loss is given by

$$|\mathbf{\Sigma}|^{\frac{1}{N}} = |\mathbf{R}|^{\frac{1}{N}} = (1-r)\left(1+\frac{r}{1-r}N\right)^{\frac{1}{N}} \tag{3.5}$$

In Figure 3.2 we plot the power loss versus the correlation factor r, by considering a set of values for N (the number of transmit antennas). As can be seen from that figure, the power loss experienced by such a system, in the high SNR regime, increases as the correlation factor (r) and the number of transmit antennas (N) increase, but for low values of r the increase is not as sharp as the one for high values of r. A typical power loss value, for moderate correlation ($r = 0.6$), is 2 dB (see Figure 3.2). Another aspect that is worth noting is that the power loss starts to saturate when the number of transmit antennas is approximately 4. This happens mainly due to the averaging of the power losses, corresponding to each of the correlation matrix eigenvalues, as N increases[1]. Namely, from equation (3.5) we note that for N tending to infinity the loss converges to $1-r$. However, as we add more antennas to the system (CAS), since the deployment space is constrained, the correlation factor will also increase, increasing the corresponding power penalty. As a consequence, we can say that as the system gets more correlated, the spectrum of the corresponding correlation matrix become worse (ill conditioned matrix), implying an increased loss.

[1] As the power loss in dB is equal to the average of the corresponding eigenvalues of $\mathbf{\Lambda}$ (in dB).

3.5 Capacity Analysis

In the previous sections, a brief overview of the benefits of a DAS over a CAS was given, namely in terms of power efficiency and diversity. Now we will focus on another measure, the channel sum-capacity. More specifically we focus on the system DCAP. In the following sections, we first quantify the system capacity gains, by the connection of additional RAUs, for the single-user case, by resorting to the DCAP definition. For that case, we initially give a brief overview of the required background to analyze this scenario. Next, we look at a specific distributed antenna deployment to find the points that benefit the most from the connection of additional transmit antennas, at the CU, and also explore the DCAP sensitivity to the SNR variation. Finally, the multi-user case is considered. For this case, we rely mostly on simulations, to extend the conclusions drawn from the single-user case.

3.5.1 Single-User Scenario

Distributed MISO system capacity

In the following, we derive the capacity expression for the single-user scenario, of a DAS. According to [12] and [14] the ergodic capacity, when only one user is considered ($K = 1$), can be expressed mathematically by

$$C = \mathbb{E}_{\mathbf{h}} \left[log \left(1 + \frac{\mathbf{h}^H . \mathbf{R}_x . \mathbf{h}}{\sigma^2} \right) \right] \tag{3.6}$$

where $\mathbf{R}_x$ is the transmit signal covariance matrix and σ^2 the noise power. The column vector $\mathbf{h}$ can be equivalently expressed by $\mathbf{h} \sim \mathbf{\Sigma}^{1/2}\mathbf{h^w}$, where $\mathbf{\Sigma}$ represent the correlation or path loss matrix, for a CAS and DAS, respectively. Let the singular value decomposition of $\mathbf{\Sigma}$ be given by $\mathbf{\Sigma} = \mathbf{U}\mathbf{\Lambda}\mathbf{U}^H$, where $\mathbf{U}$ is a unitary matrix and $\mathbf{\Lambda}$ a non-negative diagonal matrix, with each diagonal element corresponding to the eigenvalues of the matrix $\mathbf{R}$ or $\boldsymbol{\rho}$.

Hence the previous capacity expression can be rewritten as

$$\begin{aligned} C &= \mathbb{E}_{\mathbf{h}} \left[log \left(1 + \frac{\mathbf{h}^{wH}\mathbf{\Sigma}^{1/2^H}\mathbf{R}_x\mathbf{\Sigma}^{1/2}\mathbf{h}^w}{\sigma^2} \right) \right] \\ &= \mathbb{E}_{\mathbf{h}} \left[log \left(1 + \frac{\mathbf{h}^{wH}\mathbf{\Lambda}^{1/2}\mathbf{U}^H\mathbf{R}_x\mathbf{U}\mathbf{\Lambda}^{1/2}\mathbf{h}^w}{\sigma^2} \right) \right] \end{aligned} \tag{3.7}$$

To maximize the capacity, subject to the power constrain $tr(\mathbf{R}_x) = P$, $\mathbf{x}$ must be circularly symmetric complex Gaussian [1] and its correlation matrix, $\mathbf{R}_x$, must have the same eigenvectors as the covariance matrix $\mathbf{\Sigma}$ ($\mathbf{R}_x = \mathbf{U}\mathbf{D}\mathbf{U}^H$) [15, 16], where $\mathbf{D}$ is a non-negative diagonal matrix. Hence, the capacity will be only dependent on the singular values of the matrix $\mathbf{\Sigma}$. As a result, if the eigenvalues of matrices $\mathbf{R}$ and $\boldsymbol{\rho}$ are the same, for a given DAS and CAS, the corresponding capacity for the two systems is also identical. However, the DAS has more degrees of freedom/diversity available. Indeed, since for a DAS the eigenvalues change from geographical position to geographical position the system macro diversity is higher. Therefore, the probability of finding a system state with high symmetry and corresponding high-capacity gains increase. The impact of symmetry on the capacity gains will be analysed in following sections. In these sections, we verify that high symmetry imply higher capacity gains. On the other hand, for a CAS, the correlation structure is fixed implying that the corresponding

eigenvalues are fixed, and thus no inherent macro diversity is available. Thus, on average (i.e. over a given geographical area), the DAS will have higher capacity gains than a CAS. The same is true for the BER performance analysis. By using the factorization $\mathbf{R}_x = \mathbf{U}\mathbf{D}\mathbf{U}^H$, for the transmit signal covariance matrix, the channel capacity can be simplified to

$$\begin{aligned} C &= \mathbb{E}_{\mathbf{h}}\left[log\left(1+\frac{\mathbf{h}^{wH}\mathbf{\Lambda}^{1/2}\mathbf{D}\mathbf{\Lambda}^{1/2}\mathbf{h}^{w}}{\sigma^2}\right)\right] \\ &= \mathbb{E}_{\mathbf{h}}\left[log\left(1+\frac{\mathbf{h}^{wH}\mathbf{Q}\mathbf{h}^{w}}{\sigma^2}\right)\right] \end{aligned} \tag{3.8}$$

where $\mathbf{Q} = \mathbf{\Lambda}\mathbf{D}$ is a diagonal matrix since both $\mathbf{\Lambda}$ and $\mathbf{D}$ are diagonal. Let then $\mathbf{Q} = diag(Q_1, Q_2, \ldots, Q_N)$. Thus the ergodic capacity formula reduces to:

$$C = \mathbb{E}_{\mathbf{h}}\left[log\left(1+\sum_{i=1}^{N}\frac{|h_i^w|^2 Q_i}{\sigma^2}\right)\right] \tag{3.9}$$

where $\gamma_i = |h_i^w|^2 Q_i/\sigma^2$ is equal to the SNR associated to link i. According to [12] the $|h_i^w|^2$ random variable is exponential distributed and consequently γ_i. Defining γ as the sum of all links SNRs, $\gamma = \sum_{i=1}^{N}\gamma_i$, one gets

$$C = E_{\Gamma_N}[log(1+\gamma)] \tag{3.10}$$

where Γ_N is the random variable (RV) corresponding to the sum of N exponential distributed RVs with mean $\lambda_i^{-1} = Q_i/\sigma^2$ each, which obeys the PDF

$$f_{\Gamma_N}(\gamma) = \sum_{i=1}^{M}\sum_{n=1}^{K_i}\frac{a_{in}}{(n-1)!}\,\gamma^{n-1}e^{-\lambda_i\gamma} \tag{3.11}$$

In equation (3.11) M is the number of different mean SNRs, λ_i^{-1} is the mean SNR of link i, K_i is the number of antennas with SNR λ_i^{-1} and a_{in} are constants related to the partial fraction expansion [17] of the product of M Erlang distribution characteristic functions [18]. For more details on the derivation of the Γ_N RV PDF please see appendix section A.1.

According to equation (3.10) the ergodic capacity is then given by

$$C = \int_0^{\infty} log(1+\gamma) f_{\Gamma_N}(\gamma) dz \tag{3.12}$$

Using [8] or [19] for the evaluation of the integral we get

$$C = \sum_{i=1}^{M}\sum_{n=1}^{K_i}\sum_{k=0}^{n-1}\frac{a_{in}}{\lambda_i^n}\,C_i(\lambda_i, k) \tag{3.13}$$

where

$$C_i(\lambda_i, k) = \frac{(-\lambda_i)^k}{k!}\left[C_0(\lambda_i) + u(k-1)\sum_{p=1}^{k}\frac{(p-1)!}{(-\lambda_i)^p}\right]$$

$$C_0(\lambda_i) = e^{\lambda_i}E_1(\lambda_i)$$

$C_0(\lambda_i)$ is equal to the capacity of the link associated with a single transmit antenna, with SNR λ_i^{-1} and is also equal to $C_i(\lambda_i, 0)$. $E_1(x)$ is the exponential integral function, given by $E_1(x) = \int_x^{\infty} e^t/t\; dt$ and $u(n)$ is the unit step function.

Differential Capacity

In this section, we derive a recursive expression for the ergodic capacity. With this expression, we obtain a closed-form formula for the absolute differential capacity, which we define as the increase in capacity when starting with $N-1$ RAUs the terminal is connected to one more RAU. Based on that expression upper and lower bounds are derived, for the channel capacity.

Looking more carefully to the moment generating functions (MGF) and PDF of random variables Γ_N and Γ_{N-1} one can see that their difference has interesting properties. Namely, by using the MGF inverse function, $\mathcal{M}_x^{-1}[F(jw)] = \frac{1}{2\pi}\int_{-\infty}^{\infty}\varphi(jw)e^{-jwx}\,dw$, over $\varphi_{\Gamma_N}(jw)$ (the MGF of $f_{\Gamma_N}(\gamma)$) one obtains

$$\begin{aligned} f_{\Gamma_N}(\gamma) - f_{\Gamma_{N-1}}(\gamma) &= \mathcal{M}_{\Gamma}^{-1}[\varphi_{\Gamma_N}(jw) - \varphi_{\Gamma_{N-1}}(jw)] \\ &= \mathcal{M}_{\Gamma}^{-1}\left[\left[\frac{\lambda_N}{\lambda_N - jw} - 1\right]\varphi_{\Gamma_{N-1}}(jw)\right] \\ &= \frac{1}{\lambda_N}\mathcal{M}_{\Gamma}^{-1}[jw\;\varphi_{\Gamma_N}(jw)] \\ &= -\frac{1}{\lambda_N}\frac{df_{\Gamma_N}(\gamma)}{d\gamma} \end{aligned} \tag{3.14}$$

where $\varphi_{\Gamma_N}(s) = \prod_{i=1}^{M}\left(\frac{\lambda_i}{\lambda_i - s}\right)^{K_i}$. By using the random variable transformation rules one can obtain the following PDF transformation rule, from the Γ_{N-1} to the Γ_N RV

$$f_{\Gamma_N}(\gamma) = \lambda_N\, e^{-\lambda_N\gamma}\int_0^{\gamma} f_{\Gamma_{N-1}}(x)\, e^{\lambda_N x}\, dx \tag{3.15}$$

Indeed, the previous equation obeys the differential equation (3.14) and is a valid PDF function, since $\int_0^{+\infty} f_{\Gamma_N(\gamma)} = 1$. With the previous equation, one can obtain an exact recursive algorithm for the calculation of the a_{in} coefficients. Therefore, by using the previous developed tools, namely equation (3.14), we can obtain the absolute capacity difference by the user connection to one more RAU

$$\Delta C_{N-1}^{N} = C_N - C_{N-1} = I_N\lambda_N^{-1} \tag{3.16}$$

where

$$\begin{aligned} I_N &= -\int_0^{\infty}\frac{df_{\Gamma_N}(\gamma)}{d\gamma}\, log(1+\gamma)\, d\gamma \\ &= \int_0^{\infty}\frac{f_{\Gamma_N}(\gamma)}{1+\gamma}\, d\gamma = \sum_{i=1}^{M}\sum_{n=1}^{K_i}\frac{a_{in}}{\lambda_i^{n-1}}\, C_i(\lambda_i, n-1) \end{aligned} \tag{3.17}$$

Another way to express the differential capacity is (see appendix section A.2)

$$\begin{aligned} \Delta C_{N-1}^{N} = &\frac{\lambda_{N-1}}{\lambda_N}\Delta C_{N-2}^{N-1} \\ &+ \frac{1}{\lambda_N^2}\left[f_{\Gamma_N}(0) - \int_0^{\infty}\frac{f_{\Gamma_N}(\gamma)}{(1+\gamma)^2}\, d\gamma\right] \end{aligned} \tag{3.18}$$

where $f_{\Gamma_N}(0)$ is equal to 0 for $N > 1$ and equal to λ_1 for $N = 1$. This new expression can be used to obtain the following upper bound (see appendix section A.2)

$$\Delta C_{N-1}^{N} \leq \frac{\lambda_{N-1}}{\lambda_N} \Delta C_{N-2}^{N-1}, \quad N > 1 \tag{3.19}$$

Differential Capacity Bounds

The $g(\gamma) = 1/(1+\gamma)$ function is always less than one for all γ in $[0, \infty[$. Thus, we can easily get a simple upper bound for the DCAP

$$\Delta C_{N-1}^{N} = \frac{I_N}{\lambda_N} \leq \frac{1}{\lambda_N} \int_0^{\infty} f_{\Gamma_N}(\gamma)\, d\gamma = \lambda_N^{-1} \tag{3.20}$$

and by consequence

$$C_N \leq \sum_{k=1}^{N} \lambda_k^{-1} = \sum_{i=1}^{M} K_i\, \lambda_i^{-1} \tag{3.21}$$

Tighter bounds can be derived verifying that the $g(\gamma)$ function is also always greater or equal than $e^{-\gamma}$ (Bernoulli's inequality) for all γ in $[0, \infty[$, with a maximum difference of $(M_d \approx 0.204)$[2] so

$$e^{-\gamma} \leq g(\gamma) \leq e^{-\gamma} + M_d \tag{3.22}$$

and consequently

$$\frac{\varphi_{\Gamma_N}(-1)}{\lambda_N} \leq \Delta C_{N-1}^{N} \leq \frac{\varphi_{\Gamma_N}(-1)}{\lambda_N} + \frac{M_d}{\lambda_N} \tag{3.23}$$

where $\varphi_{\Gamma_N}(s)$ is the Γ_N RV MGF.

From the upper bound (3.20) and from the lower bound from equation (3.23) one can see that in the case of low SNR's the DCAP can be approximated by λ_N^{-1}, since as λ_i tends to infinity (low SNR) $\varphi_{\Gamma_N}(-1)$ tends to 1. Thus the capacity expression for low SNR's is given by

$$C_N \approx \sum_{i=1}^{N} K_i\, \lambda_i^{-1} \tag{3.24}$$

Assuming that the new mean SNR is the smallest one, it can be shown that the maximum DCAP is achieved when all RAUs have the same mean SNR, in other words, when they are co-located, see appendix section A.3

$$\begin{gathered} \Delta C_{N-1}^{N}(\lambda_1, \ldots, \lambda_N) \leq \Delta C_{N-1}^{N}(\lambda_N, \ldots, \lambda_N) \\ \lambda_N \geq \lambda_n, \forall\, n \in [1, 2, \ldots, N-1] \end{gathered} \tag{3.25}$$

In the high SNR limit the previous expression is maximal and equal to, see appendix A.4

$$\lim_{\lambda_N \to 0} \Delta C_{N-1}^{N}(\lambda_N, \ldots, \lambda_N) = \frac{1}{N-1} \tag{3.26}$$

Thus in the limit case of high SNR we can see that the DCAP value is independent of the SNR, and only depends on the number of connected RAUs to the mobile terminal. This maximum can be approached with a difference of less than 0.1 bps/Hz if all mean SNR's are

[2] Obtained numerically, and knowing that this maximum is global.

equal and higher than 17 dB. As a result, any channel asymmetry[3] in the system, either the path loss (for a DAS), or the correlation (for a CAS) imply smaller capacity gains, since they entail different mean link SNRs. This can be explained by the fact that large asymmetries in the system, at a given geographical position, imply that cooperation is not worth adding the effort of additional processing at the CU, due to the diminished expect returns.

The previous expression can be considered as a limit bound, but a tighter bound for the general case maximum achievable DCAP can be obtained (please look at appendix sections A.3 and A.4)

$$\Delta C_{N-1}^{N} \leq \frac{1}{\lambda_N + N - 1} \leq \frac{1}{N-1} \tag{3.27}$$

Therefore the DCAP, by the connection to K new antennas, is upper bounded by:

$$\Delta C_{1}^{K+1} \leq \sum_{n=2}^{K+1} \frac{1}{n-1} = \sum_{n=1}^{K} \frac{1}{n} \tag{3.28}$$

with equality if all SNR's are equal and high.

For a high number of antennas this formula can be approximated by:

$$\Delta C_{1}^{K+1} \leq \sum_{n=1}^{K} \frac{1}{n} \approx \varrho + log(K) \tag{3.29}$$

and upper bounded by:

$$\Delta C_{1}^{K+1} \leq \sum_{n=1}^{K} \frac{1}{n} \leq \varrho + log(1+K) \tag{3.30}$$

where ϱ is the Euler constant (0.577215665). So as the number of connected RAUs increase, the DCAP is smaller and smaller, because $1/K$ decreases as K increases. If the number of RAUs grows to infinity so does the capacity, but of course in practice one can only have a limited number of RAUs and the complexity will also scale up with the number of RAUs. Hence, a trade-off must be made between the number of RAUs jointly processed, and the complexity introduced.

Numerical Results

To have a better idea about the behavior of the DCAP values, let us start by looking to the DCAP values on representative geographical locations. More specifically, let us evaluate the system capacity, using (3.16), first for a user moving from point A to B, (red line Figure 3.1) and secondly for a user moving from point A to point C (green line Figure 3.1), for a DAS. The RAU coverage radius considered was 100m. As can be seen from Figure 3.3, the system capacity always increases but the amount of gain, as N increases, gets smaller, as expected. The gain becomes larger as we get farther away from RAU1, since the user is getting closer to the boundaries of the coverage area of RAU1 and of another RAU, and consequently the corresponding mean link SNRs are approaching each other, decreasing the existing asymmetries. A user moving over the red line will only cross the boundary of RAU2, at point B, and thus just the first DCAP value is big, in comparison to the other DCAP values. On the other hand, a user moving over the green line will cross two boundaries, at the same point (C), and as a result the corresponding first two DCAP values are large. The

[3]By system symmetry we mean that all average SNRs are equal.

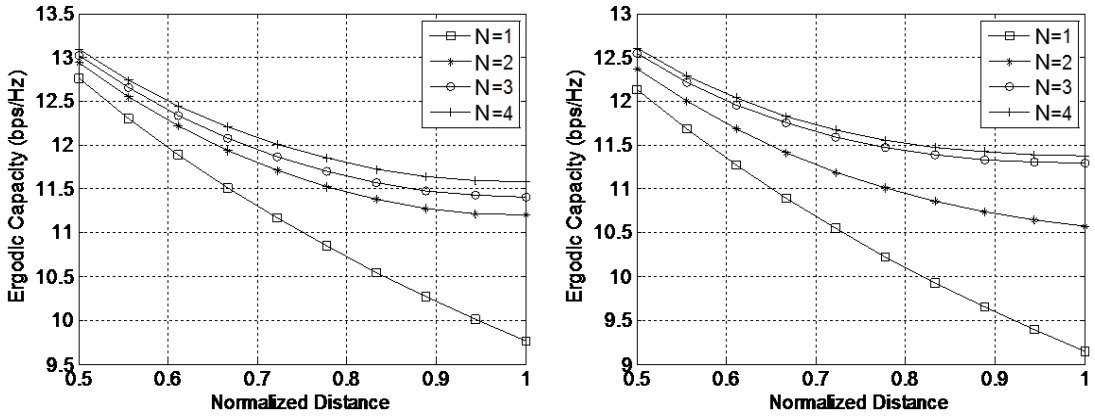

(a) Capacity variation over red line (Figure 3.1). (b) Capacity variation over green line (Figure 3.1).

Figure 3.3: Ergodic channel capacity, for different number of transmit antennas, at varying distances from RAU1 (Figure 3.1) and for a RAU coverage radius, R = 100. RAU connection order: connect first the closest antennas to the user, at each geographical position.

---

corresponding DCAP values for point (C), one of the points with the highest symmetry, and for two different RAU coverage radius are shown in Figure 3.4. In this figure we also plot the bound $1/(N-1)$, since this is the maximum DCAP that any user can get, in any position, as seen previously. As can be seen from that figure, when the new connected RAU has a mean SNR equal to a previous RAU, like RAU4 and RAU7, the DCAP is approximately equal to the beforehand connected RAU and when it changes, the DCAP value also changes, as already verified from bound (3.19). This can be explained by the DCAP ratio ($\Delta C_{N-1}^{N}/\Delta C_{N-2}^{N-1}$) bound, shown in (3.19). In a circular ring this upper bound takes the value 1, and thus the DCAP is approximately constant. However, this approximation is not always tight. To have a better insight into the sensitivity of the DCAP with the SNR variation and to verify where the bound shown in (3.19) is tight we plot in 3.5 the DCAP ratio for consecutive connected RAUs and also the previously stated bound, again for point C. As can be seen from that figure the DCAP ratio is well approximated by the ratio λ_{N-1}/λ_N, when the new mean SNR is different from the previous one and as N increases the approximation becomes tighter. For a small number of RAUs this approximation is bad and the DCAP values change even for a circular ring. Thus, one can conclude that a user in a RAU coverage boundary attains the highest DCAP values due to the existence of links with the same, or similar, mean SNRs, getting the most from the diversity of receiving simultaneously from more than one RAU.

To understand better the impact of the symmetry in the DCAP values we propose to analyze next a more symmetric geographical RAU placement, namely the one presented in Figure 3.6. In the next paragraphs, we evaluate as well the tightness of the bounds (equations (3.21), (3.23), (3.26), (3.27)) and analyze the DCAP variation as a function of the average SNRs. Additionally, we further perform an analysis of a representative area of the corresponding grid remote antenna placement, for a target capacity increase. This will allow us to see how many neighbour RAUs are able to fulfil the given capacity requirements and to attest the symmetry properties.

In Figure 3.7 we show, for the central area point (the origin $(0,0)$) and for a point that

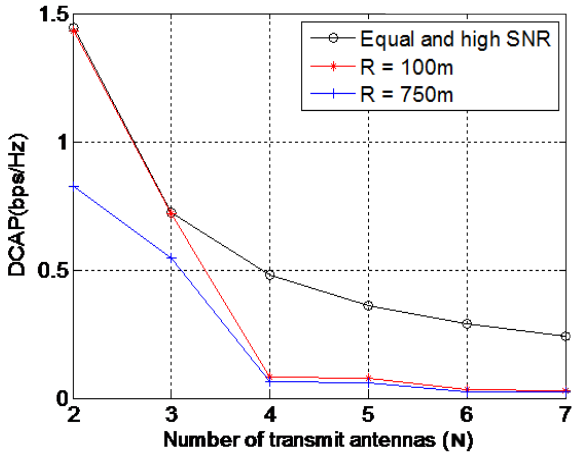

Figure 3.4: Exact DCAP values and bound $1/(N-1)$ (Nats/s/Hz), for the point C of scenario depicted in 3.1, and for two different RAU coverage radius, R = 100m and R = 750m. RAU connection order: RAU $1, 2, 3, 4, 7, 5, 6$.

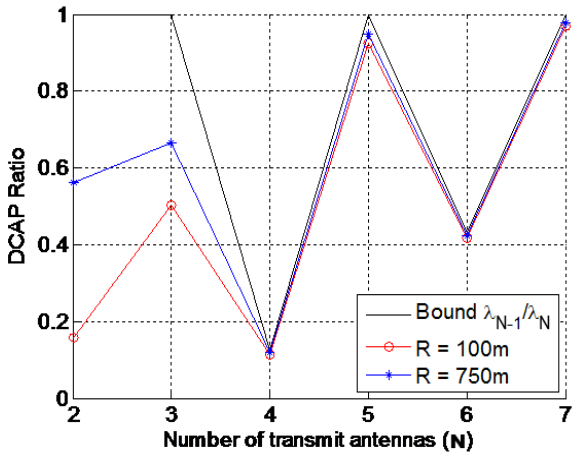

Figure 3.5: DCAP variation with respect to N, for the point C of scenario depicted in Figure 3.1, and for two different RAU coverage radius, R = 100m and R = 750m. RAU connection order: RAU $1, 2, 3, 4, 7, 5, 6$.

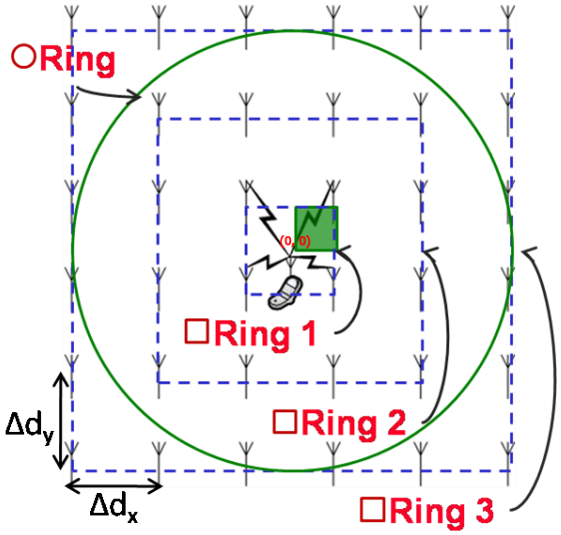

Figure 3.6: Geographical remote antenna placement.

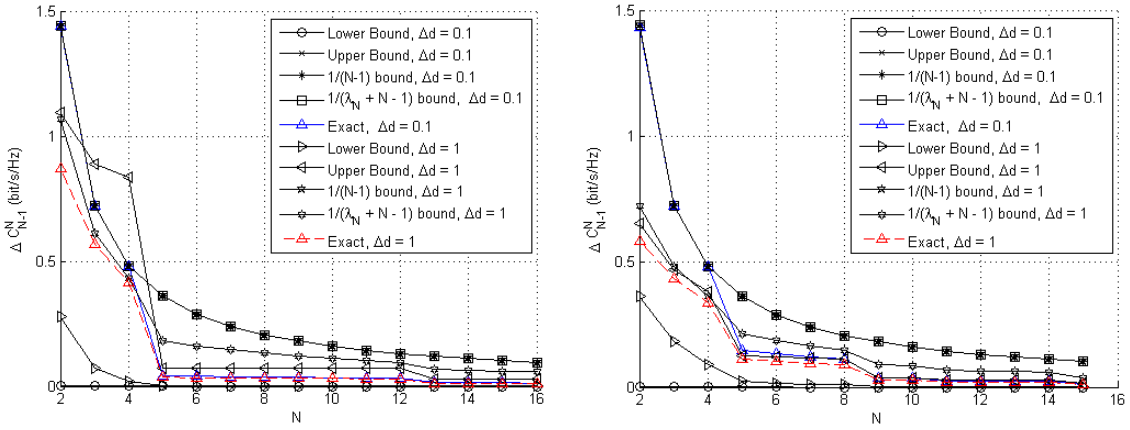

(a) Central Point.

(b) $(0.5\Delta d_x, 0.5\Delta d_y)$ Point.

Figure 3.7: Differential capacity by the connection to one more RAU, exact, upper and lower bounds.

is in the same place as one of the RAUs of the configuration in Figure 3.6, a plot of exact, upper and lower bounds of ΔC_{N-1}^{N}. In the second point we do not take into account the closest RAU. In this analysis, we evaluate the aforementioned expressions on two distinct cases, one for which the inter RAU distance is equal to $\Delta d = 1$ Kilometer and another for which $\Delta d = 0.1$ Kilometer, considering that $\Delta d_x = \Delta d_y = \Delta d$.

We can see from this figure that when we begin to connect to the next circular ring antennas the DCAP value decrease a lot and while we stay in a given circular ring, the DCAP keeps constant, as seen before. Nevertheless, for this RAU configuration, this fact is more evident due to the increased symmetry. This approximation of a constant capacity increase in a circular ring is better for rings far apart of the user. This can be explained by the fact

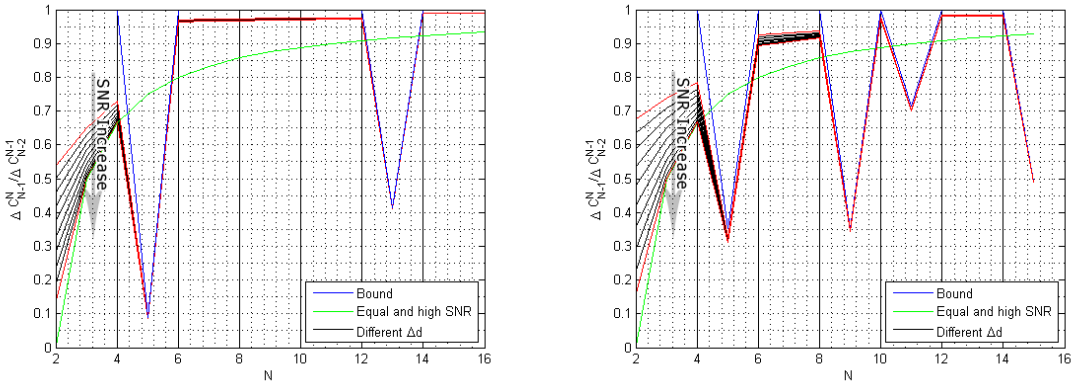

(a) Central Point.

(b) $(0.5\Delta d_x, 0.5\Delta d_y)$ Point.

Figure 3.8: Differential capacity variation with respect to N.

that in the upper bound, equation (3.23), $\varphi_{\Gamma_N}(-1)$ tends to zero as we connect to more and more RAUs. As a consequence the bound becomes independent of all SNR's, minus the new one. It can also be explained by the bound of equation (3.19) since, the ratio $\frac{\lambda_{N-1}}{\lambda_N}$ is equal to 1 for a circular ring.

This figure also shows that for high SNR's the best bound is the one from equation (3.27), but for low SNR's the upper bound provided by (3.23) is more precise. The upper bound provided by equation (3.23), for the case of $\Delta d = 0.1$ Kilometer, is not shown in this figure because its higher than the bound provided by equation (3.27) for all N. It is also important to stress that the most interesting bounds are the ones that are accurate for a small number of RAUs, equation (3.27), because the user will probably only connect to a small number of RAUs due to the diminishing returns one gets as the number of connected RAUs increases. Indeed this bound in addition of being the tightest, for a low number of connected RAUs, is also the one that requires less information to be evaluated (only the SNR of the new RAU).

These two figures, more specifically the red and blue lines, show a convergence of the DCAP to a same value as the terminal connect to more and more RAUs, in the case of SNR vectors that are multiple among themselves. It is easy to prove that as the SNR's increase this convergence occurs at a smaller N and in the case of high SNR's the DCAP cannot be higher than a given value/line, having as the ultimate line $1/(N-1)$ in the case of all equal SNR's. Showing in that way that if we bring all RAUs closer to the terminal, by a given factor, we only obtain an increase in the DCAP in the closest RAUs.

Another aspect that it is worthwhile to analyze, as seen previously, is the variation / sensitivity of the DCAP value with respect to N. In this context, we have evaluated the DCAP ratio, $\Delta C_{N-1}^{N}/\Delta C_{N-2}^{N-1}$, and plotted it in figures 3.8(a) and 3.8(b), for the same two previously used points and for a group of inter RAU distances between 0.1 and 1 Kilometer, with increments of 0.1 Kilometer, which corresponds to SNR's in the range of approximately $-10dB$ to $35dB$. As a reference a plot of the bound given by the first term of equation (3.18) and a plot of the same ratio but for the case of all equal and high SNRs is also represented in these figures, in blue and green respectively. One can see from this two figures that the ratio variation with respect to the mean SNR decreases as the number of connected RAUs increase. Therefore, for the farther RAUs the capacity ratio becomes insensitive to the SNR and is mainly

influenced by the RAU geographical positioning. Nevertheless, the same is not true for the closest RAUs. Hence, for the closest RAUs, both their geographical disposal and distance to the user influence the gains obtained by the connection of the user to new RAUs. From these figures, one can also see that the difference between the exact ratio value and the respective bound gets tighter for a higher number of transmit antennas and that at the turning points from one circular ring to another this bound is very tight.

In the next paragraphs we will perform a DCAP analysis for a representative area covered by the RAUs. For this analysis, we consider $\Delta d_x = \Delta d_y = 1$ Kilometer. Namely, we consider a target DCAP and analyze, for a given set of user positions, the number of RAUs which imply a DCAP higher than the defined target. The RAU connection order is from the closest to the farthest. In this context, the results presented in Figure 3.9 are obtained, for a target DCAP of 0.2 bps/Hz (1 bit = log(2) Nats). The region shown in this figure is the green one in Figure 3.6. Just to give an example, consider the user position, i.e. the point (0.2, 0.4). For this position, the corresponding N is equal to 2, which indicates that when the user connects to the first and second ($N = 2$) RAUs he obtains a capacity increase greater than 0.2 bps/Hz but departing from that number of RAUs, from 2 to 3, 3 to 4, ..., the capacity increase obtained is less than 0.2 bps/Hz. As can be seen from Figure 3.9, for this case, only the first ring, i.e. the four closest RAUs, is used. Moreover, this figure also shows a circular pattern in the number of RAUs needed to achieve the target. This is related to the fact that the received SNR from one RAU is always equal at a distance d from that RAU. For instance, the $(0, 0)$ point, in the middle of the area, has the greatest number of RAUs, retrieving in that way more system capacity. Such a fact stems from the high symmetry properties of this user position. Indeed for the area close to a given RAU only one RAU is needed. On the other hand, for the area on the borders of the area covered by the four RAUs the four RAUs should be used to serve the user, since each connection implies an increase in capacity higher than the target. Moreover, we can get an estimate of the number of RAUs a user should connect to, from the bounds provided in section 3.5.1. Let us consider the user position $(0, 0)$. From the upper bound $1/(N-1)$ we get that for a target increase in capacity of 0.2 bps/Hz the user must not connect to more than 8 RAUs. On the other hand, if some additional information is used, namely the mean SNR of the new connected RAU, we can get a better bound on the number of RAUs that attains the target increase in capacity. By using the fact that the SNR at a distance of 1 Kilometer from the user is 0 dB, and that the closest four RAUs are at a distance of $\sqrt{2}/2$ Kilometer we get from the $1/(\lambda_N+N-1)$ bound that the capacity increase for the fourth RAU is lower than $1/((\sqrt{2}/2)^3+4-1)/log(2) \approx 0.43$ bps/Hz (the exponent 3 corresponds to the path loss exponent). For this reason, it is possible to achieve a DCAP higher than 0.2 bps/Hz using the forth RAU. Nevertheless, for the fifth RAU their distance to the user is $\sqrt{10}/2$. Therefore, his DCAP is upper bounded by $1/((\sqrt{10}/2)^3+5-1)/log(2) \approx 0.18$ bps/Hz. As a consequence, by using just this simple upper bound we can get to the conclusion that only the four closest RAUs could lead to an increase in capacity higher than the target (0.2 bps/Hz). Therefore, one can see that for a given target DCAP it is mostly how the RAUs are distributed in a given geographical area that influences the gains obtained by the connection of the user to more RAUs and not the distance between the RAUs. Hence the importance of the symmetry in the RAUs distribution.

3.5.2 Multi-User Scenario

In the previous paragraphs, we have studied the DCAP sensitivity to the link's SNR variation, for the single-user case. Indeed, we have verified that the DCAP is maximized

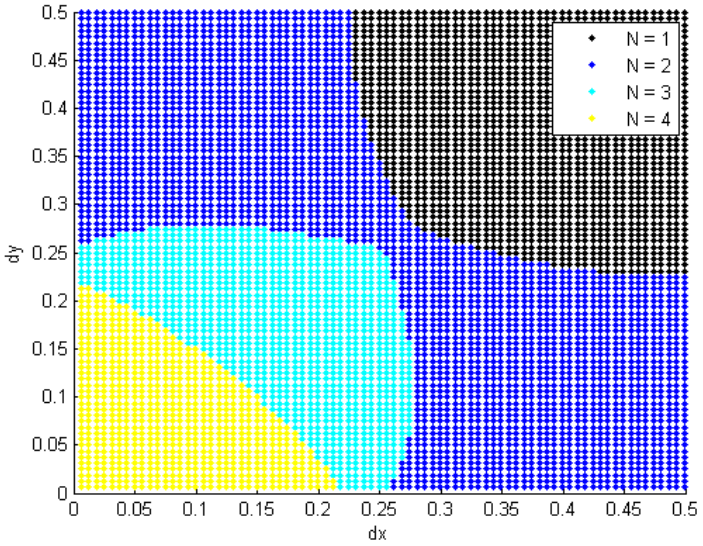

Figure 3.9: Number of RAUs till where the differential capacity is greater than 0.2 bps/Hz.

in the high SNR regime and when all RAUs have a similar link SNR. Even, if that study can provide some useful and interesting insights on the behavior of the DCAP, it is in some way limited, since, in a real system more than one user are normally available. Hence it is important to consider the multi-user case, in more detail. However, for the multi-user case the system capacity is not as easy to analyze, as the one for the single-user case, due to some additional constraints in the transmit covariance matrix and from the fact that there is no known closed-form solution, for this matrix, that maximizes the channel sum-capacity. Indeed to obtain the optimal power allocation matrix an iterative algorithm should be used [20]. Nevertheless, for the high SNR regime and for the case of more transmit than aggregate receive antennas equal power allocation is asymptotically optimal [5]. Since it is also in the high SNR regime that the DCAP is maximized, for the single-user case, from now on we only consider this regime. Hence, as an extension to the single-user scenario, we consider a multi-user scenario, both with more transmit than aggregate receive antennas and vice-versa. For simplicity, for this scenario, we first study the DCAP for the co-located antenna case, i.e. with equal path losses, considering independent channels paths. Finally, we will look to the distributed antennas case.

Broadcast Channel Sum-Capacity

A broadcast channel is a communication channel in which there is one sender and two or more receivers [21]. Recently, in [6], the authors have shown that the DPC rate region is the capacity region of the Gaussian MIMO BC. The DPC sum rate with a total power constraint, $(\sum_k q_k \leq P)$, can be expressed, from the MIMO BC-MAC duality, [22–24], by

$$\mathbf{C}_{DPC}^{(N,K)} = \max_{\sum_k q_k \leq P} log\left|\mathbf{I}_N + \sum_{k=1}^{K} \mathbf{h}_k^H q_k \mathbf{h}_k\right| = \max_{tr(\mathbf{Q})\leq P} log\left|\mathbf{I}_N + \mathbf{H}^H \mathbf{Q} \mathbf{H}\right| \tag{3.31}$$

where q_k is the transmit covariance in the dual MAC, $\mathbf{H}^H = [\mathbf{H}_1^H, \ldots, \mathbf{H}_K^H]$ denote the concatenation of all user's channels and $\mathbf{Q} = diag(q_1, \ldots, q_K)$ is a block-diagonal matrix. In the high SNR regime and for $K \leq N$, equal power allocation, $q_k = \frac{P}{KN}$, has been proven to be asymptotically optimal [5]. As a consequence, the following affine approximation to the sum-capacity can be made [5], [25].

$$\mathbf{C}_{DPC}^{(N,K)} \approx K log\, P - K log\, K + log|\mathbf{H}\mathbf{H}^H| \tag{3.32}$$

From which we can see that in the high SNR regime the sum-capacity of the MIMO BC scales like K. Unfortunately, the same cannot be said for the case of more aggregate receive than transmit antennas, $K > N$. For this case, equal power allocation is not asymptotic optimal, since for the standard degraded BC ($N = 1$) the throughput is maximized by transmitting to the best user only [26].

Differential Capacity

One aspect that is worth being investigated, for the multi-user case, is the scaling of the DCAP with the number of users. Let us consider first, for simplicity, a CAS without correlation between channels ($\mathbf{R} = \boldsymbol{\rho}_k = \mathbf{I}$) and next extend the results to a DAS. Let us start with the $N \geq K$ case and after consider the $K \geq N$ case. According to equation (3.32), for $N \geq K$, the DCAP can be expressed by

$$\begin{aligned} \Delta C_{N-1,K}^{N,K} &= \mathbb{E}[\mathbf{C}_{DPC}^{(N,K)} - \mathbf{C}_{DPC}^{(N-1,K)}] \\ &= \mathbb{E}[log|\overline{\mathbf{H}}_N \overline{\mathbf{H}}_N^H|] - \mathbb{E}[log|\overline{\mathbf{H}}_{N-1} \overline{\mathbf{H}}_{N-1}^H|] \end{aligned} \tag{3.33}$$

where $\overline{\mathbf{H}}_i$, $(i = N, N+1)$ is the channel matrix for a CAS with i transmit antennas. As a consequence, for $N \geq K$, the ergodic DCAP is only dependent on the matrix $\mathbf{H}$ distribution. On the other hand, for $K > N$, the DCAP can be expressed by

$$\begin{aligned} \Delta C_{N-1,K}^{N,K} &= \mathbb{E}[\mathbf{C}_{DPC}^{(N,K)} - \mathbf{C}_{DPC}^{(N-1,K)}] \\ &= \mathbb{E}[\mathbf{C}_{DPC}^{(N,N)} + \Delta C_{N,N}^{N,K} - (\mathbf{C}_{DPC}^{(N-1,N-1)} + \Delta C_{N-1,N-1}^{N-1,K})] \\ &= \Delta C_{N-1,N-1}^{N,N} + \Delta C_{N,N}^{N,K} - \Delta C_{N-1,N-1}^{N-1,K} \\ &= log(P) + \Delta \end{aligned} \tag{3.34}$$

where Δ is equal to $\Delta C_{N,N}^{N,K} - \Delta C_{N-1,N-1}^{N-1,K}$ plus the power offset gain provided when we pass from $N-1$ to N transmit antennas and users[4] , which is very close to $-log(e) = -1$. In the passage from the second to the third line, of equation (3.34), a slight abuse of notation has been used, since we denote the average and a given instantiation of a random variable by the same variable. However, we think that it is easy to understand and the definition of additional variables will be cumbersome. From the previous equation, we see that, for $K \geq N$, the DCAP would be power dependent, differing from the $N \geq K$ case. Hence, it is important to analyze the gain Δ, i.e. the power offset factor. This analysis is made in the following sections.

[4] $\Delta C_{N-1,N-1}^{N,N} \approx log(P) + log(N-1+\beta) + (N-1)log(N-1) - NlogN \approx log(P) - log(e)$

DCAP for $N \geq K$

In this sub-section we derive a closed-form expression for the DCAP for DPC and ZF, considering that all transmit antennas are co-located. For the general case, of a DAS, a numerical analysis is provided, please refer to section 3.5.3. For DPC, as shown in appendix (Appendix A.5), the DCAP can be expressed by

$$\begin{aligned} \Delta C_{N-1,K}^{N,K} &= \sum_{n=N-K+1}^{N} \frac{1}{n-1} = \sum_{n=N-K+1}^{N} \Delta C_{n-1,1}^{n,1} \\ &\approx log\left(1 + \frac{K}{N-1-K+\beta}\right) \end{aligned} \tag{3.35}$$

where $\beta = e^{1-\gamma} - 1$. Taking into account equation (3.35) and using the BC equivalent point to point MIMO interpretation in the high SNR regime [5], we can say that the DCAP for ZF is equal to K times the DCAP of DPC for a $(N-(K-1)) \times 1$ channel. Therefore the DCAP for ZF can be expressed by

$$\overline{\Delta C}_{N-1,K}^{N,K} \approx K log\left(1 + \frac{1}{N-1-K+\beta}\right) \tag{3.36}$$

From which we can see that asymptotically in the number of transmit antennas N, the DCAP behaves like $K/(N-K+\beta)$ for both DPC and ZF. Thus the gains are almost the same when a high number of transmit antennas is considered. However, for a finite number of transmit antennas the DCAP gains provided by DPC are lower and the difference increases with K, as can be seen by equations (3.35) and (3.36). From (3.35) it is easy to see that the DCAP scales logarithmically with the number of users, for the optimal scheme (DPC), if $N-K$ is kept constant. Thus, the gain by the connection of additional RAUs will, in some sense, saturate, since their increase rate will be smaller and smaller as more users are considered. In that way, the DCAP value that we obtain for a small number of users will be only slightly lower than the one for a higher number of users.

DCAP for $K \geq N$

When $K \geq N$ equal power allocation ceases to be asymptotically optimal, and some form of iterative water-filling algorithm must be used to allocate power between users [20]. As a result of that complication it does not appear to be possible to obtain a closed-form expression for DCAP. However, for the case of only one transmit antenna it is optimal to transmit at full power to the best user [26] and as shown in the appendix (subsection A.6), the maximum increase in capacity, when one new user is added to the system, is obtained when all users are co-located, i.e. when they have equal SNRs. Therefore, for the high SNR regime, the increase in capacity, by the connection of an additional user, for $N = 1$, can be expressed by, see appendix (subsection A.6)

$$\Delta C_{1,K-1}^{1,K} = \sum_{n=0}^{K-1} \binom{K-1}{n} (-1)^{n+1} log(n+1) \tag{3.37}$$

However to analyse the DCAP, for $K > N$, we need also to know that value for $N > 1$. Thus, in order to obtain an approximation to the increase in capacity obtained by the connection of

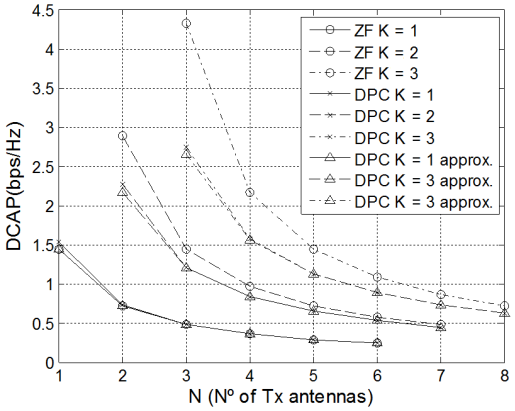

Figure 3.10: DCAP values for a multiuser co-located scenario with uncorrelated channel paths, for a number of users in the range 1 to 4, in the high SNR regime.

---

a new user to the system, when more than one transmit antenna is considered, we have done an extrapolation of equation (3.37), taking into account equation (3.35) line 1

$$\Delta C_{N,K-1}^{N,K} \approx \sum_{n=K-N+1}^{K} \Delta C_{1,n-1}^{1,n} \tag{3.38}$$

and as shown in section 3.5.3 (Figure 3.12(a)), this approximation is very close to the values obtained by numerical simulations and is better for a high number of users. This approximation will be used in section 3.5.3 to obtain an approximation for Δ in equation (3.34).

3.5.3 Numerical Results

In this section, expressions (3.35) and (3.36) are analysed to compare the DCAP gain of DPC to ZF. Next we analyse the DCAP for a DAS considering a scenario with 4 transmit RAUs and 2 users, each with only one receive antenna. Finally, for $K \geq N$ we analyse the DCAP for the case of all equal mean SNRs, namely we analyse the capacity increase provided by the connection of a new user and the power offset gain (Δ).

In Figure 3.10 we compare DPC and ZF in terms of DCAP, for a different number of users and transmit RAUs. From that figures one can see that the logarithm approximation although simple is very tight. Concerning the benefits of the connection of new transmit RAUs, ZF has higher gains than DPC and the difference increase with K. As a result of that analysis, we observe that as a scheme gets closer to the optimal one, the gains obtained by the connection of more RAUs at the transmitter side decrease. As a consequence the connection to additional RAUs/cooperation is more beneficial for lower complexity schemes, since they do not use the available resources up to the optimum performance. However, the optimal scheme has a higher sum-capacity and complexity, thus a careful choice must be made taking into account the costs/benefits ratio, for a given architecture. We can also see from Figure 3.10 that all schemes converge to the same DCAP value for a high number of transmit RAUs and that the convergence point increases with K. This happens since equations (3.35) and (3.36)

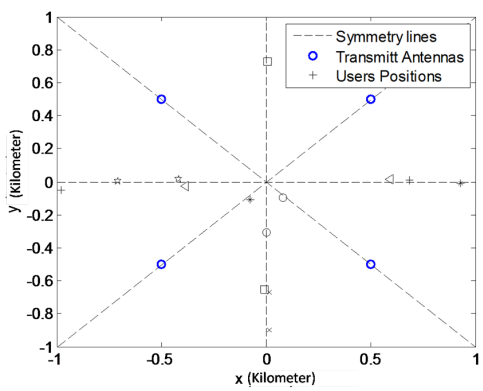

(a) User's position, where distributed DCAP is higher than co-located DCAP.

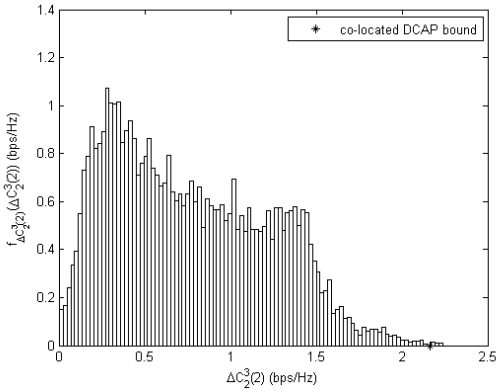

(b) DCAP distribution for $N = 2$.

Figure 3.11: Differential capacity distribution for a uniform user distribution and users positions where the distributed DCAP is higher than the co-located DCAP.

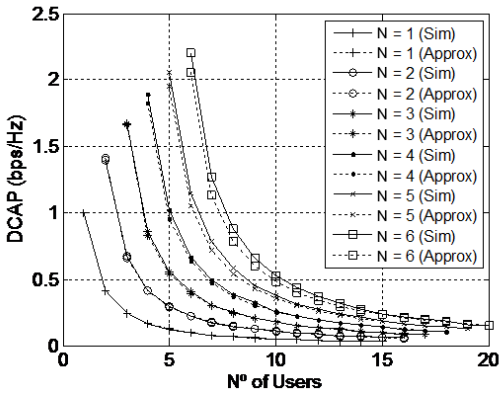

(a) Capacity increase by the connection of a new user.

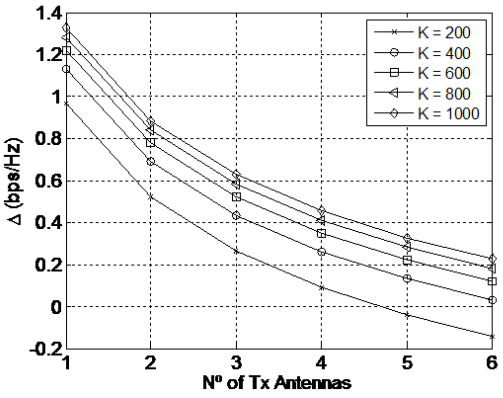

(b) Δ factor value.

Figure 3.12: Capacity increase by the connection of one more transmit RAU to the system, for $K \geq N$.

---

have identical asymptotic behaviour with N. Indeed, we think that this behaviour starts to show when the sum-capacity of both schemes get close to one another. For ZF this happens when there are enough degrees of freedom available, to cope with its not so good performance, to alleviate the properties of the matrix to be "inverted". For a higher number of users this obviously happens for a higher number of connected RAUs.

We have seen, in the single-user case, that the user positions with the highest DCAP values are the ones with highest symmetry to the RAUs. Will this be also true for the distributed case? To investigate that we have studied, in the previous paragraphs, the DCAP for a CAS with uncorrelated channel paths. However, to extend the CAS DCAP results to a DAS we will rely on numerical simulations. In that numerical simulations we have considered a scenario with 4 uncorrelated transmit RAUs (blue circles in Figure 3.11(a) and 2 users and

have evaluated the respective DCAP values, for a high number of uniformly draw positions. In the numerical simulation, for the channel model we have considered only path loss and Rayleigh multipath fading. The users positions were randomly generated according to a uniform distribution in the $[-1,1]\times[-1,1]$ Kilometer square. Ten thousand random positions were generated for each user and the DCAP was averaged over 10000 trials. The results from this simulation are shown in Figure 3.11. More precisely we plot in Figure 3.11(a) the users positions that attain the highest DCAP values, when the third RAU is connected to the CU. Each pair of equal black markers represent the positions of each user. As can be seen from that figure the users positions with the highest DCAP values are like, in the single-user case, in the symmetry lines defined by the transmit RAUs, more precisely in the coverage boundaries of each RAU. The corresponding DCAP value, for such positions, is very close to the one obtained for the uncorrelated CAS, analyzed before. In that way, the newly connected RAU has the same distribution as the previous one, in a similar manner as for the co-located case. Thus, system symmetry plays, again, an important role in obtaining most of the DCAP gains, like in the single-user scenario. Indeed, as an example, we show the distribution of the DCAP values, for the third connected RAU, in Figure 3.11. In this figure, the CAS bound of equation (3.35) is shown by a black star. From these results, one can see that most of the points have a smaller DCAP than bound (3.35). We can also notice that when we pass from 2 to 3 connected RAUs, Figure 3.11(b), 7 points exceed the bound (2.16 bps/Hz). Therefore, we can conclude that even if the DCAP for the distributed case can be higher than the DCAP for the co-located case, it will not be much higher and the number of points in that condition will be small and in a condition with high symmetry.

For the case of more aggregate receive than transmit antennas we have analysed the Δ factor in equation (3.34). To do that, a numerical analysis has been made, considering that every column of $\mathbf{H}$ is $\tilde{\mathcal{N}}_{KN}(0,\mathbf{I})$ distributed. To obtain the optimal power allocation among users the algorithm presented in [20] has been used. In Figure 3.12(a) we plot the increase in ergodic capacity, obtained by numerical simulation and averaged over 100000 trials, when one new user is added to the system, for a given number of transmit RAUs N. We also plot, in this figure, the approximation of equation (3.38), which is very close to the obtained numerical results. Indeed, the results obtained by the connection of additional users are quite similar to the ones obtained by the connection of additional RAUs, but the gains are lower. Nevertheless, the availability of users, in a network, is normally higher than the one of the RAUs. Consequently, even if these gains are lower they can be achieved more easily, if the right users are chosen. Indeed, we have verified that for the case of just one RAU $N=1$, it is the best to choose the users with the highest symmetry, i.e. with the same mean SNR. Considering the tightness of our approximation, equation (3.38), we can say, as an approximation, that the same happens if a higher number of RAUs is considered. Therefore, symmetry seems to be important both to the case of the connection of additional users and of additional RAUs. Taking into account that approximation in our analysis, in Figure 3.12(b) we plot the Δ factor values for different number of users and see that even for 1000 users this factor is small. Moreover, the power offset gain seems to be saturating with the increase of users. Consequently, for the case of more users than RAUs, after a given number of users the increase in offset power is to some point constant. Nevertheless, we should not forget that for this case, there is also a multiplexing gain.

3.6 Conclusion

In this chapter, we have shown that DAS provides an interesting alternative to CAS because of its power efficiency and diversity. Then we considered a differential measure, the DCAP, which can be useful in dynamic radio resource allocation and in the antenna planning phase. Concerning the DCAP, we have analyzed the benefits of the connection of additional RAUs to the system users of a BC, both for the single-user and multi-user cases. For the single-user case, we have analyzed the DCAP limits, its sensitivity to the links SNR variation and have also found the user positions that will benefit the most from the connection of additional transmit antennas. Furthermore, for this case, we have seen that the most relevant system property to obtain the highest DCAP values is system symmetry. It was also verified that the capacity gains obtained by a DAS, in relation to a CAS, are mainly due to the additional degrees of freedom provided by the DAS, which increase the probability of finding a user in a state with high symmetry, unlike in CAS. For the multi-user case, we have verified that the DCAP of a CAS, with uncorrelated channel paths, increases logarithmically with the number of users, for the optimal scheme (DPC). For the DAS, we have seen, by numerical simulations, that the number of user's positions with the highest DCAP values is small and that their main property is their closeness to the system symmetry lines, defined by the transmit antennas. Thus symmetry plays, like in the single-user scenario, an important role in the multi-user scenario. Hence, one can conclude that the users that will get the most benefit from the joint processing of additional RAUs, in a DAS, will be the ones at the cell borders. Additionally, one can say that a DAS has power efficiency, diversity and capacity advantages over a CAS. Consequently, a system architecture based on the DAS concept will be interesting to address the problems encountered in the current cellular systems, for users at the cell borders.

3.7 References

[1] I. E. Telatar, "Capacity of Multi-antenna Gaussian Channels," *AT&T Bell Laboratories, Murray Hill, NJ*, 1999.

[2] Fibre Optic Networks for Distributed, Extendible Heterogeneous Radio Architectures and Service Provisioning. FUTON project. [Online]. Available: http://www.ict-futon.eu/

[3] W. Choi and J. G. Andrews, "Downlink performance and capacity of distributed antenna systems in a multicell environment," *Wireless Communications, IEEE Transactions on*, vol. 6, no. 1, pp. 69–73, Jan. 2007.

[4] N. Jindal, "High SNR analysis of MIMO broadcast channels," *Information Theory, 2005. ISIT 2005. Proceedings. International Symposium on*, pp. 2310–2314, Sept. 2005.

[5] J. Lee and N. Jindal, "High SNR Analysis for MIMO Broadcast Channels: Dirty Paper Coding Versus Linear Precoding," *Information Theory, IEEE Transactions on*, vol. 53, no. 12, pp. 4787 –4792, dec. 2007.

[6] H. Weingarten, Y. Steinberg, and S. Shamai, "The Capacity Region of the Gaussian Multiple-Input Multiple-Output Broadcast Channel," *Information Theory, IEEE Transactions on*, vol. 52, no. 9, pp. 3936–3964, Sept. 2006.

[7] J. Park, E. Song, and W. Sung, "Capacity analysis for distributed antenna systems using cooperative transmission schemes in fading channels," *Wireless Communications, IEEE Transactions on*, vol. 8, no. 2, pp. 586 –592, feb. 2009.

[8] M. Dohler, A. Gkelias, and A. Aghvami, "Capacity of distributed PHY-layer sensor networks," *Vehicular Technology, IEEE Transactions on*, vol. 55, no. 2, pp. 622–639, March 2006.

[9] J. Wang and L. Milstein, "CDMA overlay situations for microcellular mobile communications," *Communications, IEEE Transactions on*, vol. 43, no. 234, pp. 603 –614, feb. 1995.

[10] J. Wang and J. Chen, "Performance of wideband CDMA systems with complex spreading and imperfect channel estimation," *Selected Areas in Communications, IEEE Journal on*, vol. 19, no. 1, pp. 152 –163, jan. 2001.

[11] A. Abouda, H. El-Sallabi, L. Vuokko, and S. Haggman, "Performance of Stochastic Kronecker MIMO Radio Channel Model in Urban Microcells," sep. 2006, pp. 1 –5.

[12] A. Goldsmith, *Wireless Communications*. Stanford University, 2005.

[13] J. Craig, "A new, simple and exact result for calculating the probability of error for two-dimensional signal constellations," in *Military Communications Conference, 1991. MILCOM '91, Conference Record, 'Military Communications in a Changing World'., IEEE*, nov 1991, pp. 571 –575 vol.2.

[14] H. Liu and G. Li, *OFDM-Based Broadband Wireless Networks: Design and Optimization*. Wiley-Interscience, 2005.

[15] E. Visotsky and U. Madhow, "Space-Time Transmit Precoding with Imperfect Feedback," 2000. [Online]. Available: citeseer.ist.psu.edu/article/visotsky00spacetime.html

[16] S. Jafar, S. Vishwanath, and A. Goldsmith, "Channel capacity and beamforming for multiple transmit and receive antennas with covariance feedback," in *Communications, 2001. ICC 2001. IEEE International Conference on*, vol. 7, 2001, pp. 2266 –2270 vol.7.

[17] S. Ghosh, *Network Theory: Analysis and Synthesis*. Prentice Hall of India, 2004.

[18] J. A. Gubner, *Probability and Random Processes for Electrical and Computer Engineers*. Cambridge University Press, 2006.

[19] I. Gradshteyn and D. Z. I.M. Ryzhik, Alan Jeffrey, *Table of Integrals, Series and Products*. Elsevier Academic Pres, 2007.

[20] N. Jindal, W. Rhee, S. Vishwanath, S. Jafar, and A. Goldsmith, "Sum power iterative water-filling for multi-antenna Gaussian broadcast channels," *Information Theory, IEEE Transactions on*, vol. 51, no. 4, pp. 1570 –1580, apr. 2005.

[21] T. Cover, "Broadcast channels," *Information Theory, IEEE Transactions on*, vol. 18, no. 1, pp. 2 – 14, jan 1972.

[22] S. Vishwanath, N. Jindal, and A. Goldsmith, "Duality, achievable rates, and sum-rate capacity of Gaussian MIMO broadcast channels," *Information Theory, IEEE Transactions on*, vol. 49, no. 10, pp. 2658 – 2668, oct. 2003.

[23] P. Viswanath and D. Tse, "Sum capacity of the vector Gaussian broadcast channel and uplink-downlink duality," *Information Theory, IEEE Transactions on*, vol. 49, no. 8, pp. 1912 – 1921, aug. 2003.

[24] W. Yu and J. Cioffi, "Sum capacity of Gaussian vector broadcast channels," *Information Theory, IEEE Transactions on*, vol. 50, no. 9, pp. 1875–1892, Sept. 2004.

[25] S. Shamai and S. Verdu, "The impact of frequency-flat fading on the spectral efficiency of CDMA," *Information Theory, IEEE Transactions on*, vol. 47, no. 4, pp. 1302 –1327, may 2001.

[26] G. Caire and S. Shamai, "On the achievable throughput of a multiantenna Gaussian broadcast channel," *Information Theory, IEEE Transactions on*, vol. 49, no. 7, pp. 1691 – 1706, july 2003.

Chapter 4

Minimum Bit Error Rate Nonlinear Precoding for Multiuser MIMO and High SNR

This chapter focuses on the minimization of the bit-error-rate, for the downlink of a multiuser MIMO channel with N transmit antennas and K single antenna users, both for co-located and distributed antenna systems. In the design of such a precoder the knowledge of the transmitted data and full channel state information, at the transmitter, are assumed. It is shown that, in the high signal to noise regime, and for co-located antenna systems, the problem simplifies from a constrained quadratic nonlinear optimization to a single quadratic program, allowing to reduce the complexity, significantly. This quadratic problem is equivalent to maximize the minimum distance between the user received symbols and corresponding decision boundaries. In contrast to zero-forcing where full inversion is required, the proposed algorithm selects and inverts part of the channel correlation matrix. This leads to an improved performance as the selection allows to get a better conditioned matrix. Additionally, this allows us to treat zero-forcing as a special case of the algorithm. By using the results obtained for the co-located case we present a two phases algorithm for distributed antenna systems and extend the obtained results for multicarrier systems. Results show that the algorithms achieve a performance close to the optimum, with low complexity.

4.1 Introduction

In recent years the quest for higher bit rates and the scarcity of spectrum have led to the use of(glossMIMO systems. Theoretically, the use of MIMO allows under certain conditions the capacity to scale linearly by a factor equal to the minimum between the number of transmit and receive antennas. This happens for rich scattering propagation environments, without resorting to an increase in spectrum usage [1–4]. Nevertheless, for limited scattering propagation environments, this is not the case, due to the strong correlation between channel links. During the last years, the DAS concept has gained more attention from the research community, since it can solve some of the problems inherent to the co-located single cell systems. Namely, such systems have a macro diversity advantage that is inherent to the widely spaced antennas and more flexibility to deal with intercell interference, which is the main limitative factor of user terminals at the cell edges [5]. MIMO systems are well studied for the single-user case,

but that is not the case for the multiuser scenario. For the multiuser scenario, MIMO allows several users to be served with the same space and time/frequency resources. However, to be able to do that some sort of precoding should be used at the transmitter side to separate the user signals, canceling in that way the multiuser interference. The concept of linear multiuser precoding for SISO systems has been introduced in [6], [7]. Such schemes have been proposed to eliminate the multiple access interference and increase the system capacity, while allowing for power allocation strategies. Multiuser linear precoding techniques for MIMO systems have been proposed in [8], [9]. A framework based on the convex optimization theory was developed in [10], [11] for designing optimum joint linear precoding and post equalization considering full CSI [10] and only CSI statistics [11]. The most common and also the lowest complexity schemes available to achieve this type of user separation are ZF and the MMSE precoder [12]. Both resort to a linear transformation of the data signal, to align it to the corresponding user subspace and to move it away from the subspace of the other users. On the other extreme of complexity we can find DPC [13], which is optimal for the MIMO multiuser Broadcast channel [14], [15].

Equally important are the works on multicell or distributed precoding techniques. In recent years relevant works on the theme have been proposed in [5, 16–21]. In [16], the inner bounds on capacity regions for downlink transmission were derived with or without Base Station (BS) cooperation and under per-antenna power or sum-power constraint. Two centralized multicell linear precoding schemes based on the waterfilling technique have been proposed in [18]. It was shown that these techniques achieve a performance, in terms of weighted sum rate, very close to the optimal. Multicell cooperation based on SVD has been proposed in [19]. The maximum achievable average transmission rate per user per antenna was derived. In [19] a clustered BS coordination was enabled through a multicell block diagonalization in order to mitigate the effects of interference in multicell MIMO systems. In [20] the linear precoder vectors were computed resorting to a SVD based algorithm in a centralized fashion and then for the power allocation the minimization of the average BER criteria was considered. Distributed multiuser linear precoding with distributed power allocation has been discussed in [21]. It was assumed that each BS has only the knowledge of local CSI and based on that the beamforming vectors were derived considering both instantaneous and statistical CSI in order to achieve the outer boundary of the achievable rate region. However, to the best of our knowledge, nonlinear precoding solutions for DAS have not been addressed in literature, yet. This has only been done for conventional co-located MIMO based systems. Namely, the nonlinear minimum BER multiuser transmission scheme (MBMUT) was, firstly, proposed for a SISO Code Division Multiple Access (CDMA) system with frequency-selective channels in [22] and was extended to multiple antenna systems in [23]. The fixed power constraint at the transmitter imposes a quadratic constraint in the problem formulation. As the merit function, i.e., the average BER is nonlinear, we are led to a quadratically constrained optimization of a nonlinear function. This can be solved using state-of-the-art nonlinear optimization methods like Sequential Quadratic Programming (SQP), but the complexity is high. To alleviate this in [24] the authors formulated the MBMUT problem by including the power constraint into the merit function, leading to an unconstrained optimization problem. This can be solved using unconstrained optimization techniques [24], but the complexity although somewhat reduced is still high.

In this chapter, we show how to reduce the complexity of the minimum BER problem by showing that the optimization task can be approximated by a single Quadratic Program (QP). To solve the aforementioned QP a low complexity algorithm is proposed, for generic M-QAM (Quadrature Amplitude Modulation) and we show that the solution has close connections to

the linear ZF scheme. Numerical results show that the proposed sub-optimal scheme achieves a performance very close to the optimal but with much lower complexity, both for conventional co-located systems and for DAS. For the DAS a two-phase algorithm is proposed: first, a solution is computed by assuming that all RAUs can jointly pool their power and in the second phase the obtained signal is multiplied by a scaling factor so that the power constraint is respected.

This chapter is organized as follows. Section 4.2 describes the system model. Next, in section 4.3, we present a brief revision of the ZF and MMSE linear precoders. Then, in section 4.4 we describe and derive the proposed two phase algorithm to approximately minimize the system BER of a DAS. To achieve that, first we solve the same minimization problem for a co-located antenna system, in section 4.4.2. Finally, we analyze the complexity of the proposed scheme and evaluate its performance, through numerical simulations, both for co-located and distributed antenna systems.

4.2 System Model

We consider a DAS system consisting of a set of RAUs which are transparently linked, by optical fiber, to a CU, where efficient joint precoding can be done, i.e., we consider the enhanced cellular architecture proposed in [25, 26]. We assume transmission from R RAUs, each with N_r antennas, to K single-antenna users, see Fig. 4.1. The total number of transmit antennas is $N = RN_r$. In such a system, the concatenation of all users received signals, $\mathbf{y}(\in \mathbb{C}^{K\times 1})$, can be mathematically described by

$$\mathbf{y} = \mathbf{H}\mathbf{x} + \mathbf{n} \tag{4.1}$$

where $\mathbf{H} = [\mathbf{h}_1, \ldots, \mathbf{h}_R](\in \mathbb{C}^{K\times N})$ denotes the concatenation of all RAUs channels, $\mathbf{x} = [\mathbf{x}_1^H, \ldots, \mathbf{x}_R^H]^H(\in \mathbb{C}^{N\times 1})$ is the transmitted vector and $\mathbf{n}(\in \mathbb{C}^{K\times 1})$ is a vector of independent complex Gaussian noise, with zero mean and variance σ^2. The transmit power at each RAU is constrained to P_{t_R}. The vector of transmitted symbols, $\mathbf{x} = [x(1), \ldots, x(N)]^T$ is obtained by a nonlinear mapping of the vector of M-ary QAM data symbols $\mathbf{d} = [d(1), \ldots, d(K)]^T$, taken from the odd complex integer grid, $\mathcal{G}$.

$$\mathcal{G} = \{I + jQ | I, Q \in \{\pm 1, \pm 3, \ldots, \pm(\sqrt{M} - 1)\}\} \tag{4.2}$$

The real valued representation of a complex vector is obtained by stacking the real and imaginary parts of the corresponding complex vectors

$$\bar{(.)} = [\mathcal{R}(.)^T \mathcal{I}(.)^T]^T \tag{4.3}$$

Using the real value representation of complex vectors, the channel model can be represented by

$$\bar{\mathbf{y}} = \bar{\mathbf{H}}\bar{\mathbf{x}} + \bar{\mathbf{n}} \tag{4.4}$$

where $\bar{\mathbf{H}}$ is the real counterpart of $\mathbf{H}$:

$$\bar{\mathbf{H}} = \begin{bmatrix} \mathcal{R}\{\mathbf{H}\} & -\mathcal{I}\{\mathbf{H}\} \\ \mathcal{I}\{\mathbf{H}\} & \mathcal{R}\{\mathbf{H}\} \end{bmatrix} = \begin{bmatrix} \bar{\mathbf{H}}_I \\ \bar{\mathbf{H}}_Q \end{bmatrix} \in \mathbb{R}^{2K\times 2N} \tag{4.5}$$

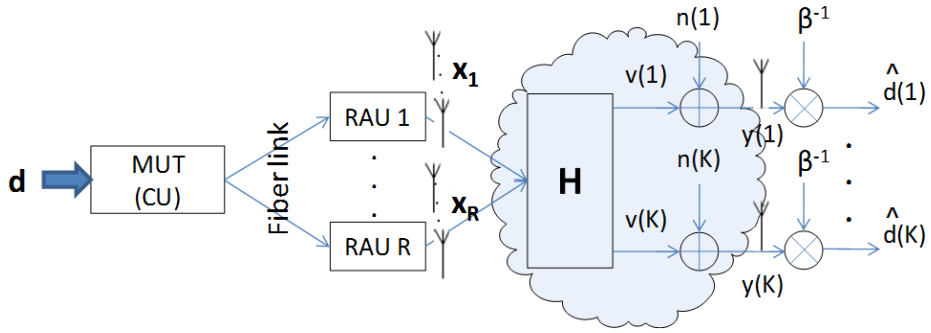

Figure 4.1: Block Diagram of Distributed Multiuser Transmission.

Hereinafter, we will use the real representation of the system, since it is easier to deal with for optimization purposes.

The proposed multiuser precoding scheme assumes perfect CSI at the transmitter side (CU), which can be acquired using the reverse-link estimation in Time-Division Duplex (TDD) or a feedback channel in Frequency-Division Duplex (FDD). Moreover, at the receiver, we assume that before hard decision the received signal is first scaled by a factor, β^{-1}, common to all receivers. This scaling parameter can be easily estimated, by the receivers, without the need to estimate the full CSI as already done, for example, for the linear ZF scheme. The received signals are scaled, by β^{-1}, so that the average power of the received QAM signals have amplitudes close to the ones of the odd complex integer grid $\mathcal{G}$.

4.3 Linear Precoding

In this section, we briefly discuss the ZF and MMSE schemes, under per-RAU power constraint. In this case, the MUltiuser Transmission (MUT) block, as shown in Figure 4.1, performs a linear operation, i.e., the input and output symbols are related by a matrix operation ($\mathbf{x} = \mathbf{Pd}$). As outlined in the introduction, for the nonlinear scheme, here, for the linear schemes, we also consider two phases: in the first phase a Total Power Constraint (TPC) is imposed, instead of a per-RAU power constraint, and in the second phase the obtained signal is multiplied by a factor, to satisfy the individual per-RAU power constraints.

4.3.1 Zero-Forcing

This scheme designs the transmitter signals in such a way that the inter-user interference, at each receiver, is zero. Under TPC, mathematically this corresponds to design the precoding matrix such that

$$\mathbf{HP} = \alpha\mathbf{I} \tag{4.6}$$

$$\mathbb{E}[\mathbf{d}^H\mathbf{P}^H\mathbf{Pd}] = tr\{\mathbf{PP}^H\} \leq P_T \tag{4.7}$$

where α is a positive constant, P_T represents the power transmitted by all RAUs, and the second condition enforces the power constraint at the transmitter. By solving

$$\mathbf{P}_{ZF} = arg\max_{\mathbf{P}} \alpha^2 \;\; s.t.\ (4.6)\ and\ (4.7) \tag{4.8}$$

one obtains the ZF precoder matrix, that is given by a scaled Moore-Penrose pseudo-inverse of the channel matrix [12].

$$\mathbf{P}_{ZF} = \psi.\mathbf{H}^H(\mathbf{H}\mathbf{H}^H)^{-1} \tag{4.9}$$

$$\psi^{-1} = \sqrt{P_T^{-1} tr\{(\mathbf{H}\mathbf{H}^H)^{-1}\}} \tag{4.10}$$

However, such a solution ($\mathbf{x} = \mathbf{P}\mathbf{d}$) must be scaled by $\eta = P_{t_R}/max\{\mathbf{x}_1^H\mathbf{x}_1, \ldots, \mathbf{x}_R^H\mathbf{x}_R\}$, where $\mathbf{x}_r$ are the rows of $\mathbf{x}$ corresponding to RAU r, so that the power constraints at each RAU are respected. After this second scaling, the constant $\beta = \eta\psi$. We call this method per-RAU Linear ZF.

4.3.2 Minimum Mean Square Error Precoding

Another commonly used criterion is the mean squared distance between received and transmitted symbols, which under TPC can be mathematically formulated as

$$\mathbf{P}_{MMSE} = arg\min_{P} \mathbb{E}\left\{\| \mathbf{d} - \hat{\mathbf{d}} \|_2^2\right\} \quad s.t.\ (4.7) \tag{4.11}$$

The solution to problem (4.11), the transmit MMSE precoding matrix, is given by [12]

$$\mathbf{P}MMSE = \psi.\mathbf{H}(\mathbf{H}\mathbf{H}^H + \sigma^2\mathbf{I})^{-1} \tag{4.12}$$

$$\psi^{-1} = \sqrt{P_T^{-1} tr\{(\mathbf{H}\mathbf{H}^H + \sigma^2\mathbf{I})^{-2}\mathbf{H}^H\mathbf{H}\}} \tag{4.13}$$

To respect the individual per-RAU power constraints, the obtained transmit signal ($\mathbf{x} = \mathbf{P}\mathbf{d}$) must be scaled by $\eta = P_{t_R}/max\{\mathbf{x}_1^H\mathbf{x}_1, \ldots, \mathbf{x}_R^H\mathbf{x}_R\}$. After this second scaling, the constant $\beta = \eta\psi$. We call this method per-RAU Linear MMSE.

4.4 Minimum BER Precoder

Differently from the MMSE criterion in which the mean squared distance between received and transmitted symbols is minimized, for the MBMUT precoder the BER is minimized directly. However, to obtain a solution, for the whole SNR regime, we should resort to numerical optimization techniques as explained in [23]. In that paper, the authors use SQP to solve the minimum BER problem, since the merit function is nonlinear and the transmitter power constraint is quadratic. Here we show how, (to alleviate the inherent complexity), to approximate this optimization problem by a simple quadratic program and present numerical results illustrating the tightness of the approximation both for co-located and distributed antenna systems.

4.4.1 Problem Formulation

Let the BER, at receiver k, conditioned on a channel realization $\bar{\mathbf{H}}$ and on a transmitted symbol $\bar{\mathbf{d}}$ be $P_{e_k}(\bar{\mathbf{x}}, \bar{\mathbf{d}}, \beta, \bar{\mathbf{H}}, \sigma)$, the average BER be $P_e(\bar{\mathbf{x}}, \bar{\mathbf{d}}, \beta, \bar{\mathbf{H}}, \sigma) = \frac{\sum_{k=1}^{K} P_{e_k}(\bar{\mathbf{x}}, \bar{\mathbf{d}}, \beta, \bar{\mathbf{H}}, \sigma)}{K}$, the goal is to find the mapping $\bar{\mathbf{d}}$ ($\in \mathbb{R}^{2K\times 1}$) $\rightarrow \bar{\mathbf{x}}$ ($\in \mathbb{R}^{2N\times 1}$) that minimizes the average BER, i.e:

$$\begin{aligned} \hat{\bar{\mathbf{x}}} =& arg\min_{\bar{\mathbf{x}},\beta} P_e(\bar{\mathbf{x}}, \bar{\mathbf{d}}, \beta, \bar{\mathbf{H}}, \sigma) \\ s.t\ \ & \bar{\mathbf{x}}_r^H\bar{\mathbf{x}}_r \leq P_{t_R}, r = \{1, \ldots, R\} \\ & \beta \geq 0 \end{aligned} \tag{4.14}$$

It should be noted that in equation (4.14) we also optimize the scaling parameter β and that the transmitted signal power is constrained to P_{t_R} at each RAU.

We consider the Gray coding to map the bits to symbols, since Gray coded bit mapping is the most common type of mapping used for quadrature amplitude modulations. For constellations of size M, where M is a perfect square, it can be shown that with a Gray mapping the region $\mathcal{R}_i^k$, where for $v \in \mathcal{R}_i^k$ implies that the probability of the i^{th} bit is decided as an i ($i = \{0, 1\}$), is given by the union of up to three different types of regions. Type 1 is a vertical (horizontal) strip left (top) limited, type 2 is a vertical (horizontal) strip right (bottom) limited and type 3 is a left and right (top and bottom) limited strip, as illustrated in Figure 4.2. A more detailed description can be found in B.1. The corresponding probability of error for

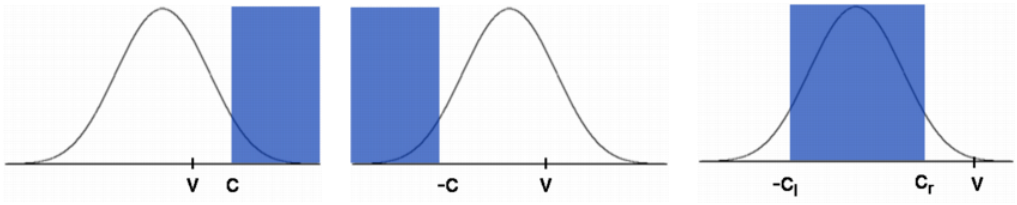

(a) Type 1. (b) Type 2. (c) Type 3.

Figure 4.2: Gray coding decision regions.

each of the three decision regions, shown in Figure 4.2, are respectively

$$\begin{aligned} P(v > c) &= Q\left(\frac{-v + c}{\sigma}\right) \\ P(v < -c) &= Q\left(\frac{v + c}{\sigma}\right) \\ P(-c_l < v < c_r) &= Q\left(\frac{-v - c_l}{\sigma}\right) + Q\left(\frac{v - c_r}{\sigma}\right) - 1 \end{aligned} \tag{4.15}$$

where for our case $v = \bar{\mathbf{h}}_k \bar{\mathbf{x}}$, $k \in \{1, \ldots, 2K\}$, $c_i = \{\beta b | b \in \{\pm 2, \ldots, \pm\sqrt{M}\}\}$. By c_i we mean both c, c_l and c_r. Indeed v is the user k received signal, without noise, and c_i a scaled version of one of the corresponding boundaries of the transmitted symbol, of the same user. From equation (4.15), one can see that the average system BER will be a scaled sum of $Q(.)$ functions minus a constant. However, to simplify the subsequent analysis and to make it more understandable we have opted by a matrix/vector notation to represent the average BER. For that we have concatenated all v variables, from equation (4.15), and corresponding signs into a vector, which can be represented by the matrix multiplication $\bar{\mathbf{A}}(\bar{\mathbf{d}})\bar{\mathbf{x}}$, where the matrix $\bar{\mathbf{A}}(\bar{\mathbf{d}})$ make explicit the sign of the v variable in the argument of the $Q(.)$ functions is not always the same and that it depends on the transmitted signal $\bar{\mathbf{d}}$. Matrix $\bar{\mathbf{A}}(\bar{\mathbf{d}})$ is defined explicitly, in the following section, for 4-QAM and 16-QAM.

Indeed $\bar{\mathbf{A}}(\bar{\mathbf{d}})\bar{\mathbf{x}}$ has close similarities to $\bar{\mathbf{H}}\bar{\mathbf{x}}$. The main differences are in the signs of the rows. The same can be done for the variable c_i, which can be represented by $\beta\bar{\mathbf{b}}$. With all that considerations, the average BER can be mathematically expressed by

$$P_e(\bar{\mathbf{x}}, \bar{\mathbf{A}}(\bar{\mathbf{d}}), \beta, \sigma) = \gamma \mathbf{1}^H \mathbf{q}\left(\frac{\bar{\mathbf{A}}(\bar{\mathbf{d}})\bar{\mathbf{x}} - \beta\bar{\mathbf{b}}}{\sigma}\right) - \zeta(\bar{\mathbf{d}}) \tag{4.16}$$

where $\mathbf{q}(\mathbf{s}) = [\ldots, Q(s_i), \ldots]^T$, with $Q(s) = 1/\sqrt{2\pi}\int_s^\infty e^{-x^2/2}dx$ and γ, and ζ are positive constants. From equation (4.15) and (4.16) we can see that the term $\bar{\mathbf{A}}(\bar{\mathbf{d}})\bar{\mathbf{x}}-\beta\bar{\mathbf{b}}$ is the distance between the received signal, without noise, to the bit decision boundaries. A detailed definition of $\bar{\mathbf{A}}(\bar{\mathbf{d}})$ is given in the next sections for 4-QAM and 16-QAM modulations, respectively. For notation simplicity, in the following, we drop the argument $\bar{\mathbf{d}}$ in $\bar{\mathbf{A}}(\bar{\mathbf{d}})$.

As already expressed, our final objective is to find the transmit vector $\hat{\bar{\mathbf{x}}}$ that minimizes the probability of error (4.16). Formally,

$$\begin{aligned} \hat{\bar{\mathbf{x}}} =& arg\min_{\bar{\mathbf{x}},\beta} \mathbf{1}^H \mathbf{q}\left(\frac{\bar{\mathbf{A}}\bar{\mathbf{x}} - \beta\bar{\mathbf{b}}}{\sigma}\right) \\ s.t\ \ & \bar{\mathbf{x}}_r^H\bar{\mathbf{x}}_r \leq P_{t_R}, r = \{1,\ldots,R\} \\ & \beta \geq 0 \end{aligned} \tag{4.17}$$

To solve (4.17) we propose a two-phase algorithm: in the first phase, we solve the associated co-located system optimization problem, by considering that all RAUs are co-located and share a common power constraint $P_T = RP_{t_R}$, i.e. the individual RAUs power constraints are replaced by a global TPC ($\bar{\mathbf{x}}^H\bar{\mathbf{x}} \leq P_T$); the second phase consists in scaling the obtained transmit signal by a factor $\eta = P_{t_R}/min\{\bar{\mathbf{x}}_1^H\bar{\mathbf{x}}_1, \ldots, \bar{\mathbf{x}}_R^H\bar{\mathbf{x}}_R\}$, so that the individual per-RAU power constraints are then respected.

4.4.2 Minimum BER Precoder for a Co-located System

In this section, we explain how to solve the first phase of the proposed algorithm efficiently. Namely, we show how to minimize approximately the BER, for the downlink of a multiuser MIMO channel with N transmit antennas and K single antenna users. It is shown that in the high signal to noise regime the problem simplifies from a constrained quadratic nonlinear optimization to a single quadratic program, allowing to reduce the complexity. Next, we present the proposed algorithm as an extension to the ZF algorithm and explain their similarities. Finally, the performance of the described algorithm is evaluated for different co-located system scenarios and its complexity analyzed.

In the first phase of the proposed two-phase algorithm we have at our hands a minimum BER optimization problem, with a global TPC. Such a problem can be mathematically described by

$$\begin{aligned} \hat{\bar{\mathbf{x}}} =& arg\min_{\bar{\mathbf{x}},\beta} P_e(\bar{\mathbf{x}}, \bar{\mathbf{d}}, \beta, \bar{\mathbf{H}}, \sigma) \\ s.t\ \ & \bar{\mathbf{x}}^H\bar{\mathbf{x}} \leq P_T,\ \beta \geq 0 \end{aligned} \tag{4.18}$$

The solution of (4.18) in general is quite difficult, since the merit function is nonlinear and non-convex. To simplify it we focus on the high SNR regime, and show that (4.18) can then be solved by a quadratic program, which is much easier to deal with.

In the high SNR regime a sum of Q-functions can be approximated by the maximum element of the sum, due to the quadratic exponential decaying behaviour of $Q(x)$ for high values of x. Therefore, the problem can be simplified to a minimax optimization, seeking to maximize the minimum distance between the received signal, without noise, and the corresponding decision boundaries

$$\hat{\bar{\mathbf{x}}} = arg\min_{\bar{\mathbf{x}},\beta} \max\{\beta\bar{\mathbf{b}} - \bar{\mathbf{A}}\bar{\mathbf{x}}\}\ \ s.t\ \bar{\mathbf{x}}^H\bar{\mathbf{x}} \leq P_T,\ \beta \geq 0 \tag{4.19}$$

The problem of (4.19) requires less complexity than the one given by (4.18); however, it is still not easy to deal, due to the non smoothness of the merit function. By using a result from [27] we can reformulate it into one with a smooth merit function

$$\hat{\bar{\mathbf{x}}} = arg \min_{z,\bar{\mathbf{x}},\beta} z \;\; s.t \; \bar{\mathbf{x}}^H \bar{\mathbf{x}} \leq P_T, \; \beta \geq 0, \; z\mathbf{1} \geq \beta \bar{\mathbf{b}} - \bar{\mathbf{A}}\bar{\mathbf{x}} \tag{4.20}$$

The problem of (4.20) is convex and all inequality constraints are affine, thus by Slater's condition [28], strong duality holds and consequently, its dual can be used to solve the primal problem. The dual of (4.20) as shown in B.2, is given by

$$\bar{\boldsymbol{\lambda}} = arg \min_{\gamma,\bar{\boldsymbol{\lambda}}} \sqrt{\bar{\boldsymbol{\lambda}}^H \bar{\mathbf{A}} \bar{\mathbf{A}}^H \bar{\boldsymbol{\lambda}}} \;\; s.t \; \mathbf{1}^H \bar{\boldsymbol{\lambda}} = 1, \; \bar{\mathbf{b}}^H \bar{\boldsymbol{\lambda}} = \gamma, \; \bar{\boldsymbol{\lambda}} \geq \mathbf{0}, \; \gamma \geq 0 \tag{4.21}$$

where $\bar{\boldsymbol{\lambda}}$ is a column vector of the Lagrange multipliers in the optimization of (4.20) [29] and is related to the transmitted vector $\mathbf{x}$ by $\bar{\mathbf{x}} = \sqrt{P_T}\bar{\mathbf{A}}^H \bar{\boldsymbol{\lambda}} / \sqrt{\bar{\boldsymbol{\lambda}}^H \bar{\mathbf{A}} \bar{\mathbf{A}}^H \bar{\boldsymbol{\lambda}}}$. As the $sqrt(.)$ function is monotonic, (4.21) is equivalent to

$$\hat{\boldsymbol{\lambda}} = arg \min_{\gamma,\bar{\boldsymbol{\lambda}}} \frac{1}{2} \bar{\boldsymbol{\lambda}}^H \bar{\mathbf{A}} \bar{\mathbf{A}}^H \boldsymbol{\lambda} \;\; s.t \; \mathbf{1}^H \bar{\boldsymbol{\lambda}} = 1, \; \bar{\mathbf{b}}^H \bar{\boldsymbol{\lambda}} = \gamma, \; \bar{\boldsymbol{\lambda}} \geq \mathbf{0}, \; \gamma \geq 0 \tag{4.22}$$

The problem of (4.22) fits under the quadratic programming framework, and since $\bar{\mathbf{A}}\bar{\mathbf{A}}^H$ is positive semidefinite the merit function is convex and admits a unique global feasible solution, for which the Karush-Kuhn-Tucker (KKT) conditions, from the problem of (4.21), are necessary and sufficient

$$\mathbf{1}^H \bar{\boldsymbol{\lambda}} = 1 \tag{4.23}$$

$$\bar{\mathbf{b}}^H \bar{\boldsymbol{\lambda}} = \gamma \tag{4.24}$$

$$\frac{\bar{\mathbf{A}}\bar{\mathbf{A}}^H \bar{\boldsymbol{\lambda}}}{\sqrt{\bar{\boldsymbol{\lambda}}^H \bar{\mathbf{A}} \bar{\mathbf{A}}^H \bar{\boldsymbol{\lambda}}}} - \beta \bar{\mathbf{b}} + z\mathbf{1} = \bar{\boldsymbol{\psi}} \tag{4.25}$$

$$\bar{\boldsymbol{\lambda}} \geq \mathbf{0}, \; \bar{\boldsymbol{\psi}} \geq \mathbf{0}, \bar{\boldsymbol{\lambda}} \circ \bar{\boldsymbol{\psi}} = \mathbf{0} \tag{4.26}$$

$$\gamma \geq 0, \; \beta \geq 0, \; \gamma\beta = 0 \tag{4.27}$$

where $\boldsymbol{\psi}$ is a vector of the Lagrange multipliers in the optimization of (4.21). From (4.25) after multiplying both sides of the equation by $\bar{\boldsymbol{\lambda}}^H$ and using equalities (4.23-4.24) and (4.26-4.27) we get that $z = -\sqrt{\bar{\boldsymbol{\lambda}}^H \bar{\mathbf{A}} \bar{\mathbf{A}}^H \bar{\boldsymbol{\lambda}}}$.

In the following sections, we show how to solve the KKT conditions for a general M-QAM constellation.

4-QAM

We start with the 4-QAM modulation, which is a constant amplitude modulation and then the algorithm is extended to non constant amplitude modulations. For 4-QAM there is no need for a scaling of the received signal since all the constellation boundaries are equal to zero. Consequently, the constraints $\gamma \geq 0$ and $\bar{\mathbf{b}}^H \bar{\boldsymbol{\lambda}} = \gamma$ do not exist and the corresponding KKT

conditions can be simplified to[1]

$$\mathbf{1}^H \bar{\boldsymbol{\lambda}} = 1 \tag{4.28}$$

$$\bar{\mathbf{A}}\bar{\mathbf{A}}^H \bar{\boldsymbol{\lambda}} + z\mathbf{1} = \bar{\boldsymbol{\psi}} \tag{4.29}$$

$$\bar{\boldsymbol{\lambda}} \geq \mathbf{0},\ \bar{\boldsymbol{\psi}} \geq \mathbf{0}, \bar{\boldsymbol{\lambda}} \circ \bar{\boldsymbol{\psi}} = \mathbf{0} \tag{4.30}$$

where $\bar{\mathbf{A}} = \bar{\mathbf{H}} \circ (\mathbf{1}_{2N}^H \otimes \bar{\mathbf{d}})$, $\bar{\mathbf{d}} \in \{-1, 1\}^{(2K \times 1)}$ is a column vector with the data symbols, and the symbol -1 represents the bit 0. A closer look to the previous system of equations shows that its solution is a scaled version of the solution of

$$\bar{\mathbf{A}}\bar{\mathbf{A}}^H \underline{\bar{\boldsymbol{\lambda}}} = \underline{\bar{\boldsymbol{\psi}}} + \mathbf{1} \tag{4.31}$$

$$\underline{\bar{\boldsymbol{\lambda}}} \geq \mathbf{0},\ \underline{\bar{\boldsymbol{\psi}}} \geq \mathbf{0}, \underline{\bar{\boldsymbol{\lambda}}} \circ \underline{\bar{\boldsymbol{\psi}}} = \mathbf{0} \tag{4.32}$$

i.e. $\bar{\boldsymbol{\lambda}} = z\underline{\bar{\boldsymbol{\lambda}}}$, $\bar{\boldsymbol{\psi}} = z\underline{\bar{\boldsymbol{\psi}}}$ and the value of z is obtained by replacing $z\underline{\bar{\boldsymbol{\lambda}}}$ in (4.28). Inspection of (4.31-4.32) shows that by setting $\underline{\bar{\boldsymbol{\psi}}} = \mathbf{0}$ one gets the standard ZF scheme, which is equivalent to remove the constraint $\bar{\boldsymbol{\lambda}} \geq 0$ from problem (4.21).

If the elements of $\underline{\bar{\boldsymbol{\lambda}}}$ that are equal to zero were known a priori, then the solution of system (4.31) would be easy to obtain. To see that, let us assume that the last m elements of $\underline{\bar{\boldsymbol{\lambda}}}$ were known a priori to be equal to zero, i.e.

$$(\underline{\bar{\boldsymbol{\lambda}}})_{(2K,1)} = [(\underline{\bar{\boldsymbol{\lambda}}}_1)_{(2K-m,1)}^H,\ \mathbf{0}_m^H]^H \tag{4.33}$$

and that the matrix $\bar{\mathbf{A}}\bar{\mathbf{A}}^H$ is split as

$$(\bar{\mathbf{A}}\bar{\mathbf{A}}^H)_{(2K,2K)} = \begin{bmatrix} (\bar{\mathbf{a}}_{11})_{(2K-m,2K-m)} & (\bar{\mathbf{a}}_{12})_{(2K-m,m)} \\ (\bar{\mathbf{a}}_{12})_{(m,2K-m)}^H & (\bar{\mathbf{a}}_{22})_{(m,m)} \end{bmatrix} \tag{4.34}$$

The assumption that the last m elements of $\underline{\bar{\boldsymbol{\lambda}}}$ are zero is not restrictive. Zeros at arbitrary m positions can be moved to the last part by applying an appropriate permutation matrix. With such representation the solution of (4.31) is just the ZF of the lower dimensional system represented by $\bar{\mathbf{a}}_{\mathbf{11}}$, and $\underline{\bar{\boldsymbol{\lambda}}}_1 = \bar{\mathbf{a}}_{11}^{-1}\mathbf{1}$. Hence the solution of the system of equations (4.31, 4.32) implies the inversion of just part of the correlation matrix $\bar{\mathbf{A}}\bar{\mathbf{A}}^H$. This sub-matrix is better conditioned than the corresponding full matrix $\bar{\mathbf{A}}\bar{\mathbf{A}}^H$ [30], since its maximum (minimum) eigenvalue is smaller (bigger) than the one of matrix $\bar{\mathbf{A}}\bar{\mathbf{A}}^H$.

Let us consider the input to $\mathbf{q}(.)$ function[2] of equation(4.17)

$$\bar{\mathbf{A}}\bar{\mathbf{x}} = \frac{\bar{\mathbf{A}}\bar{\mathbf{A}}^H\bar{\boldsymbol{\lambda}}}{\sqrt{\bar{\boldsymbol{\lambda}}^H\bar{\mathbf{A}}\bar{\mathbf{A}}^H\bar{\boldsymbol{\lambda}}}} = \frac{\bar{\mathbf{A}}\bar{\mathbf{A}}^H\underline{\bar{\boldsymbol{\lambda}}}}{\sqrt{\underline{\bar{\boldsymbol{\lambda}}}^H\bar{\mathbf{A}}\bar{\mathbf{A}}^H\underline{\bar{\boldsymbol{\lambda}}}}} \geq \frac{\mathbf{1}}{\sqrt{\mathbf{1}^H\bar{\mathbf{a}}_{\mathbf{11}}^{-1}\mathbf{1}}} \tag{4.35}$$

where the first and second equality come from the definition of vector $\bar{\mathbf{x}}$ and $\bar{\boldsymbol{\lambda}}$, respectively, and the third step, the inequality, from equations (4.31, 4.32). Therefore, the inputs to the $Q(.)$ function, for the proposed scheme, are all higher than $1/\sqrt{\mathbf{1}^H\bar{\mathbf{a}}_{\mathbf{11}}^{-1}\mathbf{1}}$ and for the ZF scheme are all equal to $1/\sqrt{\mathbf{1}^H(\bar{\mathbf{A}}\bar{\mathbf{A}}^H)^{-1}\mathbf{1}}$. By using blockwise inversion, we can show that

[1]The positive constant $\sqrt{\bar{\boldsymbol{\lambda}}^H\bar{\mathbf{A}}\bar{\mathbf{A}}^H\bar{\boldsymbol{\lambda}}}$ has been integrated into the variables z and $\bar{\boldsymbol{\psi}}$.

[2]For QPSK $\bar{\mathbf{b}} = \mathbf{0}$.

$\mathbf{1}^H(\bar{\mathbf{A}}\bar{\mathbf{A}}^H)^{-1}\mathbf{1} = \mathbf{1}^H\bar{\mathbf{a}}_{11}^{-1}\mathbf{1} + (\bar{\mathbf{a}}_{12}^H\bar{\mathbf{a}}_{11}^{-1}\mathbf{1} - \mathbf{1})^H\bar{\mathbf{E}}(\bar{\mathbf{a}}_{12}^H\bar{\mathbf{a}}_{11}^{-1}\mathbf{1} - \mathbf{1})$, where $\bar{\mathbf{E}} = (\bar{\mathbf{a}}_{22} - \bar{\mathbf{a}}_{12}^H\bar{\mathbf{a}}_{11}^{-1}\bar{\mathbf{a}}_{12})^{-1}$. Since matrix $\bar{\mathbf{E}}$ is positive definite $(\bar{\mathbf{a}}_{12}^H\bar{\mathbf{a}}_{11}^{-1}\mathbf{1} - \mathbf{1})^H\bar{\mathbf{E}}(\bar{\mathbf{a}}_{12}^H\bar{\mathbf{a}}_{11}^{-1}\mathbf{1} - \mathbf{1}) \geq 0$ thus $\mathbf{1}^H(\bar{\mathbf{A}}\bar{\mathbf{A}}^H)^{-1}\mathbf{1} \geq \mathbf{1}^H\bar{\mathbf{a}}_{11}^{-1}\mathbf{1}$. Consequently, $1/\sqrt{\mathbf{1}^H(\bar{\mathbf{A}}\bar{\mathbf{A}}^H)^{-1}\mathbf{1}} \leq 1/\sqrt{\mathbf{1}^H\bar{\mathbf{a}}_{11}^{-1}\mathbf{1}}$, i.e. the performance of the ZF scheme is always worse than the one of the proposed scheme.

Going back to the resolution of the KKT conditions, (4.31-4.32) we can see, by looking more carefully, that they fit under the framework of the nonnegative least Squares problem [31] and also of the linear complementarity problems [32] and that they are equivalent to the following optimization problem

$$\hat{\underline{\bar{\boldsymbol{\lambda}}}} = arg\min_{\underline{\bar{\boldsymbol{\lambda}}} \geq \mathbf{0}} \ \frac{1}{2}\underline{\bar{\boldsymbol{\lambda}}}^H\bar{\mathbf{A}}\bar{\mathbf{A}}^H\underline{\bar{\boldsymbol{\lambda}}} - \mathbf{1}^H\underline{\bar{\boldsymbol{\lambda}}} \tag{4.36}$$

To solve (4.36) the Projected Gauss-Seidel (PGS) algorithm [31] can be used. The PGS algorithm, to solve (4.36), is in what follows.

Algorithm: Projected Gauss-Seidel (PGS)

1. Initialization: Set $\underline{\bar{\boldsymbol{\lambda}}}^0 = \mathbf{0}$ and $\underline{\bar{\boldsymbol{\psi}}}^0 = -\mathbf{1}$
2. Repeat until stop condition is satisfied:
   For k = 1 to K
   $$\bar{\lambda}_k^{t+1} = max\left(0, \bar{\lambda}_k^t - \frac{\bar{\psi}_k^t}{\bar{\mathbf{M}}_{k,k}}\right)$$
   $$\underline{\bar{\boldsymbol{\psi}}}^{t+1} = \underline{\bar{\boldsymbol{\psi}}}^t + \left(\bar{\lambda}_k^{t+1} - \bar{\lambda}_k^t\right)\bar{\mathbf{M}}_k$$

where t is the time index, $\bar{\mathbf{M}} = \bar{\mathbf{A}}\bar{\mathbf{A}}^H$, and the stop condition used in all simulations was $F(\underline{\bar{\boldsymbol{\lambda}}}^{t-1}) - F(\underline{\bar{\boldsymbol{\lambda}}}^t) < \delta$, for $F(\underline{\bar{\boldsymbol{\lambda}}}) = \frac{1}{2}\underline{\bar{\boldsymbol{\lambda}}}^H\bar{\mathbf{A}}\bar{\mathbf{A}}^H\underline{\bar{\boldsymbol{\lambda}}} - \mathbf{1}^H\underline{\bar{\boldsymbol{\lambda}}}$ and δ a small positive constant.

The PGS algorithm coincides with the well known Gauss-Seidel algorithm, for solving linear system of equations, if the non-negativity constraints are removed. The main difference between the two methods is that the new one, has a projection step of the resulting λ_i value, at each iteration, in the non-negative orthant. Consequently, this method is commonly called Projected Gauss-Seidel algorithm.

Higher order modulations

For non constant amplitude modulations the received signal should be scaled by β^{-1} to compensate the effect of the channel as referred in section 4.2. Simulations have shown that the optimum value of β is always very close to $\sqrt{\bar{\boldsymbol{\lambda}}^H\bar{\mathbf{A}}\bar{\mathbf{A}}^H\bar{\boldsymbol{\lambda}}}$. This can be easily understood as the $\sqrt{\bar{\boldsymbol{\lambda}}^H\bar{\mathbf{A}}\bar{\mathbf{A}}^H\bar{\boldsymbol{\lambda}}}$ corresponds to scale the received signals to have the average power of a QAM signal with amplitudes $\{\pm 1, \pm 3, \ldots, \pm(\sqrt{M} - 1)\}$. To see that, let us consider equation (4.25). As the scaling factor β^{-1} is positive it preserves the phase of the received signals. Furthermore, the elements of $\bar{\mathbf{A}}\bar{\mathbf{A}}^H\bar{\boldsymbol{\lambda}}/\sqrt{\bar{\boldsymbol{\lambda}}^H\bar{\mathbf{A}}\bar{\mathbf{A}}^H\bar{\boldsymbol{\lambda}}} = \bar{\mathbf{A}}\bar{\mathbf{x}}$ have the same amplitude as the ones of $\mathbf{v}$ (see Figure 4.1). Let us consider one component and the zero forced case ($\bar{\psi}_i = 0$). Then from (4.25) we get $(\beta^{-1}\bar{\mathbf{A}}\bar{\mathbf{x}})_i = \bar{b} - \beta^{-1}z1$. As we want $(\beta^{-1}\bar{\mathbf{A}}\bar{\mathbf{x}})_i = \bar{b} + 1$, since $\bar{b} + 1 \in \bar{\mathcal{G}}$, then $\beta = -z$, which from previous considerations leads to $\beta = \sqrt{\bar{\boldsymbol{\lambda}}^H\bar{\mathbf{A}}\bar{\mathbf{A}}^H\bar{\boldsymbol{\lambda}}}$. Based on this, we simplified the algorithm by assigning to β the value $\sqrt{\bar{\boldsymbol{\lambda}}^H\bar{\mathbf{A}}\bar{\mathbf{A}}^H\bar{\boldsymbol{\lambda}}}$. With this assignment, $-z = \beta$, the general KKT conditions become similar to the 4-QAM KKT conditions. The

assignment of a value to β implies that equations (4.24) and (4.27) are no longer needed. We should emphasize that a scaling of z and β by the same factor will not affect the final solution $\bar{\mathbf{x}}$, as mentioned in the previous section and consequently, the value of β and $-z$ can be scaled to 1. To do this scaling the constant $\sqrt{\bar{\boldsymbol{\lambda}}^H \bar{\mathbf{A}} \bar{\mathbf{A}}^H \bar{\boldsymbol{\lambda}}}$ was already taken into account. With all previous assignments in mind one can formulate, like for the 4-QAM KKT conditions, a new system of equations to obtain the optimized transmit signal $\bar{\mathbf{x}} = \sqrt{P_T}\bar{\mathbf{A}}^H \underline{\bar{\boldsymbol{\lambda}}} / \sqrt{\underline{\bar{\boldsymbol{\lambda}}}^H \bar{\mathbf{A}} \bar{\mathbf{A}}^H \underline{\bar{\boldsymbol{\lambda}}}}$.

$$\bar{\mathbf{A}} \bar{\mathbf{A}}^H \underline{\bar{\boldsymbol{\lambda}}} = \underline{\bar{\boldsymbol{\psi}}} + \bar{\mathbf{b}} + \mathbf{1} \tag{4.37}$$

$$\underline{\bar{\boldsymbol{\lambda}}} \geq \mathbf{0},\ \underline{\bar{\boldsymbol{\psi}}} \geq \mathbf{0}, \underline{\bar{\boldsymbol{\lambda}}} \circ \underline{\bar{\boldsymbol{\psi}}} = \mathbf{0} \tag{4.38}$$

which can be solved with the PGS algorithm. Now $\underline{\bar{\boldsymbol{\psi}}}^0 = -\bar{\mathbf{b}} - \mathbf{1}$, in the initialization step of the PGS algorithm. Note that for the specific case of 16-QAM $\bar{\mathbf{A}} = [\bar{\mathbf{H}}_r \circ (\mathbf{1}_K \otimes \bar{\mathbf{d}}_1); -\bar{\mathbf{H}}_r \circ (\mathbf{1}_K \otimes \bar{\mathbf{d}}_2); \bar{\mathbf{H}}_r \circ (\mathbf{1}_K \otimes \bar{\mathbf{d}}_2); \bar{\mathbf{H}}_i \circ (\mathbf{1}_K \otimes \bar{\mathbf{d}}_3); -\bar{\mathbf{H}}_i \circ (\mathbf{1}_K \otimes \bar{\mathbf{d}}_4); \bar{\mathbf{H}}_i \circ (\mathbf{1}_K \otimes \bar{\mathbf{d}}_4)]$ and $\bar{\mathbf{b}} = [\mathbf{0}_K^H, 2\bar{\mathbf{d}}_2^H, 2\bar{\mathbf{d}}_2^H, \mathbf{0}_K^H, 2\bar{\mathbf{d}}_4^H, 2\bar{\mathbf{d}}_4^H]^H$, where $\bar{\mathbf{H}}_r = \mathcal{R}\{\mathbf{H}\}$, $\bar{\mathbf{H}}_i = \mathcal{I}\{\mathbf{H}\}$ and $\bar{\mathbf{d}}_i$ is the bipolar representation, $\{-1, 1\}$, of bit i. However, since we are solving a minimax problem, only the rows of $\bar{\mathbf{A}} \bar{\mathbf{A}}^H$ and $\bar{\mathbf{b}}$ corresponding to the closest boundaries, of the associated symbol, are needed as an input to the algorithm. We call this method with the η normalization per-RAU PGS ZF.

Due to the close similarities between equation (4.37) and the ZF scheme, as previously explained, we propose to regularize it, to obtain better performance, by using the Tikhonov method

$$(\bar{\mathbf{A}} \bar{\mathbf{A}}^H + 2\sigma^2 \mathbf{I}) \underline{\bar{\boldsymbol{\lambda}}} = \underline{\bar{\boldsymbol{\psi}}} + \bar{\mathbf{b}} + \mathbf{1} \tag{4.39}$$

$$\underline{\bar{\boldsymbol{\lambda}}} \geq \mathbf{0},\ \underline{\bar{\boldsymbol{\psi}}} \geq \mathbf{0}, \underline{\bar{\boldsymbol{\lambda}}} \circ \underline{\bar{\boldsymbol{\psi}}} = \mathbf{0} \tag{4.40}$$

The regularized method can still be solved by the PGS algorithm, by using matrix $\bar{\mathbf{A}} \bar{\mathbf{A}}^H + 2\sigma^2 \mathbf{I}$, instead of $\bar{\mathbf{A}} \bar{\mathbf{A}}^H$. The constant that is multiplied by the noise variance (2), comes from the fact that we are using real vectors and matrices. We call this method with the η normalization per-RAU PGS MMSE, due to its similarities to the MMSE method.

4.4.3 Equivalent Formulation

In this section, we show how to obtain the previously proposed scheme using a different formulation. This new formulation allows to get a better understanding of how it works and to propose a new method to approximate its performance.

Let us consider 4-QAM as the modulation method since it is straightforward to extend the proposed method to higher order QAM cases. Assume that now our objective is to minimize the transmit power, subject to a set of convex constraints, similarly to [33], restricting the received signal to a given region. By limiting this set of constraints to be a convex polytope, which can be described by a set of linear inequalities, the previous problem can be mathematically expressed by

$$\hat{\bar{x}} = \min_{\bar{\mathbf{x}}} \bar{\mathbf{x}}^H \bar{\mathbf{x}} \ \ s.t.\ \bar{\mathbf{B}} \bar{\mathbf{x}} \geq \bar{\mathbf{w}} \tag{4.41}$$

where $\bar{\mathbf{B}}$ is a $M \times 2N$ matrix describing the convex polytope, $\bar{\mathbf{x}}$ (the transmitted signal) is a $2N \times 1$ column vector and $\bar{\mathbf{w}}$ a $M \times 1$ column vector of constants. The KKT conditions of

this problem are

$$\bar{\mathbf{B}}\bar{\mathbf{B}}^H\bar{\boldsymbol{\lambda}} - \bar{\mathbf{w}} \geq \mathbf{0} \tag{4.42}$$

$$\bar{\boldsymbol{\lambda}} \geq \mathbf{0},\ \bar{\boldsymbol{\lambda}} \circ (\bar{\mathbf{B}}\bar{\mathbf{B}}^H\bar{\boldsymbol{\lambda}} - \bar{\mathbf{w}}) = \mathbf{0} \tag{4.43}$$

where $\bar{\boldsymbol{\lambda}}$ is a vector of the Lagrange multipliers in the optimization of (4.41) and is related to the transmit signal $\bar{\mathbf{x}}$ by $\bar{\mathbf{x}} = \bar{\mathbf{B}}^H\bar{\boldsymbol{\lambda}}$. The previous system of KKT conditions can be reduced to

$$\bar{\mathbf{B}}\bar{\mathbf{B}}^H\bar{\boldsymbol{\lambda}} = \bar{\boldsymbol{\psi}} + \bar{\mathbf{w}} \tag{4.44}$$

$$\bar{\boldsymbol{\lambda}} \geq \mathbf{0},\ \bar{\boldsymbol{\psi}} \geq \mathbf{0},\ \bar{\boldsymbol{\lambda}} \circ \bar{\boldsymbol{\psi}} = \mathbf{0} \tag{4.45}$$

where we have introduced the slack variable $\bar{\boldsymbol{\psi}}$. If $\bar{\mathbf{w}} = \mathbf{1}$ and $\bar{\mathbf{B}} = \bar{\mathbf{A}}$ the previous equations become equal to the ones presented in 4.31 and 4.32. Hence, the proposed approximate minimum BER precoder can be equivalently represented by a power minimization problem, where the received signal is constrained to be within a given region, representing the transmitted symbol, contrary to the ZF scheme where it is constrained to be exactly at the same location of the transmitted symbol. The replacement of a point by a region allows much more freedom in the transmit signal optimization process, since any point in that region has the same meaning for the receiver. Therefore, these regions define an extended constellation. As an example, in Figure 4.3, we show the 4-QAM extended constellation. As seen from that figure the minimum distance between each region is still 2, like in the original constellation.

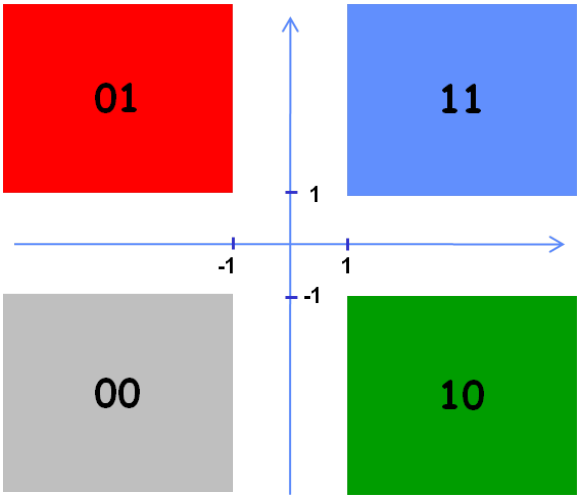

Figure 4.3: Extended 4-QAM constellation.

Approximate algorithm

To have a better insight of the proposed power minimization (minimum BER) scheme we show next how to obtain an approximate solution for it.

First, let us use the Lagrange multiplier $\bar{\boldsymbol{\lambda}}$ and the relation $\bar{\mathbf{x}} = \bar{\mathbf{B}}^H\bar{\mathbf{P}}^H\bar{\boldsymbol{\lambda}}$ to express the transmitted signal. $\bar{\mathbf{P}}$ is a given permutation matrix, that is multiplied by the channel matrix $\bar{\mathbf{B}} = \bar{\mathbf{A}}$, to relabel (order) the users. Furthermore, let us consider the QR matrix

decomposition of matrix $\bar{\mathbf{P}}\bar{\mathbf{B}} = \bar{\mathbf{R}}\bar{\mathbf{Q}}$. With that assumptions, the optimization problem 4.41 can be reformulated as

$$\hat{\bar{\boldsymbol{\lambda}}} = \min_{\bar{\boldsymbol{\lambda}}} \bar{\boldsymbol{\lambda}}^H \bar{\mathbf{R}}\bar{\mathbf{R}}^H \bar{\boldsymbol{\lambda}} \;\; s.t. \; \bar{\mathbf{R}}\bar{\mathbf{R}}^H \bar{\boldsymbol{\lambda}} \geq \mathbf{1} \tag{4.46}$$

Moreover, if we define $\bar{\mathbf{q}} = \bar{\mathbf{R}}^H \bar{\boldsymbol{\lambda}}$ it can be simplified to

$$\hat{\bar{\mathbf{q}}} = \min_{\bar{\mathbf{q}}} \bar{\mathbf{q}}^H \bar{\mathbf{q}} \;\; s.t. \; \bar{\mathbf{R}}\bar{\mathbf{q}} \geq \mathbf{1} \tag{4.47}$$

If an appropriate permutation matrix ($\bar{\mathbf{P}}$) is chosen, then the positions at which $\bar{\boldsymbol{\lambda}}$ is equal to zero are the same as the ones of variable $\bar{\mathbf{q}}$. This happens for a permutation matrix that forces to zero the last entries of the $\bar{\boldsymbol{\lambda}}$ vector, since $\bar{\mathbf{q}} = \bar{\mathbf{R}}^H \bar{\boldsymbol{\lambda}}$ and $\bar{\mathbf{R}}^H = [\bar{\mathbf{R}}_{\mathbf{11}}^H \; \bar{\mathbf{R}}_{\mathbf{12}}^H; \; \mathbf{0} \; \bar{\mathbf{R}}_{\mathbf{22}}^H]$.

To obtain an algorithm to approximate the solution of the proposed optimization problem we will first obtain an approximation for the location of the zeros in the $\bar{\boldsymbol{\lambda}}$ vector and after, with this information, the triangular inequality system, $\bar{\mathbf{R}}\bar{\mathbf{q}} \geq \mathbf{1}$ is solved, by minimizing the transmit power.

As shown in [34] the PGS algorithm does a good job to find an approximate location for the zeros of the $\bar{\boldsymbol{\lambda}}$ vector, with a quite small number of iterations. Hence, in the first step, we propose to run the PGS algorithm for a small number of iterations. This provides an approximate location of the zeros of the $\bar{\boldsymbol{\lambda}}$ vector. Next the permutation matrix can be formed and the corresponding QR decomposition $\bar{\mathbf{P}}\bar{\mathbf{B}} = \bar{\mathbf{R}}\bar{\mathbf{Q}}$, obtained. Finally, the transmit power can be minimized by solving the triangular inequality system $\bar{\mathbf{R}}\bar{\mathbf{q}} \geq \mathbf{1}$ by forward substitution. It must be stressed that at each forward substitution step the interference value can be calculated. If the inter-user interference is big enough, the corresponding inequality can be respected without any expense of more transmit power, i.e. the corresponding $\bar{\mathbf{q}}$ entry can be set to 0. Otherwise the inequality must be converted into an equality and solved.

In Figure 4.4 we present the results for the approximate algorithm for a given number of iterations of the PGS algorithm, both for a MIMO 4×4 and 8×8. In this figure, the approximate power minimization algorithm is called iPGS. For example, the label "iPGS 5", means that five iterations of the PGS algorithm are done so that and approximate ordering of the users is obtained. As can be seen as the number of iterations increases the performance of the approximate algorithm gets closer to the ones of PGS, as expected. If no user permutation is considered, i.e. $\bar{\mathbf{P}} = \mathbf{I}$, the gains relatively to ZF scheme are minimal. Nevertheless, just for 5 iterations we get around 5 dB of gains relatively to ZF. The performance of the PGS algorithm will be analysed in more detail in section 4.4.5.

4.4.4 Extension to Multicarrier Systems

In this section, we extend the previous algorithm to the case of a multicarrier distributed antenna system. Namely, we show that the previous scheme, when applied jointly to all subcarriers, is equivalent to the individual application, of the same scheme, to each subcarrier, if a final normalization factor is applied to the signal, so that the global power constraint is respected.

Let us consider the same system model, as in section 4.2, but now extended to N_c subcarriers, i.e. the sum of powers, in each RAU, is now constrained over the N_c subcarriers. Namely, this implies that the global received signal vector $\mathbf{y}$ can be expressed by

$$\bar{\mathbf{y}} = \bar{\mathbf{H}}\bar{\mathbf{x}} + \bar{\mathbf{n}} \tag{4.48}$$

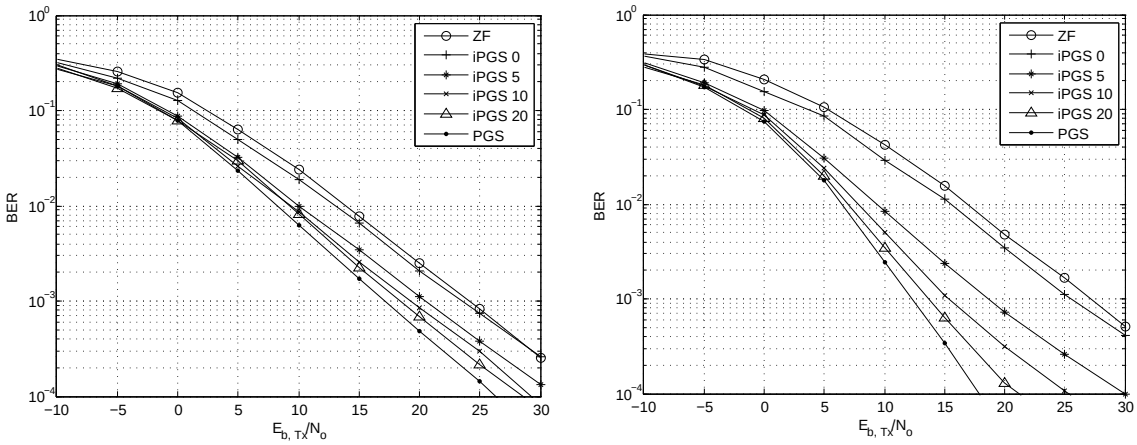

(a) $N = K = 4$ system. (b) $N = K = 8$ system.

Figure 4.4: Simulation results for 4-QAM and iPGS algorithm.

---

where $\bar{\mathbf{H}} = diag(\bar{\mathbf{H}}_1, \ldots, \bar{\mathbf{H}}_l, \ldots, \bar{\mathbf{H}}_{N_c})$, $\bar{\mathbf{H}}_l$ is the channel matrix at subcarrier l, $\bar{\mathbf{y}}^H = [\bar{\mathbf{y}}_1^H, \ldots, \bar{\mathbf{y}}_l, \ldots, \bar{\mathbf{y}}_{N_c}]$ and $\bar{\mathbf{x}}^H = [\bar{\mathbf{x}}_1^H, \ldots, \bar{\mathbf{x}}_l, \ldots, \bar{\mathbf{x}}_{N_c}]$.

Therefore, with this model one can solve the minimum BER problem approximately by running the PGS algorithm over the corresponding $\bar{\mathbf{A}}\bar{\mathbf{A}}^H$ matrix or its regularized version. However, a carefull look to the system of equations representing the KKT conditions of this problem

$$\bar{\mathbf{A}}\bar{\mathbf{A}}^H\bar{\underline{\boldsymbol{\lambda}}} = \bar{\underline{\boldsymbol{\psi}}} + \bar{\mathbf{b}} + \mathbf{1} \tag{4.49}$$

$$\bar{\underline{\boldsymbol{\lambda}}} \geq \mathbf{0},\ \bar{\underline{\boldsymbol{\psi}}} \geq \mathbf{0}, \bar{\underline{\boldsymbol{\lambda}}} \circ \bar{\underline{\boldsymbol{\psi}}} = \mathbf{0} \tag{4.50}$$

shows that it can be reduced to the solution of N_c systems of equations, one for each carrier l, since the channel matrix is diagonal

$$\bar{\mathbf{A}}_l\bar{\mathbf{A}}_l^H\bar{\underline{\boldsymbol{\lambda}}}_l = \bar{\underline{\boldsymbol{\psi}}}_l + \bar{\mathbf{b}}_l + \mathbf{1} \tag{4.51}$$

$$\bar{\underline{\boldsymbol{\lambda}}}_l \geq \mathbf{0},\ \bar{\underline{\boldsymbol{\psi}}}_l \geq \mathbf{0}, \bar{\underline{\boldsymbol{\lambda}}}_l \circ \bar{\underline{\boldsymbol{\psi}}}_l = \mathbf{0} \tag{4.52}$$

where each such system can be associated to the output $\bar{\mathbf{y}}_l = \bar{\mathbf{H}}_l\bar{\mathbf{x}}_l + \bar{\mathbf{n}}_l$. The global transmit signal vector is given by $\bar{\mathbf{x}} = \sqrt{P_T}\bar{\mathbf{A}}^{\mathbf{H}}\bar{\underline{\boldsymbol{\lambda}}}/\sqrt{\bar{\underline{\boldsymbol{\lambda}}}^H\bar{\mathbf{A}}\bar{\mathbf{A}}^H\bar{\underline{\boldsymbol{\lambda}}}}$, as previously. Thus after solving the N_c systems one should concatenate the resulting $\bar{\mathbf{x}}_l$ vectors and scale them accordingly, so that the power constraint is respected. For this reason, there is a linear increase in complexity with the number of subcarriers considered. In fact, if for each subcarrier the PGS MMSE is already used for interference cancellation between users, the only additional processing needed is a scaling of the signals obtained, by the independent processing.

Complexity of the PGS algorithm

In this section, we compare the complexity of the PGS ZF method with the one proposed in [24] which we call Broyden-Fletcher-Goldfarb-Shanno (BFGS) method and compare also the complexity of the PGS MMSE to the ZF scheme. To compare these methods, we have resorted to numerical simulations. Namely, we use as a complexity measure, the average running time to solve a problem instance. For the PGS algorithms we have used as a stopping condition

parameter $\delta = 10^{-2}$. For the BFGS algorithm the Wolfe conditions were set to $c_1 = 10^{-2}$ and $c_2 = 0.9$; see [24]. The solution of the MMSE precoder was used as a starting point for the optimization of the BFGS algorithm. Two operation points have been chosen, 0 dB and 8 dB. It should be noted that the performance of the PGS ZF and ZF schemes is independent of the noise power, contrarily to the PGS MMSE and BFGS. To assess the performance of the proposed schemes over the BFGS and ZF schemes an independent Rayleigh channel has been considered with a base station with $N \in \{2, \ldots, 12\}$ transmit antennas, $K = N$ users and the 4-QAM modulation has been chosen.

The average running time for the PGS ZF and BFGS schemes, has been measured over 10^4 trials and the one for the PGS MMSE and ZF schemes has been averaged over 10^6 runs. The gains in the execution time, i.e. the ratio between the two average running times, are plotted in Figure 4.5, for the two operation points. As can be seen from Figure 4.5(a), for 8 dB the

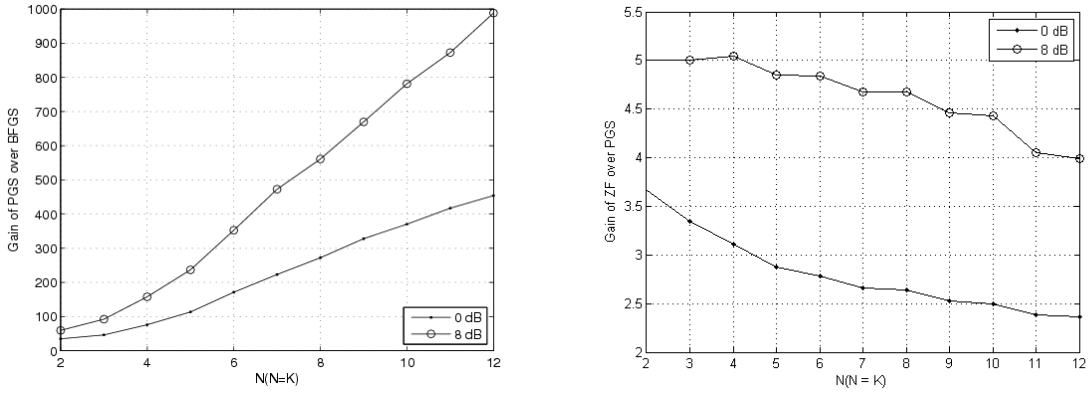

(a) Complexity comparison between PGS ZF and BFGS schemes ($time_{BFGS}/time_{PGSZF}$).

(b) Complexity comparison between PGS MMSE and ZF schemes ($time_{PGSMMSE}/time_{ZF}$).

Figure 4.5: Complexity analysis for PGS algorithm.

PGS ZF algorithm can be from 60 (2×2 MIMO) to 1000 (12×12 MIMO) times faster than the BFGS algorithm. For low values of SNR, the starting point of the BFGS is closer to the optimum value and thus a smaller number of iterations is needed. Consequently, the average running time decrease. However, we can also see a speedup of around 35 to 450 times, for 0 dB.

In Figure 4.5(b) we present the complexity results for the PGS MMSE and ZF schemes. The complexity of the nonlinear scheme is about five times higher, an order of magnitude, than the corresponding linear scheme, for the range considered, and the complexity measure seems to decrease with the number of users/transmit antennas considered. The same happens for the other two schemes, see Figure 4.5(a). This could be explained by the fact that for moderate to higher values of K and N the number of degrees of freedom of the system increases. Therefore, more alternatives to set the elements of $\bar{\boldsymbol{\lambda}}$ to zero, by the PGS algorithm, are available, reducing in that way the dimensions of the matrix to be inverted.

4.4.5 Performance Assessment

In this section, we assess the performance of the proposed schemes by resorting to numerical simulations. Namely, we start by analyzing the performance of these algorithms for conventional co-located system scenarios to evaluate the tightness of the approximations made

to the optimization problem at hand. Finally, the performance of these algorithms is analyzed in the distributed context, taking into account both phases of the algorithm, either for the single-carrier either for the multi-carrier cases.

Co-located Systems

For co-located systems we compare the PGS ZF algorithm with the optimum (MBMUT precoder), discussed in [24], and also with the MMSE and ZF precoders. For the simulations, a flat fading Rayleigh channel has been considered, without spatial correlation and with independent channel realizations. The channel is assumed to be perfectly known at the transmitter. All results presented in this section show the bit error rate over the ratio of average transmitted energy per bit to the one-sided spectral noise power density N_0. For the PGS ZF algorithm, we have used a value of 10^{-2} for the stopping condition parameter δ.

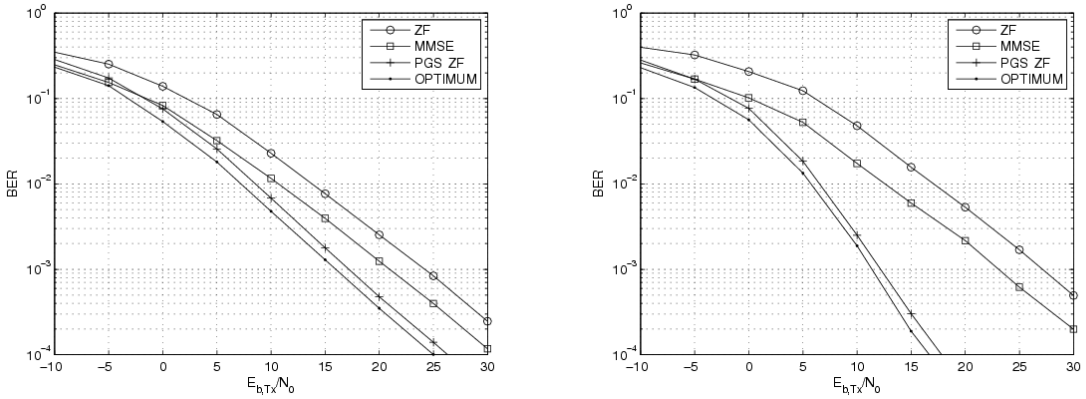

(a) $N = K = 4$ system. (b) $N = K = 8$ system.

Figure 4.6: Simulation results for 4-QAM.

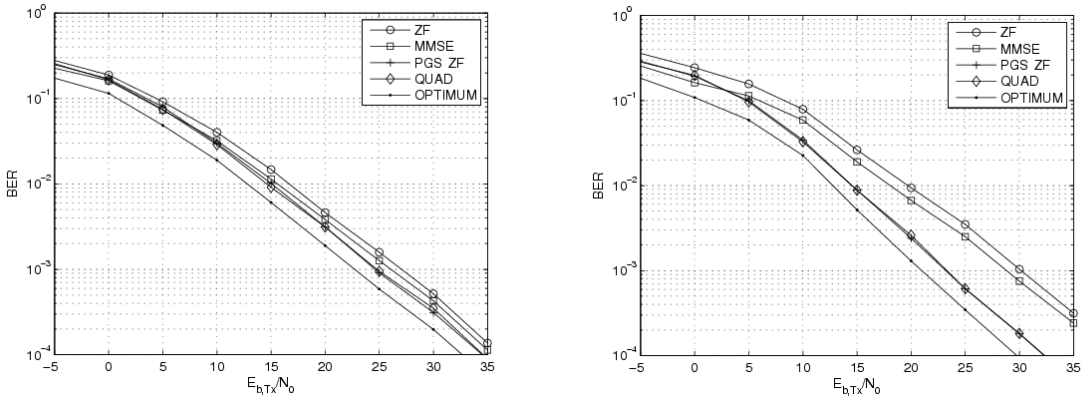

(a) $N = K = 4$ system. (b) $N = K = 8$ system.

Figure 4.7: Simulation results for 16-QAM.

In Figure 4.6, the performance of a system with $K = N = 4$ and $K = N = 8$, using

4-QAM modulation, is analyzed. As can be seen from these two figures the gain of the PGS ZF approach increases with SNR and the number of transmit antennas/user's. At low SNR, the performance of the PGS ZF and MMSE approaches is similar. However, in the high SNR regime, the PGS ZF approach has a gain of around 5 and 10 dB for a target BER of 10^{-3}, for the 4×4 and 8×8 systems, respectively. The higher gains obtained with moderate to high values of K and N can be explained by the fact that for those systems there are more degrees of freedom. Therefore, more alternatives to set the elements of $\bar{\boldsymbol{\lambda}}$ to zero are available, reducing in that way the dimensions of the matrix to be inverted. It is also clear, from these two figures, that the diversity order obtained both with the MBMUT and PGS ZF precoders is higher than the one obtained with the MMSE and ZF precoders. This is related to the fact that for the PGS case the precoder is using all the available decoding space at the decoder, contrary to the ZF and MMSE precoders. Comparing the PGS ZF precoder to the optimum, one can see a gap of 1.5 dB at BER 10^{-3}, which decreases as the number of antennas increases.

In Figure 4.7 we present the results obtained for a system with $K = N = 4$ and $K = N = 8$, using a 16-QAM constellation. For 16-QAM we also present the results obtained using a quadratic programming solver. The performance of the quadratic solver is similar to the one obtained using the PGS ZF algorithm (taking into account the assumption made for β, in section 4.4.2). The behavior of the results obtained for 16-QAM is similar to the one observed for 4-QAM. The improvement provided by the new algorithm relatively to ZF and MMSE is somewhat reduced and the penalty comparatively to the optimum slightly higher (2dB at BER 10^{-3}).

Distributed Antenna System

In order to assess the performance of the proposed algorithms, for a DAS, we have considered a scenario with four RAUs ($R = 4$), each with two transmit antennas ($N_r = 2$), and eight users ($K = 8$). The number of users per cell is considered to be two. The long-term channel powers are assumed to be one for intracell links and are uniformly distributed on the interval $[0.2, 0.6]$ for the intercell links. The performance of the proposed scheme is compared against the optimum, which we call per-RAU OPTIMUM, and also with the per-RAU Linear ZF and MMSE schemes under a flat fading Rayleigh channel without spatial correlation and with independent channel realizations. We present results also for the TPC regularized PGS algorithm (TPC PGS MMSE), which can be used as a lower bound for the other schemes. To obtain the per-RAU OPTIMUM we have used a SQP solver and the solution of the per-RAU PGS MMSE was used as a starting point. All the results are presented in terms of the average BER as a function of per-RAU SNR defined as $SNR = 1/\sigma^2$.

In Figure 4.8(a) we present the results for QPSK modulation. As can be seen the gain of the per-RAU PGS MMSE approach increases with SNR. At low SNR the performance of the per-RAU PGS MMSE and per-RAU Linear MMSE approaches are equal, as can be seen from Figure 4.8(a) and 4.8(b). However, in the high SNR regime, the PGS approach has a gain of around 15 dB and 10 dB, at a target BER of 10^{-3} over the per-RAU Linear ZF and MMSE approaches, respectively. The gap to the TPC PGS MMSE is about 3 dB and to the per-RAU OPTIMUM is about 1 dB. It is also clear, from these two figures, that the diversity order obtained by the PGS precoders is higher than the one obtained with the Linear ZF and MMSE precoders.

In Fig. 4.8(b) we present the results, for a 16-QAM constellation. The value used for β was η. The behavior of the results obtained for 16-QAM is similar to the one observed for QPSK.

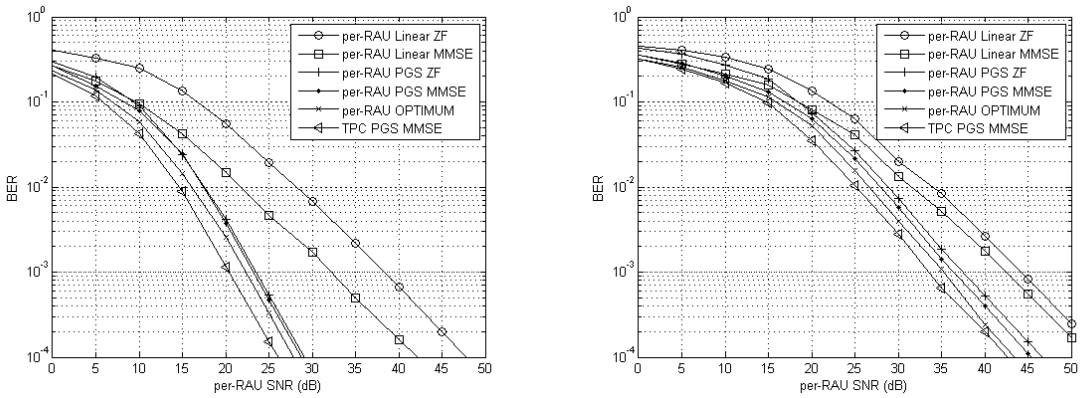

(a) QPSK and $R = 4, N_r = 2, K = 8$.

(b) 16-QAM and $R = 4, N_r = 2, K = 8$.

Figure 4.8: Performance evaluation of the proposed scheme for a DAS.

The improvement provided by the new algorithm in comparison to per-RAU Linear ZF (8 dB) and MMSE is somewhat reduced and the penalty relatively to the centralized algorithm (TPC PGS MMSE) is 3 dB and to the per-RAU OPTIMUM 1 dB.

As one can see from figures 4.6(a) and 4.6(b) the diversity order achieved for QPSK is higher than the one obtained for 16-QAM. This occurs, since the 16-QAM constellations decision regions are more constrained than the ones of the QSPK. By this we mean that for 16-QAM, the interior constellation points decoding regions are smaller than the ones of the QPSK.

Finally, from the results presented, one can see that the regularized version of the PGS method provides improvements both in the low and high SNR regime. It should be also emphasized that for low SNR values the regularized PGS method is faster than the PGS ZF counterpart since in this regime the inverted matrix $(\bar{\mathbf{A}}\bar{\mathbf{A}}^H + 2\sigma^2\mathbf{I})$ is mostly a diagonal matrix.

OFDM Distributed Antenna System

In order to evaluate the proposed multicell multiuser precoding algorithm, we consider a typical pedestrian scenario based on LTE specifications [35]. We consider four RAUs, $R = 4$, which are equipped with two antennas, $N_r = 2$, and eight single antenna users, $K = 8$. The main parameters used in the simulations are: FFT size of 1024; number of available subcarriers (N_c) set to 16, sampling frequency set to 15.36 MHz; useful symbol duration is $66.6\mu s$, cyclic prefix duration is $5.21\mu s$; overall OFDM symbol duration is $71.86\mu s$; sub-carrier separation is 15 kHz, and modulation is 4-QAM and 16-QAM. We used the ITU pedestrian channel model B, with the modified tap delays according to the sampling frequency defined on LTE standard. Concerning the MISO model, we assume that the distance between antenna elements of each RAU is far apart to assume uncorrelated antenna channels. The number of users per cell is two and the long-term channel powers are assumed to be 1 for the intracell links and are uniformly distributed on the interval $[0.2, 0.6]$ for the intercell links. All the results are presented in terms of the average BER as a function of per-RAU SNR defined as $SNR = 1/(N_c\sigma^2)$.

In Figure 4.9(a) and 4.9(a) we show the results for QPSK and 16-QAM, respectively. In

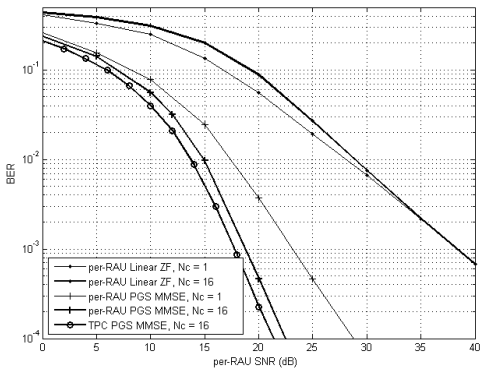

(a) QPSK and $R = 4, N_r = 2, K = 8$.

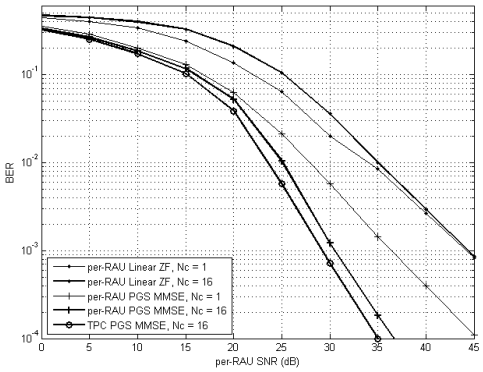

(b) 16-QAM and $R = 4, N_r = 2, K = 8$.

Figure 4.9: Performance evaluation of the proposed scheme for a OFDM DAS.

order to assess the benefits of the joint processing of the subcarriers we also plot in these figures the results obtained in the last section for one subcarrier, for reference purposes. For QPSK and for a target BER of 10^{-3} we got a gain of around 20 dB from using the per-RAU PGS MMSE algorithm over per-RAU Linear ZF. Furthermore we get around 5 dB of gain from the joint processing of the 16 subcarriers at the same target BER. As can be observed from these figures this gain comes from the additional diversity order obtained by the algorithm, when the subcarriers are jointly processed. Equally important is the fact that unlike the PGS MMSE scheme the ZF algorithm performance gets worse as the number of carriers increases. Additionally, this gain seems to be equal both for QPSK and 16-QAM as well as the gap to the lower bound (TPC PGS MMSE), around 1 dB, for both. On the other hand, for 16-QAM, the gap from per-RAU PGS MMSE to the per-RAU Linear ZF scheme, decreases and is around 14 dB, for a target BER of 10^{-3}.

4.5 Conclusion

In this chapter, we proposed and analyzed an algorithm for the minimization of the average BER, of the downlink of a multiuser DAS. The algorithm has two phases; the first phase involves the solution of a minimum BER problem, for the downlink of a conventional co-located multiuser MIMO channel. Such a problem has been tackled by considering the high SNR regime. By taking into account the properties of the BER function, in that regime, it is possible to simplify, this minimization problem, from a quadratic nonlinear optimization to a simple quadratic program. This results in a significant complexity reduction. On the other hand, such a formulation has allowed to draw connections between the standard ZF scheme and the optimum scheme, due to the close connections of the proposed scheme to ZF. For co-located systems, the algorithm has been evaluated numerically and shown to provide significant gains relatively to the conventional ZF or MMSE approaches and to be close to the optimum for moderate to high SNRs. On the other hand, the two phases algorithm has been evaluated numerically for DAS scenarios and shown to provide significant gains over the linear ZF and MMSE approaches and to be also close to the optimum. Additionally, for the multicarrier case, there was 1 dB gap from the corresponding lower bound (TPC problem),

and the diversity order achieved increased substantially. All this accomplished with a linear increase in complexity. Therefore, the algorithm is well suited for practical implementations as it combines close to optimum performance with a reduced complexity.

4.6 References

[1] I. E. Telatar, "Capacity of Multi-antenna Gaussian Channels," *AT&T Bell Laboratories, Murray Hill, NJ*, 1999.

[2] W. Yu and J. Cioffi, "Sum capacity of Gaussian vector broadcast channels," *Information Theory, IEEE Transactions on*, vol. 50, no. 9, pp. 1875–1892, Sept. 2004.

[3] N. Jindal, "High SNR analysis of MIMO broadcast channels," *Information Theory, 2005. ISIT 2005. Proceedings. International Symposium on*, pp. 2310–2314, Sept. 2005.

[4] G. J. Foschini and M. J. Gans, "On limits of wireless communications in a fading environment when using multiple antennas," *Wireless Personal Communications*, vol. 6, pp. 311–335, 1998.

[5] S. Venkatesan, A. Lozano, and R. Valenzuela, "Network MIMO: Overcoming Intercell Interference in Indoor Wireless Systems," pp. 83 –87, nov. 2007.

[6] B. Vojcic and W. M. Jang, "Transmitter precoding in synchronous multiuser communications," *Communications, IEEE Transactions on*, vol. 46, no. 10, pp. 1346 –1355, oct 1998.

[7] M. Brandt-Pearce, "Transmitter-based multiuser interference rejection for the down-link of a wireless CDMA system in a multipath environment," *Selected Areas in Communications, IEEE Journal on*, vol. 18, no. 3, pp. 407 –417, mar 2000.

[8] Q. Spencer, A. Swindlehurst, and M. Haardt, "Zero-forcing methods for downlink spatial multiplexing in multiuser MIMO channels," *Signal Processing, IEEE Transactions on*, vol. 52, no. 2, pp. 461 – 471, feb. 2004.

[9] M. Meurer, P. W. Baier, and W. Qiu, "Receiver orientation versus transmitter orientation in linear MIMO transmission systems," *EURASIP J. Appl. Signal Process.*, vol. 2004, pp. 1191–1198, January 2004.

[10] D. Palomar, J. Cioffi, and M. Lagunas, "Joint Tx-Rx beamforming design for multicarrier MIMO channels: a unified framework for convex optimization," *Signal Processing, IEEE Transactions on*, vol. 51, no. 9, pp. 2381 – 2401, sept. 2003.

[11] X. Zhang, D. Palomar, and B. Ottersten, "Statistically Robust Design of Linear MIMO Transceivers," *Signal Processing, IEEE Transactions on*, vol. 56, no. 8, pp. 3678 –3689, aug. 2008.

[12] M. Joham, K. Kusume, M. H. Gzara, W. Utschick, and J. A. Nossek, "Transmit wiener filter for the downlink of tdd ds-cdma systems," in *in Proc. IEEE ISSSTA*, 2002, pp. 9–13.

[13] M. Costa, "Writing on dirty paper (Corresp.)," *Information Theory, IEEE Transactions on*, vol. 29, no. 3, pp. 439–441, May 1983.

[14] T. M. Cover and J. A. Thomas, *Elements of information theory.* New York, NY, USA: Wiley-Interscience, 1991.

[15] H. Weingarten, Y. Steinberg, and S. Shamai, "The Capacity Region of the Gaussian Multiple-Input Multiple-Output Broadcast Channel," *Information Theory, IEEE Transactions on*, vol. 52, no. 9, pp. 3936–3964, Sept. 2006.

[16] P. Marsch and G. Fettweis, "On Downlink Network MIMO under a Constrained Backhaul and Imperfect Channel Knowledge," pp. 1 –6, 30 2009-dec. 4 2009.

[17] J. Zhang, R. Chen, J. Andrews, and R. Heath, "Coordinated Multi-cell MIMO Systems with Cellular Block Diagonalization," pp. 1669 –1673, nov. 2007.

[18] A. Armada, M. Sanchez-Fernandez, and R. Corvaja, "Waterfilling Schemes for Zero-Forcing Coordinated Base Station Transmission," pp. 1 –5, 30 2009-dec. 4 2009.

[19] W. Liu, S. Ng, and L. Hanzo, "Multicell Cooperation Based SVD Assisted Multi-User MIMO Transmission," pp. 1 –5, april 2009.

[20] R. Holakaouei, A. Silva, and A. Gameiro, "Power allocation strategies for SVD multicell MIMO-OFDM based systems," *IEEE Wireless Telecommunications Symposium, WTS 2011. IEEE*, april 2011.

[21] E. Bjo¨ andrnson, R. Zakhour, D. Gesbert, and B. Ottersten, "Cooperative Multicell Precoding: Rate Region Characterization and Distributed Strategies With Instantaneous and Statistical CSI," *Signal Processing, IEEE Transactions on*, vol. 58, no. 8, pp. 4298 –4310, aug. 2010.

[22] R. Inner, W. Rave, and G. Fettweis, "Minimum BER transmission for TDD-CDMA in frequency-selective channels," in *Personal, Indoor and Mobile Radio Communications, 2003. PIMRC 2003. 14th IEEE Proceedings on*, vol. 2, 2003, pp. 1260 – 1264 vol.2.

[23] R. Irmer, R. Habendorf, W. Rave, and G. Fettweis, "Nonlinear multiuser transmission using multiple antennas for TDD-CDMA," in *in Proc. IEEE WPMC*, 2003, pp. 251–255.

[24] R. Habendorf and G. Fettweis, "Nonlinear Optimization for the Multiuser Downlink," in *European Wireless Conference*, 2007.

[25] Fibre Optic Networks for Distributed, Extendible Heterogeneous Radio Architectures and Service Provisioning. FUTON project.

[26] F. Diehm, P. Marsch, and G. Fettweis, "The FUTON Prototype: Proof of Concept for Coordinated Multi-Point in Conjunction with a Novel Integrated Wireless/Optical Architecture," in *Wireless Communications and Networking Conference Workshops (WCNCW), 2010 IEEE*, april 2010, pp. 1 –4.

[27] J. Nocedal and S. J. Wright, *Numerical optimization.* Springer, 1999.

[28] S. P. Boyd and L. Vandenberghe, *Convex optimization.* Cambridge University Press, 2004.

[29] S. Haykin, *Adaptive Filter Theory*, 4th ed. Prentice Hall, Sep. 2001.

[30] J. K. M. Johnathan M. Bardsley and R. Vio, "THE STABILIZING PROPERTIES OF NONNEGATIVITY CONSTRAINTS IN LEAST-SQUARES IMAGE RECONSTRUCTION," 2006.

[31] V. Franc, V. Hlavac, and M. Navara, *Sequential Coordinate-Wise Algorithm for the Non-negative Least Squares Problem*, ser. Lecture Notes in Computer Science. Springer Berlin / Heidelberg, 2005, vol. 3691.

[32] R. W. Cottle, J. Pang, and R. E. Stone, *The Linear Complementarity Problem.* Academic Press, Feb. 1992.

[33] R. Muller, D. Guo, and A. Moustakas, "Vector Precoding for Wireless MIMO Systems and its Replica Analysis," *Selected Areas in Communications, IEEE Journal on*, vol. 26, no. 3, pp. 530 –540, april 2008.

[34] J. L. Morales, J. Nocedal, and M. Smelyanskiy, "An Algorithm for the Fast Solution of Symmetric Linear Complementarity Problems," 2008.

[35] 3GPP, "Evolved Universal Terrestrial Radio Access (E-UTRA); Long Term Evolution (LTE) physical layer; General description," 3rd Generation Partnership Project (3GPP), TS 36.201, Dec. 2007. [Online]. Available: http://www.3gpp.org/ftp/Specs/html-info/36201.htm

Chapter 5

Binary Dirty Paper Coding

This chapter focus on the design of a practical binary dirty paper coding scheme. In the design of such a precoder the lossy source coding subproblem is first considered. This leads to the proposal of a new algorithm for binary quantization over low density generator matrix codes. The proposed algorithm, is a modified version of belief propagation, used in the channel coding framework, and has linear complexity in the code block length. We also provide a common framework under which the proposed algorithm and some previously proposed algorithms fit. Using the previous developed framework a practical DPC scheme is proposed. It uses a low density generator matrix code concatenated with a high rate low density parity check code. In contrast to the superposition coding framework, where high-order alphabet codes are used, we propose to implement binary DPC using only binary codes. Through application of approximate density evolution and linear programming we optimize the degree distribution of the proposed code. Simulation results show that both the lossy and dirty paper coding scheme achieve close to state-of-the-art performance with reduced complexity.

5.1 Introduction

Dirty Paper Coding is a non-linear coding scheme for canceling non-causally known interference at the transmitter. This name has been proposed in a remarkable paper by Costa [1], in 1983, where it has been shown that the capacity of a Gaussian channel, when the transmitter knowns non-causally the interference, is the same of the corresponding interference free channel. Recently, driven by these results, in [2] the authors have shown that DPC is capacity achieving on the Gaussian broadcast channel. But the applications of DPC do not end here. DPC has found applications in information hiding, data embedding, watermarking [3–5] and more recently in cooperative communications [6]. The fundamental idea behind DPC is binning. Binning corresponds to the division of the set of codewords into groups ("bins") of codewords, each with the same label. Binning is not only an important concept for DPC. It is also fundamental in multi-user information theory, namely, for example, in cooperative communications. In [7] and [8], Peyman and Wei Yu, have proposed a bilayer LDPC code construction for efficient implementation of binning at the relay channel. The main idea behind their scheme is to design a LDPC code that is capable of working at two different rates: the one at the destination and the one at the relay. In this chapter, we follow a similar approach to attain the capacity of the binary dirty paper channel. However, instead of designing a dual rate LDPC code for channel coding, we now design an LDGM code, also able to work at two different rates,

but where the global code works at the channel coding level and the corresponding sub-code at the lossy source coding level. LDGM codes have emerged as a subset of LDPC codes, but with lower encoding complexity. However, LDGM codes are asymptotically bad as they exhibit an error floor that is independent of the block size considered. Nonetheless, using a proper concatenation of two codes, one can mitigate the poor distance properties, while preserving the low complexity [9]. In [10] the authors have shown that LDGM codes, as duals of LDPC codes, can saturate the rate-distortion bound of the binary erasure quantization (BEQ) problem, the dual of the BEC problem, with the help of a modified BP algorithm. Since this pioneering work, LDGM codes have been extensively used for lossy source coding. Namely, in [11] the authors propose a survey propagation (SP) based iterative quantization algorithm and in [12] the authors propose a BP based iterative quantization algorithm, to compress a binary symmetric source. However, both use a decimation process to help the respective algorithm to converge. Thus, the overall computational complexity is $\mathcal{O}(N^2)$, [13], where N is the codeword length. To overcome the complexity bottleneck, in [13], the authors propose a linear complexity algorithm to do lossy source coding with the help of LDPC codes over GF(q). However, the use of higher-order fields substantially increases the computational complexity, in comparison to the binary field. In contrast, we propose to do lossy source coding with a binary LDGM code, and with a modified BP algorithm, with computational complexity $\mathcal{O}(N)$, since no decimation is used. As a result of the good channel and lossy source coding performance of LDGM codes and also due to its inherent low complexity, LDGM codes are good candidates for the DPC problem.

This chapter is organized as follows: section 5.2 presents the general framework of binary DPC. section 5.3 provides some background about LDGM codes and about the lossy source coding problem. In section 5.3.4 we describe and derive the proposed algorithm for lossy compression. Next, in section 5.3.5 the performance of the proposed compression scheme is evaluated, by numerical simulations. In section 5.4 we describe our proposed DPC scheme, namely the code structure, respective encoding/decoding algorithms and how to optimize the proposed code, using the erasure channel and the dual code approximations [10]. Then in section 5.4.3 the performance of our scheme is assessed by numerical simulations and finally we conclude in section 5.5.

5.2 Binary Dirty Paper Coding Framework

In this section we describe the binary dirty paper framework in more detail. For the binary dirty paper channel, under the binary input $\mathbf{x} \in \{0,1\}^N$ the output takes the form $\mathbf{y} = \mathbf{x} + \mathbf{s} + \mathbf{n}$, where[1] $\mathbf{s} \sim Ber(1/2)$ is the interference signal and $\mathbf{n} \sim Ber(p)$ is the channel noise. The channel input, $\mathbf{x}$, is a function of the interference $\mathbf{s}$ and of the information bearing symbol $\mathbf{d}$, $\mathbf{x} = f(\mathbf{s}, \mathbf{d})$. The objective of binary DPC is to maximize the transmission rate subject to a distance power constraint. In the case of binary signalling the constraint can be written in terms of the hamming distance, i.e. $\mathbf{E}[\|\mathbf{x}\|_1]/N \leq D$. The capacity of this channel is given by, [14]:

$$R(D,p) = \begin{cases} H(D) - H(p), & \text{if } D_0 \leq D \leq 1/2 \\ \alpha D, & \text{if } 0 \leq D \leq D_0 \end{cases} \tag{5.1}$$

where $H(.)$ is the binary entropy function, $D_0 = 1 - 2^{-H(p)}$ and $\alpha = log((1-D_0)/D_0)$.

[1] By $\mathbf{x} \sim Ber(p)$ we mean a Bernoulli random variable with a probability p of being equal to '1'.

For this problem the binning strategy, see Figure 5.1, is to divide the set of all $2^{N(1-h(p))}$ possible[2] input binary sequences into $B = 2^{N(h(D)-h(p))}$ bins, indexed by the transmit message $\mathbf{d}$. The input set contains $2^{N(1-h(p))}$ elements drawn randomly and thus can be viewed as a channel code with rate $R_C = 1 - h(p)$, for which arbitrary small probability of error can be achieved, for channel crossover probabilities up to p. Each randomly constructed bin contains $2^{N(1-h(p))}/B = 2^{N(1-h(D))}$ elements and thus can be viewed as a lossy code with rate $R_L = 1 - h(D)$, for which, by the rate-distortion theory [15], an average distortion down to DN can be achieved.

To encode message $\mathbf{d}$ the encoder must restrict itself to bin $\mathbf{d}$ and search for the codeword that is closer to $\mathbf{s}$. After finding the closest codeword to $\mathbf{s}$, $\mathbf{u}$, the encoder inputs to the channel $\mathbf{x} = \mathbf{u} - \mathbf{s}$. At the other end, the decoder receives $\mathbf{u} + \mathbf{n}$ and wants to recover message $\mathbf{d}$. To do that, the decoder can treat the decoding problem as a standard channel decoding problem, to find the sequence $\mathbf{u}$, and after, it only needs to match sequence $\mathbf{u}$ to his respective bin, to obtain $\mathbf{d}$.

5.3 Lossy Source Coding

As stated in the previous paragraphs a dirty paper coding scheme can be divided into two main problems: the lossy source coding problem and the channel coding problem. In the following paragraphs, we start by addressing the first of these problems (lossy source coding).

5.3.1 Problem Description

In the lossy coding problem, given a realization $\mathbf{s} \in \{0,1\}^N$ of a Ber(1/2) source S we want to map it to an index $\mathbf{x} \in \{0,1\}^K$ such that approximate reconstruction of $\mathbf{s}$ is possible within a given fidelity criterion ($R = K/N$ is the compression rate). The fidelity measure used here and the most commonly used in this area, for a binary source, is the Hamming distance between the source sequence $\mathbf{s}$ and the reconstructed sequence $\hat{\mathbf{s}}$

$$d(\mathbf{s}, \hat{\mathbf{s}}) = \frac{1}{N} \sum_{i=1}^{N} |s_i - \hat{s}_i| \tag{5.2}$$

The objective of lossy compression is to minimize the average distortion $D = \mathbb{E}[d(\mathbf{S}, \hat{\mathbf{S}})]$. For such a distortion measure the asymptotic limit, designated as rate-distortion function, is well known [15] and is given by $R(D) = 1 - h(D)$, for $D \in [0, 1/2]$ and zero otherwise.

5.3.2 LDGM Code Description and Notation

An LDGM code can be represented both by its generator matrix $\mathbf{G} \in \{0,1\}^{N \times K}$ and by the associated factor graph $\mathcal{G} = (V, C, E)$. Where the sets $V = \{1, \ldots, K\}$, $C = \{1, \ldots, N\}$ and $E = \{\ldots, (a,i), \ldots\}$ denote the information bit nodes, the check nodes and the edges connecting them, respectively. We use the variables $a, b, c \in C$ to denote check nodes and variables $i, j, k \in V$ to denote information bits. We define the sets $C(i) = \{a \in C | (a,i) \in E\}$, $V(a) = \{i \in V | (a,i) \in E\}$ and use the symbol $\setminus$ to denote the set subtraction operator. A check node $a \in C$ connects to an information bit $i \in V$, $(a,i) \in E$, if $\mathbf{G}_{a,i} = 1$. In Figure

[2] By possible we mean a set of codewords for which arbitrary small probability of error, for channel crossover probabilities lower than p, is attainable.

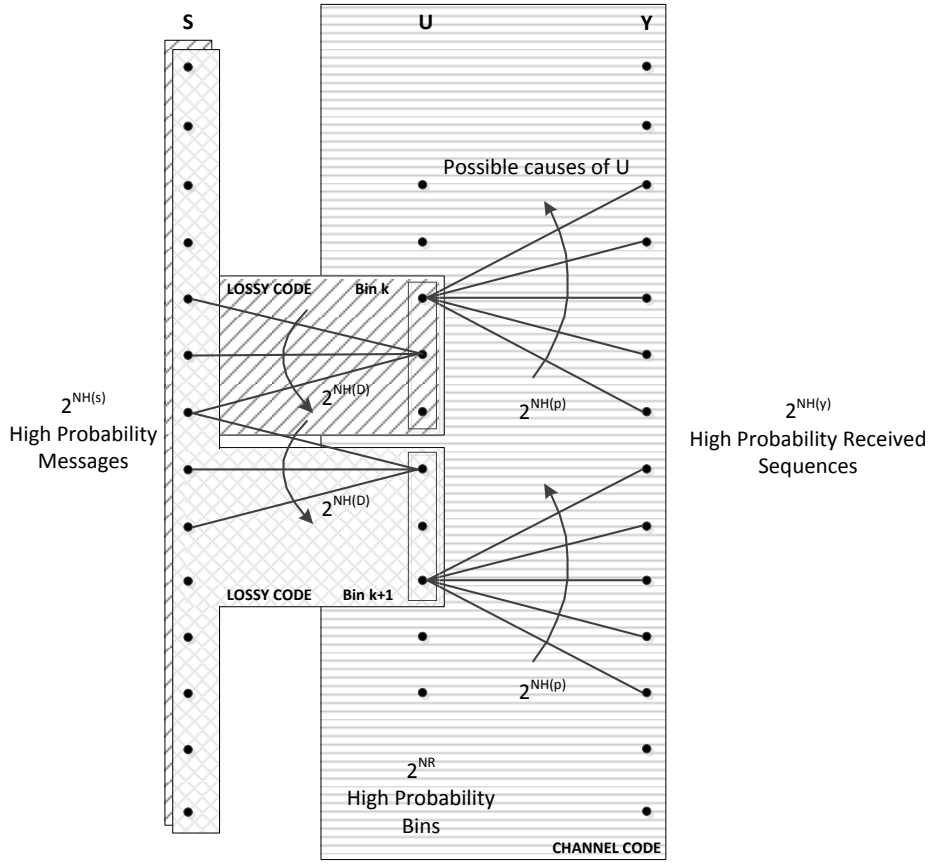

Figure 5.1: Binning Strategy Diagram, for DPC.

5.2 we depict, as an example, the factor graph of a given LDGM code with 5 check nodes, 4 information bits and 5 source bits, randomly connected between them. In this figure, the white circles denote the information bits, the squares represent the check nodes and by $\mathbf{\Pi}$ we mean a uniform drawn permutation.

The connection structure between check nodes and information bits, in a LDGM code, is specified by the correspondent check and information bit node degree distributions, from the edge perspective, (ρ, λ), $\rho(x) = \sum_i \rho_i x^{i-1}$ and $\lambda(x) = \sum_i \lambda_i x^{i-1}$. ρ_i and λ_i denote the portion of all edges connected to check nodes and information bits with degree i, respectively.

The degree of a check node is equal to the number of connected information bits, i.e. the number of connections from the squares to the circles in Figure 5.2, which is the same as the corresponding number of entries equal to 1 in row i of $\mathbf{G}$. In the case of a LDGM code, there is also a connection from the check nodes to the source bits, but this is not considered for the degree. For a LDGM code, $\mathcal{C}$, defined by the generator matrix $\mathbf{G}$, and for an index $\mathbf{x}$ the corresponding reconstructed source sequence is given by $\hat{\mathbf{s}} = \mathbf{G}\mathbf{x}$. Which due to the sparse

structure of the corresponding LDGM code can be computed in $\mathcal{O}(N)$ time, for a given index $\mathbf{x}$.

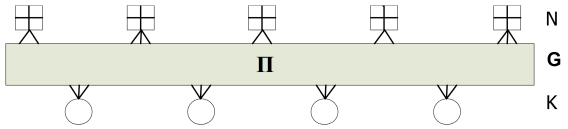

Figure 5.2: LDGM code factor graph representation.

5.3.3 Binary Erasure Quantization

In this section we analyse the simpler BEQ problem [10], to get some insights into the more complicated binary quantization problem.

The source in the BEQ problem, S, can assume three different values, $S \in \{0, 1, ?\}$, according to the probability distribution [10]

$$p_S(s) = \frac{1-\epsilon}{2}\delta(s-0) + \frac{1-\epsilon}{2}\delta(s-1) + \epsilon\delta(s-?) \tag{5.3}$$

where ϵ denotes the erasure probability and $\delta(.)$ the Dirac delta function. The objective in the BEQ is to map the source, S, with dimension N, to an index $X \in \{1, 2, \ldots, 2^{NR}\}$, such that the obtained distortion is zero. The distortion function ($d(a, b)$), for the BEQ, is $d(a, b) = 0$ if $a =?$ or $a = b$ and 1 otherwise. It is easy to get a lower bound for the rate distortion function, for this type of source. Consider that the reconstruction algorithm knows in advance the positions of the erasures, of source $\mathbf{s}$. If we have this information, we only need to know the values of the $(1-\epsilon)N$ non-erased positions to obtain a reconstructed sequence, with zero distortion. Namely, with that knowledge we can later assign any value to the erasures, without any additional distortion. Hence, it is easy to verify that the rate distortion function is lower bounded by $1-\epsilon$. To attain the bound let us consider a linear code with rate R and generator matrix $\mathbf{G} \in \{0, 1\}^{N \times RN}$. Namely let us consider that the reconstructed sequence, $\mathbf{q}$, given index $\mathbf{x}$, is $\mathbf{q} = \mathbf{G}\mathbf{x}$. By the problem definition, the source and reconstructed sequences, should be only different at the erasure positions. Assuming $\mathbf{q} = [\mathbf{q_1^T}, \mathbf{q_2^T}]^\mathbf{T}$, $\mathbf{G} = [\mathbf{G_1^T}, \mathbf{G_2^T}]^\mathbf{T}$ and that such erasures occur in the last positions of $\mathbf{q}$ and $\mathbf{s}$, the previous system of equations reduces to $\mathbf{q_1} = \mathbf{G_1}\mathbf{x}$. Thereafter, to obtain zero distortion, the reduced system of equations must have at least one solution. This happens if the system is underdetermined, i.e. if $\mathbf{G}_1$ has dimension $(1-\epsilon)N \times RN$ and $(1-\epsilon)N \leq RN$. As such R must be greater or equal to $1-\epsilon$. On the other hand, if $\mathbf{G}_1$ has dimension $(1-\epsilon)N \times (1-\epsilon)N$ and is full rank, with high probability, the previous system has just one solution, and the upper bound is met. Additionally, if the rate is higher than $1-\epsilon$ the system gets undetermined and accepts a set of indexes as its solutions. This is indeed what happens for practical codes, since the rate distortion function is only achievable in the infinite block length. Thereafter for a practical system the number of reconstruction sequences, at zero distance from the source, is higher than one, making the solution of the lossy source coding problem more difficult than the one of the channel coding problem, where just one codeword is close to the transmitted sequence.

5.3.4 Derivation of the Proposed Compression Algorithm

Almost all previously proposed algorithms for doing lossy source coding rely on a decimation step to help the iterative message passing algorithm, like BP, to converge. Namely, this type of algorithms can be divided into two phases, one where BP runs for a given number of iterations and another where the most biased information bits are decimated. Even if the resultant performance of such algorithms is very good, in practice, their inherent computational complexity is $\mathcal{O}(N^2)$ [13], since two phases are considered. One exception to this rule is the algorithm proposed in [13], [16], the reinforced BP (RBP). This algorithm does a kind of soft decimation by reinforcing the beliefs of each information bit at each iteration. Our proposed algorithm is based on the same principle, but it is applied to LDGM codes instead of LDPC codes and we also show a connection between "hard" and "soft" decimation.

In the following paragraphs, we explain how to transform the decimation step, of the previously proposed algorithms, in a soft decimation step, that is performed within each iteration. We also show how to use this simple transformation to recover the RBP algorithm as a soft version of the Bias Propagation Algorithm (BiP), [12]. This transformation results in just a slightly modification to the BP updating rules.

In the LDGM code approach to lossy source coding, the encoding phase amounts to mapping a source sequence $\mathbf{s} \in \{0,1\}^N$ to an index $\mathbf{x} \in \{0,1\}^K$, such that the Hamming distortion $d(\mathbf{Gx}, \mathbf{s})$ is minimized. Let us define the following equivalent conditional probability distribution

$$P(\mathbf{x}|\mathbf{s}) = \frac{1}{Z} e^{-\vartheta d(\mathbf{Gx},\mathbf{s})} = \frac{1}{Z} \prod_{a \in C} e^{-\vartheta d(\mathbf{G}_a\mathbf{x},\mathbf{s}_a)} = \frac{1}{Z} \prod_{a \in C} \Psi(\mathbf{x}_{V(a)}, \mathbf{s}_a) \tag{5.4}$$

where Z is a normalizing constant, $\mathbf{G}_a$ denotes row a of $\mathbf{G}$, ϑ is a parameter that is tuned via simulations to get as good performance as possible and $\Psi(\mathbf{x}_V(a), \mathbf{s_a}) = e^{-\vartheta d(\mathbf{G}_a\mathbf{x},\mathbf{s}_a)}$ represents the local constraint of check node a. It is not difficult to see, from equation (5.4), that the most probable codeword is also the one that minimizes the corresponding Hamming distortion. Indeed, the best assignment for bit x_i is obtained from the corresponding bit marginal value

$$\begin{aligned} x_i &= arg \max_{x_i \in \{0,1\}} P(x_i|\mathbf{s}) = arg \max_{x_i \in \{0,1\}} \sum_{\sim x_i} P(\mathbf{x}|\mathbf{s}) \\ &= arg \max_{x_i \in \{0,1\}} \sum_{\sim x_i} \prod_{a \in C} \Psi(\mathbf{x}_{V(a)}, \mathbf{s}_a) \end{aligned} \tag{5.5}$$

The last line of equation (5.5) can be obtained by taking into account the special structure of $P(\mathbf{x}|\mathbf{s})$ of the LDGM code. Indeed $P(\mathbf{x}|\mathbf{s})$ can be factorized in a product distribution, as shown in equation (5.4), where each element is equal to $\Psi(\mathbf{x}_V(a), \mathbf{s_a})$. The marginal value of bit i, given by equation (5.5), can be efficiently computed, if the BP/Sum-Product algorithm is used. However, unlike the channel coding problem, where the received codeword is normally at a short distance from a codeword, in the lossy source coding problem the source sequence is likely to be equidistant from more than one codeword, as seen for the BEQ problem, producing belief values, about the bit marginals, close to 1/2. Consequently, the locally operating algorithm can get confused about the direction to proceed. The usual procedure to overcome the aforementioned problem is to decimate the most biased bits, after running the BP algorithm, and to repeat the previous two steps (BP and decimation) until all bits get decimated. This allows the BP algorithm to be guided, in the search space, into the direction of just one codeword.

Belief Propagation

After some algebraic manipulations, it is not difficult to express the BP update equations (see section 2.5.1), for the lossy source coding problem, as follows, [12]:

From variable to check:

$$R_i^{n+1} = \prod_{b \in C(i)} R_{bi}^n, \qquad R_{ia}^{n+1} = \prod_{b \in C(i) \backslash a} R_{bi}^n \tag{5.6}$$

From check to variable:

$$R_{ai}^{n+1} = \frac{1 - S_{ai}^n}{1 + S_{ai}^n}, \quad S_{ai}^n = (-1)^{s_a} \frac{1 - e^{-2\vartheta}}{1 + e^{-2\vartheta}} \prod_{j \in V(a) \backslash i} B_{ja}^n \tag{5.7}$$

Variable Bias:

$$B_i^n = \frac{1 - R_i^n}{1 + R_i^n}, \qquad B_{ia}^n = \frac{1 - R_{ia}^n}{1 + R_{ia}^n} \tag{5.8}$$

where R_{ia}^n, R_{ai}^n and B_{ia}^n denote the message sent from variable node i to check node a, the message sent from check node a to variable node i and the variable i bias, without taking into account the information coming from check node a, at iteration n, respectively. By R_i^n and B_i^n we represent the ratio between the probability of variable i being equal to one and the probability of being equal to zero, and the variable i bias, respectively. The previous BP update equations can be easily converted to the log-domain, using the hyperbolic tangent function definition, as in section 2.5.1 (equations (2.50), (2.51) and (2.52))

From variable to check:

$$\bar{R}_i^{n+1} = \sum_{b \in C(i)} \bar{R}_{bi}^n, \qquad \bar{R}_{ia}^{n+1} = \sum_{b \in C(i) \backslash a} \bar{R}_{bi}^n \tag{5.9}$$

From check to variable:

$$\bar{R}_{ai}^{n+1} = 2(-1)^{s_a+1} atanh \left[\beta \prod_{j \in V(a) \backslash i} B_{ja}^n \right] \tag{5.10}$$

Variable Bias:

$$B_i^n = -tanh\left(\frac{\bar{R}_i^n}{2}\right), \qquad B_{ia}^n = -tanh\left(\frac{\bar{R}_{ia}^n}{2}\right) \tag{5.11}$$

where the top bar denotes the transformation $\bar{x} = log(x)$ and $\beta = tanh(\vartheta)$.

Hard-Decimation

The decimation step implies that the corresponding code factor graph can be reduced [12], or equivalently that the decimated information bits always send the message $+\infty$ or $-\infty$, to the neighboring check nodes. This fact can be easily incorporated into the corresponding decimated variable node update equation or into their neighboring check nodes update equations. To do that we just need to add to each check node or to each variable node or to both update

equations an indicator function, $I_d(\alpha_i, t)$, taking the value 0 (bit still not decimated), $-\infty$ (bit decimated to 0) or $+\infty$ (bit decimated to 1)

$$I_d(\alpha_i, t) = \begin{cases} -\infty, & \text{if } \alpha_i \leq -t \\ 0, & \text{if } -t \leq \alpha_i < t \\ +\infty, & \text{if } t \leq \alpha_i \end{cases} \tag{5.12}$$

where α_i can be any parameter, normally a bit bias, and t denotes a threshold parameter, after which the bit gets decimated. In the BiP algorithm $\alpha_i = -B_i$. It should be emphasized here that the decimation step is not as simple as that. For example, the decimation, in the BiP algorithm, only decimates a fixed number of information bits, at each round. More precisely, it decimates the most biased m bits, even if there are more bits that respect the threshold t. However, as we will see in the next sections, this approximation is sufficient to obtain very good results.

Soft-Decimation

The basic idea of our method is to approximate the indicator function I_d by the soft indicator function

$$\hat{I}_d(\alpha_i, t) = \frac{2}{\mu}\, atanh\left(\frac{\alpha_i}{t}\right),\ \alpha_i \in]-t, t[\tag{5.13}$$

where $\mu > 0$ is a parameter that sets the accuracy of the approximation. Figure 5.3 shows the function I_d and the approximation for several values of μ. As μ increases the approximation becomes more accurate. Assume that $\alpha_i = -B_i^n$, given by equation (5.11), and that $t = 1$

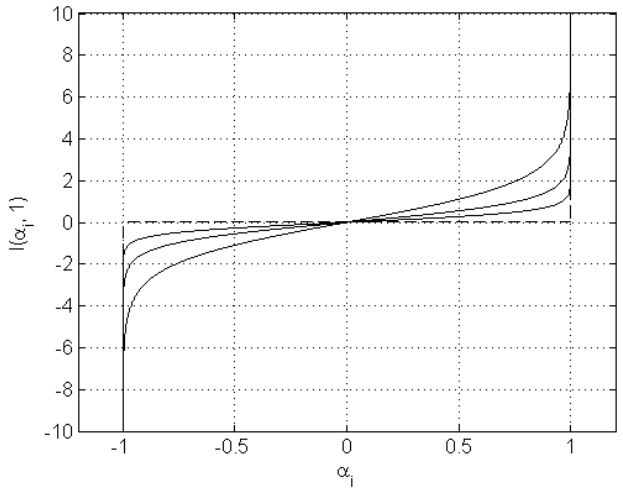

Figure 5.3: The dashed line shows the function $I_d(\alpha_i, 1)$ and the solid curves show $\hat{I}_d(\alpha_i, 1) = (2/\mu)atanh(\alpha_i)$, for $\mu = \{1, 2, 4\}$. The curve for $\mu = 4$ gives the best approximation.

(or $\alpha_i = -B_{ia}^n$ and $t = 1$) then $\hat{I}_d(-B_i^n, 1) = (1/\mu)\bar{R}_i^n$. Note that $|t|$ must be higher than 1, because as $|B_i^n| \leq 1$ the $atanh(.)$ is not defined, in the real field, using $|t| < 1$, leading to some indeterminacy. More precisely the indicator function, that represents the decimation

step, is replaced by a simple linear function. Therefore, if the indicator function is added at the variable node update equations and $\alpha_i = -B_i^n$, the BP update equations, with decimation included, can be expressed by

From variable to check nodes:

$$\bar{R}_i^{n+1} = \sum_{b \in C(i)} \bar{R}_{bi}^n, \qquad \bar{R}_{ia}^{n+1} = \frac{1}{\mu}\bar{R}_i^n + \sum_{b \in C(i)\backslash a} \bar{R}_{bi}^n \tag{5.14}$$

From check to variable nodes:

$$\bar{R}_{ai}^{n+1} = 2(-1)^{s_a+1} atanh\left[\beta \prod_{j \in V(a)\backslash i} B_{ja}^n\right] \tag{5.15}$$

Variable Bias:

$$B_i^n = -tanh\left(\frac{\bar{R}_i^n}{2}\right), \qquad B_{ia}^n = -tanh\left(\frac{\bar{R}_{ia}^n}{2}\right) \tag{5.16}$$

In this new formulation, we use a linear or 'soft' constraint function in place of a hard constraint, $I_d(.)$, like in the interior-point method [17]. A more careful look to these update equations show that, if $tanh(\vartheta) = 1$, this are indeed the log-domain RBP update equations used in [13] for doing lossy source coding, with LDPC codes over GF(q). On the other hand, if $\alpha_i = -B_{ia}^n$ and the indicator function is added to the check node update equations, the BP update equations, with decimation included, can be expressed by

From variable to check nodes:

$$\bar{R}_i^{n+1} = \sum_{b \in C(i)} \bar{R}_{bi}^n, \qquad \bar{R}_{ia}^{n+1} = \sum_{b \in C(i)\backslash a} \bar{R}_{bi}^n \tag{5.17}$$

From check to variable nodes:

$$\bar{R}_{ai}^{n+1} = \frac{1}{\mu}\bar{R}_{ia}^n + 2(-1)^{s_a+1} atanh\left[\beta \prod_{j \in V(a)\backslash i} B_{ja}^n\right] \tag{5.18}$$

Variable Bias:

$$B_i^n = -tanh\left(\frac{\bar{R}_i^n}{2}\right), \qquad B_{ia}^n = -tanh\left(\frac{\bar{R}_{ia}^n}{2}\right) \tag{5.19}$$

The main advantage of this new formulation is that the algorithm constrains the belief of the information bits, at each iteration, in the direction of the current bit belief, instead of constraining only the beliefs at the decimation step, allowing a refinement of the information bit beliefs, at each iteration. As a consequence all bits are decimated at once instead of being decimated, a fixed number of information bits, at each decimation step, as in [11] and [12]. Since, in the new algorithm, the decimation step is incorporated in the BP update equations and this amounts to just one more addition and multiplication, per edge, the overall computational complexity of the proposed algorithm is $\mathcal{O}(N)$, instead of $\mathcal{O}(N^2)$, as will be confirmed in the next section.

5.3.5 Results

To assess the performance of our algorithm we have simulated it for various code rates, source sequence lengths and different number of iterations. The modified BP update equations used in the simulations were equations (5.17), (5.18) and (5.19). The codes chosen were from degree distributions optimized for the BEC or BSC, in light of LDPC channel coding and LDGM source coding duality, in the erasure case [10]. All codes used in the simulations were generated randomly according to the correspondent degree distribution. No 4-cycles or higher-order cycles have been removed from the corresponding factor graph, only double edges. In all results presented in this section we have considered that $\beta = (1 - \xi)/(1 + \xi)$ and that $\xi = 1/\mu$, even if we have the freedom to tune both β and μ parameters independently. This parametrization has been chosen due to the inherent good performance and since it simplifies the algorithm and the task of assessing its performance.

Concerning the information bits prior value, since no apriori information is available it should be initialized to zero. However, since we are talking about a LDGM code and as is well known from the channel coding framework: if no degree 1 check nodes are available the BP algorithm never starts, it gets stuck. In [11] and [12] where a decimation step is available, this can be easily overcome since there we always have a minimum number of bits that get decimated at each iteration, even if all information bits have a lower bias than the threshold. However, for the proposed algorithm, that option is not available. Consequently, we should use a small percentage of check nodes with degree 1 or equivalently we can initialize the information bits prior with a small value, at the first iteration, and remove it in the next iteration. In all simulations presented next the information bits prior was initialized with the value 0.1, and set to zero in the second iteration.

The procedure used to quantize a given source sequence is to run the BP algorithm with soft decimation, given by equations (5.17), (5.18) and (5.19), for a fixed ξ value and for a given number of iterations, and to decimate all information bits after.

The degree distribution pair $(\lambda(x), \rho(x))$ of the rate 1/2 LDGM code used in all simulations shown in the next paragraphs was [18]

$$\lambda(x) = x^6$$
$$\rho(x) = 0.275698x + 0.25537x^2 + 0.076598x^3 + 0.39233x^8$$

Distortion versus Compression Rate

Figure 5.4 shows the obtained distortion as a function of the coding rate, for different source sequence lengths. For each code we choose ξ that achieve the lowest distortion. As can be seen from that figure the achieved distortion is very close to the theoretical limits. Even for a codeword length of 100 the achieved distortion is good, it is a little worse than the one obtained in [13] for a binary LDPC code of length 12000. We can also see, from that figure, that the distortion loss obtained by decreasing the number of iterations from 400 to 100 is small.

Distortion versus ξ

To attest the behavior of the distortion values as a stronger constraint is enforced we plot in Figure 5.5 the distortion obtained by running the proposed algorithm, during 100 iterations, for a LDGM code with rate 1/2 and for three codeword-lengths, 10^2, 10^4, 10^5. Remember that the parameter μ is inversely proportional to ξ. From Figure 5.5 it is evident that as a

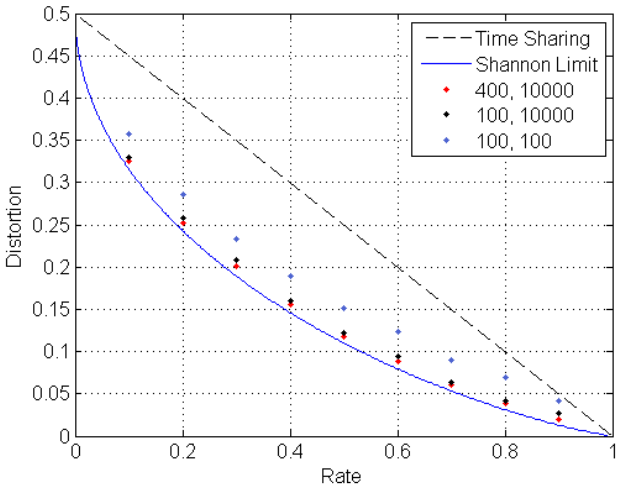

Figure 5.4: Lossy source coding performance of the proposed algorithm for different source sequence lengths (100, 10000) and for different number of iterations, (100, 400).

---

stronger constraint is imposed the distortion value decreases but after the optimal ξ value it increases abruptly, showing the existence of a threshold. As the codeword length increases the distortion value decreases even more abruptly, close to the optimal ξ value.

Distortion versus Codeword Length

Figure 5.6 presents the distortion values, as a function of the codeword length, for the rate one-half LDGM code. For each code, we choose ξ so that the average distortion is minimal. The ξ value is found by simulations. The number of iterations is fixed to 400 and the distortion was averaged over 100 trials, for codeword lengths higher than 1000, and averaged over 1000 trials otherwise. As can be observed, from figure 5.6, the average distortion obtained, as the codeword length increases, decreases exponentially and the gains obtained by the joint processing of a higher number of samples, from the source sequence, gets smaller as the codeword length increases.

Computational Complexity

In this section we analyze the number of iterations needed for convergence, as the codeword length increase. To limit the impact of the graph cycles in the results we have considered high codeword length codes only, from $N = 10^4$ to $N = 10^6$. All these codes were generated randomly with only double edges removed. To analyze the number of iterations needed for convergence, we have iterated our algorithm for 1000 iterations and averaged the corresponding obtained distortion over 1000 trials, for the rate 1/2 code and for different codeword lengths. In Figure 5.7 we plot the corresponding average distortion obtained for each iteration and for different ξ values. As can be seen from that figure the number of iterations needed for convergence decrease as the codeword length increases or as ξ increase. However, the number of needed iterations seems to be saturating as the codeword length increase, and they saturate faster for higher ξ values (weaker constraint/higher average distortion).

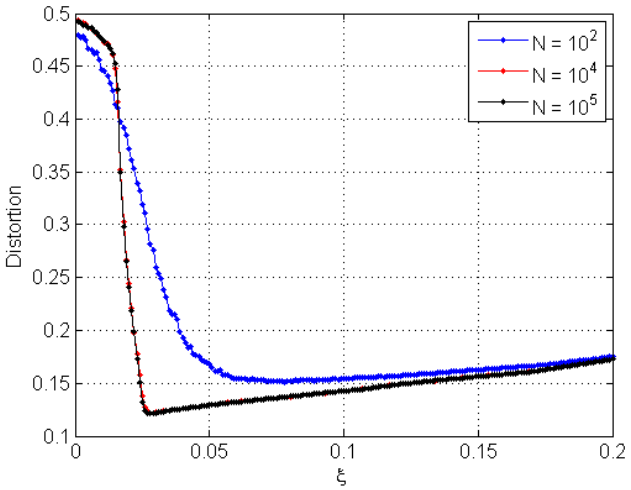

Figure 5.5: Lossy source coding performance, for 100 iterations, as a function of ξ for a randomly generated graph with rate equal to 0.5 and for three codeword lengths $N = \{10^2, 10^4, 10^5\}$.

Even if one cannot extrapolate general conclusions from these numerical results, they indicate that the number of iterations needed for convergence tend to a constant value for very high codeword lengths and a constant ξ value, supporting the $\mathcal{O}(N)$ computational complexity of the proposed algorithm.

5.4 Binary Dirty Paper Coding

In the previous sections, we have analysed the lossy source coding problem and proposed an algorithm for it. In the following sections of this chapter, we use the proposed lossy scheme as a building block to design LDGM codes for the DPC problem and analyze numerically its performance.

5.4.1 Proposed Dirty Paper Scheme

The proposed DPC code structure is presented in Figure 5.8(a). We call the proposed structure LDGM/LDPC code, since it is formed by the concatenation of a LDGM and a LDPC code. The main idea behind the proposed code structure is to use part of the information bits of a LDGM code to approximate the channel interference and to use the other part for real data transmission. However, since a LDGM code is not a good channel code the data bits are, firstly, precoded with a high rate LDPC code to remove the small distance codewords. In Figure 5.8(a) we use white circles to represent the precoded data bits and dark gray circles to denote the information bits used to approximate the channel interference. In addition, black circles represent the channel interference, and squares represent the check nodes. By $\prod_i, i \in \{1, 2, 3\}$, see Figure 5.8(a), we mean a uniformly drawn permutation. It can be seen from Figure 5.8(a) and Figure 5.8(b) that, without precoding, our proposed code structure is dual of the Bilayer expurgated code, proposed by Peyman Razaghi and Wei Yu in [7], [8], for

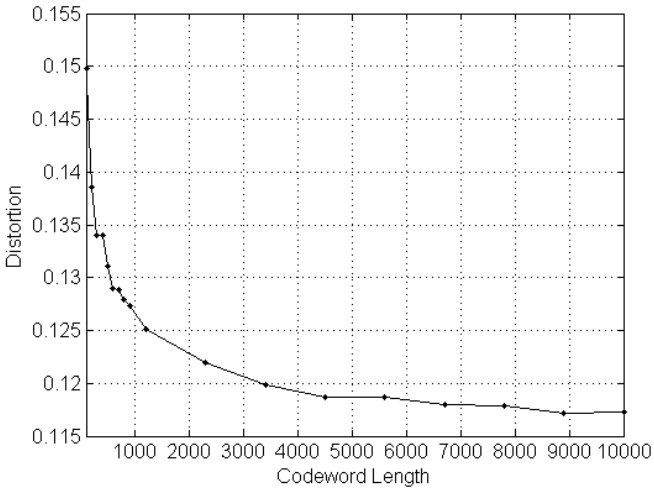

Figure 5.6: Distortion values for various codeword lengths, from 10^2 to 10^4, for a LDGM code with R = 1/2 and for 400 iterations

---

relay channels. As we will also see, in the following sections, the proposed scheme also fits, at some extent, under the superposition coding framework proposed in [14].

Encoding and Decoding

Let us consider that the upper and lower subgraphs have k_1 and k_2 variable nodes, respectively. Denote by $\mathbf{G}, \mathbf{G}_1$ and $\mathbf{G}_2$ the generator matrices of the high rate LDPC code and of the upper and lower subgraphs of the LDGM code, respectively, as shown in Figure 5.8(a). Denote by $\mathbf{H}$ the parity check matrix of the LDPC code. Thus, the upper, lower and global code can be defined by $\mathcal{C}_0$, $\mathcal{C}_1$, and $\mathcal{C}$, respectively

$$\mathcal{C}_0 = \{\mathbf{x} \in \{0,1\}^N | \ \mathbf{x} = \mathbf{G}_1\mathbf{y}, \ \forall \, \mathbf{y} \in \{0,1\}^{K_1}\} \tag{5.20}$$

$$\mathcal{C}_1 = \{\mathbf{x} \in \{0,1\}^N | \mathbf{x} = \mathbf{G}_2\mathbf{y}, \forall \, \mathbf{y} \in \{0,1\}^{K_2} : \mathbf{H}\mathbf{y} = 0\} \tag{5.21}$$

$$\mathcal{C} = \{\mathbf{x} \in \{0,1\}^N \ | \mathbf{x} = \mathbf{x}_1 + \mathbf{x}_2, \forall \, (\mathbf{x}_1, \mathbf{x}_2) \in \mathcal{C}_1 \times \mathcal{C}_2\} \tag{5.22}$$

From these definitions one can easily see that the global code ($\mathcal{C}$) is the superposition of two codes ($\mathcal{C}_0$ and $\mathcal{C}_1$), like in [14]. The main difference between our scheme and the one proposed in [14] is that in our case binary codes are sufficient and instead of a convolutional code a LDGM code is used for doing lossy source coding. Another important difference is that we propose to optimize our code within the linear programming framework.

With the previous definitions, encoding and decoding with the LDGM/LDPC code, for the binary dirty-paper channel, is as follows

ENCODING: In the encoding stage, a given message $\mathbf{d}$, is first encoded by the lower code $\mathcal{C}_1$ to obtain the lower codeword $\mathbf{c}_1 = \mathbf{G}_2\mathbf{G}\mathbf{d}$. Then, the proposed modified version of BP is

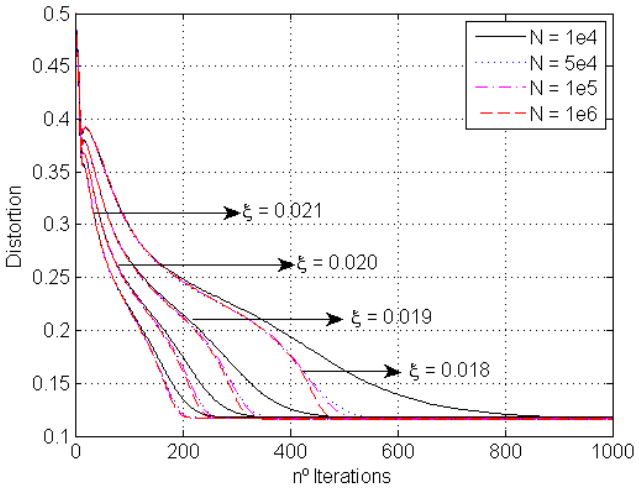

Figure 5.7: Distortion evolution over the iteration number for various codeword lengths, for a code rate of 1/2.

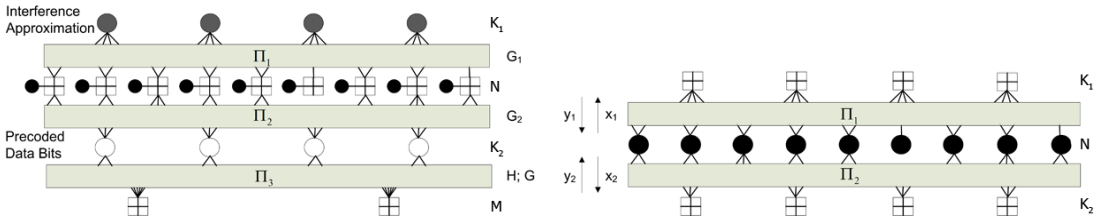

(a) LDGM/LDPC code factor graph.

(b) Dual code factor graph.

Figure 5.8: LDGM/LDPC code and dual code factor graphs.

---

run on the upper subgraph to select the codeword $\mathbf{c}_0$, belonging to $\mathcal{C}_0$, that is closest to $\mathbf{c}_1 - \mathbf{s}$. Finally the encoder inputs to the channel the sequence $\mathbf{c}_0 + \mathbf{c}_1 - \mathbf{s}$.

DECODING: The decoding problem can be cast as a standard channel decoding problem, since the received signal is given by $\mathbf{c}_0 + \mathbf{c}_1 + \mathbf{n} = \mathbf{c} + \mathbf{n}$, where $\mathbf{c}$ is a codeword of the global code $\mathcal{C}$, and $\mathbf{n}$ is the added channel noise. Thus to decode the received data we can simply run the standard BP algorithm ($\xi = 1/\mu = 0$ and $\beta = 1$, in equation (5.18)) over the overall factor graph, of code $\mathcal{C}$, to infer the transmitted data bits.

5.4.2 Code Optimization

In this section, we describe how to optimize the degree distribution of the LDGM/LDPC code for the binary dirty paper channel. In Figure 5.8(b) we present the dual of the LDGM/LDPC code, if the precoding part is not considered. For a more detailed description of dual codes, please refer to [10]. It is not difficult to realize that the dual code is, in fact, the bilayer expurgated code proposed by Peyman Razaghi and Wei Yu in [7], for relay channels. This resemblance can be used in our favor to optimize the LDGM/LDPC code, since to optimize the lossy source coding part of the LDGM/LDPC code, $\mathcal{C}_0$, the dual code approximation [10]

can be used and also because the fact that the optimization of a LDGM code amounts to not much more than translating results obtained for LDPC ensembles [19]. Thus, the optimization of the proposed code for the dirty paper channel can be approximated by the optimization of a bilayer expurgated LDPC code, for the relay channel, like in [7], [8]. However, here a further simplification is used: the binary erasure channel approximation. This choice, has been made, mainly to simplify things and in light of the connection between LDPC channel coding and LDGM source coding, in the erasure case [10]. Even if it is an approximation, the resultant performance is very good, as we will see in the next sections, showing, as a proof of concept, that the proposed scheme can be used for DPC.

Density Evolution

As stated in [7] and [8], the ensemble of bilayer expurgated LDPC codes can be characterized by a variable node degree distribution $\lambda_{i,j}, i \geq 2, j \geq 0$ and by two (upper and lower) check node degree distributions, $\rho_i^U, i \geq 2$ and $\rho_i^L, i \geq 2$. Nevertheless, we consider regular check node degree distributions, with degrees d_c^U and d_c^L, respectively for the upper and lower check nodes, due to its evidenced good performance, as will be seen in the results section, and also due to its inherent simplicity. $\lambda_{i,j}$ denotes the percentage of edges connected to a variable node with degrees (i, j), see Figure 5.9. In the ordered pair (i, j) i and j denote the upper and lower

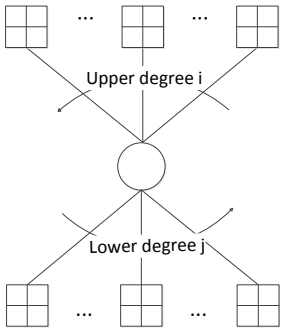

Figure 5.9: Variable node degree.

degree of the node, respectively. Let us consider a variable node with degrees (i, j). For such a case the corresponding message erasure probability, after applying the BP update equations, is given by (see section 2.5.2), $\epsilon y_1^{i-1} y_2^j$ or $\epsilon y_1^i y_2^{j-1}$, for the upper and lower edges, respectively. y_1 and y_2 represent the erasure probability of the check to variable node messages, for the upper and lower check nodes, respectively, see Figure 5.8(b). Assume that the total number of edges, in the global graph, is E. Therefore, $\lambda_{i,j}E$ is the number of edges connected to a variable node with degrees (i, j) and $\lambda_{i,j}E/(i+j)$ the corresponding number of variable nodes with degrees (i, j). Hence, $i\lambda_{i,j}E/(i+j)$ represent the number of upper edges connected to a variable node with degrees (i, j) and the corresponding percentage of upper edges is $i\lambda_{i,j}E/(i+j)/E^U$ (E^U denote the number of edges in the upper graph). This value corresponds also to the percentage of messages, in the upper graph, emanating from a variable node with degree (i, j). As a

consequence, after averaging over the code ensemble, the following erasure probabilities result

$$\mathbf{x} = \begin{bmatrix} \frac{\epsilon}{\eta} \sum_{i,j} i \frac{\lambda_{i,j}}{i+j} y_1^{i-1} y_2^j \\ \frac{\epsilon}{\gamma} \sum_{i,j} j \frac{\lambda_{i,j}}{i+j} y_1^i y_2^{j-1} \end{bmatrix} \tag{5.23}$$

where $\mathbf{x} = [x_1, x_2]$ correspond to the densities of the messages sent by variable nodes, $\mathbf{y} = [y_1, y_2]$ to the ones sent by the check nodes, $\eta = E^U/E$ corresponds to the percentage of upper edges in the overall graph, $\gamma = 1 - \eta$, and ϵ is the channel erasure probability.

Using conventional density evolution and the erasure channel approximation the densities of the messages sent by the check nodes, $\mathbf{y} = [y_1, y_2]$ are given by (like in section 2.5.2)

$$\mathbf{y} = \begin{bmatrix} 1 - (1 - x_1)^{d_c^U - 1} \\ 1 - (1 - x_2)^{d_c^L - 1} \end{bmatrix} \tag{5.24}$$

As a consequence, the overall probability of erasure, at a given variable node, is

$$P_e = \epsilon \sum_{i,j} \lambda_{i,j} y_1^i y_2^j \tag{5.25}$$

Code Design

To decode a codeword successfully, the overall erasure probability, equation (5.25), should decrease at each iteration and converge to zero. This can be enforced by constraining y_1 and y_2 to decrease at each iteration and converge to zero, in the large block length limit. Due to the one to one correspondence between y_1 and x_1 and between y_2 and x_2, this is equivalent to both x_1 and x_2 decrease, which can be formulated as

$$\frac{\epsilon}{\eta} \sum_{i,j} i \frac{\lambda_{i,j}}{i+j} y_1^{i-1} y_2^j < x_1 \qquad\qquad \frac{\epsilon}{\gamma} \sum_{i,j} j \frac{\lambda_{i,j}}{i+j} y_1^i y_2^{j-1} < x_2 \tag{5.26}$$

where y_1 and y_2 should be replaced by their respective expressions, given by equation (5.24).

The design of a bilayer expurgated LDPC code involves finding $\lambda_{i,j}$, d_c^U, d_c^L and η, such that the overall code and respective upper sub-code are capacity approaching for a channel erasure probability ϵ and $\epsilon_U (< \epsilon)$, respectively. One way to formulate the design problem, like in standard LDPC code optimization (see section 2.5.2), is to fix the check node degree distribution, (d_c^U, d_c^L), and jointly optimize the parameters $\lambda_{i,j}$ and λ_i^U (upper code variable degree distribution).

Based on iterative linear programming, a rate maximization problem can be formulated, to optimize the bilayer LDPC code as follows. The rate of the overall code is given by $R = 1 - (\sum_i \rho_i/i)/(\sum_i \lambda_i/i)$, where ρ_i and λ_i are the degree distribution of the check nodes and of the variable nodes of the global code, respectively. Fixing the check node degrees, d_c^U and d_c^L , the rate of the global code depends on the $\lambda_{i,j}$ parameters. Therefore, the rate maximization problem is equivalent to the maximization of $\sum_i \lambda_i/i = \sum_{i,j} \lambda_{i,j}/(i+j)$. As a consequence, the following linear program can be formulated to optimize the proposed

LDGM/LDPC code, for η, ϵ, ϵ_U, d_c^U, d_c^L and maximum upper and lower variable degrees known

$$\max_{\lambda_{i,j},\lambda_i^U} \quad \sum_{i,j} \lambda_{i,j}/(i+j) \tag{5.27}$$

$$s.t. \quad \sum_{i,j} \lambda_{i,j} = 1; \quad 0 \leq \lambda_{i,j},\ i \geq 2, j \geq 0 \qquad \sum_{i,j} \frac{i}{i+j}\lambda_{i,j} = \eta \tag{5.28}$$

$$\sum_{j} \frac{i}{i+j}\lambda_{i,j} - \eta\lambda_i^U = 0 \qquad \frac{\epsilon}{\eta}\sum_{i,j} i\frac{\lambda_{i,j}}{i+j} y_1^{i-1} y_2^j < x_1 \tag{5.29}$$

$$\frac{\epsilon}{\gamma}\sum_{i,j} j\frac{\lambda_{i,j}}{i+j} y_1^i y_2^{j-1} < x_2 \qquad \epsilon_U \sum_i \lambda_i^U (1-(1-x)^{d_c^U}) < x \tag{5.30}$$

Equation (5.28), on the right side, enforces that the percentage of upper edges in the global code should be equal to η, equation (5.29), left side, expresses the relation between distribution λ_i^U and $\lambda_{i,j}$ and equation (5.30), on the right side, enforces that the error probability of the optimized upper sub-code should decrease at each iteration and converge to zero (to obtain a good lossy code).

5.4.3 Results

To assess the LDGM/LDPC code performance, we have optimized a code for a channel coding rate of 1/2 (considering the high rate LDPC code) and for a lossy source coding rate of 1/8, which gives a dirty paper rate of 3/8. For the aforementioned rates, the corresponding channel coding threshold is $p = 0.11$, and the lossy source coding threshold is $\delta = 0.295$, which is equivalent to an input constraint of 0.295. For the optimization process, a maximum upper and lower variable degree of 7 and 10 has been considered, respectively, for the dual code. For the upper and lower check nodes a degree of 20 and a degree of 6 has been considered, respectively. The check node degrees have been obtained experimentally by testing several different pairs of values. However, for the upper check degree, we can get an idea of the optimal value by looking to LDPC optimized degree distributions, for a code rate of $1 - 1/8 = 7/8$, since the upper sub-code will work "alone" at the encoding stage. Nevertheless, its distribution will influence the global code degree distribution. To remove the low weight codewords of the LDGM code, a regular $(3, 60)$ LDPC code (Rate = 0.95) has been used. The optimized degree distribution, obtained from the code optimization, is shown in Table 5.1. As can be seen from that table, a small percentage of degree $(1, 0)$ check nodes has been added to the obtained optimized degree distribution, to help the iterative process to start, likewise, for LDGM codes in the channel coding setting. The code used for simulations has been generated randomly and the codeword length considered was 10^5. The optimal distortion value for a code with rate 1/8 is 0.295. In our simulations, for 100 trials and for 400 iterations of the modified BP algorithm, we have got an average distortion of 0.304 ($\xi = 0.008$), and for 100 iterations, a distortion of 0.306 ($\xi = 0.01$). In Figure 5.10 the BER performance of the LDGM/LDPC code is shown. These results were obtained for 100 iterations of the BP algorithm over the global code, having as a stop criterion, for each channel crossover probability, 200 received frames in error. One iteration of the global code corresponds to one iteration at the LDGM code and another at the LDPC code. As a reference the capacity limit for this code rate, $p = 0.11$, is also presented. As can be seen from that curve, at BER $= 2 \times 10^{-5}$ the threshold of our code is $p^* = 0.094$, with a gap to capacity of 0.016, similar to superposition coding proposed

Table 5.1: Optimized LDGM/LDPC variable node degree distribution, for an upper and lower check node degree of 20 and 6. An entry (i, j) corresponds to the percentage of edges connected to check nodes with upper degree i and lower degree j.

(i,j)	$j=0$	$j=1$	$j=2$	$j=4$	$j=5$	$j=6$	$j=7$	$j=8$	$j=9$	$j=10$
i = 1	0.0012	0	0	0	0	0	0	0	0	0
i = 2	0.0502	0.0179	0.3875	0.0048	0.0477	0.0033	0	0	0	0
i = 3	0.0322	0.0304	0.0452	0.0273	0.0683	0.0421	0.0182	0.0004	0	0
i = 4	0.0190	0	0	0	0.0180	0.0160	0.0080	0	0	0
i = 5	0.0096	0	0	0	0	0.0085	0	0	0	0.0231
i = 6	0	0	0	0	0	0	0	0	0.0007	0.0431
i = 7	0	0	0	0	0	0	0	0	0.0320	0.0453

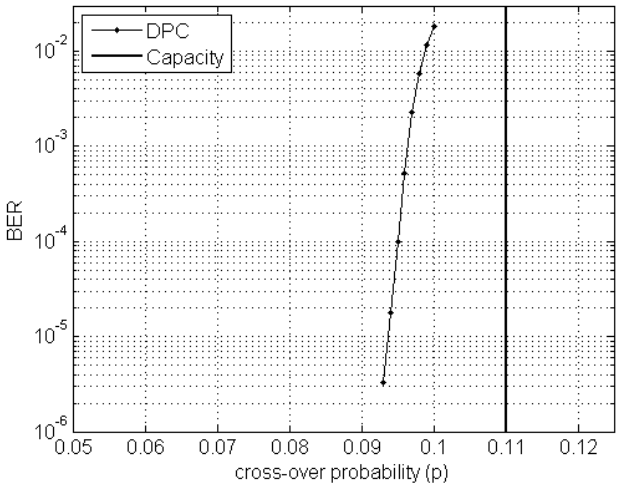

Figure 5.10: Bit-error-rate performance.

---

in [14]. However our system is only based on binary codes and instead of a convolutional code a LDGM code is used for implementing the lossy source coding part of DPC.

It is worth noting that in the optimization, we constrained the check nodes to have regular degree distribution. Further improvement could be achieved allowing irregularity. However, due to its simplicity and evidenced good performance, we have focused only on regular check dual codes, as in standard LDPC code design. Another aspect that should be emphasized here is that instead of a high rate LDPC code a high rate LDGM code could be used to remove the inherent LDGM code error floor [9], reducing further the complexity of the proposed scheme.

5.5 Conclusion

In this chapter, we have proposed a new algorithm for lossy source coding, using LDGM codes. The main idea behind the proposed algorithm was to transform the hard decimation step, present in almost all previously proposed algorithms, into a soft-decimator and to in-

clude it in the BP algorithm. To do that we have first obtained an equivalent representation of the decimation step, with the help of an indicator function, and have included it into the BP update equations. Next, a new formulation has been proposed, for the aforementioned algorithm, using a linear or 'soft' constraint function instead of a 'hard' constraint. The derived algorithm has linear complexity in the code block length, unlike the ones based on hard decimation, where it grows with $\mathcal{O}(N^2)$. Simulation results indicate that the performance is very close to the one achieved with state-of-the-art algorithms, based on hard decimation, with much lower complexity. Additionally, a practical scheme for implementing binary dirty paper coding with only binary low density codes has been proposed. The main idea behind the proposed code is to divide the information bits of a LDGM code in two parts and to use one part to transmit data and the other part to approximate the channel interference. However, due to the inherent LDGM error floor, the data bits are, firstly, precoded by a high-rate code, namely a LDPC code. To optimize the LDGM/LDPC code a simple linear programming approach has been proposed. An important element, for code optimization, has been the analogy verified between the bilayer LDPC code approach, for the relay channel, and the proposed LDGM/LDPC code. This analogy has enabled the use of research that exists for bilayer LDPC code optimization, simplifying our task significantly. Simulation results indicate reliable transmission, close to the Shannon limit, with reduced complexity.

5.6 References

[1] M. Costa, "Writing on dirty paper (Corresp.)," *Information Theory, IEEE Transactions on*, vol. 29, no. 3, pp. 439–441, May 1983.

[2] H. Weingarten, Y. Steinberg, and S. Shamai, "The Capacity Region of the Gaussian Multiple-Input Multiple-Output Broadcast Channel," *Information Theory, IEEE Transactions on*, vol. 52, no. 9, pp. 3936–3964, Sept. 2006.

[3] J. Eggers, J. Su, and B. Girod, "A blind watermarking scheme based on structured codebooks," in *Secure Images and Image Authentication (Ref. No. 2000/039), IEE Seminar on*, 2000, pp. 4/1 –4/21.

[4] M. Miller, G. Doerr, and I. Cox, "Applying informed coding and embedding to design a robust high-capacity watermark," *Image Processing, IEEE Transactions on*, vol. 13, no. 6, pp. 792 –807, june 2004.

[5] C. Peel, "On "Dirty-Paper coding"," *Signal Processing Magazine, IEEE*, vol. 20, no. 3, pp. 112 – 113, may 2003.

[6] N. Fawaz, D. Gesbert, and M. Debbah, "When network coding and dirty paper coding meet in a cooperative ad hoc network," *Wireless Communications, IEEE Transactions on*, vol. 7, no. 5, pp. 1862 –1867, may 2008.

[7] P. Razaghi and W. Yu, "Bilayer LDPC Codes for the Relay Channel," in *Communications, 2006. ICC '06. IEEE International Conference on*, vol. 4, June 2006, pp. 1574–1579.

[8] ——, "Bilayer Low-Density Parity-Check Codes for Decode-and-Forward in Relay Channels," *Information Theory, IEEE Transactions on*, vol. 53, no. 10, pp. 3723–3739, Oct. 2007.

[9] J. Garcia-Frias and W. Zhong, "Approaching Shannon performance by iterative decoding of linear codes with low-density generator matrix," *Communications Letters, IEEE*, vol. 7, no. 6, pp. 266–268, June 2003.

[10] E. Martinian and J. S. Yedidia, "Iterative Quantization Using Codes On Graphs," *CoRR*, vol. cs.IT/0408008, 2004.

[11] M. J. Wainwright and E. N. Maneva, "Lossy source encoding via message-passing and decimation over generalized codewords of LDGM codes," *CoRR*, vol. abs/cs/0508068, 2005.

[12] T. Filler and J. J. Fridrich, "Binary quantization using Belief Propagation with decimation over factor graphs of LDGM codes," *CoRR*, vol. abs/0710.0192, 2007.

[13] A. Braunstein, F. Kayhan, and R. Zecchina, "Efficient LDPC Codes over GF(q) for Lossy Data Compression," *CoRR*, vol. abs/0901.4467, 2009.

[14] A. Bennatan, D. Burshtein, G. Caire, and S. Shamai, "Superposition coding for side-information channels," *Information Theory, IEEE Transactions on*, vol. 52, no. 5, pp. 1872–1889, May 2006.

[15] T. M. Cover and J. A. Thomas, *Elements of information theory*. New York, NY, USA: Wiley-Interscience, 1991. [Online]. Available: http://portal.acm.org/citation.cfm?id=129837

[16] A. Braunstein, F. Kayhan, G. Montorsi, and R. Zecchina, "Encoding for the Blackwell Channel with Reinforced Belief Propagation," in *Information Theory, 2007. ISIT 2007. IEEE International Symposium on*, 24-29 2007, pp. 1891 –1895.

[17] S. P. Boyd and L. Vandenberghe, *Convex optimization*. Cambridge University Press, 2004.

[18] A. Amraoui. LTHC:"LdpcOp". [Online]. Available: http://ipgdemos.epfl.ch/ldpcopt/

[19] T. Richardson and R. Urbanke, *Modern Coding Theory*. Cambridge University Press, Mar. 2008.

Chapter 6

Conclusions and Future Work

6.1 Conclusions

The wireless communications industry has evolved significantly, since its birth. Over the years, the spectral efficiencies have increased substantially. This progress has been made possible due to the many advances made in the signal-processing field. One of the main impairments of communication systems is the noise. In 1948, Shannon has shown [1] that it is possible to communicate reliably, at a positive rate, in the presence of noise, using coding. The introduction of channel coding, mainly of modern coding designs (like turbo and LDPC codes) [2–10] made possible reliable transmission of information at rates close to the theoretical limits defined by Shannon. This in conjunction with the fact that the cells are becoming smaller, to achieve higher rates and to cope with a higher density of users, implies that interference is becoming the main limiting factor for the evolution/scaling of the spectral efficiencies [11]. Interference can be alleviated using cooperation techniques [11], as in LTE [12]. Consequently, the interference can be treated as a known signal and cancelled with the help of joint processing between the BSs included in the cooperation. On the other hand, there has been also an intensive research on the field of information theory to achieve a better understanding of the topic (interference) and to characterize the capacity region of the interference channel [13–19].

The work developed in this thesis is within the scope of signal processing techniques for distributed multiuser systems and has contributed with low complexity precoding techniques for interference cancellation, both for the unidimensional as for the multi-dimensional cases. Results show close to optimum performance, for the proposed schemes.

In the following paragraphs, we will summarize the outcomes and outline the main conclusions of this thesis. Concerning chapter 3 they can be summarized as

- The capacity increase, by the connection of additional transmit antennas, is maximal when all antennas have the same mean link SNR. This can be verified by the differential capacity measure. It implies that the highest performance improvement will be for the users located at the edge of the cells, which in fact are the ones that in average more need it.
- The BER and capacity of a DAS(CAS) can be described by the singular values of the associated path loss (correlation) matrix. For a DAS the singular values, which

correspond to the path losses (diagonal matrix) change from geographical position to geographical position. On the other hand, the ones of a CAS are fixed since they are mostly dependent on the transmit antennas configuration. Hence the DAS has more flexibility and diversity to attain improved performance.

- The introduced differential measure, the DCAP, can be useful in dynamic radio resource allocation since it provides a measure of how beneficial the joint processing of an additional RAU is to the system. The increase in capacity is bounded and simple/accurate upper bounds exist, for its calculation. Such bounds can be used for example to discard from the scheduling pool some of the RAUs.

- As a final conclusion, of this chapter, one can say that a system architecture based on the DAS concept will be able to address most of the problems encountered in the current cellular systems, for users at the cell borders, since are those the ones with the highest symmetry properties, to the system RAUs.

From chapter 4 the following conclusions can be made

- To obtain a solution to the minimum BER problem, of a multiuser system, a quadratic constrained nonlinear program must be solved. This requires the use of sequential quadratic programming tools. However, such a high complexity can be reduced by considering the high SNR regime. Namely, for this regime the previous problem can be approximated by a simple quadratic problem.

- The transformation of the interference signal into an useful signal, instead of considering it as disturbance, that has to be nullified or minimized, allows to achieve high performance gains, relatively to the standard ZF and MMSE schemes and close to the optimum performance. This can be done by allowing the transmitter to assign power to a given user symbol, only if the interference of the signal is not enough to recover it. Additional gains can be obtained by carefully selecting the user processing order. This allows to make the interference as useful as possible.

- The proposed scheme achieves a higher diversity gain than ZF/MMSE schemes, since instead of constraining the received signal to be equal to the transmitted symbol or close to it (like in ZF/MMSE) the received signal can lie in any point of the decoding region of the corresponding symbol. Hence, the proposed scheme uses all the available decoding space. Indeed, it is proven that, unlike ZF, the new scheme only inverts part of the correlation matrix ($\mathbf{H}\mathbf{H}^H$) which is better conditioned than the corresponding global matrix. Thus, noise enhancement is less pronounced.

- For higher constellation orders (M-QAM) the signal decoding space gets more constrained. As a result, the gap, of the optimum and new scheme, relatively to ZF gets reduced. Indeed for high constellations orders the ZF scheme will be close to the optimum and therefore, can be used.

- In the high SNR regime the approximate solution to the minimum BER problem is linearly dependent on the available transmit power. This allows to treat the joint processing of a group of sub-carriers as if they were processed separately. Indeed, the main difference between the two cases is that in the former the joint signal is normalized to

meet the power constraint, instead of doing a normalization for each sub-carrier signal. This fact allows the joint processing of a group of sub-carriers to have the same complexity as the independent processing. Nevertheless, diversity gains are obtained.

- The case of a distributed system introduces additional constraints, in the minimum BER problem, i.e. the per-RAU power constraints. To approximate the solution of the minimum BER problem a global power constraint can be imposed instead. Nevertheless, the resulting signal, for each RAU, must be normalized (by a common factor) so that each local power constraint is respected. This allows to treat, again, the initial problem as a quadratic program, reducing significantly the complexity. Such an approximation enables close to optimum performance.

- Finally, one can conclude that the good performance of the proposed scheme makes it well suited for practical implementations as it combines close to optimum performance with a reduced complexity.

From chapter 5 the conclusions can be compiled as follows

- By converting the hard decimation step of the belief propagation algorithm into a soft decimator the complexity is significantly reduced. This can be achieved by using the framework of interior point methods, i.e. by using a linear approximation for the corresponding indicator function. Indeed linear complexity, in the blocklength can be achieved with close to state-of-the art performance, as can be corroborated by the numerical results presented.

- A DPC scheme can be implemented using only a LDGM code. Nevertheless, the information bits of the code should be divided into two parts, unlike in the channel coding setting, where no division is necessary. One for data transmission and another to approximate the channel interference. Such a fact allows to decouple the DPC problem into two sub problems. The first of which is a channel coding problem and the second a lossy source problem. Nevertheless, to achieve reliable communication over the channel the bits used for data transmission should be precoded, since a LDGM code is not a good channel code.

- Using existing research on the topic of bilayer codes, for the relay channel, one can simplify the task of DPC code optimization significantly. Indeed, a similar linear programming problem can be formulated to optimize the structure of the proposed bilayer LDGM code.

- As a concluding remark one can say that by combining a lossy coding algorithm and a LDGM code, reliable transmission over the DPC channel is possible, with performance close to the Shannon limit and reduced complexity.

6.2 Future Work

This thesis has focused on interference cancellation, for distributed wireless systems. The work carried out can be divided into three topics (capacity analysis, one dimensional and multidimensional precoding). In this study, some problems are left open for future research. In relation to chapter 3 the following aspects might be of interest

- In the proposed capacity analysis, it was considered an ideal situation, i.e. no interference, perfect CSI, no delay between cooperating BSs and no synchronization issues. The study of the impact of each of these imperfections, on the distributed antenna system, is of special importance, since it will make worse the improvement obtained by the joint processing of additional DAS, than the one presented.

In the context of one dimensional precoding the following topics are regarded as interesting for future research

- Normally, in the design of a precoder, it is assumed that the set of users, to be precoded, is given (by an upper layer function). Indeed this is the case of the described precoder. But, as seen in the analysis, the performance improves when the order by which the different users are processed is carefully chosen. Hence, it is of interest to see the impact of the users scheduling in its performance and design.

- The proposed precoder uses all the available decoding space, of the symbol to be transmitted, to find the best signal to be sent through the channel. In the derivation of the new scheme Gray mapping was considered. Nevertheless, it is not know if this is optimal. Indeed we think that by carefully choosing the available decoding space, for each bit, better performance can be achieved. In principle, larger decoding spaces should be better, but a search over the possible decoding spaces should be done to verify if there is any with better performance than the one provided by Gray mapping.

- The availability of CSI at BSs is always limited, since it implies the existence of feedback channels, whose capacity is limited. Several assumptions can be made about it. Namely, it can be global (i.e. a BS knows the CSI of all users), local (i.e. a BS knows only the CSI of a small set of users) and it can be quantized (i.e. not exact). In the design of the proposed precoder it was assumed exact global CSI. An interesting extension is to consider quantized and/or local CSI, since it reflects best a real-world scenario.

- The proposed algorithm can handle the case of multiple receive antennas by, for example, considering that each antenna belongs to a different user. Nevertheless, a scheme specially designed for this setup could provide performance improvements. The correct matching between the precoder and equalizer can achieve this.

In the context of multidimensional precoding, the topics that one thinks need to be further addressed are

- In the work presented the proposed schemes where designed for the binary case. However, for a practical system this is not the case, and a more general design should be considered. For example, Gaussian noise and the existence of a set of users, for precoding, should be considered.

- A possible extension to extend the proposed DPC scheme, from the binary setting to the more general case, is by merging the two coding schemes (the one dimensional and multidimensional), i.e. use concepts from one into the other.

- The investigated lossy source coding algorithm has good performance. A theoretical analysis, in the limit of infinite block length, would be interesting, both to get an upper bound on the performance of the scheme as to design better codes, shaped/optimized for the algorithm.

- To make the lossy algorithm to track just one solution of the lossy coding problem, the most biased bits are "soft" decimated. Other ways to guide the algorithm exist. We think that one which is worth pursuing is the one yielding the sparsest solution.

6.3 References

[1] C. E. Shannon, "A mathematical theory of communication," *Bell System Technical Journal*, vol. 27, pp. 379–423 and 623–656, July and October 1948.

[2] F. Kschischang, B. Frey, and H. Loeliger, "Factor graphs and the sum-product algorithm," *Information Theory, IEEE Transactions on*, vol. 47, no. 2, pp. 498–519, 2001.

[3] D. MacKay and R. Neal, "Near Shannon limit performance of low density parity check codes," *Electronics Letters*, vol. 33, no. 6, pp. 457–458, Mar 1997.

[4] M. Davey and D. MacKay, "Low density parity check codes over GF(q)," in *Information Theory Workshop, 1998*, Jun 1998, pp. 70–71.

[5] T. Richardson, M. Shokrollahi, and R. Urbanke, "Design of capacity-approaching irregular low-density parity-check codes," *Information Theory, IEEE Transactions on*, vol. 47, no. 2, pp. 619–637, 2001.

[6] T. Richardson and R. Urbanke, "The capacity of low-density parity-check codes under message-passing decoding," *Information Theory, IEEE Transactions on*, vol. 47, no. 2, pp. 599–618, Feb 2001.

[7] S.-Y. Chung, J. Forney, G.D., T. Richardson, and R. Urbanke, "On the design of low-density parity-check codes within 0.0045 dB of the Shannon limit," *Communications Letters, IEEE*, vol. 5, no. 2, pp. 58–60, Feb 2001.

[8] C. Berrou, A. Glavieux, and P. Thitimajshima, "Near Shannon limit error-correcting coding and decoding: Turbo-codes. 1," vol. 2, 1993, pp. 1064–1070 vol.2.

[9] R. McEliece, D. MacKay, and J.-F. Cheng, "Turbo decoding as an instance of Pearl's ldquo;belief propagation rdquo; algorithm," *Selected Areas in Communications, IEEE Journal on*, vol. 16, no. 2, pp. 140 –152, feb 1998.

[10] M. Tuchler, R. Koetter, and A. Singer, "Turbo equalization: principles and new results," *Communications, IEEE Transactions on*, vol. 50, no. 5, pp. 754 –767, may 2002.

[11] D. Gesbert, S. Hanly, H. Huang, S. Shamai Shitz, O. Simeone, and W. Yu, "Multi-Cell MIMO Cooperative Networks: A New Look at Interference," *Selected Areas in Communications, IEEE Journal on*, vol. 28, no. 9, pp. 1380 –1408, december 2010.

[12] T. Tran, Y. Shin, and O. Shin, "Overview of enabling technologies for 3GPP LTE-advanced," *EURASIP Journal on Wireless Communications and Networking*, vol. 2012, no. 1, p. 54, 2012.

[13] H. Sato, "The capacity of the Gaussian interference channel under strong interference (corresp.)," *Information Theory, IEEE Transactions on*, vol. 27, no. 6, pp. 786–788, 1981.

[14] T. Han and K. Kobayashi, "A new achievable rate region for the interference channel," *Information Theory, IEEE Transactions on*, vol. 27, no. 1, pp. 49–60, 1981.

[15] V. Cadambe and S. Jafar, "Interference alignment and degrees of freedom of the-user interference channel," *Information Theory, IEEE Transactions on*, vol. 54, no. 8, pp. 3425–3441, 2008.

[16] R. Etkin, D. Tse, and H. Wang, "Gaussian interference channel capacity to within one bit," *Information Theory, IEEE Transactions on*, vol. 54, no. 12, pp. 5534–5562, 2008.

[17] I. Sason, "On achievable rate regions for the Gaussian interference channel," *Information Theory, IEEE Transactions on*, vol. 50, no. 6, pp. 1345–1356, 2004.

[18] S. Jafar and M. Fakhereddin, "Degrees of freedom for the MIMO interference channel," *Information Theory, IEEE Transactions on*, vol. 53, no. 7, pp. 2637–2642, 2007.

[19] S. Jafar and S. Vishwanath, "Generalized Degrees of Freedom of the Symmetric Gaussian User Interference Channel," *Information Theory, IEEE Transactions on*, vol. 56, no. 7, pp. 3297–3303, 2010.

Appendix A

Distributed Antenna System Overview

A.1 pdf Evaluation

A exponential RV X, with mean λ^{-1}, has his MGF given by [1]

$$\varphi_X(s) = \left(1 - \frac{s}{\lambda}\right)^{-1} \tag{A.1}$$

For a RV, Γ, which is the sum of N independent RV, the corresponding MGF is the product of the N independent RV MGFs. If we have K_i antennas for each group i of M, with each channel gain magnitude obeying a Rayleigh distribution, or equivalently an exponential distribution, for power, the MGF of Γ is

$$\varphi_\Gamma(s) = \prod_{i=1}^{M} \varphi_{X_i}(s)^{Ki} = \prod_{i=1}^{M} \left(\frac{\lambda_i}{\lambda_i - s}\right)^{K_i} \tag{A.2}$$

which can be expanded in partial fractions as

$$\varphi_\Gamma(s) = \sum_{i=1}^{M} \sum_{n=1}^{K_i} \frac{a_{in}}{(\lambda_i - s)^n} \tag{A.3}$$

where a_{in} are the partial fraction coefficients given by [2]:

$$a_{in} = \frac{1}{(K_i - n)!} \frac{d^{(K_i - n)}}{ds^{(K_i - n)}} [(\lambda_i - s)^{K_i} \varphi_\Gamma(s)] \Big|_{s=\lambda_i} \tag{A.4}$$

Having that we can evaluate the Γ RV pdf as

$$\begin{aligned} f_\Gamma(\gamma) &= \mathcal{M}_\Gamma^{-1}[\varphi_\Gamma(jw)] \\ &= \sum_{i=1}^{M} \sum_{n=1}^{K_i} \frac{a_{in}}{\lambda_i^n} \mathcal{M}_\Gamma^{-1} \left[\frac{\lambda_i^n}{(\lambda_i - jw)^n}\right] \end{aligned} \tag{A.5}$$

where $\mathcal{M}_x[f(x)]$ and $\mathcal{M}_x^{-1}[F(jw)]$ are the moment generating function and inverse moment generating function, respectively

$$\mathcal{M}_x[f(x)] = \int_{-\infty}^{\infty} f(x) e^{jwx}\, dx \tag{A.6}$$

$$\mathcal{M}_x^{-1}[F(jw)] = \frac{1}{2\pi} \int_{-\infty}^{\infty} F(jw) e^{-jwx}\, dw \tag{A.7}$$

The $\mathcal{M}_{\Gamma}^{-1}$ part in the second equality of equation (A.5) is well known. It is the pdf of an Erlang distribution [3], or equivalently the PDF of a Gamma distribution with an integer shape parameter. Therefore the pdf of the Γ RV is

$$f_{\Gamma}(\gamma) = \sum_{i=1}^{M} \sum_{n=1}^{K_i} \frac{a_{in} \gamma^{n-1} e^{-\lambda_i \gamma}}{(n-1)!} \tag{A.8}$$

A.2 Differential Capacity

From equation (3.17) the differential capacity is given by

$$\Delta C_{N-1}^{N} = \int_0^{\infty} \frac{f_{\Gamma_N}(\gamma)}{1+\gamma} \, d\gamma \tag{A.9}$$

and the corresponding Γ_N RV probability distribution, (3.15), by

$$f_{\Gamma_N}(\gamma) = \lambda_N \, e^{-\lambda_N \gamma} \int_0^{\gamma} f_{\Gamma_{N-1}}(x) \, e^{\lambda_N x} \, dx \tag{A.10}$$

Therefore, after some manipulations to the first expression we get

$$\begin{aligned}
\Delta C_{N-1}^{N} &= \int_0^{+\infty} \frac{e^{-\lambda_N \gamma}}{1+\gamma} \int_0^{\gamma} f_{\Gamma_{N-1}}(x) e^{\lambda_N x} dx d\gamma \\
&= \left[-\frac{e^{-\lambda_N \gamma}}{\lambda_N} \frac{1}{1+\gamma} \int_0^{\gamma} f_{\Gamma_{N-1}}(x) e^{\lambda_N x} dx \right]_0^{+\infty} - \\
&\int_0^{+\infty} \left(-\frac{e^{-\lambda_N \gamma}}{\lambda_N} \right) \left[-\frac{1}{(1+\gamma)^2} \int_0^{\gamma} f_{\Gamma_{N-1}}(x) e^{\lambda_N x} dx d\gamma \right] + \\
&\int_0^{+\infty} \frac{e^{-\lambda_N \gamma}}{\lambda_N} \left[\frac{1}{1+\gamma} f_{\Gamma_{N-1}}(\gamma) e^{\lambda_N \gamma} \right] d\gamma \\
&= \left[-\frac{1}{\lambda_N^2} \frac{f_{\Gamma_N}(\gamma)}{1+\gamma} \right]_0^{+\infty} - \frac{1}{\lambda_N^2} \int_0^{+\infty} \frac{\lambda_N e^{-\lambda_N \gamma}}{(1+\gamma)^2} \int_0^{\gamma} f_{\Gamma_{N-1}}(x) e^{\lambda_N x} dx d\gamma + \frac{1}{\lambda_N} \int_0^{+\infty} \frac{f_{\Gamma_{N-1}}(\gamma)}{1+\gamma} d\gamma \\
&= \frac{1}{\lambda_N^2} \left[f_{\Gamma_N}(0) - \int_0^{+\infty} \frac{f_{\Gamma_N}(\gamma)}{(1+\gamma)^2} d\gamma \right] + \frac{\lambda_{N-1}}{\lambda_N} \Delta C_{N-1}
\end{aligned} \tag{A.11}$$

The result of the integral in the last equation is always positive, since its argument is greater than zero for all $\gamma \geq 0$. Hence, the DCAP ratio can be upper bounded by

$$\frac{\Delta C_{N-1}^{N}}{\Delta C_{N-2}^{N-1}} \leq \frac{\lambda_{N-1}}{\lambda_N} \tag{A.12}$$

A.3 Maximum DCAP

We know from equations (3.16) and (3.17) that the capacity increase by the connection of one more antenna to the user reduces to

$$\Delta C_{N-1}^{N} = \frac{1}{\lambda_N} \int_0^{\infty} \frac{f_{\Gamma_N}(\gamma)}{1+\gamma} \, d\gamma \tag{A.13}$$

Thus its derivative in relation to λ_i, for all i different from N, is given by

$$\frac{d\Delta C_{N-1}^{N}}{d\lambda_i} = \frac{1}{\lambda_N}\int_0^\infty \frac{\mathcal{M}_\Gamma^{-1}[\frac{d\varphi_\Gamma(jw)}{d\lambda_i}]}{1+\gamma}\,d\gamma \tag{A.14}$$

Since the derivative of the MGF of the Γ RV in order to λ_i is:

$$\frac{d\varphi_\Gamma(jw)}{d\lambda_i} = -jw\frac{K_i}{\lambda_i^2}\frac{\lambda_i}{\lambda_i - jw}\varphi_\Gamma(jw) \tag{A.15}$$

we have

$$\begin{aligned}\frac{d\Delta C_{N-1}^{N}}{d\lambda_i} &= \frac{K_i}{\lambda_i^2}\frac{1}{\lambda_N}\int_0^\infty \frac{df_{\Gamma_{N+1}}(\gamma)}{d\gamma}\frac{1}{1+\gamma}\,d\gamma \\ &= \frac{K_i}{\lambda_i^2}\frac{1}{\lambda_N}\left[-\lambda_1\delta_{N1} + \int_0^\infty \frac{f_{\Gamma_{N+1}}(\gamma)}{(1+\gamma)^2}\,d\gamma\right]\end{aligned} \tag{A.16}$$

where δ_{ij} is the Kronecker delta function. Hence, for $i \neq N$, we have that

$$\begin{aligned}\frac{d\Delta C_{N-1}^{N}}{d\lambda_i} &\geq 0, N > 1 \\ \frac{d\Delta C_{N-1}^{N}}{d\lambda_i} &\leq 0, N = 1\end{aligned} \tag{A.17}$$

Thus the capacity increase, decreases with the SNR increase for the case of more than one antenna connected to the user, and increases with the SNR increase for the case of only one antenna connected to the user. Being aware of that and assuming that the new connected antenna has the smallest SNR of all them, the capacity increase by the connection to one more antenna can be upper bounded by

$$\begin{aligned}\Delta C_{N-1}^{N}(\lambda_1,\ldots,\lambda_N) &\leq \Delta C_{N-1}^{N}(\lambda_N,\ldots,\lambda_N) \\ &\leq \frac{1}{\lambda_N + N - 1} \leq \frac{1}{N-1}\end{aligned} \tag{A.18}$$

The second inequality follows from section A.4.

A.4 DCAP for the Case of Equal SNRs

For the case of all equal mean SNRs the global pdf reduces to:

$$f_\Gamma(\gamma) = \frac{\lambda^N}{(N-1)!}\,\gamma^{N-1}e^{-\lambda\gamma} \tag{A.19}$$

Thus, from equation (3.16) the capacity increase by the connection to 1 more antenna is given by

$$\begin{aligned}\Delta C_{N-1}^{N} = C_1(\lambda, N-1) &= \frac{1}{\lambda}\int_0^\infty \frac{f_{\Gamma_N}(\gamma)}{1+\gamma}\,d\gamma \\ &= \int_0^\infty \frac{(\lambda\gamma)^{N-1}e^{-\lambda\gamma}}{(1+\gamma)(N-1)!}\,d\gamma \\ &= \int_0^\infty \frac{\gamma^{N-1}e^{-\gamma}}{(\lambda+\gamma)(N-1)!}\,d\gamma\end{aligned} \tag{A.20}$$

From the third line of equation (A.20) we can see that as the SNR, λ^{-1}, increases the DCAP also increases, since

$$\gamma \geq 0 \ \wedge \ \lambda \ \geq \lambda_0 \geq 0 \Leftrightarrow \frac{\gamma^{N-1}e^{-\gamma}}{(\lambda+\gamma)(N-1)!} \leq \frac{\gamma^{N-1}e^{-\gamma}}{(\lambda_0+\gamma)(N-1)!} \tag{A.21}$$

Thus the derivative of this function in order to λ, $\frac{d\Delta C_{N-1}^{N}}{d\lambda}$, is always lower than zero.

$$\begin{aligned}
\frac{d\Delta C_{N-1}^{N}}{d\lambda} &= \int_0^\infty \frac{d\frac{(\lambda\gamma)^{N-1}e^{-\lambda\gamma}}{(1+\gamma)(N-1)!}}{d\lambda}\, d\gamma \\
&= \int_0^\infty \frac{(N-1)\gamma(\lambda\gamma)^{N-2}e^{-\lambda\gamma} + (\lambda\gamma)^{N-1}(-\gamma)e^{-\lambda\gamma}}{(1+\gamma)(N-1)!} d\gamma \\
&= \frac{N-1}{\lambda}\int_0^\infty \frac{(\lambda\gamma)^{N-1}e^{-\lambda\gamma}}{(1+\gamma)(N-1)!} d\gamma - \int_0^\infty \frac{\gamma}{\lambda}\frac{\lambda^N\gamma^{N-1}e^{-\lambda\gamma}}{(1+\gamma)(N-1)!} d\gamma \\
&= \frac{N-1}{\lambda}\Delta C_{N-1}^{N} - \frac{1}{\lambda}\int_0^\infty \frac{\gamma}{(1+\gamma)} f_{\Gamma_N}(\gamma) d\gamma \\
&= \frac{N-1}{\lambda}\Delta C_{N-1}^{N} - \frac{1}{\lambda}\int_0^\infty \frac{1+\gamma}{(1+\gamma)} f_{\Gamma_N}(\gamma) d\gamma + \frac{1}{\lambda}\int_0^\infty \frac{1}{(1+\gamma)} f_{\Gamma_N}(\gamma) d\gamma \\
&= \frac{N-1}{\lambda}\Delta C_{N-1}^{N} - \frac{1}{\lambda} + \Delta C_{N-1}^{N} \\
&= \left(\frac{N-1}{\lambda} + 1\right)\Delta C_{N-1}^{N} - \frac{1}{\lambda} \leq 0
\end{aligned} \tag{A.22}$$

In the evaluation of the derivative of ΔC_{N-1}^{N} over λ we have just used the definition of DCAP (equation 3.16) and of Γ_N RV pdf (equation (A.19)). Therefore the DCAP can be upper bounded by

$$\Delta C_{N-1}^{N} \leq \frac{1}{N-1+\lambda} \leq \frac{1}{N-1} \tag{A.23}$$

Additionally the upper bound $1/(N-1)$ can be obtained in the limit of $\lambda = 0$, by evaluating the third line of equation (A.20).

A.5 DCAP Derivation for the Multiuser Case

For the co-located transmit antennas case $\overline{\mathbf{H}}_i\overline{\mathbf{H}}_i^H$, $(i = N-1, N)$, is $\tilde{\mathcal{W}}_K(i, \boldsymbol{\Xi})$ distributed. But since $\overline{\mathbf{H}}_i\overline{\mathbf{H}}_i^H \sim \boldsymbol{\Xi}^{1/2}\mathbf{A}_i\boldsymbol{\Xi}^{1/2}$, where $\mathbf{A}_i$ is $\tilde{\mathcal{W}}_K(i, \mathbf{I}_K)$ distributed, the DCAP can be expressed by:

$$\begin{aligned}
\Delta C_{N-1,K}^{N,K} &= \mathbb{E}[log|\overline{\mathbf{H}}_N\overline{\mathbf{H}}_N^H|] - \mathbb{E}[log|\overline{\mathbf{H}}_{N-1}\overline{\mathbf{H}}_{N-1}^H|] \\
&= \mathbb{E}[log|\mathbf{A}_N|] - \mathbb{E}[log|\mathbf{A}_{N-1}|] \\
&= \left[\sum_{l=0}^{K-1}\Psi(N-l) - \sum_{l=0}^{K-1}\Psi(N-1-l)\right] \\
&= \sum_{n=N-K+1}^{N}\frac{1}{n-1} \approx \log\left(1 + \frac{K}{N-1-K+\beta}\right)
\end{aligned} \tag{A.24}$$

where $\Psi(l) = -\varrho + \sum_{n=1}^{l-1} 1/n$, is the Euler's digamma function. The result from the second line comes from the determinant property ($|\mathbf{AB}| = |\mathbf{A}||\mathbf{B}|$) and the result from the third line from lemma 1 of [4] ($(\mathbb{E}[log|\mathbf{A}_i|] = \sum_{l=0}^{K-1} \Psi(i-l))$). To obtain an approximation to the partial sum of the harmonic series we have used $\sum_{n=1}^{N} 1/n \approx \varrho + log(N+\beta)$ (ϱ is the Euler Constant) which has a maximum error of 4.1×10^{-3}.

A.6 Capacity Increase by the Connection of One More User, for N=1

For $N = 1$ the broadcast channel ergodic sum-capacity, equation (3.31), simplifies to, [5]

$$\overline{\mathbf{C}}_{DPC}^{1,K} = \mathbb{E}\left[log\left(1 + P \max_{k=1\ldots K}(\xi_k^{1/2} h_k^H h_k \xi_k^{1/2})\right)\right] = \mathbb{E}[log(1+Px)] \tag{A.25}$$

where ξ_k is the average SNR of user k, $h_k \sim \tilde{\mathcal{N}}(0,1)$ and $x = \max_k(\xi_k h_k^H h_k)$. Hence the cumulative distribution of x is given by [6] $F_X(x) = \prod_{k=1}^{K} F_{Y_k}(x)$, where $y_k = \xi_k h_k^H h_k$. Since Y_k is exponential distributed with mean $\mu_k^{-1} = \xi_k$, $F_{Y_k}(y) = 1 - e^{-u_k y}$, $F_X(x) = \prod_{k=1}^{K}(1 - e^{-u_k x})$ and $f_X(x) = dF_X(x)/dx = \sum_{k=1}^{K} u_k e^{-u_k x} \prod_{i=1, i\neq k}^{K}(1 - e^{-u_i x})$. Using this information to evaluate the expectation operator of equation (A.25) we get

$$\begin{aligned}
\overline{\mathbf{C}}_{DPC}^{1,K} &= \int_0^\infty log(1+Px) f_X(x) dx \\
&= \int_0^\infty log(1+Px) \sum_{k=1}^{K} u_k e^{-u_k x} \prod_{i=1, i\neq k}^{K} (1 - e^{-u_i x}) dx \\
&= [log(1+Px) f(x)]_0^\infty - \int_0^\infty \frac{P f(x)}{1+Px} dx, \quad f(x) = \int \sum_{k=1}^{K} u_k e^{-u_k x} \prod_{i=1, i\neq k}^{K} (1 - e^{-u_i x}) dx \\
&= \left[log(1+Px)\left(\prod_{k=1}^{K}(1 - e^{-u_k x}) - 1\right)\right]_0^\infty - \int_0^\infty \frac{P}{1+Px}\left(\prod_{k=1}^{K}(1 - e^{-u_k x}) - 1\right) dx \\
&= -\int_0^\infty \frac{P}{1+Px}\left(\prod_{k=1}^{K}(1 - e^{-u_k x}) - 1\right) dx
\end{aligned} \tag{A.26}$$

In the third line we have used integration by parts and in fourth line used the fact that $f(x)$ is the integral of $f_X(x)$ and thus is up to a constant equal to $F_X(x)$. In this case the constant is equal to -1 since $F_X(x) = 1 + g(x)$, where $g(x)$ is a sum of exponential functions, and therefore the constant 1 is removed in the derivation.

With the help of the capacity expression obtained in the previous derivation we can obtain

the capacity increase by the connection of an additional user, which is given by

$$\begin{aligned}
\Delta C_{1,K-1}^{1,K} &= \overline{\mathbf{C}}_{DPC}^{1,K} - \overline{\mathbf{C}}_{DPC}^{1,K-1} \\
&= -\int_0^\infty \frac{P}{1+Px}\left(\prod_{k=1}^{K}(1-e^{-u_k x})-1\right)dx + \int_0^\infty \frac{P}{1+Px}\left(\prod_{k=1}^{K-1}(1-e^{-u_k x})-1\right)dx \\
&= \int_0^\infty \frac{P}{1+Px}\left[\prod_{k=1}^{K-1}(1-e^{-u_k x})[-(1-e^{-u_K x})+1]+1-1\right]dx \\
&= \int_0^\infty \frac{P}{1+Px}e^{-u_K x}\prod_{k=1}^{K-1}(1-e^{-u_k x})dx \\
&= \int_0^\infty \frac{1}{1+y}e^{-\nu_K y}\prod_{k=1}^{K-1}(1-e^{-\nu_k y})dy, \quad y = Px, \quad \nu_k = u_k/P
\end{aligned} \tag{A.27}$$

Thus its derivative in relation to u_k, for all k different from K is given by

$$\frac{d\Delta C_{1,K-1}^{1,K}}{du_k} = \int_0^\infty \frac{P}{1+Px}e^{-u_K x}u_k e^{-u_k x}\prod_{n=1,n\neq k}^{K-1}(1-e^{-u_n x})dx \tag{A.28}$$

$$\frac{d\Delta C_{1,K-1}^{1,K}}{du_K} = \int_0^\infty \frac{P}{1+Px}(-u_K)e^{-u_K x}\prod_{n=1}^{K-1}(1-e^{-u_n x})dx \tag{A.29}$$

Since, for all $x \geq 0$, the integrand in equation (A.28) is always positive and in equation (A.29) always negative, we have

$$\begin{aligned}
\frac{d\Delta C_{1,K-1}^{1,K}}{du_k} &\geq 0, \quad k \neq K \\
\frac{d\Delta C_{1,K-1}^{1,K}}{du_K} &\leq 0
\end{aligned} \tag{A.30}$$

Therefore using the same arguments as in section A.3 we get to the conclusion that the maximum increase in capacity by the connection of an additional user is obtained when all u_k are equal, i.e. $u_k = u$, $k = 1, \ldots, K$. For this case of all equal mean SNRs we can get a closed form solution for $\Delta C_{1,K-1}^{1,K}$. Indeed, from the fourth line of equation (A.27), we see that $\Delta C_{1,K-1}^{1,K}$ is maximal when P goes to infinite (High SNR), since $P_0 > P_1 \Leftrightarrow P_0/(1+P_0 x) \geq P_1/(1+P_1 x)$. As a consequence the maximum capacity increase is given by

$$\begin{aligned}
\Delta C_{1,K-1}^{1,K} &= \int_0^\infty \frac{1}{x}e^{-ux}(1-e^{-ux})^{K-1}dx = \int_0^\infty \frac{1}{y}e^{-y}(1-e^{-y})^{K-1}dy, \quad y = ux \\
&= -\int_0^1 \frac{(1-z)^{K-1}}{log(z)}dz = \sum_{n=0}^{K-1}\binom{K-1}{n}(-1)^{n+1}log(n+1), \quad z = e^{-y}
\end{aligned} \tag{A.31}$$

The last equality is a known result (equation (57) of [7]).

A.7 References

[1] S. M. Ross, *Introduction to probability models.* Academic Press, 2007.

[2] S. Ghosh, *Network Theory: Analysis and Synthesis.* Prentice Hall of India, 2004.

[3] J. A. Gubner, *Probability and Random Processes for Electrical and Computer Engineers.* Cambridge University Press, 2006.

[4] J. Lee and N. Jindal, "High SNR Analysis for MIMO Broadcast Channels: Dirty Paper Coding Versus Linear Precoding," *Information Theory, IEEE Transactions on*, vol. 53, no. 12, pp. 4787 –4792, dec. 2007.

[5] G. Caire and S. Shamai, "On the achievable throughput of a multiantenna Gaussian broadcast channel," *Information Theory, IEEE Transactions on*, vol. 49, no. 7, pp. 1691 – 1706, july 2003.

[6] H. Liu and G. Li, *OFDM-Based Broadband Wireless Networks: Design and Optimization.* Wiley-Interscience, 2005.

[7] J. Guillera and J. Sondow, "Double integrals and infinite products for some classical constants via analytic continuations of lerch's transcendent," *Ramanujan J. 16 (2008) 247-270*, 2005.

Appendix B

Minimum Bit Error Rate Nonlinear Precoding for Multiuser MIMO and High SNR

B.1 Gray Mapping and Corresponding Decision Regions

In this appendix we review Gray mapping for a square M-ary constellation, in the odd complex integer grid $\mathcal{G}$. By doing so our objective is to show that every decision region has a specific geometry that can be easily used in our benefit to obtain the corresponding probability of error of the corresponding bit. So to start we show how Gray mapping can be done, for

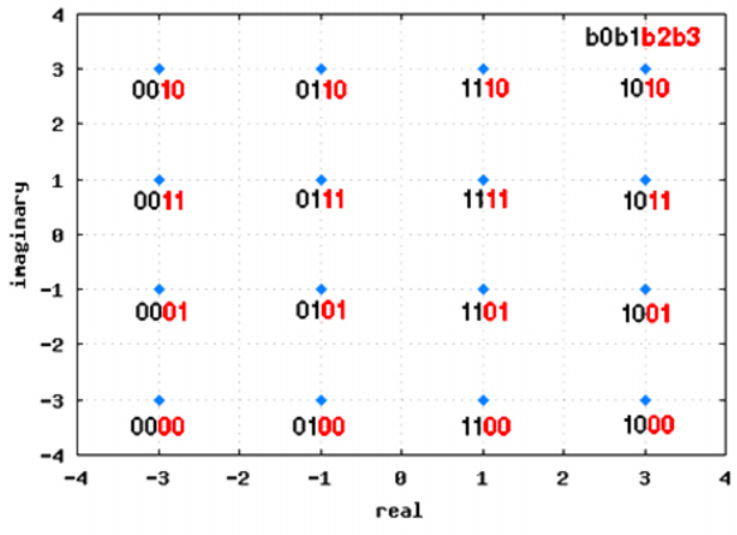

Figure B.1: Gray mapping 16-QAM.

a given M-ary constellation. Since we are considering a square M-ary constellation, and by that we mean that M is a square number, the bits can be divided into two groups, $\mathcal{G}_I$ and $\mathcal{G}_Q$.

Namely we divide them into two groups, because $\mathcal{G}_I$ is used to do the Gray mapping in the In-Phase component and $\mathcal{G}_Q$ is used to do the Gray mapping in the Quadrature component. By doing that we impose that only one bit changes in each direction (In-Phase and Quadrature), between adjacent symbols. We also impose the decision regions to be only limited in one of the directions, and not both in the In-Phase and Quadrature directions.

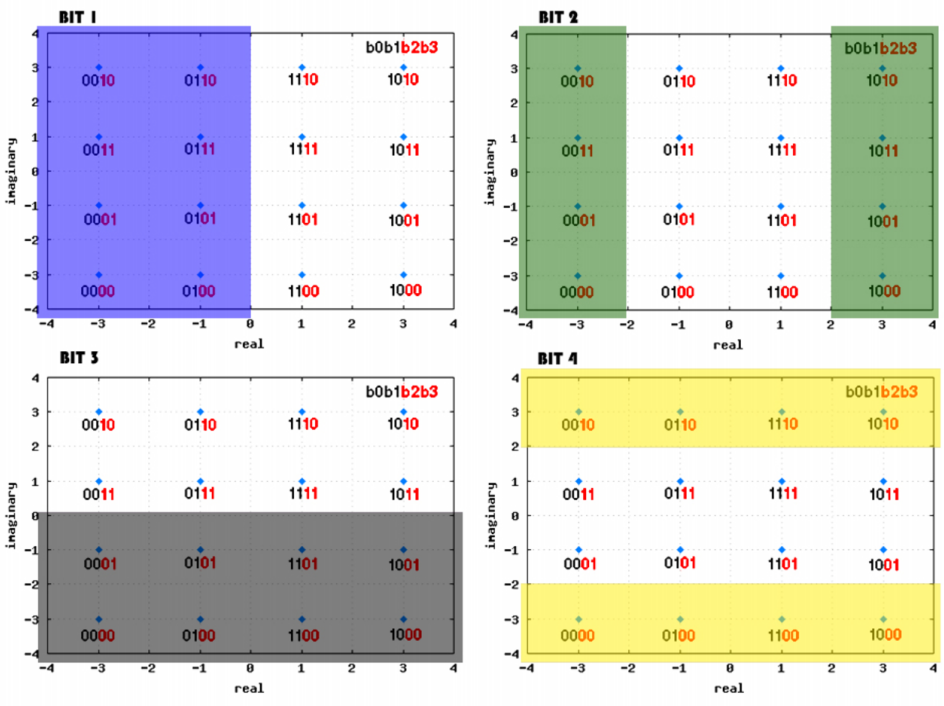

Figure B.2: Gray mapping 16-QAM.

To exemplify the aforementioned explanation in the following paragraphs we show how to do the Gray mapping for a 16-QAM constellation and the corresponding decision regions. Such a mapping is shown in figure B.1. Consider that we use the first two bits for the In-Phase component ($\mathcal{G}_I$), and the last two bits for the Quadrature component ($\mathcal{G}_Q$). The bits of group $\mathcal{G}_I$ and the ones from group $\mathcal{G}_Q$ are represented in black and red, respectively. By doing that we see, if we only look from left to right (in the In-Phase component direction) that only one bit changes between adjacent symbols. The same happens in the quadrature direction. With that in mind it is not difficult to see that, by doing such a mapping, only one bit changes between adjacent symbols, in both directions. Thus is also not difficult to see that the decision regions for each bit of the symbol ('0000') are the ones shown in Figure B.2 and that the corresponding probability of error can be expressed by the sum of Q-functions, as mentioned in section 4.4.

B.2 Dual Problem

The aim of this appendix is to derive the dual problem of (4.20). The Lagrangian [1, 2] associated with the aforementioned problem is

$$L(z,\beta,\mathbf{x},u,\gamma,\boldsymbol{\lambda}) = z + u(\mathbf{x}^H\mathbf{x} - P_T) + \boldsymbol{\lambda}^H(\beta\mathbf{b} - \mathbf{A}\mathbf{x} - z\mathbf{1}) - \gamma\beta \tag{B.1}$$

The variables u ($u \geq 0$), γ ($\gamma \geq 0$) and the vector $\boldsymbol{\lambda}$ ($\boldsymbol{\lambda} \geq \mathbf{0}$) are called the dual variables and the variables z, β, and the vector $\mathbf{x}$ are called the primal variables [1]. The Lagrange dual function can be obtained as the minimum value of the Lagrangian over the primal variables [1]. Since $L(z,\beta,\mathbf{x},u,\gamma,\boldsymbol{\lambda})$ is quadratic in $\mathbf{x}$ and a linear function of z and β we can find the minimizing pair $(z,\beta,\mathbf{x})$ from the corresponding KKT conditions [3], that are necessary and sufficient:

$$\begin{aligned}
&\frac{\partial L(z,\beta,\mathbf{x},u,\gamma,\boldsymbol{\lambda})}{\partial z} = 1 - \mathbf{1}^H\boldsymbol{\lambda} = 0 \\
&\frac{\partial L(z,\beta,\mathbf{x},u,\gamma,\boldsymbol{\lambda})}{\partial \beta} = \mathbf{b}^H\boldsymbol{\lambda} - \gamma = 0 \\
&\frac{\partial L(z,\beta,\mathbf{x},u,\gamma,\boldsymbol{\lambda})}{\partial \mathbf{x}} = 2u\mathbf{x} - \mathbf{A}^H\boldsymbol{\lambda} = 0 \Leftrightarrow \mathbf{x} = \frac{\mathbf{A}^H\boldsymbol{\lambda}}{2u}
\end{aligned} \tag{B.2}$$

Such conditions imply that Lagrange dual function [1], $g(u,y,\boldsymbol{\lambda})$ is given by

$$g(u,\gamma,\boldsymbol{\lambda}) = \begin{cases} -\frac{\boldsymbol{\lambda}^H\mathbf{A}\mathbf{A}^H\boldsymbol{\lambda}}{4u} - u, & 1 - \mathbf{1}^H\boldsymbol{\lambda} = 0;\ \mathbf{b}^H\boldsymbol{\lambda} - \gamma = 0 \\ -\infty, & \text{otherwise} \end{cases} \tag{B.3}$$

Consequently, the Lagrange dual problem [1, 4, 5] of (4.20) is to maximize $g(u,\gamma,\boldsymbol{\lambda})$ subject to the positivity of the dual variables:

$$\min_{u,\gamma,\boldsymbol{\lambda}} \frac{\boldsymbol{\lambda}^H\mathbf{A}\mathbf{A}^H\boldsymbol{\lambda}}{4u} + uP_T \ \ s.t. \mathbf{1}^H\boldsymbol{\lambda} = 1, \mathbf{b}^H\boldsymbol{\lambda} = \gamma, \boldsymbol{\lambda} \geq \mathbf{0}, u \geq 0, \gamma \geq 0 \tag{B.4}$$

However the dual problem can be further simplified since the value of u can be obtained analytically $\left(2u = \sqrt{\boldsymbol{\lambda}^H\mathbf{A}\mathbf{A}^H\boldsymbol{\lambda}/P_T}\right)$, consequently, the dual problem can be shown to be equal to

$$\hat{\underline{\boldsymbol{\lambda}}} = arg\min_{\gamma,\boldsymbol{\lambda}} \sqrt{\boldsymbol{\lambda}^H\mathbf{A}\mathbf{A}^H\boldsymbol{\lambda}} \ \ s.t. \mathbf{1}^H\boldsymbol{\lambda} = 1, \mathbf{b}^H\boldsymbol{\lambda} = \gamma, \boldsymbol{\lambda} \geq \mathbf{0}, \gamma \geq 0 \tag{B.5}$$

B.3 References

[1] S. P. Boyd and L. Vandenberghe, *Convex optimization.* Cambridge University Press, 2004.

[2] S. Haykin, *Adaptive Filter Theory*, 4th ed. Prentice Hall, Sep. 2001.

[3] H. Kuhn and A. Tucker, "Nonlinear programming," in *Proceedings of the second Berkeley symposium on mathematical statistics and probability*, vol. 1. California, 1951, pp. 481–492.

[4] D. P. Bertsekas, *Nonlinear programming.* Athena Scientific, 1999.

[5] R. Boţ, G. Wanka, and S. Grad, *Duality in vector optimization.* Springer Verlag, 2009.